TECHNISCHE UNIVERSITÄT DARMSTADT

Flavors of biotin ligases: From research tools towards biopharmaceutical applications

Vom Fachbereich Chemie
der Technischen Universität Darmstadt

zur Erlangung des akademischen Grades eines
Doctor rerum naturalium (Dr. rer. nat)

genehmigte

Dissertation

eingereicht von

Sebastian Harald Bitsch, M.Sc.

Referent: Prof. Dr. Harald Kolmar
Korreferent: Prof. Dr. Viktor Stein

Darmstadt 2023

Bitsch, Sebastian Harald: Flavors of biotin ligases: From research tools towards biopharmaceutical applications
Darmstadt, Technische Universität Darmstadt
Jahr der Veröffentlichung der Dissertation auf TUprints: 2023
URN: urn:nbn:de:tuda-tuprints-242067
URI: https://tuprints.ulb.tu-darmstadt.de/id/eprint/24206

Tag der Einreichung: 11. Mai 2023
Tag der mündlichen Prüfung: 26. Juni 2023

Die vorliegende Arbeit wurde unter der Leitung von Herrn Prof. Dr. Harald Kolmar am Clemens-Schöpf-Institut für organische Chemie und Biochemie der Technischen Universität Darmstadt von Juni 2019 bis Mai 2023 angefertigt.

Für Mama

…du weißt,
warum beim Verfassen dieser Arbeit,
meine Gedanken mehr als einmal
zu dir gegangen sind!

Publications derived from this work:

Kubitz L.*, **Bitsch S.***, Zhao X.*, Schmitt K., Deweid L., Roehrig A., Barazzone E. C., Valerius O., Kolmar H., & Béthune J. (2022). Engineering of ultraID, a compact and hyperactive enzyme for proximity-dependent biotinylation in living cells. *Communications Biology* 2022 5:1, 5(1), 1–14.

Baalmann M.*, Neises L.*, **Bitsch S.**, Schneider H., Deweid L., Werther P., Ilkenhans N., Wolfring M., Ziegler M. J., Wilhelm J., Kolmar H., & Wombacher R. (2020). A Bioorthogonal Click Chemistry Toolbox for Targeted Synthesis of Branched and Well-Defined Protein–Protein Conjugates. *Angewandte Chemie International Edition*, 59(31), 12885–12893.

Contributions to related projects:

Becker B.*, Englert S.*, Schneider H., Yanakieva D., Hofmann S., Dombrowsky C., Macarrón Palacios A., **Bitsch S.**, Elter A., Meckel T., Kugler B., Schirmacher A., Avrutina O., Diederichsen U., & Kolmar H. (2021). Multivalent dextran hybrids for efficient cytosolic delivery of biomolecular cargoes. *Journal of Peptide Science*, 27(4).

Elter A.*, Bock T., Spiehl D., Russo G., Hinz S. C., **Bitsch S.**, Baum E., Langhans M., Meckel T., Dörsam E., Kolmar H., & Schwall G. (2021). Carbohydrate binding module-fused antibodies improve the performance of cellulose-based lateral flow immunoassays. *Scientific Reports,* 11, 7880.

Ali A.*, Happel D., Habermann J., Schoenfeld K., Macarrón Palacios A., **Bitsch S.**, Englert S., Schneider H., Avrutina O., Fabritz S., & Kolmar H. (2022). Sactipeptide Engineering by Probing the Substrate Tolerance of a Thioether-Bond-Forming Sactisynthase. *Angewandte Chemie - International Edition*, *61*(45).

Hadjabdelhafid-Parisien A.*, **Bitsch S.**, Macarrón Palacios A., Deweid L., Kolmar H., & Pelletier J. N. (2022). Tag-free, specific conjugation of glycosylated IgG1 antibodies using microbial transglutaminase. *RSC Advances*, 12(52), 33510–33515.

Contributions to conferences:

Poster presenter at PEGS Europe 2022 – Protein & Antibody Engineering Summit: Engineering of ultraID, a compact and hyperactive enzyme for proximity-dependent biotinylation in living cells.

Contents

1 Zusammenfassung

Biotin-Ligasen sind Enzyme, die den Biotin-Transfer auf Biotin-abhängige Enzyme katalysieren, welche wiederum für essenzielle Stoffwechselwege wie die Gluconeogenese oder die Fettsäuresynthese von grundlegender Bedeutung sind. In Zeiten des *Protein-Engineerings* und *Genome Editings* können diese Enzyme jedoch auch auf andere, vielfältige Weise genutzt werden. In dieser Arbeit wurden Biotin-Ligasen für verschiedene Anwendungen eingesetzt, angefangen als Hilfsmittel zum grundlegenden Verständnis der Zellbiologie bis hin zu biopharmazeutischen Ansätzen.

Zunächst wurde durch gerichtete Evolution ein neuartiges Enzym namens ultraID für Protein-Protein-Interaktionsstudien entwickelt. Dieses Unterfangen wurde durch *Error-Prone PCR* Mutagenese und *Yeast Surface Display* in Kombination mit fluoreszenzaktivierter Zellsortierung realisiert. Das identifizierte Enzym, das auf einer Biotin-Ligase aus *Aquifex aeolicus* basiert, wies einen massiv verbesserten katalytischen Umsatz auf, der auf eine einzige Mutation im aktiven Zentrum zurückgeführt werden konnte. Bislang ist ultraID eines der kleinsten und effizientesten Enzyme für die *proximity-dependent biotin identification* Methode.

Als nächstes wurde die randomisierte Biotin-Ligasen Bibliothek auf ein modifiziertes Biotin Substrat durchmustert. Dabei wurde ein Propargyl-funktionalisiertes Biotin Derivat auf Enzymumsatz untersucht. Trotz der Anwendung verschiedener Präsentations- und Assay-Strategien konnte ein Propargyl-Biotin umsetzendes Enzym nicht identifiziert werden.

Darüber hinaus wurden grundlegende Experimente zur Herstellung eines Antikörper-Wirkstoff-Konjugats durch Biotin-Ligasen durchgeführt. Eine aus *Pyrococcus horikoshii* stammende Biotin-Ligase wurde genutzt, um Propargyl-Biotin und Desthiobiotin-Azid an den therapeutischen Antikörper Trastuzumab zu konjugieren, der zuvor mit einer Biotin-Akzeptordomäne ausgestattet wurde. Es konnte erfolgreich gezeigt werden, dass eine chemoenzymatische Modifizierung durch Konjugation eines Fluorophors an den Antikörper möglich ist. Die Verwendung von Desthiobiotin-Azid als Substrat machte die Biotin-Ligase jedoch unspezifisch, sodass bei zukünftigen Ansätzen Optimierungen vorgenommen werden müssen. Parallel dazu wurde ein Antikörper-Wirkstoff-Konjugat mit einer anderen Konjugationsstrategie hergestellt. Die Liponsäure-Ligase A aus *Escherichia coli* wurde zum Anbringen eines Click-Chemie kompatiblen Moleküls an einen mit Enzym-Erkennungsmotiv modifizierten Trastuzumab verwendet. Das anschließende Funktionalisieren mit einem Monomethyl-Auristatin-E Toxin führte zur Herstellung eines Antikörper-Wirkstoff-Konjugats mit einer Wirksamkeit im picomolaren Bereich. Darüber hinaus wurde gezeigt, dass die angewandte Konjugationsstrategie keinen Einfluss auf die Affinität des Antikörpers hatte und die enzymatische Modifizierung innerhalb weniger Minuten abgeschlossen war.

Zuletzt wurde die Identifizierung von internalisierenden *single-chain variable fragments* aus Phagen-Display-Bibliotheken von Patienten, welche an systemischem Lupus erythematodes leiden, durchgeführt. Dabei wurden verschiedene Anreicherungsstrategien untersucht, die eine Inkubation auf Säugetierzellen und eine Biotinylierung der Phagen nach erfolgreicher Zellpenetration beinhalteten. Letztendlich konnte kein internalisierender Binder gefunden werden, aber es wurden wichtige Erkenntnisse über die Anreicherung von zellpenetrierenden Bindern mittels Phagen-Display gewonnen.

2 Abstract

Biotin ligases are enzymes commonly attaching biotin to biotin-dependent enzymes, which are fundamental for essential metabolic pathways like gluconeogenesis or fatty acids synthesis. However, in times of protein engineering and genome editing those enzymes can be utilized in versatile ways. In this work biotin ligases were deployed in different fields of research starting with a tool for fundamental understanding of cell biology and culminating in biopharmaceutical approaches.

First, a novel enzyme called ultraID applicable for protein-protein interaction studies was engineered by directed evolution. This undertaking was carried out by error-prone PCR mutagenesis and yeast surface display in combination with fluorescence activated cell sorting. While based on a biotin ligase derived from *Aquifex aeolicus* the novel enzyme exhibited a massively improved catalytic turnover, which was tracked back to one single mutation in the active site. To date, ultraID is one of the smallest and most efficient enzymes for the proximity-dependent biotin identification method.

Second, screening of the randomized biotin ligase library was conducted towards a modified biotin substrate. Hereby, a propargyl functionalized biotin derivative was examined for enzyme turnover. Even tough different yeast surface presentation and assay strategies were analyzed a propargyl biotin using enzymes was not identified.

Third, fundamental experiments for the generation of an antibody-drug conjugate by biotin ligases were performed. A biotin ligase derived from *Pyrococcus horikoshii* was exploited to conjugate propargyl biotin and desthiobiotin azide to the therapeutic antibody trastuzumab, which was equipped with a biotin acceptor domain. It was successfully demonstrated that chemoenzymatic modification was feasible by conjugating a fluorophore to the antibody. However, the usage of desthiobiotin azide as a substrate renders the biotin ligase unspecific and consequently, optimizations must be done in future approaches. In parallel an antibody-drug conjugate was generated by a different approach. Lipoate-protein ligase A derived from *Escherichia coli* was used to conjugate a click chemistry moiety to a tagged trastuzumab. Subsequent attachment of a Monomethyl auristatin E toxin led to the generation of an antibody-drug

conjugate with potency in the picomolar range. Additionally, it was shown that the applied conjugation strategy had no impact on the antibodies affinity and enzymatic conjugation was complete within a few minutes.

Last, identification of internalizing single-chain variable fragments out of systemic lupus erythematosus phage display library was executed. Hereby different enrichment strategies were examined involving incubation on mammalian cells and biotinylation of phages upon successful cell penetration. Ultimately, discovery of an internalizing binder was not achieved but crucial knowledge on phage display-based enrichment of cell penetrating binders was obtained.

3 Introduction

Several projects were performed in this thesis that all make use of the enzyme biotin ligase and another small molecule coupling ligase, called lipoic acid ligase, as tool enzymes. The projects are aimed at providing better tools for the study of protein-protein interactions in cells, improving the generation of antibody drug conjugates in frame of cancer therapy or isolation of cell-penetrating antibodies for potential future therapeutic use. In the following chapters state of the art aspects of cancer therapy, generation, and mode of action of antibody-drug conjugates as well as current strategies for cell internalization of protein cargos are highlighted. This also includes latest methods for functional improvement of biotin ligases as required in frame of this thesis (see also chapter 4).

3.1 Cancer – an overview

Next to cardiovascular diseases, cancer remains the second most leading cause of death worldwide[1]. In 2020, there were 19.3 million new diagnoses and nearly 10 million cancer-related deaths[2]. Furthermore, cancer prevalence increased continuously since 1975 and prognosis say it will increase even more[3–5]. To top it all off, financial burden associated with cancer was projected to be $21.1 billion dollar in 2019 in the US[6]. As depicted by this data cancer has a huge impact on society worldwide and therefore reliable cancer treatments are mandatory. For a better understanding of targets addressed by common therapies, it is crucial to understand cancer biology and cell behavior.

On a cellular level, there are unique hallmarks that allow the differentiation of cancer cells from healthy cells[7,8]. First, cancer cells divide continuously and independently of external growth stimuli. Second, they ignore inhibitory growth signals and are resistant to the so-called “programmed cell death” or apoptosis both leading to unrestricted cell division and expansion of cell mass. Third, cancer cells migrate into healthy tissue, displacing prevalent cells. It is also possible that they detach and travel through the body in blood vessels or the lymph system, to form metastasis in a different body area. Usually, cancerous cells are generated in our body every day, however they are commonly eliminated by the immune system. Consequently, the fourth hallmark of cancer is the ability to escape the immune system, often trough the expression of inhibitory immune checkpoints. Next, due to the expression of telomerases, cancer cells avoid cell cycle arrest, exhibiting replicative immortality. Cells are usually bound to the Hayflick limit, which describes a cell division limit of ~ 50 replications, due to truncated telomere regions of chromosomes[9]. To satisfy the huge nutritional requirements, sufficient transport systems to and away from the solid tumor are crucial. Therefore, formation of blood and lymphatic vessels is promoted. Angiogenesis and lymph angiogenesis can be achieved by the secretion of more than a dozen different activators e.g., vascular endothelial growth factor (VEGF) or basic fibroblast growth factor (bFGF)[10].

Another hallmark promoting further degeneration is the overall genome instability of tumor cells. Deletions or duplications are not uncommon, even doubling of chromosomes may occur. Finally, tumors often exhibit a completely altered metabolism[11]. For example, glycolysis is enhanced, even in an aerobic environment. Hereby, so-called aerobic glycolysis increases the availability of precursors for anabolic pathways and therefore tumor progression[12].

To develop new therapeutic strategies or improve current treatments, deeper knowledge on cancer metabolism and cellular molecular mechanisms in general is required. Therefore, studying cancer cells is necessary, which could be carried out e.g., by protein-protein interactions studies (PPIs). A widely used PPIs approach called BioID was often conducted studying various cancer-related proteins[13–16].

3.1.1 Protein-protein interaction studies based on BioID

Proximity-dependent bio**t**in **id**entification (BioID) is a method used in protein-protein interaction studies. The method was pioneered by Roux *et al.* in 2012[17] and is based on the small molecule biotin, also known as vitamin H or B_7 and its unique interaction with avidin or streptavidin. Being essential for the correct function of many carboxylases e.g., pyruvate-carboxylase or acetyl-CoA-carboxylase *in vivo*, it exhibits upon binding to avidin and streptavidin a dissociation constant of $\sim 10^{-15}$ - 10^{-16} M and $\sim 10^{-14}$ M, respectively[18,19].

For BioID, a protein of interest (POI) is first chosen to be analyzed for its cellular interaction partners. A crucial requirement is a promiscuous biotin ligase, which in initial experiments was derived from *Escherichia coli* (*E. coli*). Being promiscuous the enzyme uses adenosine triphosphate (ATP) and biotin to form biotinyl-adenosine monophosphate (biotinyl-AMP), which is released into the solvent (Figure 1). The mentioned promiscuity is often enabled by mutagenesis of a specific arginine within the active site of the enzyme. Obviously, in an unmodified ligase the intermediate is bound tightly in the enzymes binding pocket and is only released when a suitable and specific acceptor protein is recognized. To carry out a PPIs the biotin ligase is genetically fused to the POI and expressed in its natural environment. The activated biotin released by the enzyme is highly reactive and conjugates to any lysine within close proximity. Consequently, a “cloud” of biotinyl-AMP is formed next to the biotin ligase fusion, leading to biotinylation of proteins interacting with the POI (Figure 2). The “cloud” is estimated to be $\sim$ 10 nm in diameter before presumable hydrolysis with water deactivates the biotinyl-AMP[20]. Initial experiments showed that biotinylation of proximal proteins occurs and that there is no unspecific widespread biotinylation[17]. To get meaningful results, it is important that the enzyme fusion is evenly expressed in all cells of a given population. Therefore, generation of a stable cell line is mandatory and consequently the rate-determining step of the method.

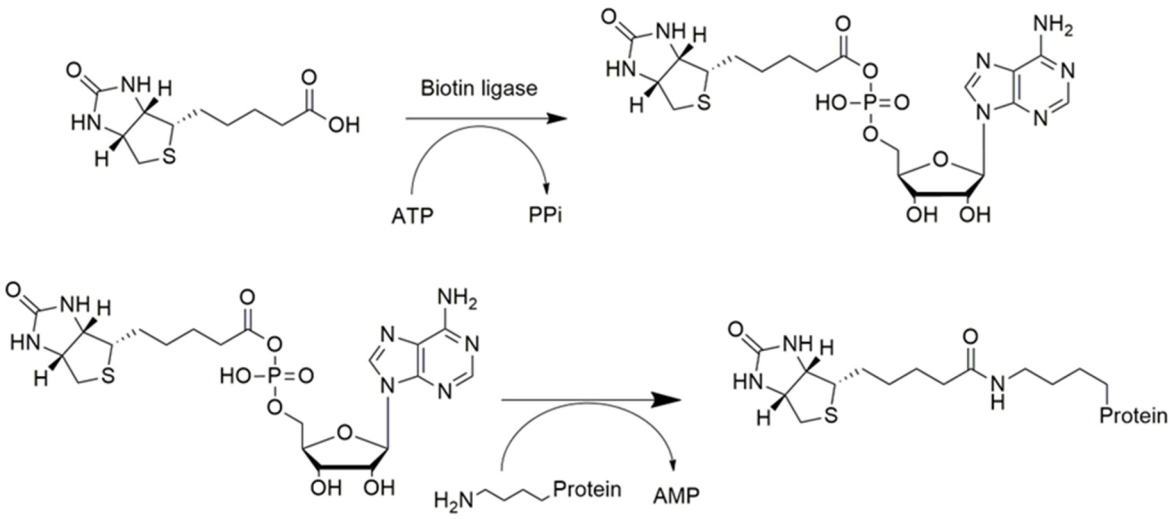

Figure 1: Reaction catalyzed by a promiscuous biotin ligase. Biotin is activated in the presence of ATP and biotin ligase to form biotinyl-AMP. In context of BioID, the released molecule reacts with any lysine of a proximate protein. Visualized using ChemDraw.

After expression of the BioID fusion protein and incubation in the presence of additional biotin, the cells are lysed, and the extract is purified via streptavidin. Selected biotinylated proteins can either be analyzed directly by mass spectrometry or the mixture can be hydrolyzed by trypsin to generate peptides. These undergo mass spectrometry analysis and machine-supported algorithms matching the detected masses with databases to identify POI interacting proteins. With this data in hand fundamental knowledge to a protein of choice can be generated, improving overall understanding of certain mechanisms in living cells.

Initial BioID experiments were performed with a biotin ligase derived from *E. coli*, where a single R118G mutation renders the enzyme abortive in a way that it releases biotinyl-AMP from the active site and is responsible for its promiscuity. However, the enzyme suffers from numerous disadvantages. Besides its size and bulkiness, its overall turnover is weak, hampering a solid proteomic analysis. In general, size of the ligase has an impact on the experimental outcome. Since the POI and ligase form a covalent unit, it cannot be precluded that the enzyme prevents interactions with proteins occurring in a natural context. As a consequence, the biotin ligase should be as small as possible[21,22]. Therefore, novel biotin ligases were introduced (see Table 1), e.g., BASU[23] which was derived from *Bacillus subtilis* or BioID2[21] derived from *Aquifex aeolicus*. The latter is the smallest biotin ligase known and is lacking the class II biotin ligase DNA binding domain. Comparable to the *E. coli* counterpart a single R40G mutation introduces promiscuity. However, while both enzymes show improved catalytic activity, they still lack in their ability to carry out very short labeling experiments of approximately 10 min. This is desirable since processes in cells could be investigated in much higher resolution. Consequently, enzyme engineering was performed by applying yeast surface display.

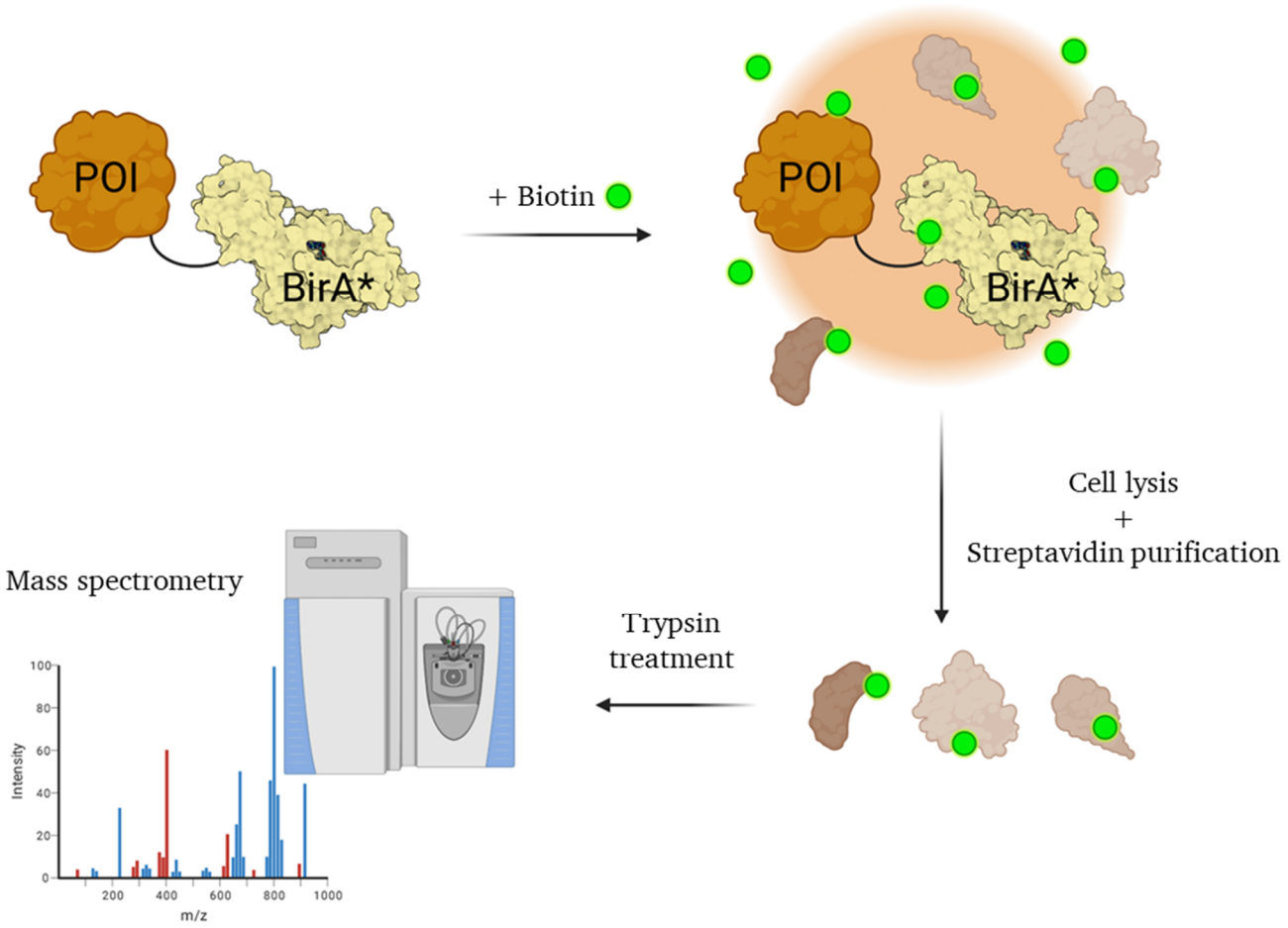

Figure 2: General workflow of a BioID experiment. In presences of additional biotin, an area with activated biotin is generated around the protein of interest. Proteins entering this space are unspecifically biotinylated and can be purified by streptavidin. These proteins are hydrolyzed by trypsin and the resulting peptides are analyzed with mass spectrometry. Database alignments reveal the peptide origin and help to identify POI interacting proteins. Visualized using Biorender.com.

Branon *et al.*[24] randomized *E. coli* biotin ligase using error-prone polymerase chain reaction (PCR) and performed various screening approaches ending up in the identification of TurboID and miniTurbo. Labeling kinetics were massively improved, reducing incubation times from 18 h to 10 min with comparable signal and an overall bigger proteome, increased by 46 %. Nevertheless, both enzymes are still relatively large (35 and 28 kDa, respectively) and background labeling occurs even when no additional biotin is added. Last there is an enzyme called AirID, which was identified by metagenome data mining. Having a molecular weight of 37 kDa, it is faster than the non-engineered counterparts however still relatively bulky[25]. All mentioned enzymes are suitable for BioID experiments and have been successfully applied in past studies. Nonetheless, there is still the need to find an enzyme combining a small size with high labeling turnover to improves PPIs.

To sum it up, BioID is a powerful tool to improve protein-protein interaction studies and became a reliable method in fundamental research over the last years.

Table 1: Overview of BioID suitable biotin ligases.

Name	Organism	Properties
BirA* or BioID	*E. coli*	Bulky (35 kDa), slow labeling kinetics (18 h)[17]
BASU	*B. subtilis*	Small (28 kDa), slow labeling kinetics (18 h)[23]
BioID2	*A. aeolicus*	Small (27 kDa), slow labeling kinetics (18 h)[21]
AirID	Multiple ancestral organisms	Bulky (37 kDa), medium labeling kinetics (3 h)[25]
TurboID	*E. coli*	Bulky (35 kDa), fast labeling kinetics (10 min)[24]
miniTurbo	*E. coli*	Small (28 kDa), fast labeling kinetics (10 min)[24]

3.2 Cancer therapies

Today, cancer therapies are as versatile as cancer types existing. Besides local removal of tumors *via* surgery, the most prominent courses of action are chemo- and radiation therapy. Both strategies result in unspecific cell killing, in the hope that healthy cells will replace malignant ones. While chemotherapy is based on the application of at least one cytotoxic drug, radiation therapy uses ionizing radiation. The latter leads to fatal DNA damage or generation of reactive oxygen species due to radiolysis, resulting in cell death. Chemotherapy targets essential pathways in e.g., cell cycle, cell division or DNA replication forcing the cell to stop proliferating or ultimately in cell death. However, both therapies go hand-in-hand with severe side-effects for the patient, ranging from hair loss, tiredness and fatigue to anemia or organ damage. Nonetheless, they remain one of the most potent tools for the treatment of several cancer types in most cases[26–31]. Besides those there are more specialized treatments which must be evaluated individually to be deployed.

For instance, there are hormone therapies relying on cancer types which are hormone-dependent for growth. Consequently, this method targets the proprioceptive hormone production or prevents the molecules from binding to the tumor cells. While effective, this therapy is limited to certain types of cancer e.g., breast, prostate, or adrenal cancer[32–34].

Another example is “hyperthermia therapy”, where areas of the body are heated to 41-50°C. This should help damaging cancer cells with little to no harm on healthy tissue[35,36]. In general, malignant cells aren´t more sensitive to heat than the healthy counterpart however heat selectively kills chronically hypoxic, acidotic, and nutritionally deficient cells[37]. These are all properties featured in tumor cells.

A more complex treatment is photodynamic therapy. Applying photosensitizer molecules, the whole approach is based on illumination with light, which is harmless compared to radiation used in radiation therapy. The photosensitizer agents are non-dangerous and enrich in tumor-associated tissue over time. After illumination, radicals are formed in the malignant cell ultimately leading to cell death. With limited side-effects on healthy cells, photodynamic therapy is restricted to tumors under the skin or the lining of internal organs, due to the limited penetration distance of light into deeper tissues[38,39]. While all these treatment classes bring their own advantages and disadvantages, the complexity of cancer requires novel therapies that may lower side-effects and spare healthy cells.

3.3 Immunotherapies

Over the last decade, the interest in immunotherapy for treatment of different diseases has massively increased. In terms of numbers, the 2021 market size was determined to be $44.4M in the US and calculations predict an annual increase of 7.2 % from 2020 to 2030[40]. Advantages of this quickly growing class of therapy is a significantly higher long-term survival rate, a higher specificity which decreases side-effects and a wide adaptability to multiple types of tumors[41]. In addition to that, personalized care is available, due to the high diversity of immunotherapies available, usually discriminated in active and passive approaches[42–45]. A few of them are mentioned in the following section.

To start with an active strategy, adoptive cell therapy (ACT) is a method relying on antitumor properties of lymphocytes. Therefore, e.g., tumor-infiltrating lymphocytes are taken from tumor tissue and expanded *in vitro*. T-cells are stimulated by cytokines and reinfused into the same patient. This approach circumvents the immune suppressive tumor environment and resulting deactivation of T-cells[45–47].

Another active approach are cancer vaccines. Some of them target oncogenic agents and serve as a prophylaxis e.g., human papillomavirus which could lead to cervical cancer[48] or hepatitis B virus causing liver cancer[49]. Vaccines targeting cancer cells directly by combining adjuvants or virus particles with patient-derived tumor cells, aiming for an immune response failed in clinical trials, due to missing benefit[50]. In addition to that, there are preclinical studies trying to identify neoantigens by next-generation sequencing[51,52]. Synthesis of personalized peptides could mimic tumor-associated antigens and lead to subsequent activation of the immune system.

Cytokines are also used as support for cancer therapy as they can manipulate cancer grow and metabolism or stimulate and boost the immune system. For example, Aldesleukin is an engineered and recombinantly produced interleukin 2[43], which enhances T- and natural killer-cell (NK-cell) proliferation and promotes further cytokine release[53]. These effects could facilitate and improve therapeutic outcome especially in renal and kidney lymphoma[42,43,54].

A novel approach is chimeric antigen receptor T-cell (CAR-T-cell) therapy. Hereby, T-cells are taken from the patient and are genetically modified to present a chimeric antigen receptor on their surface. Being trained for a new antigen, the cell should proliferate and introduce a strong immune response against the cancer cells after re-administration into the patient[45,46]. CAR-T-cell treatment is usually used for B-cell lymphoma for young people under the age of 25. As is it a personalized therapy it is associated with high costs of ~ $373000 per $2*10^6$ CAR-T cells/kg[55].

Finally, monoclonal antibodies are a big part of modern immunotherapy. They are usually applied in a naked, unmodified form or as a conjugate carrying e.g., a toxin or radiolabel. Their structural characteristics, biophysical properties and mode of action are highlighted in the next sections.

3.4 Immunoglobulins – Antibodies (Abs)

Immunoglobulins (Ig), also known as antibodies, are B-cell secreted glycoproteins, which play a major role in the adaptive immune system. In humans there are five main Ig classes, namely IgA, IgE, IgD, IgG and IgM, dividing the proteins by their function, structure, and localization in the body[56]. Being separated into four isotypes, the most abundant class is IgG with ~ 75 – 80 % of in blood circulating Igs (Figure 3)[57]. The glycoprotein is made up of two identical heavy (~ 50 kDa) and light chains (~ 25 kDa), resulting in a Y-shape-like structure with around 150 kDa in molecular weight. Intra- and interchain disulfide bonds as well as the glycosylation stabilize the whole immunoglobulin. The latter is also very important in antibody recognition by various immune cells. Being a relatively large protein, the whole molecule is still very flexible due to the hinge region. As no secondary protein structure is formed in this area, the fragment antigen binding (Fab) can rotate freely, enabling flexibility in antigen binding. Hereby, the paratope on top of the Fab fragment interacts specifically with the epitope of the antigen, forming a non-covalent complex[58]. The interface relies on hydrogen bonds, ionic and Van-der-Waals forces as well as hydrophobic interactions. All amino acids involved in antigen binding are located in the complementarity-determining region (CDRs). For IgG molecules, they consist of twelve surface-exposed loops (three per domain) on top of the heavy chain variable domain (V_H) and light chain variable domain (V_L)[59]. In addition, antibodies are usually distinguished between monoclonal (mAb) and polyclonal (pAb). While both detect a single antigen mAbs are derived from one B-cells or a synthetic source and only recognizes one epitope on the one antigen whereas pAbs are a mixture of Abs, often derived from rabbit or goat sera, which detect different epitopes on one single antigen.

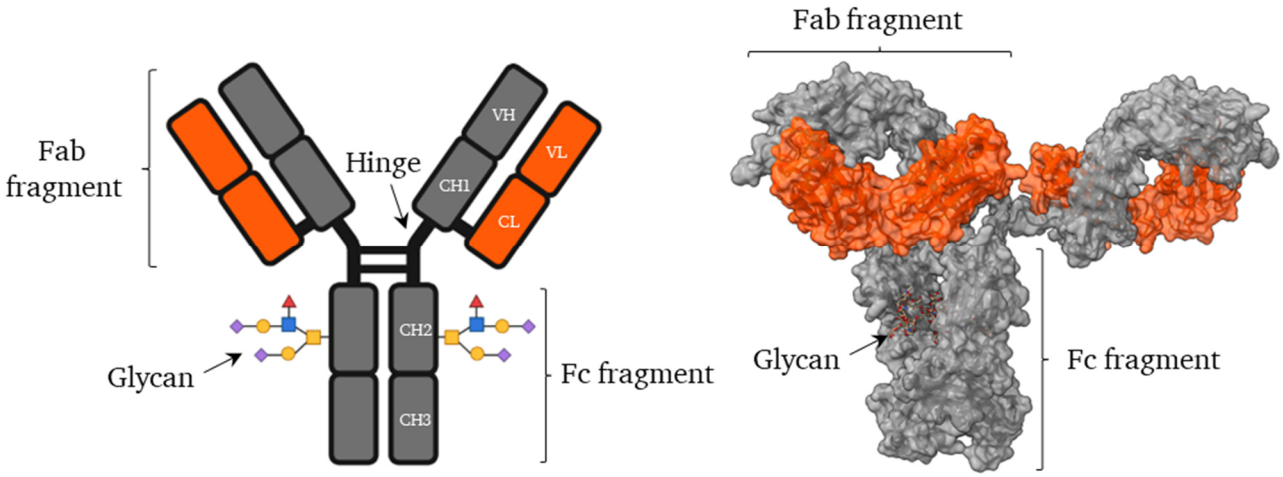

Figure 3: General structure of an IgG1 antibody. Schematic depiction of an IgG antibody (left) and crystal structure of a human IgG antibody against HIV-1 (right). The light chain is highlighted in orange, the heavy chain in grey. Structure downloaded from RCSB PDB (ID: 1HZH). Visualized using UCSF ChimeraX and Biorender.com.

The main function of antibodies is the binding to pathogens like viruses or bacteria for neutralization and marking for the immune system. In the context of viruses, binding of the antibody can prevent further infection of healthy cells by hampering the interaction between the virion and the cell surface. For bacteria, antibodies can act in different ways. On the one hand, toxins secreted by bacteria are neutralized in the same manner as viruses. On the other hand, the organisms can be targeted directly. Bound by an antibody, opsonized bacteria are eliminated by the complement system, which is a part of the innate immune system composing proteolytic or inflammation promoting proteins (referred to as complement-dependent cytotoxicity, CDC). Additionally, attachment of bacteria to host cells is inhibited by antibodies. Pathogens can also be destroyed by effector functions mediated through the Fc fragment. Therefore, the proportion is recognized by a variety of Fc receptors expressed on various immune cells. For example, phagocytes like macrophages or dendritic cells can identify antibody-bound bacteria and induce phagocytosis to digest the whole organism, a mechanism referred to as antibody-dependent cellular phagocytosis (ADCP). Furthermore, virus infected cells are marked by immunoglobulins, which again recruit NK-cells, neutrophiles and eosinophiles via the Fc fragment. This leads to the secretion of cytoplasmatic granules and the death of the infected cell through antibody-dependent cellular cytotoxicity (ADCC)[60–62].

To sum it up the combination of a high specificity with the inherent ability to activate the immune system, helps antibodies to get more and more important in cancer immunotherapy. A closer look to that topic will be taken in the next section.

3.4.1 Monoclonal antibodies for cancer therapy

Pursuing cancer with therapeutic antibodies was a huge progress in improving therapy. This is reflected by the fact that there have been 23 Food and Drug Administration (FDA) approved monoclonal antibodies for cancer treatment in 2023[63]. Comparable to the defense of pathogens, they may mediate different modes of action. Besides the previously described effector functions (ADCC, CDC and ADCP), surface-exposed receptors or their ligands can be blocked by the antibodies, leading to signal inhibition. Often targeted receptors are e.g., growth factor receptors to stop proliferation signals or check-point inhibitors to prevent immune escape by cancer cells. For an efficient accumulation of the antibody at the tumor site and to minimize off-target and side-effects, the target should be overexpressed on cancerous cells compared to healthy cells.

To give some examples of antibodies and their applications, an often-addressed target is CD20 which is overexpressed in different types of non-Hodgkin lymphoma and myeloma. Occurring only on B-cells, CD20 is bound by the therapeutic antibodies obinutuzumab, ofatumumab and rituximab, which all mediate ADCC, CDC and direct apoptosis[63–67].

Another target is the programmed cell death protein 1 receptor (PD-1) and its ligand 1 (PD-L1), known as immune checkpoints. Normally, cancer cells would receive a signal by T-cells to undergo apoptosis. However, PD-L1 can inhibit T-cell activation and mediates the immune system escape of the degenerated cell. By blocking the PD-1 / PD-L1 axis, this effect is prevented, and apoptosis can be induced. Immunoglobulins acting this way are e.g., avelumab, nivolumab or pembrolizumab[68–70] which are known as immune checkpoint inhibitors.

Since tumors have a huge nutritional demand, supply via the bloodstream is necessary. This can be achieved by angiogenesis into the tumor. Bevacizumab and ramucirumab targeting this phenomenon by binding to and inhibiting vascular endothelial factors (VEGF), which leads to decreased angiogenesis and ultimately decreased tumor growth[71,72].

Trastuzumab and pertuzumab are mAbs used for the treatment of breast cancer, among others. Both targeting the human epidermal growth factor receptor 2 (HER2/neu) also called erb-b2 receptor tyrosine kinase 2 (ERBB2) which has great implications in cancer diagnostic and therapy. While HER2 is involved in cell proliferation and apoptosis inhibition it is overexpressed in cancerous tissue. Both antibodies mediate inhibition of HER2 proliferation signals as well as ADCC and ADCP[73–77]. However, they exhibit small differences in their mode of action. On the one hand, trastuzumab binds to the IV subdomain of HER2, preventing ligand-independent dimerization of the receptor and subsequent signaling. Consequently, this does not apply for ligand-dependent heterodimerization with other receptor family

members e.g., HER2-HER3. Besides that, cleavage of the HER2 receptor is inhibited by trastuzumab, which also circumvents activation[78]. On the other hand, pertuzumab interacts with the extracellular domain II preventing ligand-dependent heterodimerization[79,80]. Therefore, combination therapy with both antibodies promises a higher success in therapy[81].

Trastuzumab is a humanized monoclonal IgG1 kappa antibody, which is recombinantly produced in CHO cells[82–84]. Having been approved for cancer therapy in 1998, it remains on the list of the best-selling drugs ever, even though patent protection expired and biosimilars are becoming more and more common[85–87].

3.4.2 Antibody-drug conjugates

Antibody-drug conjugates (ADC) are, as their name suggests, a combination of a therapeutic antibody and a cytotoxic drug, exploiting the high specificity of the mAb with the high toxicity of the drug to result in increased anti-cancer potency. Until 2023 there are 14 FDA approved ADCs on the market[88] and 169 are in clinical trials (late 2022)[89]. Like mAbs, the high number of ADCs under clinical development highlights their potential for improved cancer therapy.

In general, an ADC consists of three individual parts (Figure 4, A), all being crucial for its function. First, the monoclonal antibody serves to deliver the cytotoxic drug to the tumor microenvironment and bind specifically to malignant cells. Thereby, affinity needs to be tuned to a degree where specific binding is ensured and off-target effects are reduced (high affinity necessary), however good penetration in solid tumors must also be possible (lower affinity necessary)[90]. Next, the cytotoxic drug is the key part for inducing apoptosis and cell death. Since only a few percent of the administered ADC actually delivers its payload, these drugs have to be very potent with nano to picomolar half maximal inhibitory concentration (IC_{50})[91–93]. Common targets are microtubules or the DNA in the nucleus. An example is the microtubule inhibitor monomethyl auristatin E (MMAE), which is an often used payload for ADCs and exhibits IC_{50} values in the low triple to double digit picomolar range[94]. Lastly, ADCs consist of a linker between the small molecule and the mAb. Biophysical properties of the linking moiety have to be tuned in order to ensure stability in the bloodstream to prevent a premature release of the drug but must also facilitate delivery when necessary[88]. Therefore, linkers are usually divided into either cleavable or non-cleavable linkers. The latter relies on complete degradation of the ADC in the cell, rendering a site-specific hydrolysis unnecessary.

In contrast, cleavable linkers enable specific release of the cytotoxic drug in a unique tumor-associated environment. FDA approved ADCs with this linker-type carry either protease-cleavable or pH-sensitive molecules. Regarding protease labile linkers, valine-citrulline or valine-alanine serves as a motive being

recognized by cysteine protease cathepsin B, enabling the release of the drug in lysosomes[88,95]. This technique is for example exploited by Zynlonta® [96]. Also addressing endosomal and lysosomal delivery e.g., hydrazones are used for pH sensitive release. This linker types are applied in Besponsa® and Mylotarg® [97,98].

For the general mode of action (Figure 4, B)[99–101], the antibody and drug form a stable unit, which is not toxic in the bloodstream and exhibits weak off-target effects. Carrying the small molecule to the tumor site or cancerous cell, the ADC is eventually internalized, releasing its payload after degradation of the antibody in the endosome/lysosome[102,103]. Due to its high toxicity and direct delivery, only a few molecules are required for mediation of cell death. Alongside direct delivery, membrane-permeable drugs are also able to diffuse out of the targeted cell to kill other cells in spatial proximity. This effect is called "*bystander effect*" and is beneficial in a solid tumor context, however it could also lead to side-effects when healthy cells are affected[104]. Independent of the drug impact, ADCs often retain their Fc-mediated effector functions or inhibition of receptor signaling (see section 3.4 and 3.4.1)[105–107].

Synthesis of an antibody-drug conjugate is a non-trivial process, especially for therapeutic agents, therefore common methods are highlighted in the next section.

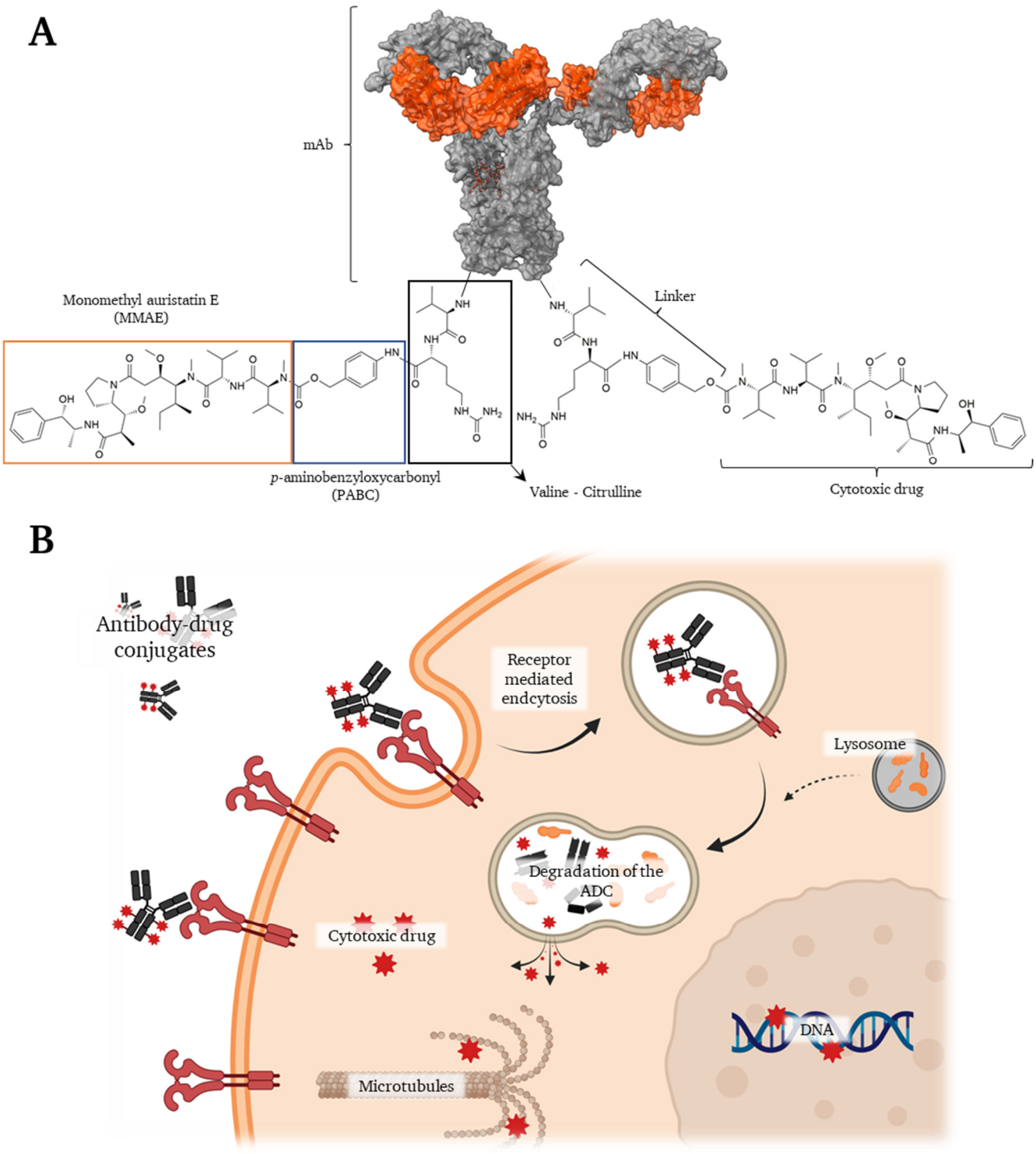

Figure 4: Schematic depiction of an antibody-drug conjugate with two MMAE toxins (A) and mode of action (B). The antibody is conjugated to two ValCit-PAB-MMAE moieties. ValCit is a motif known to be cleaved by lysosomal proteases. PABC, also known as PAB, linker serves as a decarboxylation agent to supply an unmodified MMAE toxin. Structure downloaded from RCSB PDB (ID: 1HZH). For the mode of action, the ADC binds to its specific receptor and is subsequently internalized by receptor mediated endocytosis. Consequently, the molecule is degraded in the lysosome releasing its cytotoxic drug at the latest, which leads ultimately to cell death. Visualized using UCSF ChimeraX, Biorender.com and ChemDraw.

3.4.3 Generation of antibody-drug conjugates

Manufacturing an antibody-drug conjugate is a complicated process, which needs to be reliable and reproducible, especially for subsequent human application. Batch-to-batch consistency needs to be ensured, since conjugation variations go hand-in-hand with alterations of physicochemical attributes of the molecule[108], ending up in unpredictable consequences for patients. In this context all ADCs being approved by FDA are generated by chemical methods[109]. This means, that the antibody is produced independently by recombinant sources and afterwards conjugation of the drug is carried out. The most common labelling reaction is carried out at the cysteines of the antibody via maleimide Michael addition (Figure 5, upper row) leading to drug-to-antibody ratios (DAR) from ~ 2.3 (Zynlonta®)[96] to ~ 8 (Enhertu®)[110].

Independent of ADCs used in actual cancer therapy, there are various conjugates mentioned in literature involving chemoenzymatic or enzymatic conjugation strategies. Usage of enzymes is beneficial since a site-specific modification of the antibody is achieved, leading to more homologous constructs and batch-to-batch consistency. However, upscaling of the reaction will increase costs due to necessity of large amounts of enzyme and additional downstream purification. On top of that the antibody often requires slight alterations to enable a modification by the enzyme. In many cases this is achieved by introducing short peptide tags to the C-terminus of the heavy and/or light chain. Nevertheless, in some cases direct modification with an enzyme is also possible. Examples for both are given in the next section.

An example of a chemoenzymatic approach is the use of a mushroom derived tyrosinase[111]. After deglycosylation of the antibody, Y300 becomes accessible to the enzyme, oxidizing it to an ortho-quinone (Figure 5, middle row). This functional group is unique in the whole molecule enabling site-specific Strain-Promoted Oxidation-Controlled Cyclooctyne–1,2-Quinone Cycloaddition (SPOCQ).

Another approach was published by van Geel and coworkers[112], where the glycan of an antibody served as an attachment site for the cytotoxic drug. Therefore, the glycan was trimmed to its core by an endoglycosidase and a modified sugar was attached by a glycosyl transferase. Exhibiting an azide handle this sugar served as the basis for Strain-Promoted Alkyne–Azide Cycloaddition (SPAAC) with a drug.

Being more versatile, Sortase A is an enzyme that can be used for chemoenzymatic and direct conjugation (Figure 5, lower row). In 2017, Xu and coworkers[113] introduced the recognition motif LPETG to the C-terminus of the anti-CD20 antibody ofatumumab, enabling modification with molecules exhibiting a triple glycine with a free N-terminus. In their work, a chemoenzymatic approach was chosen by applying a GGG-PEG-N_3 molecule as well as a direct enzymatic method with a GGG-Val-Cit-PAB-

MMAE. Interestingly, direct conjugation yielded a DAR of 1.4, whereas the chemoenzymatic approach led to a ratio of 3.3.

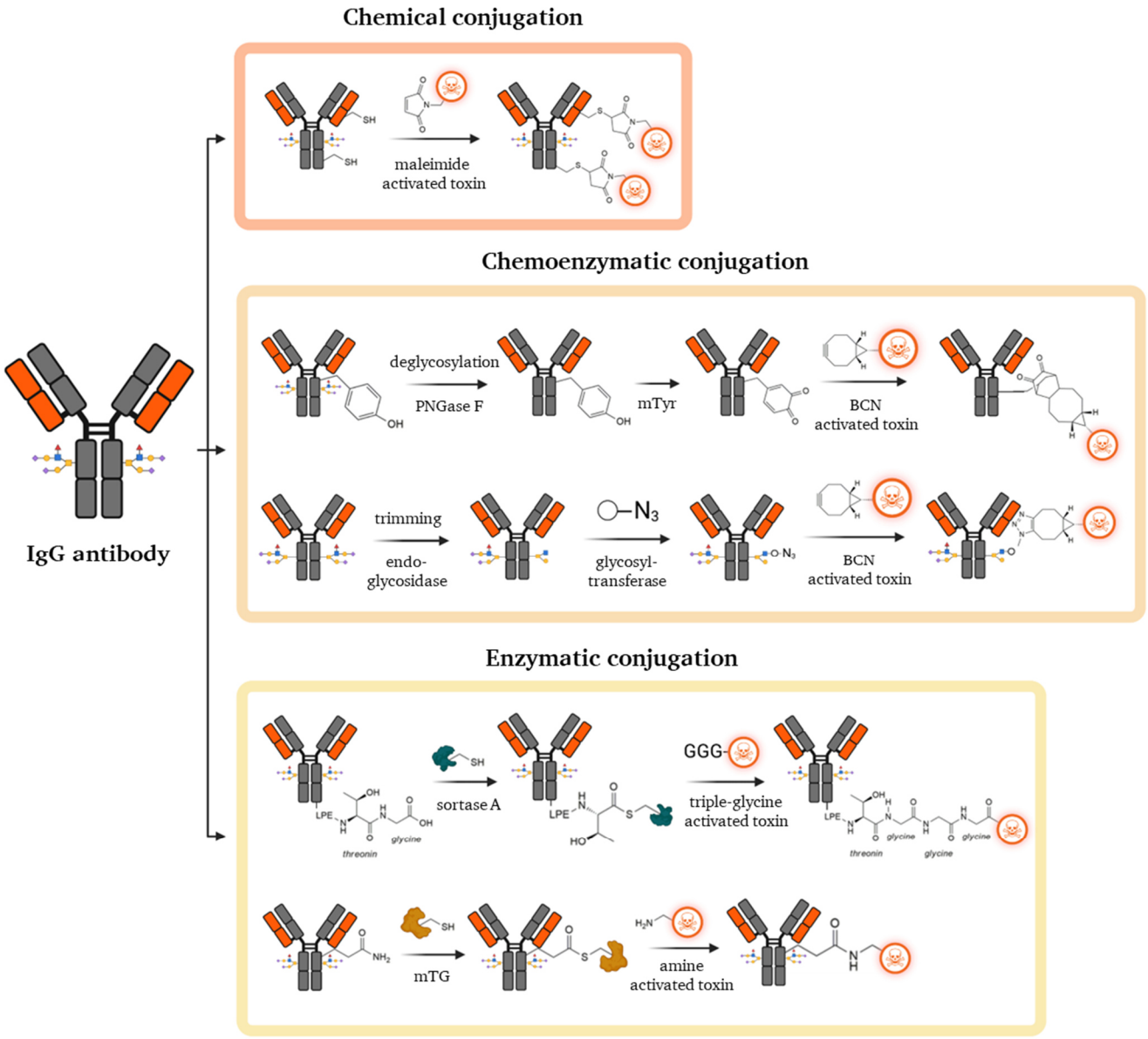

Figure 5: Schematic depiction of different ADC generation approaches. All ADCs approved by FDA are conjugated by chemical methods like Michael addition of cysteines to maleimides (upper row). However, there are also chemoenzymatic (middle row) or enzymatic (lower row) approaches mentioned in literature. For the sake of convenience conjugations to the antibody is only shown on one chain of the molecule. Visualized using Biorender.com and ChemDraw.

Another commonly used enzyme for the generation of an ADC is microbial transglutaminase (mTG). This enzyme crosslinks glutamines with primary amines derived from lysine's or small molecules to form a stable isopeptide bond. Exhibiting no clear recognition motif, mTG should be ideal to conjugate even

wild-type antibodies and avoids the introduction of any conjugation tag. However, studies have shown this not to be the case as, contrary to expectation, the enzyme does not recognize any glutamine in a native IgG antibody[114,115]. As a workaround, the group of Roger Schibli reported that deglycosylation of the immunoglobulin enables successful conjunction at Q295, generating an ADC[116,117]. Since glycosylation plays a role in antibody stability and function, its removal is disadvantageous, especially in the case of a therapeutic agent. In 2020, Dickgiesser and coworkers[118] presented an engineered enzyme variant being able to recognize fully glycosylated IgGs and additionally demonstrated stability and efficacy of the conjugates. In parallel Philipp Spycher a post-doc of Roger Schibli discovered that also the amine substrate is crucial for the glutamine modification location. Based on this finding a Paul Scherer Institute spin-off was founded marketing the technology and substrates[119].

The construction of antibody-drug conjugates includes a plethora of conjugation strategies, with the mentioned approaches just being an excerpt. While designing novel ADCs, the most fitting strategy must be chosen based on downstream applications and evolving technologies. Besides the above listed, there is the formyl glycine-generating enzyme[120], prenyltransferase[121], the THIOMAB technology[122] or incorporation of unnatural amino acids[123] and many more.

3.5 Bond forming enzymes for ADC generation

As presented in the last section, bond forming enzymes are a specific way to generate antibody-drug conjugates. Although many different enzymes have been applied for this approach, there are still unused variants left, which could potentially increase the enzymatic conjugation toolbox. Two are further highlighted in the next two sections.

3.5.1 Lipoate-protein ligase A

E. coli lipoate-protein ligase A (LplA) is a ~ 38 kDa monomeric enzyme (Figure 6, A) catalyzing the transfer of lipoic acid to the ε-amino group of a specific lysine within a lipoate acceptor domain. Lipoate itself is an important cofactor of the 2-oxo dehydrogenase complexes and the glycine-cleavage pathway in *E. coli*[124,125]. Being dependent on ATP and Mg^{2+}-ions the enzyme binds both substrates first, lipoate and ATP, and catalyzes the formation of lipoyl-AMP, which is fixated in the U-shaped like binding pocket. Upon identification of the lipoate acceptor domain the lipoyl-AMP reacts with a certain lysine forming an amide bond and releasing AMP (Figure 6, C)[126]. Due to the dependency of Mg^{2+} ions enzyme activity is inhibited by chelating agents such as EDTA.

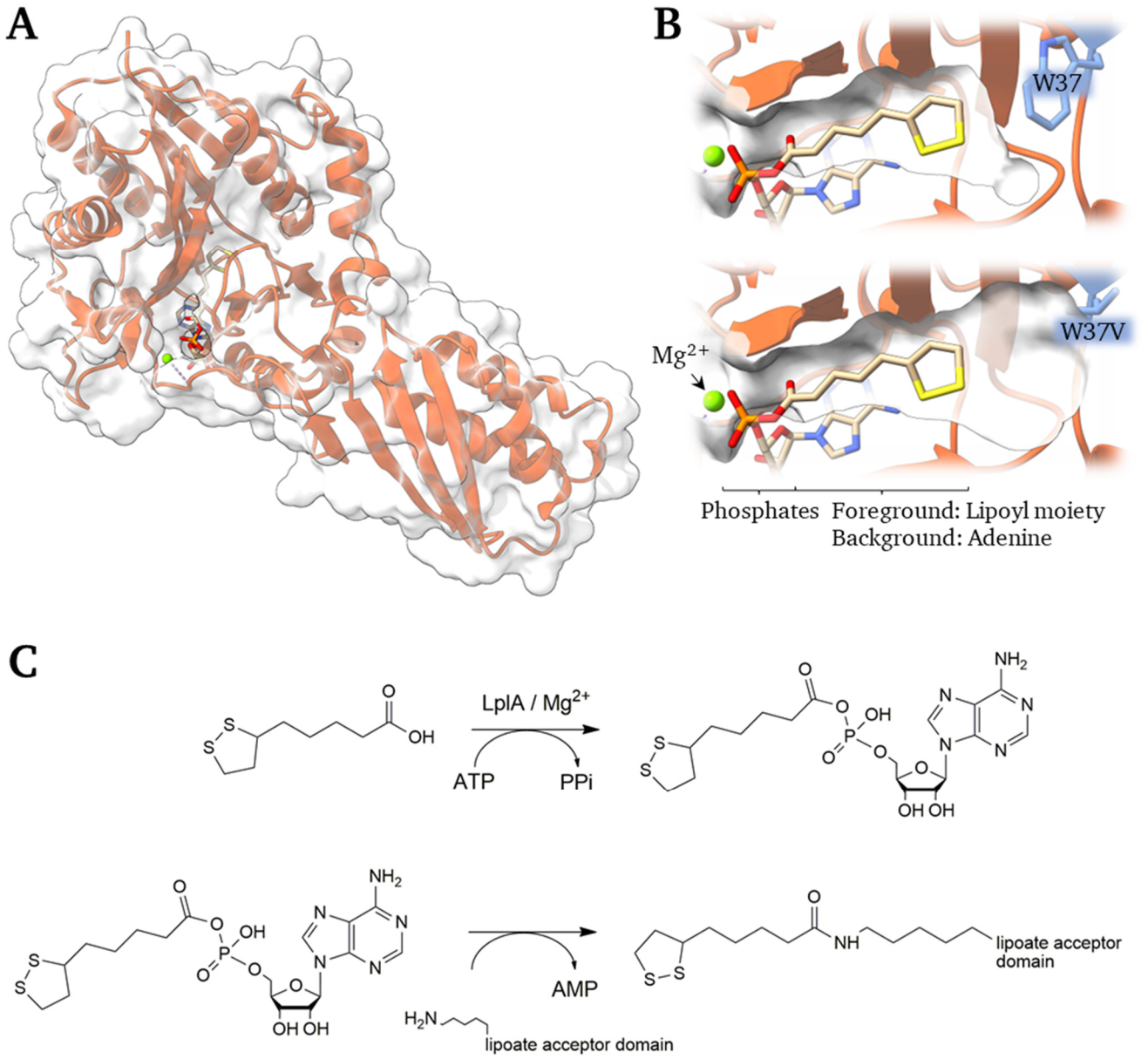

Figure 6: Crystal structure of lipoate-protein ligase A (A), magnification of the active site with the wild-type W37 and mutant W37V (B) and reaction catalyzed (C). Structure downloaded from RCSB PDB (ID: 3A7R). Visualized using UCSF ChimeraX and ChemDraw.

For biotechnological / biopharmaceutical application the enzyme was only partially usable. On the one hand, introduction of lipoic acid in e.g., an antibody is not useful. On the other hand, conjugation requires modification of the protein of interest with the lipoate acceptor domain since no recognition sequence was known. Both problems were addressed by Fernández-Suárez and coworkers[127] by identifying a LplA acceptor peptide (LAP) and synthesizing lipoate derivatives with different functional groups. For engineering of the recognition sequence, rational design was applied by comparing different lipoate acceptor proteins from different species. Out of seven initial peptides and subsequent site-directed mutagenesis the 22-amino acid long LAP-tag was identified exhibiting a 2.3-fold lower k_{cat} than

the original counterpart. Despite the decreased turnover rate introduction of a small peptide modification might be more desirable than the attachment of the entire lipoate acceptor domain. In parallel the dithiolane group of lipoate was substituted by an azide- or an alkyne-function and the aliphatic chain length was varied from four to ten carbon atoms. Turnover was analyzed and compared to the natural substrate. Interestingly, an azide variant harboring seven carbons in the aliphatic chain showed 55.4 % conversion and was the best performing substrate variant. Using both, the LAP-tag, and the azide substrate, labeling of surface proteins in mammalian cells was possible by applying a chemoenzymatic approach with click-chemistry. Consequently, this publication introduced the enzyme to novel applications in biotechnology. Two years later, a follow up paper was published presenting a truncated LAP-tag with more than 70-fold improved kinetics[128]. The screening of different substrates already showed that the enzymes actives site seemed to be sterically demanding. For a broader scope turnover of bulky substrates was desirable. Baruah *et al.* identified a single W37V mutation, which enlarges the active site to bind an aryl azide (Figure 6, B)[129]. Until today, LplA W37V in combination with the truncated LAP-tag is the gold standard for conjugation with this enzyme and was applied in various approaches[130–132]. In 2019 a one-pot approach with microbial transglutaminase was presented by Thornlow *et al.* Here an LAP-modified trastuzumab was conjugated with two fluorophores at the same time[133]. However, generation of an actual antibody-drug conjugate is still lacking.

3.5.2 Biotin-protein ligase

Biotin-protein ligases (BPL) are enzymes catalyzing the transfer of biotin to biotin-dependent proteins, like carboxylases. Those proteins are essential in gluconeogenesis or fatty acid metabolism, among others, which are both crucial pathways in living cells. Even though biotinylation occurs ubiquitously in nature, the modification itself is rare. Inside a cell, there are ≤ 5 proteins being conjugated with the small molecule[134], so biotinylation appears to be highly specific and efficient.

The catalyzed reaction is comparable to that of LplA and was already mentioned in section 3.1.1 (see also Figure 1). However, in contrast to a promiscuous biotin ligase, biotinyl-AMP is not released unspecifically but rather bound in the active site until a specific lysine of the biotin carboxyl carrier protein (BCCP) is recognized.

In general, BPLs are divided into three classes distinguished by their functionalities[135]. Class I biotin ligases are solely catalyzing the transfer of biotin to the respective acceptor domain. In contrast, class II enzymes exhibit an additional transcription repressor function. Lastly, the class III ligases contain an N-terminal extension being involved in further discrimination of biotin acceptor enzymes[136]. Nonetheless, this class of BPLs only occurs in higher organisms like mammals.

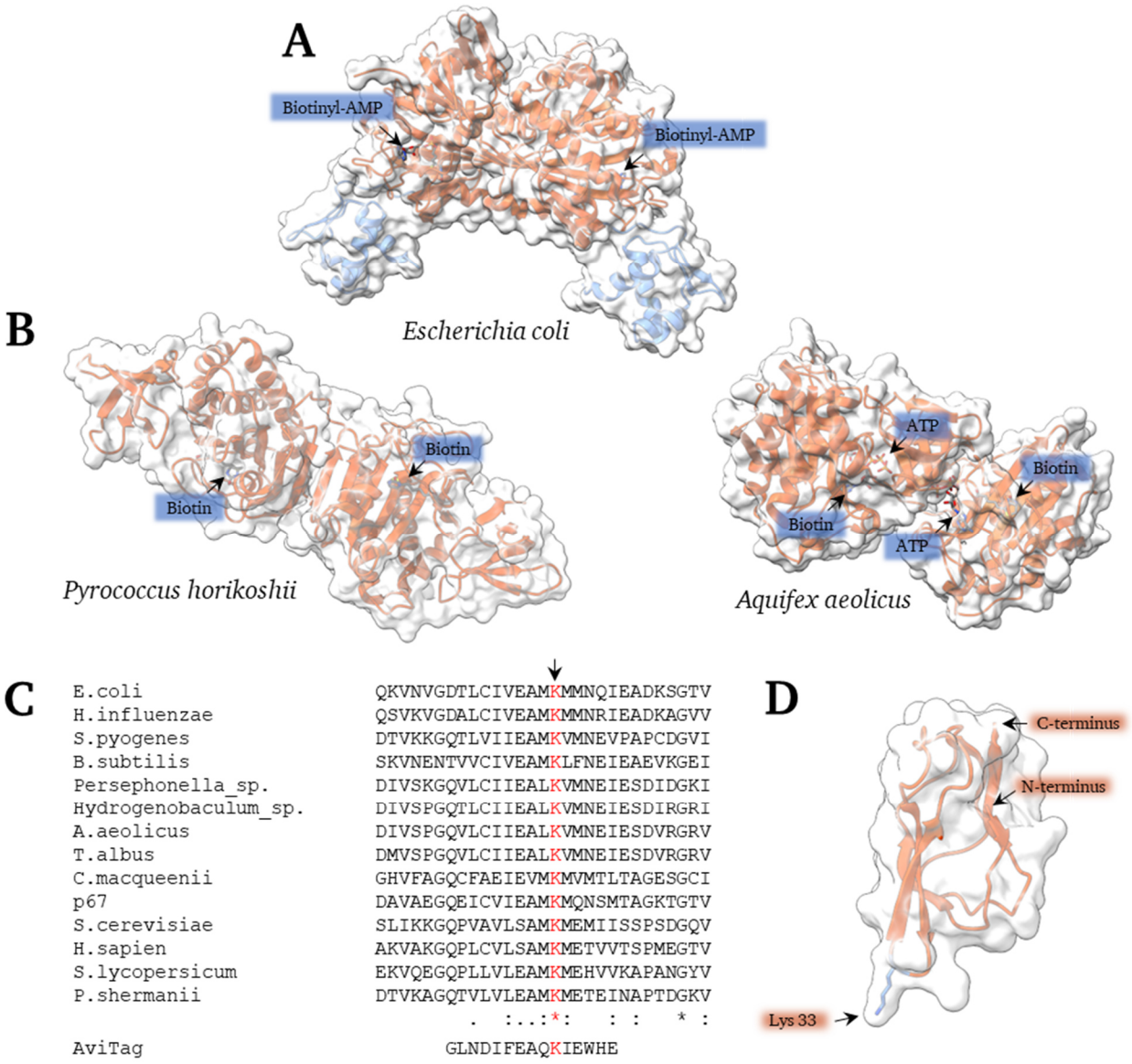

Figure 7: Crystal structure of *Escherichia coli* (A), *Pyrococcus horikoshii* and *Aquifex aeolicus* biotin protein ligase (B), multiple sequence alignment of BCCPs from diverse species (C) and structural prediction of p67 (D). DNA-binding domain of *E. coli* BPL is colored in blue. Biotin ligase structure downloaded from RCSB PDB (IDs: 2EWN / 1WPY / 3EFS). Sequences of BCCPs were derived from UniProt and aligned by Clustal Omega – Multiple Sequence Alignment. Biotinylated lysines are highlighted in red and with an arrow. Structure of p67 domain (last 67 amino acids of propionyl-CoA carboxylase alpha chain) was predicted by AlphaFold using P05165 as input. Biotinylation site (lysine 33) of p67 is highlighted. Visualized using UCSF ChimeraX.

One of the best understood and examined class II BPL is derived from *E. coli.* The enzyme, often called BirA, is 33.5 kDa in size and is made up of an N-terminal DNA-binding domain (Figure 7, A, blue) and a C-terminal domain (orange) responsible for biotin transfer[137,138]. As they contain a repressor function, the enzyme can bind to DNA at a specific condition, preventing the transcription of gene(s). In case of *E. coli,* the whole *bio*-operon is regulated by the ligase involving genes for biotin synthesis. To perform regulation, binding to the operator occurs when the enzyme is loaded with biotinyl-AMP. This is only

the case, if all BCCP molecules in the cells are biotinylated and therefore no free biotin is needed. Subsequently, biotin synthesis is inhibited until cellular demand for the small molecule grows. Consequently concentration of unbiotinylated BCCPs increases, BPLs start to biotinylate their substrate again and therefore fall off of the operator[139]. The different interaction potential of the enzyme with DNA is achieved by structural changes upon binding and release of biotinyl-AMP.

Biotin ligases of *Pyrococcus horikoshii* and *Aquifex aeolicus* are thermophilic, class I enzymes of ~ 26 kDa in size. Even though the DNA-binding domain is missing in both the ligases are still made up of the catalytic N-terminal and a C-terminal domain[140,141]. In contrast to *E. coli* BirA, which only forms a dimeric state, when binding to DNA is desired (induced by bound biotinyl-AMP), the other two enzymes form a homodimer even in the absence of the substrates (see Figure 7, B). This attribute may contribute positively to the thermostability of the proteins.

This section often pointed out that BCCPs serve as an acceptor for biotin, which is crucial for correct function of the biotin-dependent enzyme. Since biotinylation occurs only on a few proteins the biotin carrier proteins need to exhibit structural or sequential motifs being recognized by the biotin ligase. Indeed, there are four subfamilies of BCCPs differing in minor changes in primary structure, but all in all sharing comparable tertiary structure[142]. As depicted in Figure 7 C, sequence alignment of different species reveals a relatively conserved region around the biotinylated lysine considering the phylogenetic distance of the organisms. Structural similarities were also shown indirectly by Slavoff and coworkers, which used a biotin acceptor domain derived from human propionyl-CoA carboxylase and showed that it was recognized by many biotin ligases of different species[143]. The acceptor domain consists of the last 67 amino acids of the carboxylase and can be expressed solitary as a small 7 kDa protein called p67 (Figure 7, D). Having a small acceptor for biotin ligase mediated conjugation may be a promising tool, especially in context of ADC generation. Fundamental experiments towards this approach were also done by Slavoff *et al.* by synthesis of biotin derivatives with addressable functional groups[143].

3.6 Click-Chemistry

As introduced in section 3.4.3 antibody-drug conjugates can be generated by chemoenzymatic methods involving a chemical conjugation step, which is necessary for toxin coupling. Most of these reactions being grouped by the name “click chemistry” were neglected in the last sections and will be highlighted next.

The “inventors” of the name trace back to Sharpless and coworkers, who published an article at the beginning of this millennium[144]. Hereby, the term “click-chemistry” was introduced and describes

reactions that, need to proceed under given conditions and fulfill various requirements. Emphasizing the impact of this class of reactions in the field, Barry Sharpless, Morten Meldal and Carolyn Bertozzi received the Nobel Prize in Chemistry in 2022 for their work[145].

In general, click-chemistry reactions are modular, wide in scope and lead to very high yields. It is necessary that byproducts can be removed easily, and product formation occurs stereospecifically. Performing these reactions should be simple, involving no or harmless solvents with water as well as oxygen being largely tolerated.[144] Decades later, click chemistry has become the most applied approach for conjugation in biological systems or proteins of interest. A reason for that is the orthogonality to all reactive groups occurring in nature e.g., amines, thiols and many more. Bioorthogonality was proven many times, including the work of Bertozzi by mapping cells[146,147].

Especially in the context of protein or peptide conjugation, three reactions are very prominent. As reported by Meldal *et al.*[148] the first is the copper-catalyzed azide-alkyne cycloaddition (CuAAC). Here, a stable triazole is formed out of an azide and a terminal alkyne in the presences of Cu^+. The copper ions are essential for the activation of the alkyne and stabilization of the triazolyl intermediate[149]. Even though there are many examples where proteins have been conjugated via CuAAC[150–152], the toxicity of Cu^+ ions in biological systems is a big drawback, that prevents unrestricted applications.

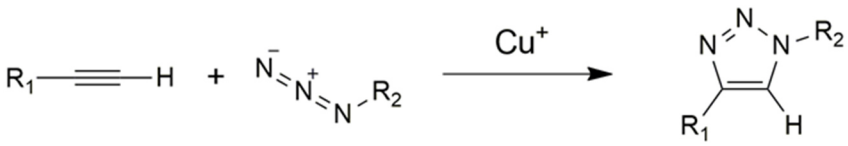

Figure 8: Copper-catalyzed azide-alkyne cycloaddition. A terminal alkyne reacts with an organic azide in presence of Cu^+ to form a stable triazole.

Therefore, the so-called strain-promoted azide-alkyne cycloaddition (SPAAC) was rediscovered. Uncovered more than 60 years ago this reaction experiences a renaissance as an copper-free alternative to CuAAC[153]. Hereby, an azide reacts with a strained alkyne ring to form a triazole (Figure 9). Without the need for a catalyst, there are various examples of SPAAC being used in protein chemical or biological applications, like covalent linkage of a DNA aptamer with a fluorescent dye[154], incorporation of an unnatural azide amino acid in a glutathione S-transferase with subsequent dye conjugation[155] or imaging of a calcium channel on HEK293 cells[156].

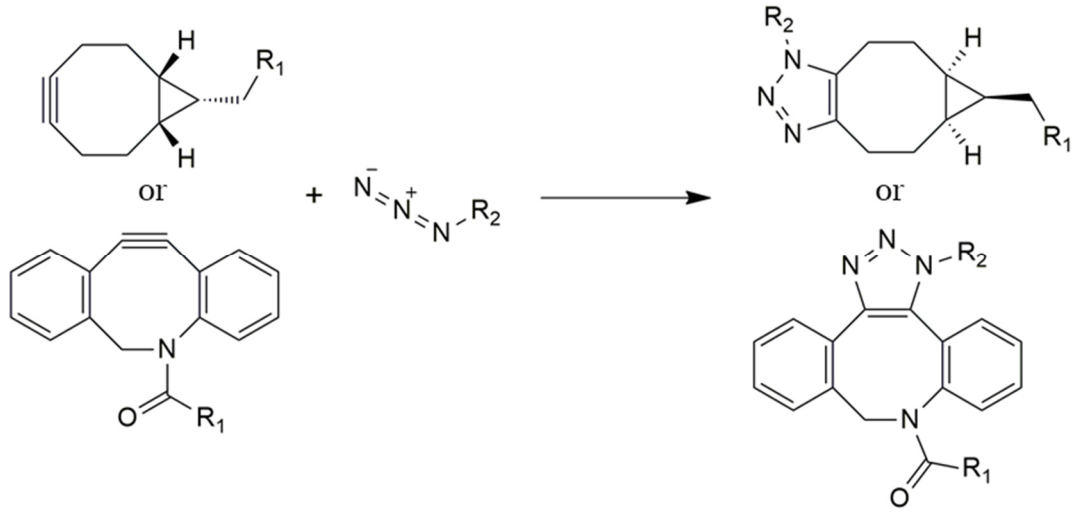

Figure 9: Strain-promoted azide-alkyne cycloaddition. Examples for a SPAAC reaction. A bicyclononyne- (BCN) or a dibenzocyclooctyne-moiety (DBCO) reacts with an organic azide to form a stable triazole.

Last, the strain-promoted inverse electron demand Diels-Alder cycloaddition (SPIEDAC) proved to be the state-of-the-art reaction regarding click chemistry. It combines excellent kinetics with orthogonality and biocompatibility[157,158]. Commonly, 1,2,4,5-tetrazines are used to react with various olefins like bicyclononyne (BCN) or norbornene. Besides the pyridazine, elementary nitrogen is formed as a byproduct of the reaction. In literature SPIEDAC was applied for live-cell labeling[132] and imaging[159] as well as selective marking of RNA[160] and many more applications.

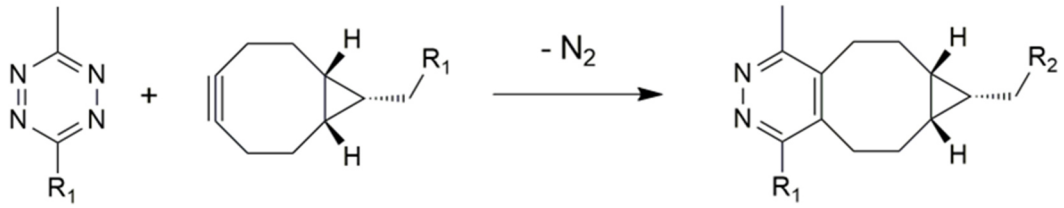

Figure 10: Strain-promoted inverse electron demand Diels-Alder cycloaddition. Example for a SPIEDAC reaction. A 6-methy-1,2,4,5-tetrazine reacts with a BCN to form a pyridazine and elementary nitrogen.

Comparing the three presented reactions, SPIEDAC is the fastest proceeding coupling with $\sim 1 - 10^6$ $M^{-1}s^{-1}$, followed by the CuAAC with $\sim 10 - 100$ $M^{-1}s^{-1}$. SPAAC is the slowest reaction with a turnover of around $10^{-2} - 10$ $M^{-1}s^{-1}$ [157].

All in all, SPIEDAC combines both, the high reactions rate of CuAAC and the independence from catalysts of the SPAAC. However, from a synthesis point of view, educts for CuAAC or SPAAC are often easier to synthesize, hence reaction choice remains a serious consideration.

3.7 Directed evolution and display technologies

Previously, improved enzyme variants or antibodies engineered to gain desired properties were mentioned. All of them are optimized *in vitro* by an approach often referred as directed evolution. Aiming for tailer-made proteins this attempt is divided in three parts: diversification, screening / selection, and characterization.

To start with diversification, a protein of interest must be randomized to generate different variants, potentially generating a desired version. Due to the massive progress in molecular biology over the past decades there are numerous methods for variant generation, ranging from random diversification to rational site-specific modification. Very prominent for random mutagenesis is e.g., error-prone PCR[161–164]. The methodology relies on incorporation of errors during DNA amplification, which is enabled by e.g., application of a low-fidelity or defective engineered polymerase, additives like Mn^{2+} and/or unequal amounts of the deoxy nucleoside triphosphates (dNTPs). A more rational approach is the site-directed (saturation) mutagenesis[165–167]. Hereby, partially mismatching DNA oligos are used to amplify and in parallel modify a gene at a desired position with a defined or undefined mutation (depended on oligo design). A more complex approach is gene shuffling which can be carried out if combination of homologous genes is wanted[168,169]. After partial hydrolysis of the coding DNA by a DNase or restriction enzyme the genes are restored by a primer less PCR exploiting the homology to each other. This approach is particularly suitable for combination of phylogenetic neighboring genes or as a follow up for already evolved proteins.

For the screening approach, randomized libraries must be examined for improved variants. As for the diversification, technologies for this purpose also increased massively. For evolution of ligand binding DNA or RNA systematic evolution of ligands by exponential enrichment (SELEX) is common[170,171]. Incubation of the oligonucleotides with an immobilized target enables removal of non-bound molecules and an enrichment of good performing molecules. Very powerful are display-based technologies. Hereby, phenotype-genotype coupling is achieved by different mechanisms enabling the selection for desired properties and analysis of the underlying DNA sequence. Bacterial[172,173], ribosome[174] and mammalian[175,176] as well as yeast surface and phage display are all prominent examples. The last two are further highlighted in 3.7.1 and 3.7.2. Most of those methods are usually combined with fluorescence-activated cell sorting (FACS) or *in vitro* compartmentalization (IVC) to be able to handle the big library sizes.

Last, characterization is usually carried out, when promising variants are identified. Those are taken out of the library context and get tested individually in the demanded setup. This final step determines if directed evolution was a success.

3.7.1 Yeast surface display

Previously mentioned is yeast-surface display (YSD) a robust and widely applied engineering platform. Supported by FACS for screening of interesting candidates, YSD libraries with an average size of $\sim 10^8 - 10^9$ clones can be handled and have been generated for protein engineering approaches, in the past.

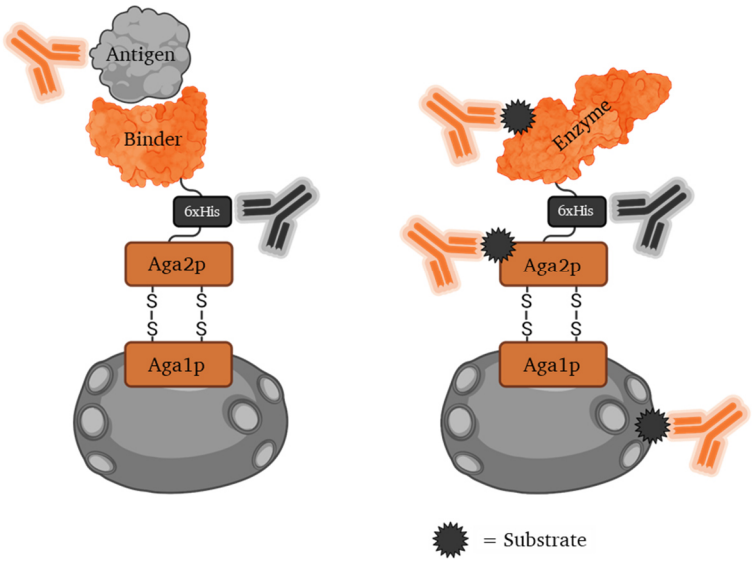

Figure 11: Conceptual depiction of yeast-surface display. Left: Presentation of a binder molecule (orange) with its bound antigen (grey). Staining of the yeasts to confirm protein presentation can be carried out via 6xHis-Tag, and detection of antigen binding can also be measured. Right: Presentation of an enzyme (orange). The catalyst reaction is performed on the cell with an addressable substrate, which can be attached to the surface. Staining is carried out against the 6xHis tag and the substrate.

YSD was pioneered in 1997 by Boder and Wittrup, by presentation and subsequent screening of an antibody single-chain variable fragment library[177]. Combining easy handling and genetic modification with a eukaryotic expression machinery the bakery yeast *Saccharomyces cerevisiae* is the organism of choice for YSD. For fusion of the protein of interest to the surface, there are various anchors known[178]. However with around $\sim 3*10^4$ proteins on a yeast cell[177] the a-agglutinin system is probably one of the most prominent examples. α-agglutinin and a-agglutinin are proteins involved in yeast mating and mediate binding of two yeast cells with different mating type to each other[179]. The latter protein is made up of two subunits, namely Aga1p and Aga2p, which are linked by two disulfide bonds. Hereby, Aga1p is directly connected to the cell wall of the yeast, whereas Aga2p is only attached to Aga1p. For yeast surface display, the POI is genetically fused to Aga2p resulting in the display of the fusion protein on

Aga1p and consequently the cell wall (Figure 11). Incorporation of affinity tags like 6xHis-tag or myc-tag (EQKLISEEDL) in the Aga2p:POI molecule allows for staining of the yeast cells with fluorescently labeled antibodies or comparable proteins followed by flow cytometry analysis or FACS. On the genetic level, Aga1p is untouched and encoded genomically, whereas the Aga2p fusion is encoded on a plasmid under control of an inducible Gal1-promoter enabling control over yeast cell presentation.

3.7.2 Phage display

Another widely used display technology is phage display as first reported by Smith in 1985[180]. Usually up to 10^{10} individual clones presenting peptides or proteins can be screened by bio panning. Display of the protein of interest is realized by a genetic fusion to one of the different coat proteins of filamentous phage M13. Hereby, phenotype-genotype coupling is secured, since M13 phage carries a single-stranded DNA (ssDNA) phagemid with the encoded POI. Usually, fusion is carried out to the minor coat protein pIII ending up in one to five proteins or peptides being expressed on the phage, depending on the presentation strategy. In many cases, display rate is tuned by an amber stop codon in between the POI and pIII on the phagemid. Most of the time, only the first encoded protein is translated, however the usage of *E. coli* amber codon suppressor strains circumvents this fact. Therefore, occasionally the stop codon is ignored and a pIII fusion is translated and incorporated in a phage. Afterwards the packaged libraries are incubated with an immobilized antigen (bio panning) to mediate association of phages. All unbound phages are removed by stringent washing steps, the bound phages are eluted from the antigens and amplified by infection of *E. coli* cells. Repeating the procedure will eventually enrich specific binders, that can be expressed and subsequently characterized[180–182].

Especially for the identification of binders, phage display is a powerful tool and is applied widely until today. There are also numerous therapeutic antibodies derived from phage display libraries[183], for example atezolizumab (lung cancer)[184], ixekizumab (Psoriasis)[185] or caplacizumab[186] (thrombotic thrombocytopenic purpura) to name just a few.

Besides the classical phage display approaches, there are also possible variations, for example where the presentation on M13 phages is exploited for more complex screens involving cell internalizing proteins or peptides.

In 2012, Kim *et al.* showed that M13 phages equipped with an internalizing transbody (termed 3D8) could enter living cells and remain there for more than 12 h. On top of that, phages retained their ability to infect *E. coli* after cell lysis and therefore can be amplified after treatment[187]. Some years later, this breakthrough was the basis for a novel platform technology. Hoffmann and coworkers[188] pioneered a

method for the identification of cell-penetrating peptides. Therefore, M13 phages presenting phylomer peptides enable endosomal escape and therefore mediate cell penetration. In addition, the AviTag™, a short biotin acceptor tag (GLNDIFEAQKIEWHE) for *E. coli* biotin ligase, is also presented. Upon internalization into cells expressing the biotin ligase, the phages are biotinylated and can be captured and by streptavidin beads. The potential of peptides identified by this platform technology were successfully validated in an *in vivo* model of Duchenne muscular dystrophy[188].

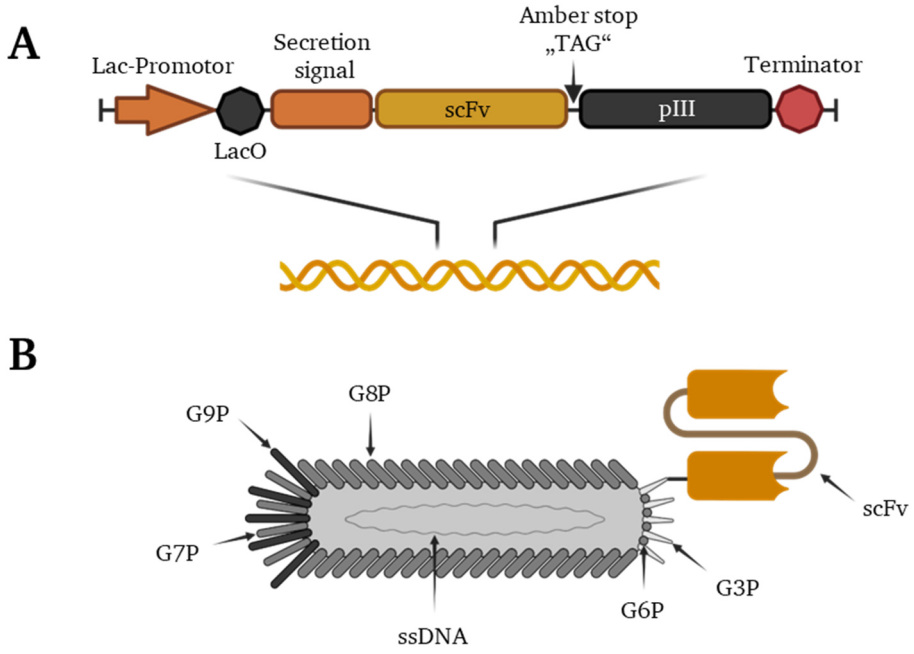

Figure 12: Schematic depiction of the expression cassette in a phagemid (A) and M13 filamentouse phage presenting an scFv (B). In a typical phagemid like the pPD1 or pHAL expression of scFv:pIII is under control of Lac-promoter and its corresponding operator. For phage assembly the fusion protein needs to be secreted in the periplasm and therefore signaling via secretion sequence is necessary. The protein of interest (e.g., scFv) is separated from the pIII by the amber stop codon "TAG". Consequently, the fusion protein is only expressed, when amber codon suppression takes place, else the solitary scFv is expressed.

3.8 Systemic lupus erythematosus and internalizing antibodies

Systemic lupus erythematosus (SLE) is an autoimmune disease with different and complex non-specific symptoms such as arthritis, low fever, fatigue, among others[189]. The disorder is mediated by autoantibodies, that facilitate inflammation, formation of immune complexes and ultimately organ damage. There are 16000 new cases estimated per year of which 90% of patients are female[190].

An important role in SLE formation, progress and diagnostic are so called antinuclear antibodies (ANAs)[191,192]. As the name implies antigens are DNA, RNA and nucleic acid associated proteins like histones. Consequently, any cell debris of apoptotic cells can be recognized by these ANAs, which

promotes the formation of immune complexes paired with complement activation, cytokine release and inflammation. Moreover, it is known, that anti-DNA antibodies in SLE can internalize into living cells[193], also inducing interleukin 8 (IL-8) and tumor necrosis factor α (TNF-α) release[194]. Usually, antibodies are not able to enter living cells, which is problematic in a therapeutic context when targets are not expressed on the cell surface. In the context of cancer, many tumor-associated targets are only expressed intracellularly and cannot be accessed by biomacromolecule, limiting therapeutic success[195]. However, there are some known antibodies internalizing in living cells or methods to improve penetration of the binders. On the one hand, usage of cell penetrating peptides (CPPs) as fusion partners could mediate internalization. This was demonstrated by e.g., Gaston *et al.* in 2019[196]. They used CPPs from different sources like Pep-1 (semi-synthetic, partially nuclear localization signal of simian virus 40), TAT (transactivator of transcription sequence of HI-virus) or MTS (12 amino acid membrane translocation sequences of Kaposi fibroblast growth factor) and fused them to various positions of an antibodies. For some constructs they enhanced penetration into the cytosol, however this had to be optimized in following studies. On the other hand, specific amino acids motifs were identified, enabling cell penetration and could in theory be grafted onto any IgG antibody rendering it cell penetrable. Hereby, a so called TMab4 antibody with a ht4 light chain was reported, which successful escapes the endosome by a pH-dependent conformational change[197]. This light chain is based on the humanized VL of the earlier mentioned 3D8 transbody[198,199]. Furthermore, there is an anti-dsDNA antibody called 2C10 which was derived from SLE-patients[200]. Internalization is presumably mediated by many positively charged amino acids in the CDR3-V_H interacting with negatively charged sulfate polysaccharides or glycosaminoglycans on the cell surface followed by endocytosis[201]. And lastly, there are binders with the inherent ability to pass cell membranes, despite specific motifs or structural elements not being identified yet. An example for this is the anti-STAT3 VHH[202,203] by Singh biotechnology, which gained orphan drug designation and is also patented[204].

Even though there are some moieties realizing internalization available options are still limited to a few molecules. Additionally, overall penetration efficiency is modest and decreases even more when other molecules should be transported in parallel. Therefore, demand on these proteins is still present.

4 Objective

In this work biotin ligases as a tool enzyme were intended to be developed and applied in several individual projects for different applications and demands. First, BioID is a widely applied method for proximity labeling of intracellular protein-protein interaction partners and was used in the past to improve understanding of protein interaction networks in living cells. Until today biotin ligases suitable for this approach are bulky and / or suffer from weak catalytic efficiency. Therefore, identification of a small enzyme with high turnover is desired. In cooperation with the Béthune group from Hamburg, former Heidelberg, a truncated version, and consequently very small biotin ligase derived from *Aquifex aeolicus* should be engineered by directed evolution and yeast surface display to improve its catalytic efficiency. This should ultimately complement the BioID enzyme repertoire by addition of a novel enzyme combining both, small size, and very fast labelling.

Since a yeast surface display library of biotin ligase would be available from the first project, the same library could be used to identify biotin ligase variants for a different purpose. Presented in a publication by Slavoff *et al.* in 2008, biotin derivatives are accessible which introduced click chemistry substrates to biotin ligases. In a protein conjugation context this could enable versatile capabilities e.g., the generation of an antibody-drug conjugate (ADC) in frame of cancer therapy. Therefore, identification of an enzyme using efficiently propargyl biotin as a substrate was desired ultimately being able to generate an ADC mediated by biotin ligase. Engineering of biotin ligases towards biotin derivatives was already done in the past e.g., for desthiobiotin[205] so identification of variants using click chemistry based derivates should be feasible.

In context of ADC generation lipoate-protein ligase A (LplA) is a promising bond-forming enzyme used for various protein conjugation experiments in the past. Since the catalyzed reaction is relatively similar to the one of biotin ligases, LplA should also be explored for ADC generation. In cooperation with the Wombacher group from University of Heidelberg, click chemistry-based lipoate derivatives are accessible. As for the biotin ligase approach, the therapeutic antibody trastuzumab should be attached with the enzymes engineered recognition motif (LAP-tag) allowing construction of a toxin carrying antibody.

While mAbs are extensively used in the clinic particularly for cancer therapy by recognizing extracellular or cell-surface exposed targets, they are, with a few exceptions, unable to pass the cytoplasmic membrane barrier. Consequently, intracellular targets remain unaddressed by mAbs. Patients suffering from the autoimmune disease SLE are known to have antibodies internalizing in cells. Their identification and analysis of the origin of their penetration properties might shed some light on their

mode of action in regard of cell penetration and might allow for their use as intracellular transporters of any kind of protein cargo. Hence this project aimed at establishing a screening method for cell penetrating antibodies again making use of biotin ligase, this time expressed by a reporter cell line. Basis for this project were phage display libraries derived from *Merck Healthcare KGaA* presenting antibody fragments (scFvs) of SLE patients. As published by Kim *et al.*[187] those phages can internalize in living cells when a penetrating protein is presented on their surface and remain intracellularly for various hours in an intact state. So, as aim for this project, the libraries should be incubated with living cells to identify the internalizing scFvs. As shown by Hoffmann and coworkers[188] intracellular expressed biotin ligases might improve screening stringency by (specific) biotinylation of the internalizing phages and subsequent affinity purification. This technology should be applied in frame of this thesis for the isolation of internalizing SLE associated antibodies.

5 Material

5.1 Bacterial strains

Bacterial strain	Genotype
Escherichia coli DH5α	*F⁻ φ80lacZΔM15 Δ(lacZYA-argF)U169 recA1 endA1 hsdR17(rK–, mK+) phoA supE44 λ–thi-1 gyrA96 relA1*
Escherichia coli TOP10	*F⁻ mcrA Δ(mrr-hsdRMS-mcrBC) φ80lacZΔM15 ΔlacX74 recA1 araD139 Δ(ara-leu)7697 galU galK λ–rpsL(StrR) endA1 nupG*
Escherichia coli BL21 (DE3)	*fhuA2 [lon] ompT gal (λ DE3) [dcm] ΔhsdS* *λ DE3 = λ sBamHIo ΔEcoRI-B int::(lacI::PlacUV5::T7 gene1) i21 Δnin5*
Escherichia coli XL1-Blue	*recA1 endA1 gyrA96 thi-1 hsdR17 supE44 relA1 lac [F' proAB lacIqZΔM15 Tn10 (Tetr)]*
Escherichia coli K12 ER2738	*F' proA+B+ lacIq Δ(lacZ)M15 zzf::Tn10(TetR)/ fhuA2 glnV Δ(lac-proAB) thi-1 Δ(hsdS-mcrB)5*

5.2 Yeast strains

Yeast strain	Genotype
Saccharomyces cerevisiae EBY100	*MATa AGA1::GAL1-AGA1::URA3 ura3-52 trp1 leu2- Δ200 his3- Δ200 pep4::HIS3 prbd1.6R can1 GAL*

5.3 Mammalian cell lines

Cell line	Cell type	Adherent	Culture medium
SK-BR-3	Human mammary gland (adenocarcinoma)	yes	DMEM + 10 % (v/v) FBS + 1 % (v/v) P/S
CHO-K1	Chinese hamster ovary	yes	DMEM / F12 ham + 10 % (v/v) FBS + 1 % (v/v) P/S

HeLa-EM2-11ht	Human cervix (adenocarcinoma)	yes	DMEM + 10 % (v/v) FBS + 1 % (v/v) P/S 0.2 mg/ml G418 0.2 mg/ml Hygromycin
HEK Expi293F™	Human embryonic kidney	no	Expi293F™ Expression medium + 1% P/S

5.4 Enzymes and proteins

Protein	**Supplier**
Anti-His antibody	*QIAGEN N.V.*
Anti-Human IgG Fc – phycoerythrin antibody	*Thermo Fisher Scientific*
Anti-M13 pIII monoclonal antibody	*New England Biolabs*
Anti-Mouse IgG (whole molecule) - FITC antibody	*Merck KGaA*
BamHI	*New England Biolabs*
Blue Prestained Protein Standard, Broad Range (11 – 250 kDa)	*New England Biolabs*
Bovine serum albumin (BSA) fraction V	*Carl Roth GmbH*
BsaI-HFv2	*New England Biolabs*
DpnI	*New England Biolabs*
EcoRI-HF	*New England Biolabs*
MfeI-HF	*New England Biolabs*
NcoI-HF	*New England Biolabs*
NeutrAvidin Protein, DyLight™ 650	*Thermo Fisher Scientific*
NotI-HF	*New England Biolabs*
One*Taq*®Quick Load DNA Polymerase	*New England Biolabs*
Q5® High-Fidelity DNA Polymerase	*New England Biolabs*
SapI	*New England Biolabs*
Shrimp Alkaline Phosphatase (rSAP)	*New England Biolabs*
Streptavidin alkaline phosphatase-conjugat	*Roche Holding AG*
Streptavidin - allophycocyanin-conjugate	*Thermo Fisher Scientific*
T4 DNA Ligase	*New England Biolabs*

5.5 Oligos

Table 2: Oligos used in 7.1. Recognition motifs for restriction enzymes are in bold.

Primer name	Sequence 5‘ → 3‘
microID library gap lo	TCTACACTGTTGTTATCAGATCTCGAGCTATTAATGGTGATGGTGATGATG
microID library gap up	GTGGTGGTGGTTCTGGTGGTGGTGGTTCTGAACAAAAACTCATCTCAGAAGAGGATCTC
microID SDM G40R/L41P	GGGCAGAGGCCGCCCGGGCAGAAAGTGGCTGAGCCAGG
microID SDM lo	TTGGTCTGTCTGTCGGCCACC
microID SDM R40G/L41P	GGGCAGAGGCGGCCCGGGCAGAAAGTGGCTGAGCCAGG
ultraID EcoRI lo	TATTAT**GAATTC**TTAATGGTGATGGTGATGATGCTTCTC
ultraID NcoI up	ATAATA**CCATGG**GCGAACAAAAACTCATCTCAGAAGAGGATCTC

Table 3: Oligos used in 7.2.

Primer name	Sequence 5‘ → 3‘
microID Co Display up	GGTGGTGGTGGTTCTGGTGGTGGTGGTTCTGGTGGTGGTGGTTCTGAACAAAAACTCATCTCAGAAGAGGATCTCG
BCCP Co gap lo	TTTGTTACATCTACACTGTTGTTATCAGATTTAATGATGATGATGATGATGAACGTTAGTGTCGATCAAGAACAATGGTTG
microID Co Display lo (GGGSE linker)	ACCTTCAGATCCACCTCCTTCAGAACCACCTCCTCCTTCAGAACCTCCACCACCCTTCTCCTTGAACTTCTTCAGGTTCTCG
BCCP Co Display up (GGGSE linker)	GGTGGTGGAGGTTCTGAAGGAGGAGGTGGTTCTGAAGGAGGTGGATCTGAAGGTATGATGGACAAGGACTTCATCAAGGAATTG
microID Co gap lo (GGGS linker)	AGAACCTCCACCACCCTTCTCCTTGAACTTCTTCAGGTTCTCG
BCCP Co gap up (GGGS linker)	AAGTTCAAGGAGAAGGGTGGTGGAGGTTCTGGAGGAGGTGGTTCTATGATGGACAAGGACTTCATCAAGGAATTG
Double Display gap up	TATACTTTAACGTCAAGGAGAAAAAACCCCGGATCGAATTCCCTACTTCATACATTTTCAATTAAGATGCAACTATTAAGG
Aga2p lo	AAACACATACTGGGTATTAATAGGTGATCCTTTTGATG
Aga2p up	CAGGAGTTAACCACAATTTGCGAGC
Double Display gap lo	TTGTTACATCTACACTGTTGTTATCAGATCTCGAGTCAGTGGTGGTGGTGGTGGTGCAC

Table 4: Oligos used in 7.3. Recognition motifs for restriction enzymes are in bold. In case of Type IIS enzymes resulting, sticky ends are underlined.

Primer name	Sequence 5‘ → 3‘
BirA* EcoRI lo	TATTAT**GAATTC**TCAGTGATGATGGTGATGGTGCTTCTCTGCGCTTCTCAGGG
PhBL BsaI up	ATAATA**GGTCTC**GAGCGGCATGTTAGGGCTCAAGACGTCGATTATTGG

PhBL His6 BsaI lo	TATTAT**GGTCTC**CTCATTCAATGATGATGATGATGATGAAGAAATCTTAAGCTTACATCGCCATAAATC ACC
yBL BsaI up	ATAATA**GGTCTC**GAGCGGCATGAATGTATTAGTCTATAATGGCCCAGGG
yBL His6 BsaI lo	TATTAT**GGTCTC**CTCATTTAATGATGATGATGATGATGACTCTGAACCTTTTTAGCAATTAAGCTCTTG AAGATATC
p67 BsaI up	ATAATA**GGTCTC**GAGCGGCCTCAGATCCCCCATGCCCGG
p67 His6 BsaI lo	TATTAT**GGTCTC**CTCATTCAATGATGATGATGATGATGCTCTAACTCTACGAGTAAATCTCCCTCGC
p67 BamHI lo (HC)	TATTAT**GGATCC**TCACTCTAACTCTACGAGTAAATCTCC
p67 CH3 Tras up	GAAGTCCCTGAGCCTGAGCCCCGGCCTCAGATCCCCCATGCCCG
Tras CH2 MfeI up	ATAATA**CAATTG**GTACGTGGACGGCG
Tras CH3 p67 lo	CTACGACGCCGGGCATGGGGGATCTGAGGCCGGGGCTCAGGCTC
Tras GGGS overlap lo	GAGGCTGCCACCGCCGCTACCGCCACCGCTGCCGCCGCCGGGGCTCAGGCTCAG
p67 GGGS overlap up	CCCCGGCGGCGGCAGCGGTGGCGGTAGCGGCGGTGGCAGCCTCAGATCCCCCATGCCCGG
Tras LC EcoRI up	ATAATA**GAATTC**GCCACCATGAAGCTGC
Tras LC p67 overlap lo	GACTACGACGCCGGGCATGGGGGATCTGAGAGATCCCCCTCCGCCACTTC
p67 LC overlap up	GAGGCGGAAGTGGCGGAGGGGGATCTCTCAGATCCCCCATGCCCG
p67 BamHI lo (LC)	TATTAT**GGATCC**TCACTCTAACTCTACGAGTAAATCTCCCTCGC
Trastuzumab N297Q up	GGAACAGTACCAGAGCACCTACCGGGTGGTGTCC
CH2 SDM lo	TCTCTGGGCTTGGTCTTGGCGTTG

Table 5: Oligos used in 7.5. Recognition motifs for restriction enzymes are in bold. In case of Type IIS enzymes resulting, sticky ends are underlined.

Primer name	Sequence 5‘ → 3‘
MHVH1f	ATAATA**GCTCTTC**TATGGCGCAGGTBCAGCTGGTGCAGTCTGG
MHVH1/7f	ATAATA**GCTCTTC**TATGGCGCARRTSCAGCTGGTRCARTCTGG
MHVH2f	ATAATA**GCTCTTC**TATGGCGCAGRTCACCTTGAAGGAGTCTGG
JokVH3f1	ATAATA**GCTCTTC**TATGGCGSAGGTGCAGCTGGTGGAGTCTGG
JokVH3f2	ATAATA**GCTCTTC**TATGGCGGARGTGCAGCTGKTGGAGTCTGG
MHVH4f1	ATAATA**GCTCTTC**TATGGCGCAGGTGCARCTGCAGGAGTCGGG
JokVH4f2	ATAATA**GCTCTTC**TATGGCGCAGGTGCAGCTACARCAGTGGGG
JokVH4f3	ATAATA**GCTCTTC**TATGGCGCAGCTGCAGCTGCAGGAGTCSGG
MHVH5f	ATAATA**GCTCTTC**TATGGCGGARGTGCAGCTGGTGCAGTCTGG
MHVH6f	ATAATA**GCTCTTC**TATGGCGCAGGTACAGCTGCAGCAGTCAGG

MHIgGCH1r	ATAATA**GCTCTTC**TACCGACCGATGGGCCCTTGGTGGA
MHVK1f1	ATAATA**GCTCTTC**TTCTGACATCCAGATGACCCAGTCTCC
MHVK1f2	ATAATA**GCTCTTC**TTCTGMCATCCRGWTGACCCAGTCTCC
MHVK2f	ATAATA**GCTCTTC**TTCTGATRTTGTGATGACYCAGWCTCC
MHVK3f	ATAATA**GCTCTTC**TTCTGAAATWGTGWTGACRCAGTCTCC
MHVK4f	ATAATA**GCTCTTC**TTCTGACATCGTGATGACCCAGTCTCC
MHVK5f	ATAATA**GCTCTTC**TTCTGAAACGACACTCACGCAGTCTCC
MHVK6f	ATAATA**GCTCTTC**TTCTGAWRTTGTGMTGACWCAGTCTCC
MHkappaCLr	ATAATA**GCTCTTC**TCGCGAAGACAGATGGTGCAGCCACAGT
MHkappaCL-Avir	ATAATA**GCTCTTC**TCGCTTCGTGCCATTCGATTTTCTGAGCTTCGAAGATGTCGTTCAGACCGAAGACA GATGGTGCAGCCACAGT
MHVL1f1	ATAATA**GCTCTTC**TTCTCAGTCTGTGCTGACTCAGCCACC
MHVL1f2	ATAATA**GCTCTTC**TTCTCAGTCTGTGYTGACGCAGCCGCC
MHVL2f	ATAATA**GCTCTTC**TTCTCAGTCTGCCCTGACTCAGCCT
MHVL3f1	ATAATA**GCTCTTC**TTCTTCCTATGWGCTGACWCAGCCACC
MHVL3f2	ATAATA**GCTCTTC**TTCTTCTTCTGAGCTGACTCAGGACCC
MHVL4f1	ATAATA**GCTCTTC**TTCTCTGCCTGTGCTGACTCAGCCC
MHVL4f2	ATAATA**GCTCTTC**TTCTCAGCYTGTGCTGACTCAATCRYC
MHVL5f	ATAATA**GCTCTTC**TTCTCAGSCTGTGCTGACTCAGCC
MHVL6f	ATAATA**GCTCTTC**TTCTAATTTTATGCTGACTCAGCCCCA
MHVL7/8f	ATAATA**GCTCTTC**TTCTCAGRCTGTGGTGACYCAGGAGCC
MHVL9/10f	ATAATA**GCTCTTC**TTCTCAGSCWGKGCTGACTCAGCCACC
MHLambdaCLr	ATAATA**GCTCTTC**TCGCAGAGGASGGYGGGAACAGAGTGAC
MHLambdaCL-Avir	ATAATA**GCTCTTC**TCGCTTCGTGCCATTCGATTTTCTGAGCTTCGAAGATGTCGTTCAGACCAGAGGAS GGYGGGAACAGAGTGAC
VHH13 DsbA EcoRI up	ATAATA**GAATTC**ATTAAAGAGGAGAAATTAACCATGAAAAAAATCTGGCTGGCTCTGGCTGGTCTGGT TCTGGCTTTCTCTGCTTCTGCTGCTCAGCATGTGCAGCTGGTGGAGTCTG
VHH13 NotI lo	TATTAT**GCGGCCGC**TGAGGAGACAGTGACCTGGGTC

5.6 Plasmids

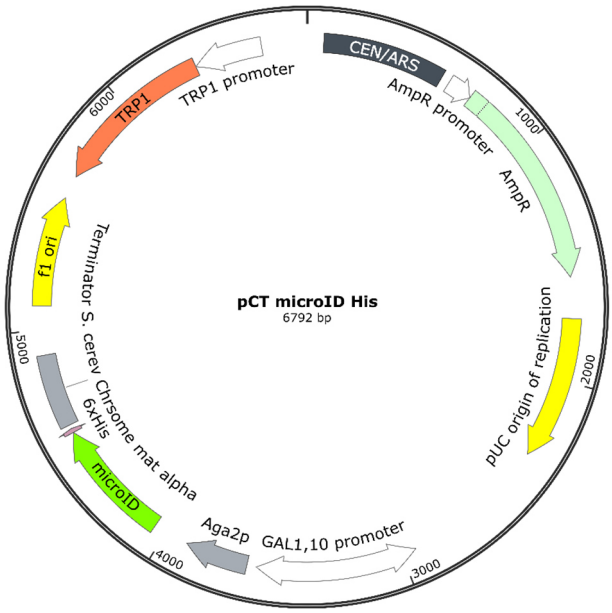

Figure 13: pCT microID His vector used for directed evolution. CEN/ARS: *S. cerevisiae* CEN6 centromere fused to an autonomously replicating sequence; **AmpR:** Ampicillin resistance gene; **GAL1,10 promotor:** Divergent promotor region of *S. cerevisiae* galactose promotor; **Aga2p:** A-agglutinin from *S. cerevisiae*; **microID:** Truncated and mutated (R40G) biotin ligase derived by *Aquifex aeolicus*; **6xHis:** C-terminal Histidine-tag; **f1 ori:** f1 bacteriophage origin of replication **TRP1:** Phosphoribosyl anthranilate isomerase, required for tryptophan biosynthesis.

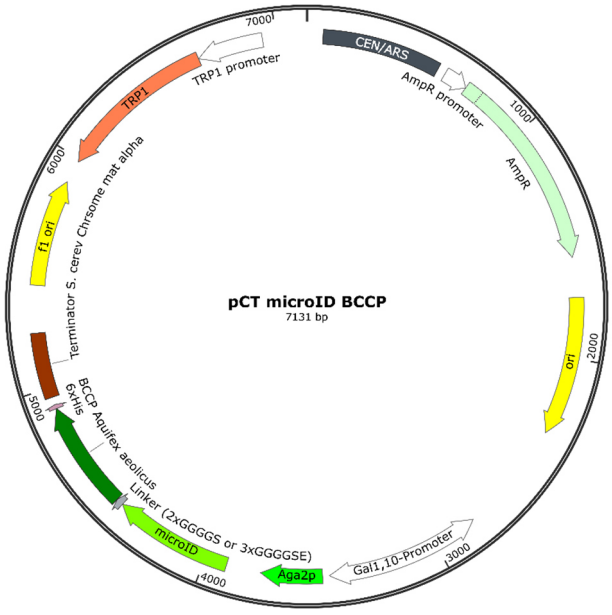

Figure 14: pCT - yeast surface display vector used for display of microID and *A. aeolicus* BCCP. CEN/ARS: *S. cerevisiae* CEN6 centromere fused to an autonomously replicating sequence; **AmpR:** Ampicillin resistance gene; **GAL1,10 promotor:** Divergent promotor region of *S. cerevisiae* galactose promotor; **Aga2p:** A-agglutinin from *S. cerevisiae*; **microID:** Truncated and mutated (R40G) biotin ligase derived by *Aquifex aeolicus*; **6xHis:** C-terminal Histidine-tag; **f1 ori:** f1 bacteriophage origin of replication **TRP1:** Phosphoribosyl anthranilate isomerase, required for tryptophan biosynthesis.

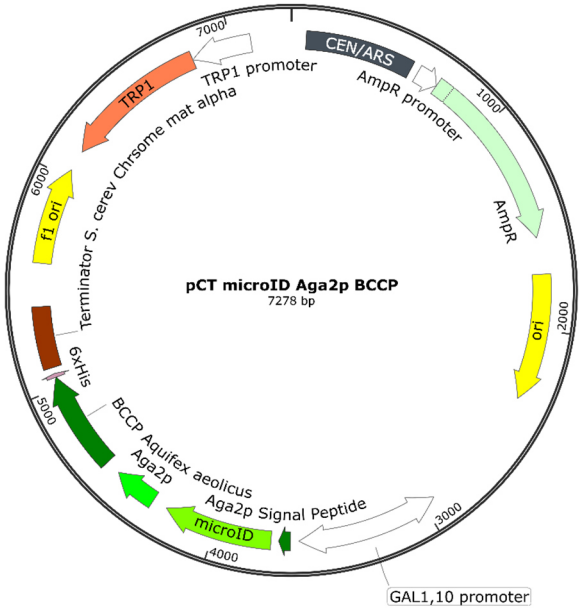

Figure 15: pCT - yeast surface display vector used for N- and C-terminal Aga2p display of microID and *A. aeolicus'* BCCP. *S. cerevisiae* CEN6 centromere fused to an autonomously replicating sequence; **AmpR:** Ampicillin resistance gene; **GAL1,10 promotor:** Divergent promotor region of *S. cerevisiae* galactose promotor; **Aga2p Signal Peptide:** Secretion signal of Aga2p; **microID:** Truncated and mutated (R40G) biotin ligase derived by *Aquifex aeolicus*; **Aga2p:** A-agglutinin from *S. cerevisiae*; **6xHis:** C-terminal Histidine-tag; **f1 ori:** f1 bacteriophage origin of replication **TRP1:** Phosphoribosyl anthranilate isomerase, required for tryptophan biosynthesis.

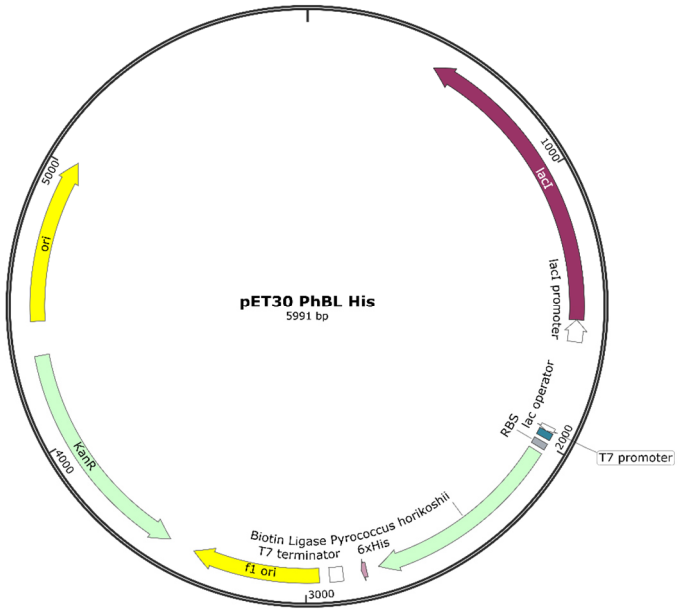

Figure 16: Exemplary depiction of pET30 vector used for recombinant protein expression in *E. coli*. lacI: Lac repressor; **RBS:** efficient ribosome binding site from bacteriophage T7; **6xHis:** C-terminal Histidine-tag; **f1 ori:** f1 bacteriophage origin of replication; **KanR:** confers resistance to kanamycin in bacteria; **ori:** high-copy-number ColE1 origin of replication.

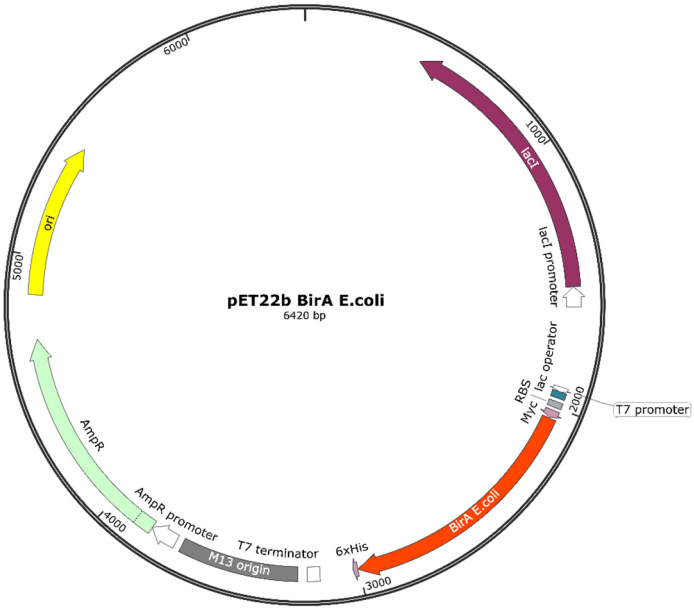

Figure 17: Exemplary depiction of pET22b vector used for recombinant protein expression in *E. coli*. lacI: Lac repressor; **RBS:** efficient ribosome binding site from bacteriophage T7; **Myc:** Myc (human c-Myc oncogene) epitope tag; **6xHis:** C-terminal Histidine-tag; **f1 ori:** f1 bacteriophage origin of replication; **AmpR:** Ampicillin resistance gene; **ori:** high-copy-number ColE1 origin of replication.

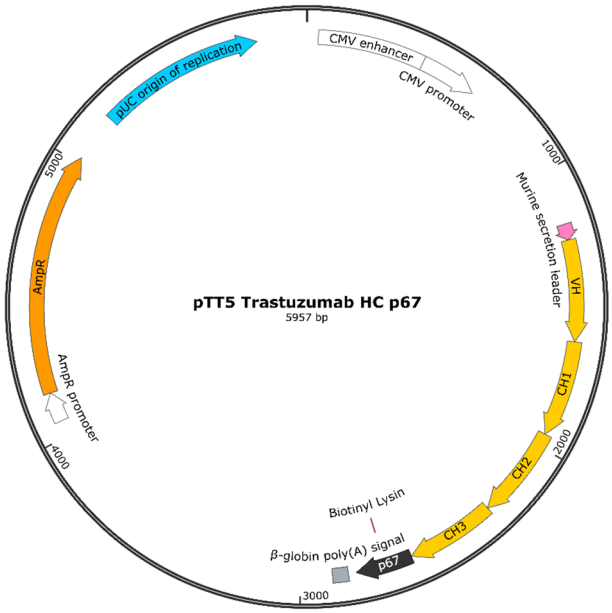

Figure 18: Exemplary depiction of pTT5 vector used for recombinant protein expression in HEK Expi293F™ cells. CMV enhancer: human cytomegalovirus immediate early enhancer; **CMV promotor:** human cytomegalovirus (CMV) immediate early promoter; **VH, CH1, CH2, CH3**: Trastuzumab heavy chain gene; **p67:** Last 67 amino acids of human propionyl-CoA carboxylase; **β-globin poly(A) signal:** rabbit β-globin polyadenylation signal; **AmpR:** Ampicillin resistance gene.

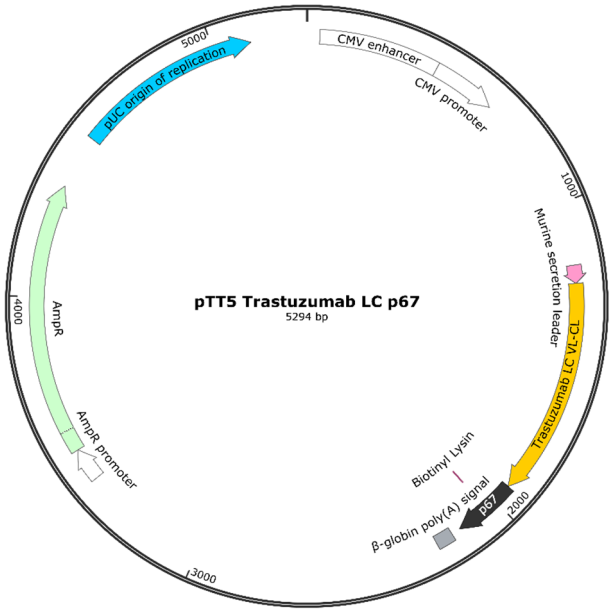

Figure 19: Exemplary depiction of pTT5 vector used for recombinant protein expression in HEK Expi293F™ cells. CMV enhancer: human cytomegalovirus immediate early enhancer; **CMV promotor:** human cytomegalovirus (CMV) immediate early promoter; **Trastuzumab LC VL-CL**: Trastuzumab light chain gene; **p67:** Last 67 amino acids of human propionyl-CoA carboxylase; **β-globin poly(A) signal:** rabbit β-globin polyadenylation signal; **AmpR:** Ampicillin resistance gene.

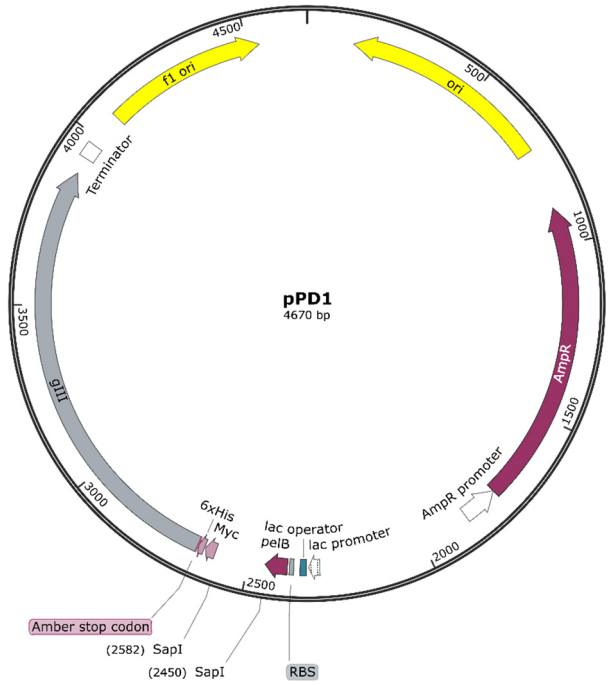

Figure 20: Empty pPD1 destination phage display vector. ori: high-copy-number ColE1 origin of replication. **AmpR:** Ampicillin resistance gene; **RBS:** strong bacterial ribosome binding site; **pelB:** leader peptide for secretion; **Myc:** Myc (human c-Myc oncogene) epitope tag; **6xHis:** Poly-Histidine-tag; **f1 ori:** f1 bacteriophage origin of replication; **gIII**: Codes for M13 phage pIII minor coat protein. *SapI* restriction sites were used for golden gate assembly.

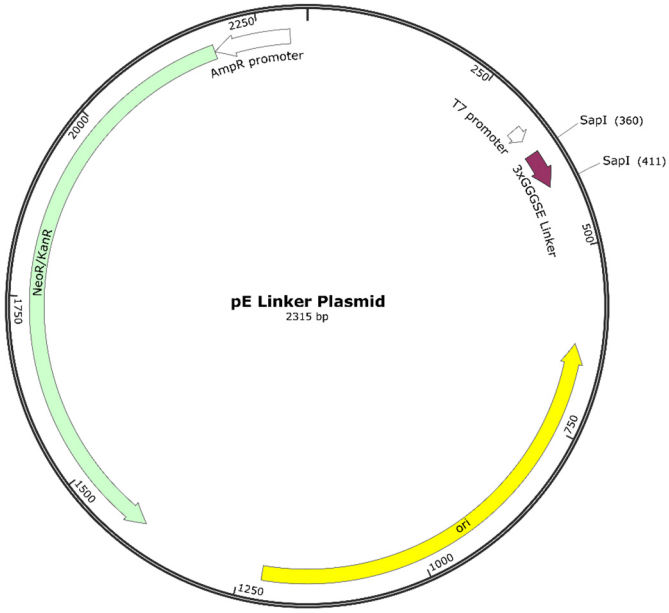

Figure 21: pE vector containing linker sequence for scFv assembly. ori: high-copy-number ColE1 origin of replication. **KanR:** confers resistance to kanamycin in bacteria. Linker sequence which is flanked by *SapI* restriction sites served as insert for golden gate assembly.

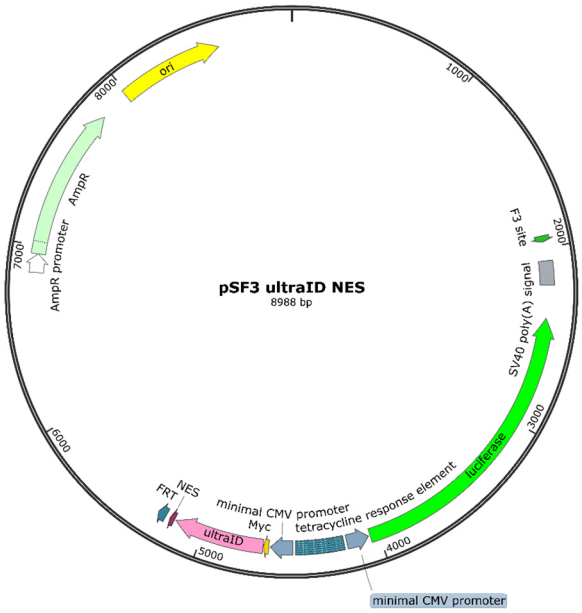

Figure 22: pSF3 vector used for integration in HeLa-EM2-11ht cell line. F3 site: Upstream integration site for double reciprocal crossover by Flp-recombinase; **SV40 poly(A) signal:** SV40 polyadenylation signal; **Luciferase:** enhanced *luc+* version of the luciferase gene; **minimal CMV promotor:** Minimal human cytomegalovirus (CMV) immediate early promoter; **tetracycline response element:** contains seven copies of the tetracycline operator *tetO;* **Myc:** Myc (human c-Myc oncogene) epitope tag; **NES:** nuclear export signal from the HIV Rev protein; **FRT:** Downstream integration site for double reciprocal crossover mediated by Flp-recombinase.

5.7 Chemicals

Chemical	Supplier
(D)-Biotin	*Merck KGaA*
(D)-Galactose	*Carl Roth GmbH & Co. KG*
(D)-Glucose	*Carl Roth GmbH & Co. KG*
[Bis(2-hydroxyethyl) amino] acetic acid (Bicine)	Carl Roth GmbH & Co. KG
2-Mercaptoethanol	*Carl Roth GmbH & Co. KG*
5-Carboxytetramethylrhodamine-PEG3-Azide	*Carl Roth GmbH & Co. KG*
5-(and-6)-Carboxytetramethylrhodamine-Azide	*Synthesized by Kolmar Group*
5-(and-6)-Carboxytetramethylrhodamine-bicyclononyne	*Synthesized by Kolmar Group*
Acetic acid	*Carl Roth GmbH & Co. KG*
Acrylamid/Bisacrylamid (37.5:1)	*Carl Roth GmbH & Co. KG*
Adenosin-5'-triphosphat-Dinatriumsalz (ATP)	*Carl Roth GmbH & Co. KG*
Agar-Agar, Kobe I	*Carl Roth GmbH & Co. KG*
Agarose	*Carl Roth GmbH & Co. KG*
Ammonium persulfate (APS)	*Carl Roth GmbH & Co. KG*
Ammonium sulfate	*Carl Roth GmbH & Co. KG*
Ampicillin, sodium salt	*Carl Roth GmbH & Co. KG*
Ascorbic acid	*Merck KGaA*
Bacto Casamino acids	*Becton, Dickinson and Company*
Bromophenol blue	*Carl Roth GmbH & Co. KG*
Chloramphenicol	*Carl Roth GmbH & Co. KG*
cis-/trans-propargyl biotin	*Synthesized by Peter Bitsch (Kolmar Group)*
Citric acid	*Carl Roth GmbH & Co. KG*
Coomassie Brilliant Blue-G250	*Carl Roth GmbH & Co. KG*
Coomassie Brilliant Blue-R250	*Carl Roth GmbH & Co. KG*
Copper (II) sulfate pentahydrate	*Carl Roth GmbH & Co. KG*
Desthiobiotin azide	*Synthesized by Ingo Bork (Kolmar Group)*
Difco yeast nitrogen base	*Becton, Dickinson and Company*
Dimethyl sulfoxide (DMSO)	*Thermo Fisher Scientific Inc.*
Disodium hydrogen phosphate dihydrate	*Carl Roth GmbH & Co. KG*
Dithiothreitol (DTT)	*Carl Roth GmbH & Co. KG*

dNTP mix	*New England BioLabs*
Dry milk powder	*Carl Roth GmbH & Co. KG*
Ethanol	*Carl Roth GmbH & Co. KG*
Ethylenediaminetetraacetic acid disodium salt (EDTA)	*Carl Roth GmbH & Co. KG*
Glycerol	*Merck KGaA*
HCl	*Carl Roth GmbH & Co. KG*
HDGreen™ DNA/RNA staining reagent	*Intas Science Imaging*
Imidazole	*Carl Roth GmbH & Co. KG*
Isopropanol	*Carl Roth GmbH & Co. KG*
Isopropyl β-D-1 thiogalactopyranoside(IPTG)	*Carl Roth GmbH & Co. KG*
Lithium acetate	*Carl Roth GmbH & Co. KG*
Magnesium acetate tetrahydrate	*Carl Roth GmbH & Co. KG*
Magnesium chloride hexahydrate	*Merck KGaA*
Nickel chloride	*Merck KGaA*
Penicillin-Streptomycin (P/S)	*Merck KGaA*
Potassium chloride	*Carl Roth GmbH & Co. KG*
Sodium chloride (NaCl)	*Carl Roth GmbH & Co. KG*
Sodium dihydrogen phosphate	*Carl Roth GmbH & Co. KG*
Sodium dodecyl sulfate (SDS)	*Carl Roth GmbH & Co. KG*
Sodium hydroxide (NaOH)	*Carl Roth GmbH & Co. KG*
Sorbitol	*Carl Roth GmbH & Co. KG*
Tetramethylethylenediamine (TEMED)	*Merck KGaA*
Tris-(hydroxymethyl)-aminomethane (TRIS)	*Carl Roth GmbH & Co. KG*
Trisodium citrate	*Carl Roth GmbH & Co. KG*
Triton X-100	*Carl Roth GmbH & Co. KG*
Trypan Blue Solution 0.4	*Thermo Fisher Scientific Inc.*
Tryptone/Peptone from casein, granulated	*Carl Roth GmbH & Co. KG*
TWEEN-20	*AppliChem GmbH*
Yeast extract	*Merck KGaA*

5.8 Media for bacterial cultivation

For preparation of agar plates 1.2 % (w/v) agar-agar was added before sterilization.

Medium	Composition
Double concentrated Yeast Tryptone (dYT)	1.6 % (w/v) tryptone / peptone 1 % (w/v) yeast extract 0.5 % (w/v) NaCl
Terrific broth (TB)	2.4 % (w/v) yeast extract 1.2 % (w/v) tryptone / peptone 0.4 % (v/v) glycerol 17 mM KH_2PO_4 72 mM K_2HPO_4
Super optimal broth (SOC)	0.5 % (w/v) yeast extract 2 % (w/v) tryptone / peptone 10 mM NaCl 2.5 mM KCl 10 mM $MgCl_2$ 10 mM $MgSO_4$ 20 mM glucose

5.9 Media for yeast cultivation

For preparation of agar plates 1.2 % (w/v) agar-agar was added before sterilization.

Medium	Composition
Yeast extract peptone dextrose (YPD)	1 % (w/v) Yeast-extract 2 % (w/v) Tryptone 2 % (w/v) Glucose
Synthetic defined without tryptophane (SD_{-Trp})	0.86 % (w/v) NaH_2PO_4 0.54 % (w/v) Na_2HPO_4 0.5 % (w/v) $(NH_4)_2SO_4$ 2 % (w/v) Glucose 0.17 % (w/v) Yeast nitrogen base 0.5 % (w/v) Bacto casamino acids
Synthetic defined with galactose and without glucose / tryptophane (SG_{-Trp})	0.86 % (w/v) NaH_2PO_4 0.54 % (w/v) Na_2HPO_4 0.5 % (w/v) $(NH_4)_2SO_4$ 2 % (w/v) Galactose 0.17 % (w/v) Yeast nitrogen base 0.5 % (w/v) Bacto casamino acids

5.10 Media for mammalian cell culture

Medium	Composition
Dulbecco's modified eagle medium (DMEM)	*Merck KGaA*
Dulbecco's modified eagle medium and Ham F-12 Nutrient Mixture (DMEM / F12 Ham)	*Merck KGaA*
Expi293™ expression medium	*Thermo Fisher Scientific Inc.*
Fetal bovine serum (FBS) superior	*Merck KGaA*
Trypsin-EDTA solution	*Merck KGaA*

5.11 Buffers and solutions

Buffer / Solution	Composition
AP buffer	100 mM Tris-HCl, pH 9.1100 mM NaCl 5 mM $MgCl_2$
Conditioning buffer	2.5 mM DTT 1 M Tris-HCl, pH 8.0
Coomassie brilliant blue staining solution	0.2 % (w/v) Coomassie brilliant blue R-250 0.2 % (w/v) Coomassie brilliant blue G-250 30 % (v/v) Isopropanol 7.5 % (v/v) Acetic acid
Coomassie destaining solution	10 % (v/v) Acetic acid
Electroporation buffer	1 M Sorbitol 1 mM $CaCl_2$
HIC A buffer	20 mM Tris-HCl, pH 7.2 1.5 M $(NH_4)_2SO_4$
HIC B buffer	20 mM Tris-HCl, pH 7.2
IMAC A buffer	50 mM Tris-HCl, pH 7.5 300 mM NaCl 20 mM Imidazole
IMAC B buffer	50 mM Tris-HCl, pH 7.5 300 mM NaCl 500 mM Imidazole
SDS-PAGE separation buffer	3 M Tris-HCl, pH 8.8 4 g/l SDS
SDS-PAGE stacking buffer	0.5 M Tris-HCl, pH 6.8 4 g/l SDS

SDS-PAGE Loading dye (5x)	250 mM Tris-HCl 75 g/l SDS 25 % (v/v) Glycerol 12.5 % (v/v) β-Mercaptoethanol 0.25 g/l Bromophenol blue
SDS-PAGE running buffer	50 mM Tris-HCl, pH 8.8 190 nM Glycine 1 g/l SDS
Strep W buffer	100 mM Tris-HCl, pH 8.0 150 mM NaCl 1 mM EDTA
Phosphate buffered saline (PBS)	140 mM NaCl 10 mM KCl 6.4 mM Na_2HPO_4 2 mM KH_2PO_4
Phosphate buffered saline TWEEN®20 (PBS-T)	140 mM NaCl 10 mM KCl 6.4 mM Na_2HPO_4 2 mM KH_2PO_4 0.1 % (v/v) TWEEN20
Protein A elution buffer	90 mM Citric acid 20 mM Trisodium citrate

5.12 Kits and consumables

Kit / Consumable	**Supplier**
Amicon® Ultra - 0.5 mL Centrifugal Filter Device	*Merck KGaA*
Cell culture 96 well plates	*Carl Roth GmbH & Co. KG*
Cell culture flasks, T25 / T75	*Corning Inc.*
Centrifuge tubes, 15 / 50 ml	*Sarstedt AG & Co. KG*
Centrifuge tubes, 50 ml	*Sarstedt AG & Co. KG*
Dialysis membrane Spectra/Por® MWCO 8000	*Carl Roth GmbH & Co. KG*
Electroporation cuvette	*Bio-Rad Laboratories Inc.*
Erlenmeyer cell culture flasks	*Corning Inc.*
GeneMorph II Random Mutagensis Kit	*Agilent Technologies Inc.*
HisTrap HP, 1 ml	*Cytiva*
HiTrap Protein A HP, 1 ml	*Cytiva*
Nunc™ MaxiSorp™ ELISA plates	*Thermo Fisher Scientific Inc.*

Petri dishes, 92x16 mm und 150x20 mm	*Sarstedt AG & Co. KG*
PureYield™ Plasmid Midiprep System	*Promega corporation*
Reaction tubes, 1.5 / 2 ml	*Sarstedt AG & Co. KG*
Strep-Tactin®XT 4Flow® resin	*IBA Lifesciences*
Wizard Plus® SV Minipreps DNA Purification System	*Promega corporation*
Wizard® SV Gel and PCR Clean-Up System	*Promega corporation*

5.13 Software

Software	**Supplier**
BioRender	*Science Suite Inc.*
ChemDraw	*PerkinElmer Inc.*
ChimeraX	*UCSF Resource for Biocomputing, Visualization, and Informatics*[206]
FlowJo	*Becton, Dickinson and Company*
GraphPad PRISM	*GraphPad Software Inc.*
mMass - Open Source Mass Spectrometry Tool	*By Martin Strohalm © 2010-2023*
SnapGene	*Dotmatics*

5.14 Instruments

Device	**Manufacturer**
ÄKTA Start	*Cytiva*
ÄKTA Purifier UPC-900 P900 Frac-920	*Cytiva*
BD Influx™ Cell Sorter	*Becton, Dickinson and Company*
BioSpec-nano Micro-volume UV-Vis Spectrophotometer	*Shimadzu Cooperation*
CLARIOstar Plus	*BMG LABTECH GmbH*
CytoFLEX	*Beckman Coulter Cooperation*
GelDoc-It 2 Imaging System	*UVP LLC*
Infinite® 200 PRO	*Tecan Group AG*
LC-MS-2020	*Shimadzu Cooperation*

NanoDrop™ One/OneC	*Thermo Fisher Scientific Inc.*
NGC Quest system	*Bio-Rad Laboratories Inc.*
Series 1100 HPLC system	*Agilent Technologies Inc.*
Series 1260 HPLC system	*Agilent Technologies Inc.*
SH800S Cell Sorter	*Sony Biotechnology*

6 Methods

6.1 Microbiological methods

6.1.1 Sterilization of solutions and media

Sterilization of heat-stable solutions was carried out for 20 min at 121°C and 2 bars. Antibiotics were added after cooling of the solution. Sterile filtration was done with heat-labile solutions by 0.2 μm syringe or bottle top filters.

6.1.2 Determination of optical density

Photometric measurement of optical density was performed at 600 nm (OD_{600}) to get information about the growth state of a certain culture. Cultivation media served as a blank and cultures were diluted 1:10 if the OD_{600} was > 1.

6.1.3 Cultivation of *E. coli*

Cultivation of *E. coli* was done on agar plates or in liquid medium. For agar plate cultivation, cells were generally spread out on antibiotic containing dYT agar plates and incubated overnight to obtain single colonies. Plates were stored at 4°C. For submerged cultivation a single E. coli colony was inoculated into antibiotic containing dYT medium and cultivated overnight at 37°C and 180 rpm. The culture was further used to inoculate a recombinant production or isolate plasmids.

Table 6: Working concentrations of different antibiotics used for microbial selection.

Antibiotic	Final concentration [μg/ml]
Ampicillin	100
Chloramphenicol	25
Kanamycin	75
Tetracycline	20

6.1.4 Cultivation of *S. cerevisiae*

Cultivation of *wild type S. cerevisiae* was done in liquid YPD medium or YPD agar plates containing an antibiotic of choice to prevent growth of bacterial contaminations. For selection of transformed yeast cells, SD_{-Trp} or SG_{-Trp} media were used, also incorporating exhibiting an antibiotic of choice. Incubation in liquid medium was carried out at 30°C and 180 rpm until turbidity was visible (usually after 1-3 days). Cultivation of agar was also done at 30°C until colonies were visible (1-3 days). Storage happened at 4°C.

6.1.5 Cryopreservation

For cryopreservation cells from a liquid culture were taken. After centrifugation at 4000 × g, cells were resuspended in a small volume of medium (~ 500 µl). For *E. coli* 10 % DMSO, for *S. cerevisiae* 50 % glycerol was added. Sample tubes were stored at -80°C.

6.2 Molecular biological methods

6.2.1 Determination of DNA concentration

DNA concentrations were measured at 260 nm with *NanoDrop One* (*ThermoFisher*) or *BioSpec-nano*^{TM} (*Shimadzu*). The ratio of A260/A280 and A260/A230 gave information of e.g., protein or ethanol impurities. A value of ~ 1.8 resembles a pure DNA preparation.

6.2.2 Plasmid isolation

Conventional *E. coli* plasmid isolation was carried out with *PureYield*^{TM} *Plasmid Miniprep System* (*Promega*) in accordance to the manufacturer´s protocol. When high plasmid yields were required *PureYield*^{TM} *Plasmid Midiprep System* (*Promega*) was conducted. Incorporating an endotoxin wash, this plasmid preparations was also suitable for cell culture transfection.

Plasmid isolation from yeast cells was performed using *Zymoprep Yeast Plasmid Miniprep Kit* (*Zymo research*), also in accordance with the manufacturer´s protocol.

6.2.3 Agarose gel-electrophoresis

Agarose gel-electrophoresis is used to separate DNA size-dependently. For preparation of a gel up to 2% (w/v) of agarose was dissolved in 1x TAE buffer and mixed with HDGreen. Samples were diluted 6:1 with Gel Loading dye (*New England BioLabs*) and were applied to the gel. Separation was carried out at 120 V until dye front reached at least half of the gel. Visualization was done with ultraviolet light.

6.2.4 DNA cleavage with restriction enzymes

Cleavage of plasmids and inserts for conventional or gap repair cloning was done with restriction enzymes. Therefore, reactions were performed according to the supplier's manual. Generally, 1 U of enzymes hydrolyzes 1 µg of DNA within 1 h at 37°C. Usually DNA amounts were used in extend of the applied enzyme units; however, digestions was carried out overnight.

6.2.5 Polymerase chain-reaction (PCR)

The polymerase chain-reaction[207] was applied to amplify small amounts of DNA or for analytical purpose in a colony PCR. In this work the thermostable polymerases *Q5® High-Fidelity DNA-polymerase* (*New*

England BioLabs) and *OneTaq® DNA polymerase* (*New England BioLabs*) were used according to Table 7. Temperatures for denaturation and elongation were used as described by manufacturer´s manual. Annealing temperatures were determined with *NEB Tm calculator*[208]. PCR products were always analyzed via agarose gel.

Table 7: Reaction composition for conventional PCR using *OneTaq®* or *Q5®*-polymerase

Reagents	*OneTaq® DNA polymerase*	*Q5® High-Fidelity DNA-polymerase*
Template < 100 ng	1 µl	1 µl
Primer forward 10 µM	1 µl	2.5 µl
Primer reverse 10 µM	1 µl	2.5 µl
dNTP-mix 10 mM	1 µl	1 µl
Reaction buffer	10 µl (OneTaq® Quick-Load® Reaction Buffer)	10 µl (Q5® reaction buffer)
H_2O	35.5 µl	32.5 µl
Polymerase	0.5 µl (2.5 U)	0.5 µl (1 U)

Colony PCR was carried out to primarily investigate a successful introduction of a DNA insert into a vector. Therefore, colonies of *E. coli* or *S. cerevisiae* were picked and mixed with 10 µl of H_2O or 20 mM NaOH, respectively. After incubation at 95°C for 15 min, 1 µl of the lysate was used as a template with the composition listed in Table 8. To distinguish between successful introduced inserts and unmodified vectors, primers were selected carefully. PCR product was also evaluated by agarose gel.

Table 8: Composition of a colony PCR sample. Usually, a master mix for at least eight reactions was prepared. After aliquotation á 24 µl the lysate was added, and sample was used directly for PCR.

Reagents	*OneTaq® DNA polymerase*
Template – cell lysate	1 µl
Primer forward 10 µM	0.5 µl
Primer reverse 10 µM	0.5 µl
dNTP-mix 10 mM	0.5 µl
Reaction buffer	5 µl (OneTaq® Quick-Load® Reaction Buffer)
H_2O	17.38 µl
Polymerase	0.125 µl (2.5 U)

6.2.6 Error-Prone PCR

Error-Prone PCR was carried out using the *GeneMorph II Random Mutagensis* Kit (*Agilent*) in accordance with the manufacturer´s protocol. For randomization of microID, three individual PCRs with different mutation rates ranging from low to high were performed. Subsequently, PCRs were united, purified and used as template for conventional PCR.

6.2.7 Purification of PCR products or hydrolyzed plasmid DNA

After successful amplification of DNA or hydrolyzation of plasmids by restriction enzymes, DNA was purified using *Wizard® SV Gel and PCR Clean-Up System* (*Promega*), following the manufacturer´s protocol.

If DNA could not be amplified without side products and a pure insert was necessary, gel extraction was carried out. Therefore, an agarose gel was done, and the desired band was cut out. The slice was used for DNA extraction in accordance with *Wizard® SV Gel and PCR Clean-Up System* (*Promega*) manual.

6.2.8 Generation of electrocompetent *E. coli*

To obtain *E. coli* cells for electroporation, cells were inoculated in 50 ml dYT medium, usually without antibiotics. After reaching an OD_{600} of ~ 0.7 cells were centrifugated at 4000 × g and washed three times with 50 ml of cold, deionized H2O. Cells were resuspended in 500 µl H2O and used directly for electroporation or stored as cryostocks at – 80°C.

6.2.9 Generation of electrocompetent *S. cerevisae*

To generate electrocompetent yeast cells for library generation, the protocol of Benatuil *et al.* [209] was used.

For a small batch, yeasts were grown in 50 ml YPD at 30°C and 200 rpm to an OD_{600} of ~ 1.0 – 1.3. Subsequently, 1 ml conditioning buffer was added followed by another incubation for 10 min. Cells were washed three times and resuspended in 500 µl with ice cold electroporation buffer. Yeast cells were used directly for electroporation.

6.2.10 Transformation of electrocompetent cells via electroporation

Usually, 50 µl of electrocompetent E. coli cells were mixed with 100 – 1000 ng of plasmid DNA and were transferred to a prechilled electroporation cuvette. Subsequent transformation was carried out with *Gen Pulser Xcell* (*Bio-Rad Laboratories, Inc.*) and an electric pulse (2500 V, 25 µF, 200 Ω). SOC medium was added immediately after electroporation and cells were regenerated at 37°C for 1 h. Bacteria was spread out on agar plates with an appropriate antibiotic.

Electroporation of yeast cells was done comparable to *E. coli*. However, cells were regenerated in YPD medium for 1 h at 30°C.

6.2.11 Restriction-ligation cloning and golden gate cloning

Conventional restriction-ligation cloning was performed with previously hydrolyzed insert and plasmid DNA. Both were mixed in a plasmid-insert-ratio of 1:3. 10x T4-DNA ligase buffer (*New England BioLabs*) and 400 U of T4-ligase were applied. The total reaction volume was 20 μl and the sample was incubated at 16°C for at least 15 min. Form the reaction sample 5 μl were transformed in *E. coli* cells.

Golden gate cloning is a method to efficiently perform DNA fragment assembly and cloning in a one-pot reaction[210,211]. The method is based on type IIS restriction enzymes, removing their own recognition sequence during hydrolyzation by skilled designing plasmid and primer sequences. In a cycle-based restriction and ligation protocol, successfully ligated plasmid is enriched. DNA and insert were mixed in T4-DNA ligase buffer in a plasmid-insert-ratio of 1:3. 400 U of T4-ligase and 30 U of the restriction enzyme were added. Samples were incubated in a PCR cycler applying (37°C for 2 min → 16°C for 2 min) x 30 + 80°C for 20 min. Following, 5 μl reaction were used for transformation in *E. coli*.

6.2.12 Golden gate cloning for assembly of SLE libraries

Generation of SLE phage libraries was done by golden gate cloning. Therefore, pPD1 phagemid, a vector containing the scFv linker sequence and genes of the V_H- and V_L-domain were mixed. Assembly took place in between the three fragments (V_H, V_L, GGGSE-linker derived from pE vector) and the destination vector. PCR cycler was used to perform (37°C for 5 min → 16°C for 5 min) x 30 + 60°C for 5 min. Ligation products were purified by *Wizard® SV Gel and PCR Clean-Up System* (*Promega*) and used for transformation in F^+ *E. coli* cells.

Table 9: Reaction sample (1x) of golden gate assembly for SLE-libraries. For each library containing either κ or λ V_L a 10x sample of the reaction mixture was used.

Reagent	Amount
pPD1 – destination vector	220 ng (3 nM)
pE – linker containing vector	110 ng (3 nM)
Insert VH	30 ng (3 nM)
Insert VL κ or λ	30 ng (3 nM)
SapI	15 U
T4-Ligase	1000 U
T4 Ligase buffer	1x
H_2O	Fill up to 20 μl

6.2.13 Gap repair cloning

Gap repair cloning in yeast is based on homologous recombination. Therefore, linearized vector and a fragment carrying at least 30 bp homologous regions at the 5' and 3' were mixed in an insert-vector-ratio of 5:1 and applied to electrocompetent yeast cells. Subsequently, electroporation was carried out (2500 V, 25 μF, 200 Ω) with *Gene Pulser Xcell* (*Bio-Rad Laboratories, Inc.*). Following steps were performed as for traditional electroporation.

6.2.14 Preparation of yeast genome for amplification

Yeast genome preparation for amplification of the yBL gene was done as described by Lõoke *et al.* in 2011[212].

6.2.15 DNA sequencing

For determination of successful cloning, DNA sequencing was used as a final validation. Sequencing was done at *SeqLab Göttingen GmbH* using Sanger sequencing[213]. Therefore, 500 - 1200 ng of plasmid DNA were mixed with 30 pmol of a primer.

6.3 Protein chemical methods

6.3.1 Determination of protein concentration

Protein concentrations was determined by measuring the extinction at 280 nm using *NanoDrop One* (*ThermoFisher*) or *BioSpec-nano*^{TM} (*Shimadzu*). Respective extinction coefficient were calculated by *Expasy ProtParam*[214].

6.3.2 Sodium dodecyl sulfate-polyacrylamide gel electrophoresis (SDS-PAGE)

SDS-PAGE is one of the standard methods in protein chemistry. First mentioned by Laemmli 1970 [215] this method is used to separate a mixture of proteins based on their size/molecular weight. An acrylamide SDS-gel consists of a 15 % separation and a 4 % stacking gel. For analysis, a sample was mixed with SDS-loading dye and heated up to 98°C for 5 min. After loading of the gel, proteins were separated applying 300 V and 45 mA until the dye front reached the end of the gel. Usually, the gel was stained with Coomassie brilliant blue or was used for a western blot.

Table 10: Recipe for one acrylamid SDS-gel

	Stacking gel 4 %	Separation gel 15 %
Rotiphorese 40 (37.5:1)	2.4 ml	13 ml
Separation Tris buffer	-	6.5 ml
Stacking Tris buffer	3.6 ml	-
dH_2O	8.4 ml	6.5 ml
TEMED	10.8 μl	9.8 μl
APS 10 % (w/v)	130 μl	195 μl

6.3.3 Western blot

Western blot is a method for immune-based detection of proteins. Therefore, an unstained acrylamide SDS-gel is used and blotted onto a nitrocellulose membrane by applying 25 V and 300 mA for 35 min. Subsequently, the membrane was saturated and blocked with 3 % of skim milk powder in PBS-T for 1 h. Following, a primary antibody and subsequently a secondary antibody or streptavidin conjugated with alkaline phosphates were each applied for 1h in 15 ml PBS-T. In between each handling step the membrane was washed three times with PBS-T. Staining reaction was carried out with 15 ml AP-buffer containing 75 μl 5-Bromo-4-chloro-3-indolyl phosphate (BCIP) (50 mg/ml in DMF) and 25 μl nitro blue tetrazolium chloride (NBT) (75 mg/ml in 70 % DMF) until protein bands were visible. Reaction was stopped with 10 % acetic acid.

6.3.4 Recombinant expression of proteins

Expression of proteins was carried out in *E. coli* BL21 (DE3) or *E. coli* BL21 Gold cells. One day before expression, an overnight culture was prepared by inoculating cells in 50 ml dYT with antibiotics. This culture was used to inoculated 1 L of TB-medium with antibiotics to an OD_{600} of 0.1. The main culture was incubated at 37°C and 200 rpm until OD_{600} reached ~ 0.6. Protein expression was induced by the addition of 0.5 mM (final) IPTG and was carried out overnight at 25°C. The next day, cells were harvested by centrifugation at 4000 × g. The centrifugate was either stored at -80°C or was directly used for purification.

6.3.5 Cell lysis

In order to lyse *E. coli* cells sonification was performed. Therefore, cell centrifugate was resuspended in 25 ml of the primary purification buffer, usually IMAC A. Sonification procedure was carried out at ~50 % of maximal power five times with one minute pause in between. Subsequently, the lysate was centrifugated at 15000 × g for 20 min at 4°C and the supernatant was filtered with an 0.4 μm syringe filter. The sample was ready for purification.

6.3.6 Protein dialysis

Proteins were dialyzed to remove salts or buffer components derived from purification e.g., imidazole or citric acid. The protein solution was filled into dialysis tube with a smaller molecular weight cut off than the protein of interest and was dialyzed against 5 L of the desired buffer. Usually, biotin ligases were dialyzed against 50 mM Tris pH 7.5, 150 mM NaCl and 5 mM $MgCl_2$ and antibodies against PBS.

6.3.7 ELISA-based biotin ligase activity assay

Activity of biotin ligase was performed in an ELISA-based assay. To begin with a 96 well Nunc MaxiSorp™ (*Thermo Fisher Scientific*) microtiter plate was coated with 200 μl of 40 mg/ml bovine serum albumin fraction V (BSA) solution for 1 h. Plate was washed three times with PBS-T. Subsequently, the biotinylation reaction was carried out by addition of prewarmed 2.5 mM ATP, 50 μM biotin and 2.7μM (0.06 mg/ml) biotin ligase in 50 mM Tris, 150 mM NaCl and 5 mM $MgCl_2$ for 10 min at 37°C. Afterwards the reaction was stopped with 0.25 M EDTA and three following washing steps with PBS-T were conducted. 50 μl of streptavidin-alkaline phosphatase conjugate (1:5000) solution was added and incubated for 1 h. Next, wells were washed again three times and equilibrated with AP-buffer. Staining was carried out for 20 min using 1 mg/ml para-nitrophenyl phosphate in AP-buffer. Subsequently, absorbance was measured at 405 nm using *TECAN Infinite® 200 PRO* or *BMG LABTECH CLARIOstar Plus*. The method was slightly adapted when non-promiscuous enzymes were measured. Hereby, 50 μM p67, 5 mM $Mg(OAc)_2$, 5 mM ATP, 1 mM biotin and 5 μM biotin ligase were mixed in PBS and incubated for 2 h at 37°C. Afterwards, the reactions mixture was coated onto a 96 well Nunc MaxiSorp™ (*Thermo Fisher Scientific*) microtiter plate for 1 h. The microtiter plate was washed three times with PBS-T and the protocol was continued as mentioned above, with the addition of streptavidin-alkaline phosphatase conjugate.

6.3.8 Biotin ligase meditated protein conjugation

Protein conjugation by different biotin ligases was performed to modify p67 fused trastuzumab with biotin derivatives. The enzymatic reaction was usually carried out at 37°C overnight. If not stated differently following components and concentrations were applied (Table 11).

Table 11: Reactants for biotin ligase meditated conjugation.

Component	Final concentration
p67 modified protein	As desired
Bicine, pH 8.0	50 mM
$Mg(OAc)_2$	5 mM
ATP	5 mM
Biotin ligase	0.1 equivalents
Biotin derivative	50 equivalents
H_2O	Filled up to desired volume

6.3.9 LplA mediated protein conjugation

Protein conjugation by LplA was done to introduce click chemistry-based handles into a POI. The reaction was carried out at 37°C for 1 h. Applied components and concentrations are shown in Table 12. When necessary, reaction was stopped using 0.25 M EDTA (final).

Table 12: Reactants for LplA meditated conjugation.

Component	Final concentration
LAP-tagged Protein	As desired
Sodium phosphate, pH 7.0	25 mM
$Mg(OAc)_2$	5 mM
ATP	5 mM
LplA W37V	0.1 equivalents
Substrate	50 equivalents
H_2O	Filled up to desired volume

6.3.10 Determination of on-cell K_D by flow cytometry

Determination of K_D was done to evaluate affinity of trastuzumab-HC:LAP conjugates. Hereby, Her2 positive SK-BR-3 cells were used and aliquoted á $2*10^5$ cells in a 96-well microtiter plate. After three washing steps with PBS containing 1 % BSA (w/v) the antibody conjugates were added in varying

concentrations. Incubation was done for 30 min on ice followed by three consecutive washing steps. The samples containing unmodified trastuzumab-HC:LAP were additionally incubated with 1:100 anti-human IgG phycoerythrin conjugate for 20 min. This was not necessary for the eGFP and rhodamine conjugates. Last, cells were washed three times again and were analyzed by FACS. The normalized fluorescence was plotted against the antibody concentration and was used for determination of the K_D.

6.3.11 LplA mediated chemoenzymatic generation of an ADC

Generation of an ADC by chemoenzymatic conjugation with LplA was carried out in accordance with 6.3.9. After enzymatic conjugation the BCN activated trastuzumab-HC:LAP was purified by a protein A spin column (*Cytiva*) and the antibody was retained in an immobilized state. Subsequently, 50 equivalents of azido-Val-Cit-PAB-MMAE were added and conjugation was performed at 37°C overnight. The ADC was eluted from protein A column with protein A elution buffer and directly neutralized by addition of 1 M Tris-HCl pH 9.0. Subsequently the protein was dialyzed against PBS and concentrated using ultracentrifugation.

6.3.12 CuAAC and SPAAC to address biotin derivatives

For modification of enzymatically activated antibodies CuAAC or SPAAC was performed. To carry the former out $CuSO_4$ was mixed with 2 equivalents ascorbic acid and if desired 6 equivalents of BTTAA, separately. Next, 1 – 10 equivalents of Cu^+ and 5 – 50 equivalents of the azide bearing TAMRA were added to the previously purified and propargyl biotin functionalized antibody. Reaction was carried out from 1 – 72 h at room temperature or 37°C.

SPAAC was carried out by mixing 5 – 50 equivalents of BCN-TAMRA with the previously purified and desthiobiotin azide functionalized antibody for 72 h at room temperature or 37°C.

6.4 Chromatography methods

6.4.1 Immobilized metal ion chromatography

Immobilized metal ion chromatography (IMAC) is a method to purify poly-histidine tagged proteins. It relies on the ability of the imidazole side chain of histidine's to form complexes with Ni^{2+} ions. As a consequence, His-tagged proteins can bind to the IMAC column and can be separated from a crude lysate or protein mixture. Elution of the protein of interest can be carried out by high concentrations of imidazole (0.25 – 1 M) or a low pH (≤ 4).

IMAC purification were performed on an *ÄKTA Start, ÄKTA Purifier (Cytiva)* or an *NGC Quest system (BioRad)* by applying the protein sample to the HisTrap column (Cytiva). After loading of the sample,

the column was washed with IMAC A buffer until the UV signal stabilized. In order to remove unspecifically bound proteins, another washing step was conducted applying 5 % IMAC B buffer. The protein of interest was eluted by a linear gradient to 100 % IMAC B over 15 min. Elution fractions were analyzed by SDS-PAGE and protein containing samples were dialyzed to remove imidazole.

6.4.2 Protein A purification

Protein A is a 42 kDa protein derived from *Staphylococcus aureus* and binds with high affinity to the Fc-fragment of antibodies. This characteristic is used, to enable specific purification of those immunoglobulins.

Protein A purification were performed on an *ÄKTA Start, ÄKTA Purifier (Cytiva)* or an *NGC Quest system (BioRad)* by applying the PBS mixed cell culture supernatant (1:2 ratio) to the Protein A column (Cytiva). Subsequently, the column was washed with PBS until the UV signal normalized. Elution of the antibody was performed with 100 % of Protein A elution buffer. In order to neutralize the eluate, collection tubes were filled prior to elution with 200 μl 1 M Tris pH 9. Fractions were analyzed by SDS-PAGE and the citric acid / Tris mixture was removed from the antibody by dialysis.

6.4.3 Hydrophobic interaction chromatography (HIC)

Hydrophobic interaction chromatography was used, when conjugation of small molecules to an antibody was performed and reaction success and conjugation quantity needed to be analyzed. Therefore, ~ 35 μg of the antibody was injected into a TSKgel® Butyl-NPR column (*Tosoh Bioscience GmbH*) and absorbance was measured at 220 nm. The sample was eluted using a gradient of 0 to 100 % HIC B buffer over 35 min with a flow rate of 0.9 ml/min.

6.4.4 Reversed phase high-performance liquid chromatography (RP-HPLC)

RP-HPLC was used to determine CuAAC reaction success. Therefore, samples were applied to an Eclipse Plus RP column C-18, 3 µm, 100×4.6 mm, 95 Å (*Agilent Technologies Inc.*). Separation of the samples was monitored by measurement of the absorbance at 220 and 550 nm at a flow rate of 0.6 ml/min. The conducted eluents consisted of eluent A (0.1 % (v/v) trifluoroacetic acid in water) and eluent B (0.1 % trifluoroacetic acid in 90 % (v/v) aqueous acetonitrile).

6.5 Mass spectrometry methods

6.5.1 Liquid chromatography-mass spectrometry (LC-MS)

LC-MS was used to determine CuAAC reaction success. Hereby, sample were separated using a Synergy 4 µm Hydro-RP 80 Å C-18, 250 × 4.6 mm column (*Phenomenex Ltd.*) with a flow rate of 0.7 ml/min. The conducted eluents consisted of eluent A (0.1 % (v/v) formic acid in water) and eluent B (0.1 % (v/v) formic acid in acetonitrile). Mass spectra were obtained by electrospray ionization (ESI).

6.5.2 Matrix-assisted laser desorption/ionization – time of flight (MALDI-TOF/TOF)

MALDI-TOF/TOF was conducted to determine desthiobiotin azide conjugation by PhBL to the light chain of trastuzumab-HC:p67. Analysis was performed in the MS department of the TU Darmstadt using an *Autoflex speed TOF/TOF, Bruker Daltonik* and a 2,6-dihydroxyacetophenone (DHAP) matrix.

6.6 Cell culture methods

6.6.1 Culturing adherent cell lines

Adherent cells were cultured in T25 or T75 flask under standard conditions (37°C, 5% CO_2). Cells were passaged after reaching ~ 90% confluency (generally every 3 – 4 days) cells were passaged. Therefore, cells were washed with 5 – 10 ml of PBS. Subsequently, 0.5 – 1 ml of trypsin/EDTA solution was applied and incubated at 37°C until cells detached from the flask surface. This was controlled by microscopy. Addition of 4 times the volume of serum containing medium stopped the trypsin reaction. Afterwards, cells were diluted 1:4 to 1:10 and the flask was filled up with pre-warmed medium. Incubation of cells was continued until the next passage.

6.6.2 Expression of antibodies

Expression of antibodies was performed in *ThermoFisher Scientific* HEK Expo293F™ cells. Prior to transfection with a mammalian expression vector (usually pTT5), cell titer was set to 2.5 – 3*10^6 cells/ml. Plasmids encoding for the heavy or light chain of the antibody were mixed together with polyethylenimine (PEI). Dependent on the expression scale, 25 or 50 μg of each plasmid and 120 or 240 μg of PEI were used for 30 or 60 ml expression cultures, respectively. The DNA-PEI mixture was incubated for 20 min at room temperature and was added to the cells while the flask was constantly swayed. Expression was carried out for 5 days at 37°C, 125 rpm and 8 % CO_2. The day after transfection 0.85 or 1.7 ml of sterile 10 % tryptone solution was added to the cells. For purification of the antibody cells were centrifugated at 4000 × g and supernatant was sterile filtered to remove remaining cells or debris. With this, supernatant was ready for Protein A chromatography.

6.6.3 Generation of stable HeLa cell line

For generation of a stable HeLa cell line expressing the biotin ligases microID or ultraID, a FLP-recombinase based method was performed. In general, the workflow was completed as described in the original paper by Weidenfeld *et al.*[216] and [217]. HeLa EM2-11ht cell line needed for this approach was kindly provided by the Béthune group in Hamburg, formerly Heidelberg.

In brief, $5*10^5$ cells were seeded 24 h before transfection in DMEM containing 10 % FBS, 1 % penicillin-streptomycin, 0.2 mg/ml G418 and hygromycin. Transfection of 2 μg of the plasmid of interest and 2 μg of pPGKFLPobpA (Addgene 13793) coding for the Flp recombinase was mediated by Lipofectamine 2000, following the manufacturer´s manual. The following day, cells were passaged in a 10 cm petri dish and cultivated in DMEM mentioned above without hygromycin selection marker. After 2 days, medium was changed to DMEM containing 10 % FBS, 1 % penicillin-streptomycin, 0.2 mg/ml G418 and 40 μM ganciclovir. Cultivation was continued for 7 days or until single cell colonies were formed. Ganciclovir leads to cell death, where no recombination event happened. For each transfection, six single colonies were isolated by cloning cylinders, seeded in 24 well plates and expanded further for a week. After passaging in a T25 cell culture flask, stable HeLa cells were ready for analysis of protein of interest expression.

6.6.4 Cell proliferation assay

As a functional test of the generated ADCs, a cytotoxicity assay was conducted. Therefore, 0.5 - $1*10^4$ HER2-positive SK-BR-3 and HER2-negative CHO cells were seeded in a 96-well microtiter plate. After incubation for 24 h at 37°C and 5 % CO_2 cells were treated with the respective ADC or unconjugated antibody as negative control and incubated further for 72 – 80 h. Afterwards cell proliferation was determined using *CellTiter96® AQueous One Solution Cell Proliferation Assay (Promega)* in accordance with manufacturer´s protocol.

6.7 Yeast surface display

6.7.1 Induction of surface presentation

Expression of the protein of interest on the yeast surface was regulated *via* the Gal1,10-promotor. Therefore, surface presentation could be induced in the presence of galactose and absence of glucose. Usually, a yeast culture, previously cultivated in SD medium, was inoculated to an OD_{600} of 1 in a 50 ml flask containing SG_{-trp}-medium and was incubated over-night at 30°C and 180 rpm. Yeast on agar plates

were either cultivated in SD_{-trp}-medium before being transferred to SG or were directly inoculated in autoinduction medium (mixture of SD and SG 1/5).

6.7.2 Generation of a yeast surface display library

Yeast surface display library generation for directed evolution of microID was done as described by Benatuil *et al.*[209].

6.7.3 Yeast surface biotinylation assay (YSBA)

For a yeast-surface biotinylation assay $5*10^7 – 1*10^8$, yeast cells were transferred to a micro reaction tube and were washed twice with PBS. The cells were resuspended in 1 ml PBS and 50 μM biotin and 2.5 mM ATP were added. Incubation was carried out for 17 h at 30°C and 900 rpm to prevent settling of the cells. Afterwards, cells were washed twice and stained in 100 μl of PBS. This was using anti-penta His antibody (1:100) and streptavidin APC conjugate (1:100). As a secondary antibody, an anti-mouse FITC-conjugated antibody (1:50) was used. For the propargyl biotin screens NeutrAvidin Dylight™ 650 was applied 1:100 as well as the self-generated Avidin-ATTO 647 conjugate, which was used 1:20. Finally, cells were resuspended in 1 ml of PBS being ready for FACS.

6.8 Phage display

6.8.1 Generation of phage display libraries

E. coli F^+ cells were grown in 300 ml dYT medium supplemented with 20 μg/ml tetracycline. Upon reaching an OD_{600} of ~ 0.6 cells were centrifuged for 10 min at 4000 × g. Subsequently three washing steps with ice cold dH_2O were conducted and ultimately cells were resuspended in 1 ml of H_2O. For transformation 90 μl cell suspension was mixed with 10 μl of golden gate assembled pPD1-scFv vector and electroporated using 2500 V, 25 μF, 200 Ω. For regeneration each electroporation was directly mixed with 1 ml of prewarmed SOC medium and incubated at 37°C for one hour at 180 rpm. Last, cells were serially diluted 1:10 for nine times to determine the libraries diversity and remaining cells were plated out on 30 cm agar plates containing dYT supplemented with ampicillin and tetracycline. The next day cells were scraped off and stored at – 80°C after addition of 10 % DMSO.

6.8.2 Amplification of M13KO7 helper phage

In general, throughout this work *E. coli* XL1-blue and ER2738 were used as hosts for phage generation and titer determination, since both express the F-pilus.

For amplification of M13KO7 helper phage, a freshly grown *E. coli* culture (OD_{600} ~ 0.4) was aliquoted á 200 μl and mixed with 10 μl of different M13KO7 phage solutions, which were serially diluted 1:10

priorly. Mixtures were incubated for 30 min at room temperature and were subsequently added to 3 ml of molten top agar (45°C), which was poured on pre-warmed dYT-agar plates. The next day, a small plaque was picked into 5 ml of a freshly grown F^+ *E. coli* culture. After incubation for 2 h at 37°C this culture was transferred into a 2 l flask with 500 ml dYT medium and further incubated for 1 h. Subsequently, kanamycin was added, and cultivation was continued over night at 30°C and 200 rpm. The next day, the culture was centrifuged, and 1/5 volume phage precipitation buffer was added to the supernatant. The sample was incubated for 1 h at 4°C in the fridge and was subsequently centrifuged at 4000 × g for 45 min. The centrifuge beaker was stored upside down to remove excess phage precipitation buffer from the obtained phage pellet. Next, the pellet was resuspended in 10 ml of PBS and the whole procedure was repeated, starting with addition of 1/5 volume of phage precipitation buffer. The final M13KO7 pellet was resuspended in 5 ml PBS and centrifuged at 13000 × g to remove remaining *E. coli* cells. Titer of M13KO7 was determined and the final product was mixed with 50 % glycerol and stored at -80°C.

6.8.3 Packaging of phage libraries

Packaging of SLE libraries was performed as described by Kügler *et al.*[218].

6.8.4 Titer determination

For phage titer determination the phage solution was serially diluted 1:100 for six times (10^{-2} to 10^{-12}) in sterile PBS buffer. 10 μl of the solution was added to 90 μl of freshly grown F^+ *E. coli* cells ($OD_{600} \sim 0.4$) and incubated for 30 min at room temperature. Afterwards, the sample was plated out on dYT agar plates containing either ampicillin (SLE libraries) or kanamycin (M13KO7). The next day, each colony represented one colony forming phage (cfu).

Additionally, to the serial dilution and infection of *E. coli,* spectrometric determination of phage titer was performed using this formula[219,220]:

$$\frac{Virions}{ml} = \frac{(A_{269} - A_{320}) * 6 * 10^{16}}{bases\ phage\ genome}$$

Determination of phage titer via serial dilution was conducted when the expected titer was low or phage containing solutions exhibited impurities e.g., proteins or cell fragments. Spectrometric determination was performed when a pure phage preparation existed.

6.8.5 Incubation of M13 phages on mammalian cells

For incubation of M13 phages on mammalian cells, methodology was adapted from Kim *et al.*[187]. Experiments done in 7.5.1 and 7.5.3 were performed exactly as described in the publication except from

incubation with serum-free DMEM medium (instead of TOM™) and washing of the cells at room temperature (instead of 25°C).

For screening with microID / ultraID expressing cells, HeLa-EM2-11ht were seeded in a 6-well plate to a final cell count of $0.3*10^6$ cells/well. After 24 h expression of biotin ligase was induced by addition of 1 μg/ml doxycycline. As substrate 50 μM biotin was supplemented as well. Subsequently, phages were applied to the cells. The following day washing, and lysis was done in accordance with the protocol of Kim *et al.* Obtained lysates were mixed with 50 μl of Strep-Tactin® agarose bead slurry and incubated at room temperature for 10 min. Beads were washed three times with Strep W buffer and phages were directly eluted in freshly prepared F^+ *E. coli* cells.

7 Results and Discussion

7.1 A novel biotin ligase for proximity dependent biotinylation

Proximity-dependent biotinylation with subsequent mass spectrometry is an important method in protein-protein interaction studies as outlined in the introduction section 3.1.1. It relies on the use of a biotin ligase variant, fused to a protein of interest, that releases biotinyl-AMP. The latter biotinylates nonspecifically proteins in close proximity thus allowing for their identification in frame of defining an interaction network for a given protein analysis. There have been different enzymes used for the widespread approach called BioID[17]. Besides its bulky size, the initial *E. coli* BirA* suffered from slow labeling kinetics and was therefore optimized with yeast surface display[24]. In order to solve both problems, a mutated biotin ligase (R40G) to enable promiscuity derived from *Aquifex aeolicus* was investigated (BioID2)[21]. After deletion of its C-terminal domain, the enzyme (termed microID) should be engineered to improve its catalytic activity by yeast surface display. Since microID was the starting point of this directed evolution approach the enzyme will be termed as “wild-type” variant even though it is drastically different to its original counterpart. This project was a cooperation with the working group Béthune in Hamburg (previously in Heidelberg).

7.1.1 Generation of an error-prone PCR yeast library

In order to enable randomization of the microID biotin ligase gene three individual error-prone PCRs were carried out. Increasing the amount of template, the mutation rate was set from high to low. The purified PCR products were pooled and further amplified by conventional PCR, introducing 30 base pair (bp) flanking overhangs for the pCT destination vector and subsequent gap-repair cloning in yeast. Using the protocol of Benatuil *et al.*[209], a yeast surface display library was generated with a diversity of approximately $8*10^7$ microID variants and an average mutation rate of 2.2 amino acids exchanged per enzyme (Supplementary figure 1).

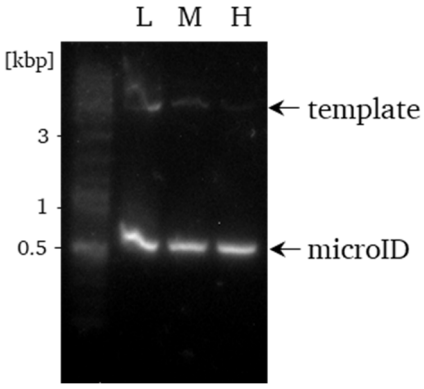

Figure 23: Error-prone PCR of the microID gene. For the randomization of microID three individual error-prone PCRs with different mutagenesis rates ranging from low (L), medium (M) to high (H) were carried out and analyzed by agarose gel electrophoresis.

7.1.2 Screening of improved microID variants

In order to identify enzyme variants capable of faster proximity biotinylation a yeast surface biotinylation assay (YSBA) was performed with the yeast library. Therefore, after induction of biotin ligase gene expression, yeasts were incubated with biotin and ATP, leading to an unspecific biotinylation of the cell surface in correlation with enzyme activity. Subsequently, the cells were stained for surface presentation with an anti-penta His and an anti-mouse FITC antibody for enzyme detection, and a streptavidin-APC conjugate for activity. Cells showing surface presentation and strong activity compared to the "wild-type" enzyme were sorted out by FACS. Following this procedure, three consecutive enrichment rounds were carried out, resulting in 0.77, 2.24 and 0.53 % of the cells being enriched in rounds 1, 2 and 3, respectively.

To begin with the "wild-type" enzyme, it was shown, that 17 h of biotinylation was sufficient for a strong biotin-coupling derived fluorescence signal. This was also true for the initial library, which showed comparable activity (Figure 24 and Supplementary figure 2). However, there were also cells presenting enzyme variants with no or weak activity. This was not surprising since randomization with error-prone PCR is a non-biased and non-rational mutagenesis method and may consequently result in unfunctional proteins.

As the aim of the directed evolution approach was a higher turnover of the enzyme, reaction time was decreased with every enrichment round and for every outcome validation. This led to a loss of activity of the "wild-type" enzyme when reaction times were 1 h or lower (Supplementary figure 2). Interestingly, activity of the library remained almost constant during the whole evolution process indicating enrichment of improved enzyme variants. Additionally, there was a subpopulation after the first and second round that showed no surface presentation but an activity signal. A reason for this could be an unwanted bystander biotinylation of other yeast cells by the biotin ligases, in combination with long reaction times.

Finally, enriched cells in the 3rd round were capable to biotinylate the yeast surface within 10 min (Figure 24). Of the analyzed cells, 49.1 % shifted to the upper right (Q2), whereas for the "wild-type" enzyme there were only 6.39 %. This, once again, emphasizes the assumption of a successful enrichment of improved biotin ligases variants.

Considering the strong activity of the round 3 library compared to the "wild-type", screening was stopped, and single-clone analysis was carried out.

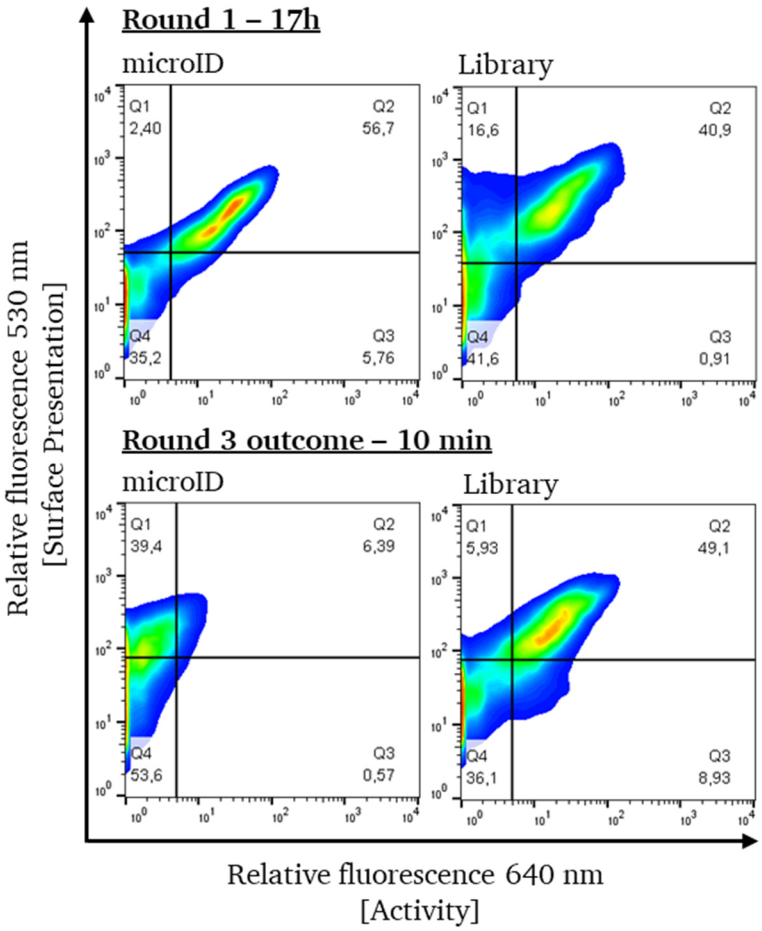

Figure 24: Comparison of initial microID yeast library and outcome of Round 3. For enrichment of improved microID variants, the microID library and yeasts displaying the "wild-type" enzyme were used for YSBA. Hereby, yeast cells were incubated in presence of 50 µM biotin and 2.5 mM ATP and were incubated for decreasing time periods (17h, 1h and 15 min) at 30°C and 900 rpm. Cells showing surface presentation and strong activity compared to the "wild-type" cells were sorted out, cultivated and used again for another enrichment round. This procedure was repeated three times. Surface presentation was stained with an anti-penta His and an anti-mouse FITC antibody (y-axis), activity was evaluated by a streptavidin-APC conjugate (x-axis). Figure taken from [221].

7.1.3 Single clone analysis

After FACS, the microID library was analyzed to identify improved biotin ligase variants. Hence, cells sorted after the third round of screening were subsequently streaked on agar plates. Eight single clones were cultivated and induced in liquid medium, followed by another YSBA and analysis by FACS.

As shown in Supplementary figure 3, all analyzed single clones showed activity after 10 min of surface biotinylation. However, clones 3 and 8 exhibited weaker turnover than all the other clones. Consequently, the remaining six clones were sequenced (Supplementary figure 4), revealing three unique enzyme sequences referred to as variant 1 - 3 (Table 13). Obtaining completely identical clones out of this small sample size implies a successful enrichment during the directed evolution approach and a low remaining library diversity.

Examining the sequencing results variant 2 and 3 showed the same L41P mutation, which might be a reason for the improved activity. Variant 1 carried a single mutation namely L67P, and interestingly, the stop codon at the end of the gene was lost due to a nucleotide deletion leading to a 22 amino acid extension (NSSRSDNNSVDVTKSTLFPLYF) of the protein. This phenomenon was not to be expected from an error-prone PCR, since the stop codon was primer encoded. It is likely that the mutation happened during homologous recombination in yeast. Considering the additional lysine in the amino acid extension, activity improvement could be a result of an additional biotin acceptor in proximity of the enzyme and not due to a higher turnover. Thus, further evaluation of the enzymes, especially variant 1 was crucial.

Table 13: Summary of single clone sequencing. Cells sorted after 3 rounds of screening were streaked on agar plates. Eight single clones were cultivated and induced in liquid medium, followed by another YSBA and analysis by FACS. The six clones showing highest activity during single-clone analysis were sequenced. Clone 1 + 6 (enzyme variant 1) as well as clone 2 + 4 + 7 (enzyme variant 2) revealed completely identical amino acid sequence. Clone 5 (enzyme variant 3) was unique.

Variant	Clone	Mutations
1	1, 6	L67P, mutated stop codon
2	2, 4, 7	S24C, L41P, K169R
3	5	L41P, K115M, K156E

7.1.4 Crystal structure analysis of microID

For a better understanding of the introduced mutations, the enzyme structure was visualized (Figure 25) with ChimeraX and mutation positions were investigated.

To begin with, variant 1 showed one L67P mutation at the beginning of an alpha-helix with some distance to the active site. The influence of this mutation on the activity of the enzyme is hard to estimate. Due to the distance to the binding pockets, it is possible that the effect is low. However, proline has special properties compared to the other 20 canonical amino acids. Its cyclic structure leads to a higher conformational rigidity and is also known as a secondary structure disruptor. An existing proline at the beginning of an alpha-helix may end up in a different arrangement of the overall enzyme structure, ultimately influencing the catalysis efficiency. Thus, impact of this mutations remained unclear.

Next, variant 2 and 3 exhibited many mutations (S24C, K169R, K115M, K156E) being solely surface exposed and in large distance to the active site. Additionally, the exchanges mostly kept the biophysical property of the original amino acid (serin to cysteine: polar; lysine to arginine and lysine to glutamic

acid: charged). Hence, these mutations likely did not influence the overall activity of the enzyme in a significant manner.

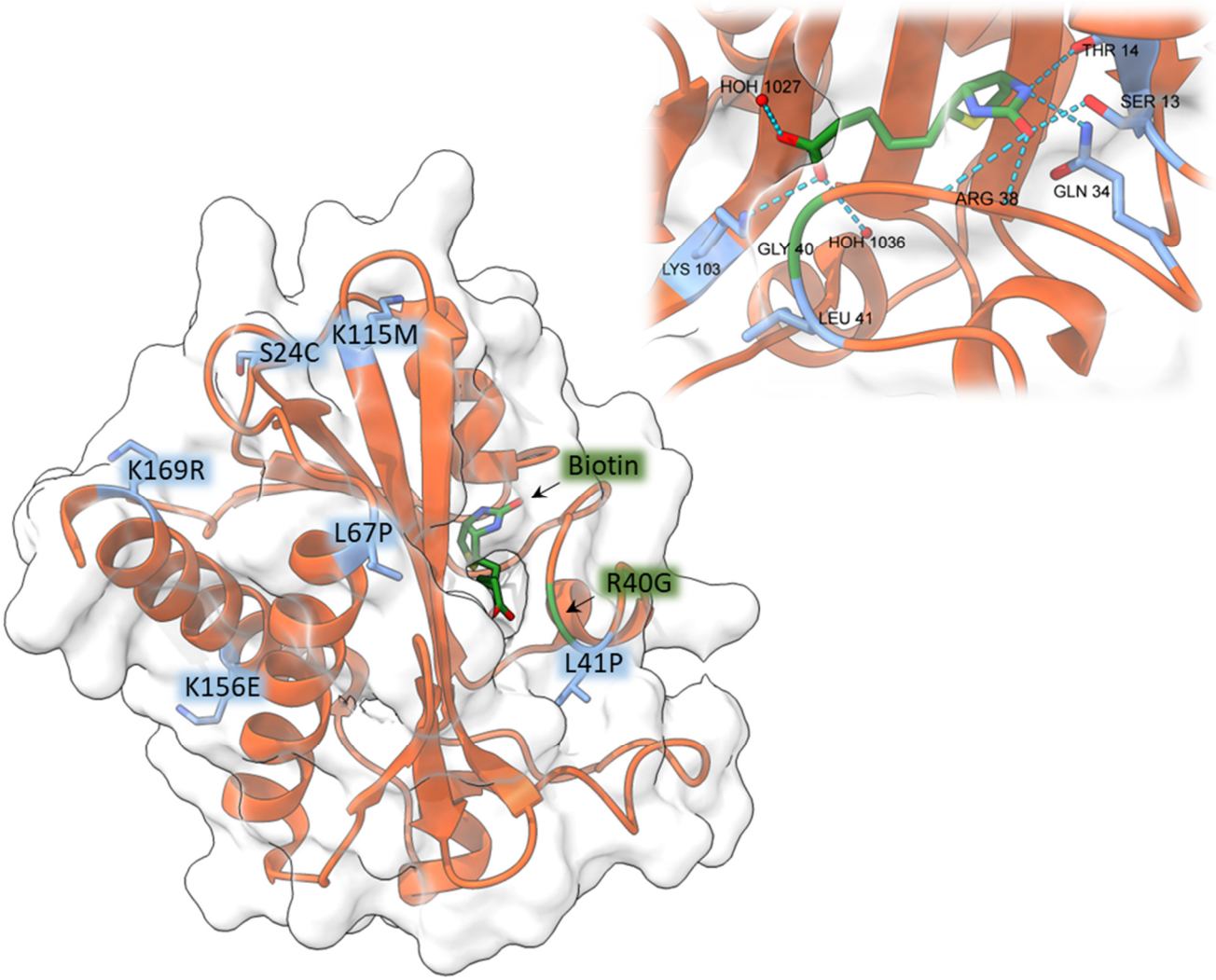

Figure 25: Crystal structure of C-terminally truncated R40G biotin ligase derived by Aquifex aeolicus. Left: Entire biotin ligase. Mutated amino acids of improved variants are highlighted in blue. R40G mutation necessary for promiscuity is marked in green. Right: Zoom into biotin binding pocket. Hydrogen bounds formed to bind biotin are shown. All amino acids forming hydrogen bonds with the molecule and R40G, L41 are labeled. Structure downloaded from RCSB PDB (ID: 3EFR). Visualized using UCSF ChimeraX.

Nonetheless, both variants carry an L41P mutation. This position is close to the active site and biotin binding pocket. In addition, it is next to R40, which must be mutated in order to render the enzyme promiscuous. Similar to variant 1, a proline was the exchanged amino acid, which may have a bigger structural impact than any other amino acid. Being placed in a turn region next to the active site could result in an enlarged entry and facilitate the release of biotinyl-AMP. Considering the results from section 7.1.3 and the structure analysis, mutation L41P was presumably the reason for the improved activity of variants 2 and 3.

7.1.5 Promiscuity verification of microID mutants

As determined by single-clone analysis and sequencing, enzyme variant 1 lost its original stop codon leading to a 22 amino acid extension with an addition lysine. To investigate whether activity resulted from the additional biotin acceptor or the L67P mutation, enzyme variant presenting yeast cell were incubated with 100 mM DTT after YSBA. This treatment reduces the disulfide bonds between Aga1p and Aga2p, releasing the enzyme in the supernatant. If improved promiscuous biotinylation occurred before, the biotinylation is still detectable by streptavidin-APC and FACS. However, preferred self-biotinylation would lead to decreased detectable activity.

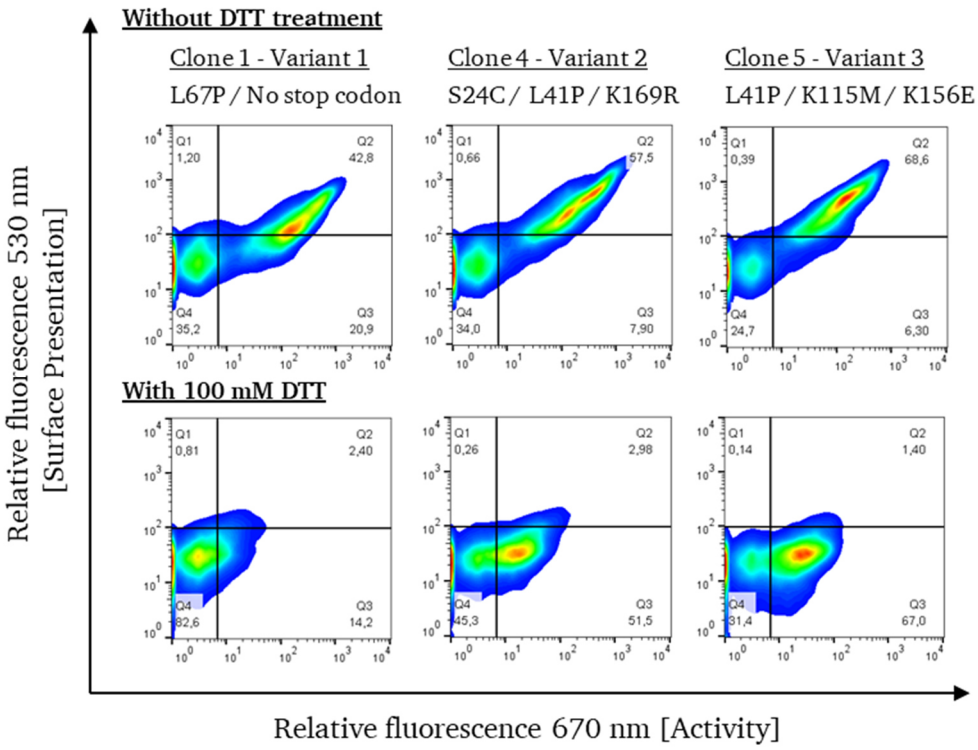

Figure 26: Promiscuity verification of microID mutants. Yeast cells presenting mutant variants 1-3 were used in a YSBA. After two washing steps with PBS, cells were incubated at 30°C for 15 min in presences of 100 mM DTT. Staining was carried out after two PBS washing steps with an anti-penta His, an anti-mouse FITC antibody (y-axis) and streptavidin-APC (x-axis). Analysis was done with FACS. Figure taken from [221].

YSBA revealed a strong activity signal for all tested yeasts presenting an enzyme variant (Figure 26). These results correlate with the single-clone analysis (7.1.3) done after 3rd round of screening. Comparing the DTT treated with the non-treated sample of variant 2 and 3, a strong decrease of surface presentation due to the reduction of disulfide bonds between Aga1p and Aga2p was observed. However, activity remained unchanged (shift Q3 quadrant), which represents a promiscuous biotinylation of the whole yeast surface by the biotin ligase. In comparison no shift occurred for variant 1 after DTT

treatment, supporting the notion that the additional lysine in the 22 amino acids extension served as an easy biotin acceptor.

For additional characterization of the enzymes, solitary expression in *E. coli* was necessary. Since, variant 2 and 3 looked most promising those two were considered further. Variant 2 (S24C, L41P, K169R) was named ultraID-4, whereas variant 3 (L41P, K115M, K156E) was termed ultraID-5.

7.1.6 Expression and stability examination of ultraID variants

In order to characterize the biotin ligase mutants, the enzymes were expressed in *E. coli*. Consequently, genes were amplified from the YSD vector pCT and subcloned into pET22. Additionally, the "wild-type" enzyme microID was cloned. On top of that, a R40G / L41P (microID + L41P) construct and a L41P-only (intact R40) variant was generated with site-directed mutagenesis to further investigate the influence of the L41P mutation. After transformation in *E. coli* BL21 (DE3), production of the enzymes was carried out and subsequently purified *via* IMAC due to the incorporated C-terminal His_6-tag also used priorly for staining on the yeast surface. Purified biotin ligases were dialyzed and analyzed by SDS-PAGE.

Expression of all five enzymes was successful. Yields ranged from 10 – 25 mg enzyme per liter *E. coli* culture. Analysis by SDS-PAGE showed mostly pure enzymes (Figure 27 A). There were some high molecular impurities, however overall enzyme purity was estimated to be > 95%. With the purified enzymes, a thermal shift assay to determine melting temperature (T_M) was performed to investigate any potential mutation impact on the stability of the enzymes. Interestingly, biotin ligase variants exhibited different melting temperatures, even though amino acid sequence was mostly identical. As shown in Figure 27 B, microID and ultraID-K4 had the highest melting temperatures of 64 and 64.5°C, respectively. The latter displayed two individual melting points, which may arise from the S24C mutation and formation of intermolecular disulfide bonds. For the mutants R40G / L41P and L41P-only, a weak decrease in thermal stability was observed to 63 and 60.5°C, respectively. Regarding the L41P-only enzyme the combination of the R40 with P41 may be unfavorable for stability. Of all the tested proteins, ultraID-5 showed the lowest temperature permanence, with a T_M of 52°C. This can be explained by the K115M and K156E mutations, where a charged amino acid was exchanged to a hydrophobic one and a positively charged against a negatively charged, respectively.

All in all, expression of pure enzymes with high yields was successful. While small to significant effects were detectable in thermal stability, even in a solitary state, all melting temperatures were > 50°C, which should be sufficient for protein interaction studies in most living cells.

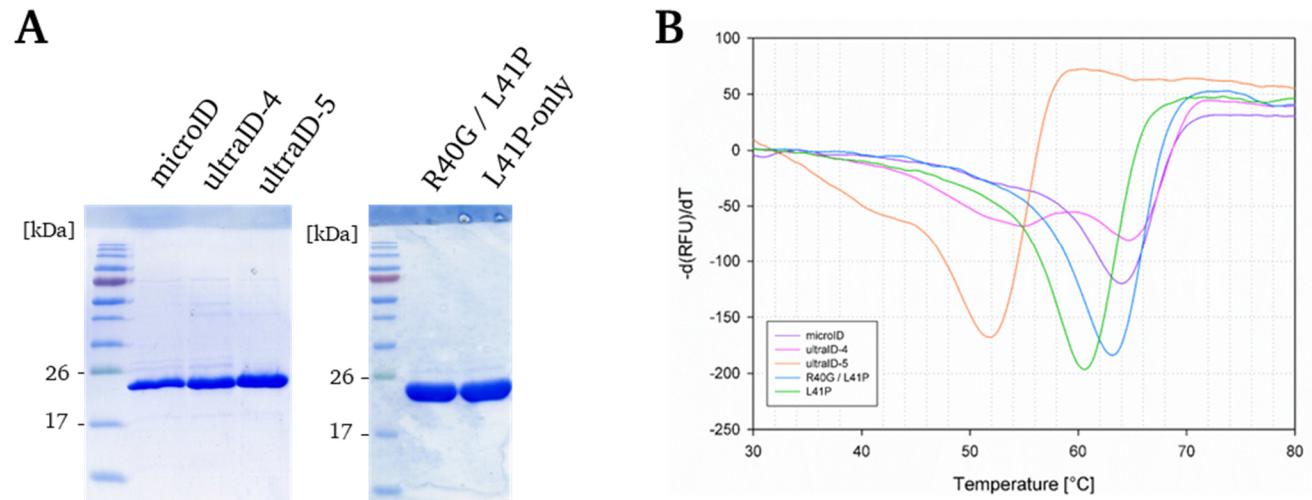

	Melting points [°C]	
microID	64	
ultraID-4	55	64.5
ultraID-5	52	
R40G/L41P	63	
L41P-only	60.5	

Figure 27: Expression of microID and ultraID variants and thermal shift assay for stability investigation. *E. coli* BL21 (DE3) were used for expression of the biotin ligase enzymes. Production was carried out in TB-medium overnight at 30°C. Subsequently, cells were harvested, lysed by sonification and the protein was purified by IMAC. After dialysis enzymes were characterized by thermal shift assay in order to investigate temperature stability. Figure adapted from [221].

7.1.7 ELISA-based biotin ligase activity assay

With the successful expression of microID and ultraID variants activity determination was necessary. Therefore, a microtiter plate was first coated with BSA, and biotin, ATP and a biotin ligase were subsequently added (Figure 28). During 10 min incubation at 37°C, BSA should be biotinylated by the promiscuous ligase. Enzymes with a higher turnover should lead to a higher degree of labeling.

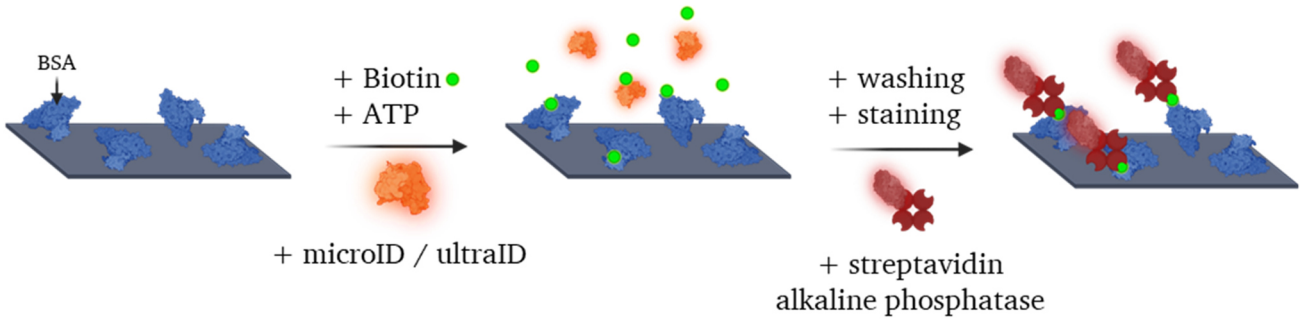

Figure 28: Schematic depiction of the ELISA-based activity assay. A BSA-coated microtiter plate was used for promiscuous biotinylation by microID / ultraID. Therefore biotin, ATP and the enzyme were added to the wells and incubated for 10 min at 37°C. Finally biotinylated BSA was stained with a streptavidin alkaline phosphatase conjugate.

As also determined by YSBA, ultraID variants exhibited improved activity compared to the “wild-type” microID. In this experimental setup ultraID-4 and 5 had improved activity of 167% and 183%, respectively (Figure 29). For the R40G / L41P variant turnover was even higher with 207%. So, L41P could finally be identified as the origin for the activity improvement. At least in this experiment all other mutations found in ultraID-4 and 5 had an unfavorable effect on biotinylation, since R40G / L41P was the best performing enzyme. On top of that, L41P-only had the same effect as the R40G mutation and seemed to be sufficient to render the enzyme abortive. This also led to a stronger activity.

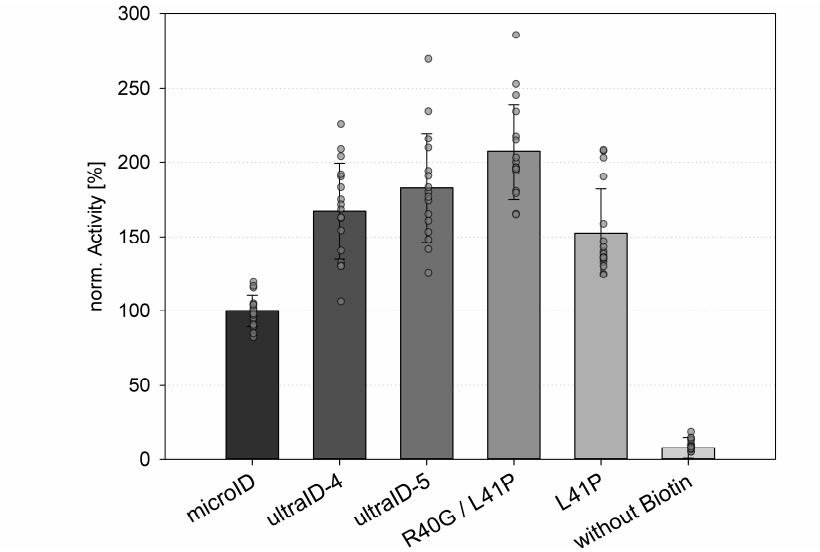

Figure 29: Activity measurement of microID variants with an ELISA-based biotinylation assay. A BSA coated microtiter plate was used for promiscuous biotinylation. Therefore biotin, ATP and the enzyme were added to the wells and incubated for 10 min at 37°C. Reaction was stop by addition of 0.25 M EDTA. Measurements were performed in five individual experiments in triplicates or quadruplicates. Norm. activity refers to the microID absorbance at 405 nm set to 100 %. Error bars indicate standard deviations. Figure taken from [221].

Interestingly, results from YSBA and this experiment were contradictory. On the yeast surface microID displayed neglectable biotinylation when incubation time was less than one hour. The improved ultraID variants showed strong activity even at shorter reaction times of 10 min. Intuitively, these circumstances should end in an improvement factor of at least six. However, the ELISA results displayed an improvement factor of ~ 2. Reasons for this could be a result of the artificial conditions in the ELISA-based assay, where only biotinylation occurring at the bottom of the well was detected. Consequently, the only acceptor for biotin, which was detected, was BSA. Biotinylation occurring in the “supernatant” (mostly self-biotinylation of the enzymes) of the well was washed away during staining of the microtiter plate. This may also hint at the high deviation achieved in this assay. In addition, a saturation of free lysine may happen. As biotinyl-AMP is an unstable molecule, hydrolyzing in water, it is likely that after a certain point of BSA biotinylation hydrolysis reactions became more prominent than the attachment of biotinyl-AMP to a free lysines. In contrast, on the yeast surface new proteins are constantly produced

by the cell and the ratio between enzyme to other proteins is higher, assuming presentation of only ~ 10^5 enzymes per cell[177,222]. In a real proximity-dependent biotinylation assay, saturation of lysines is not possible since the cytoplasm of cells is a dynamic environment and proteins are also expressed and degraded in a constant matter. Thus, while this ELISA-based activity assay may provide a general overview and ranking of activity between different variants, further evaluation might be required with orthologous activity assays.

7.1.8 Summary and interim conclusion

All in all, a novel biotin ligase with improved catalytic properties was investigated originating from a YSD screening. The enhanced turnover could be attributed to a key position/mutation namely L41P. Consequently, all other mutations identified after YSD were redundant which led to the naming of ultraID for the R40G / L41P and C-terminally truncated biotin ligase derived from *A. aeolicus* (see 10.4 Abbreviations for naming of the enzymes). Lastly, testing of the enzyme in authentic PDB experiments was necessary, to ensure that the enzyme was useful for its desired application. These experiments were done by our colleagues in Hamburg, and ultraID outperformed all other known promiscuous biotin ligases used for protein-protein interaction studies[221].

7.2 Screening for propargyl biotin using microID-variants

As shown in the previous chapter evolution of the promiscuous and truncated version of *Aquifex aeolicus* biotin ligase was a straightforward approach. Using this library screening for other substrates was desirable. In 2008, Slavoff *et al.*[143] synthesized different biotin derivatives with additional functional groups. They introduced e.g., an azide or a propargyl group, which are interesting candidates for click-chemistry and possible chemoenzymatic generation of an ADC. Identifying another biotin ligase using this substrate could enable the site-specific introduction into a protein of interest. Therefore, the R40G mutation needed to be reverted after the isolation of interesting variants. For easier screening with YSD, R40G stayed intact at first glance.

7.2.1 Qualitative HABA/Avidin assay

The publication of Slavoff *et al.*[143] showed that binding of propargyl biotin to the binding pocket of a biotin ligase is not trivial, especially in combination with YSD, as the detection method for activity is using streptavidin APC leading to potential difficulties with activity staining. Consequently, binding to streptavidin is also debatable. Since it would be impossible to distinguish if lacking activity is correlated to an enzyme not recognizing the propargyl biotin or a lack of binding by streptavidin, other staining methods needed to be established.

Like streptavidin, avidin is also a biotin binder found in egg white, with the advantage that there is a method to confirm binding of biotin to the molecule. This so-called HABA/Avidin assay is based on the small molecule 4'-hydroxyazobenzene-2-carboxylic acid (HABA), which exhibits an increased absorbance at 500 nm when bound to avidin. Nevertheless, it is displaced in presence of biotin, losing its absorbance. Usually, this assay is used for quantitative determination of biotin in a sample (amount of biotin conjugated to a protein or biotin contamination in a sample). However, in this context it was used as a qualitative evaluation whether binding of propargyl biotin to avidin occurs.

The HABA/Avidin-solution exhibited an absorbance of ~ 0.8 in a non-bound biotin state (Figure 30). Upon addition of biotin, the signal vanished, confirming binding. Remarkably, *cis*- as well as *trans*-propargyl biotin seemed to bind to avidin. Interestingly, *trans*-propargyl biotin showed a better binding to the protein as the *cis* counterpart, likely due to higher steric demand for the latter. As all biotin molecules were dissolved in DMSO, solvent mediated effects were also investigated. While the addition of DMSO also led to a decrease in absorbance, the effect was not as pronounced as for the biotin molecules. With these results confirming the binding of both *cis*- and *trans*-propargyl biotin to avidin, detection of activity for YSD could be considered with an avidin fluorophore conjugate to overcome the aforementioned problems.

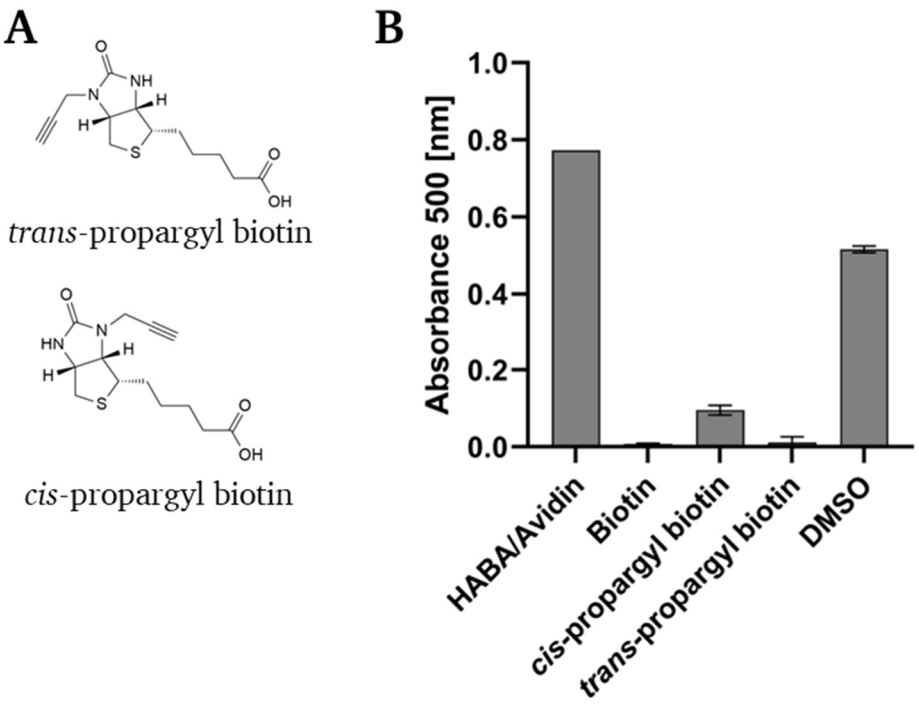

Figure 30: Structure of propargyl biotin derivatives (A) and qualitative HABA/Avidin assay (B). For determination of propargyl biotin binding to avidin a qualitative HABA/Avidin assay was conducted. Therefore, HABA/Avidin solution was mixed with 50 µM of the biotin reagent and absorbance was measured at 500 nm. Error bars resemble standard deviation for n = 3.

7.2.2 Library screening for propargyl biotin using enzymes

Since the HABA/Avidin assay showed propargyl biotin binding to avidin, an avidin-ATTO 647 conjugate was generated. Commercially available avidin was modified by *N*-Hydroxysuccinimide (NHS)-ATTO 647 fluorophore, the conjugate was purified with a PD10 column and subsequently used for staining.

Using microID "wild-type" yeast cells in a YSBA, without a biotin substrate followed by avidin-ATTO-647 staining revealed that the self-generated conjugate was suitable for specific staining as low unspecific binding was observed in the absence of biotin (Figure 31). On the other hand, cells incubated with substrate exhibited a strong shift to the right top (Q2) quadrant of 75.2 %. For the library, which was incubated with a mixture of *cis*- and *trans*-propargyl biotin, a shift of 13.2 % occurred, indicating propargyl biotin turnover. Thus, yeast cells were sorted, and analysis was carried out after cultivation and induction.

As depicted in Figure 31, a population in the lower right quadrant (Q3) was heavily enriched, resembling no surface display but activity. This behavior should not be possible, and a contamination may have likely occurred. However, in the FSC against SSC plot no other population besides yeast debris which usually emerged after the long incubation and many washing steps was detected

(Supplementary figure 5). Repetition of first round sorting led to the same results, with the ultimate origin and identity of this enriched population remaining unclear. Nevertheless, the expected yeast population in Q2 was sorted for a further sorting round. Notably, the outcome of the second screening round showed no activity at all (Figure 31) and was comparable to the negative control without biotin. Since enrichment attempts were repeated various times and no satisfying results could be achieved, screening approaches were stopped.

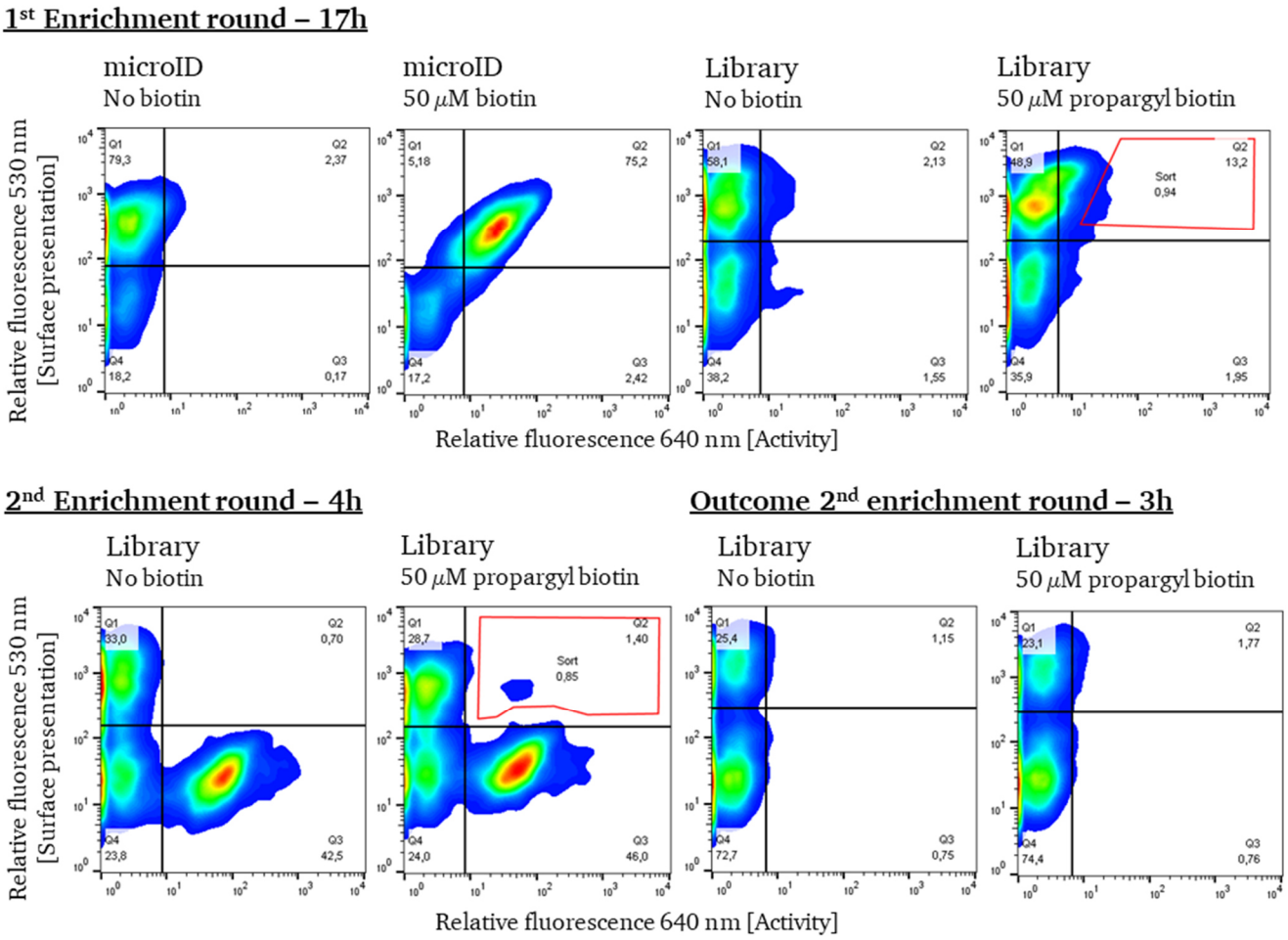

Figure 31: Screening for propargyl biotin using enzymes. For identification of propargyl biotin using microID variants, the error-prone PCR based library was incubated in the presences of 50 µM *cis*-/*trans*-propargyl biotin and 2.5 mM ATP. Two consecutive enrichment rounds were performed. Surface presentation was stained with an anti-penta His and an anti-mouse FITC antibody, activity was evaluated by a Avidin-ATTO 647 conjugate.

Overall, there exist several reasons for the failed enrichment approach. On the one hand, it could be correlated to the enzyme and/or the library itself. It is possible that the active site of the enzyme is sterically not able to bind propargyl biotin, even in a mutated state or that the library did not contain a variant with the right mutations. On the other hand, the YSBA assay was not perfectly established in this context. As there was no positive control on hand, it was not possible to evaluate the FACS signals and

distinguish between actual hits and possible artifacts. Since presented enzymes are remained promiscuous and were not directly applicable for the desired use case, presentation strategy should be changed.

7.2.3 Presentation of biotin ligase-biotin carboxyl carrier protein fusions

To establish a method for non-promiscuous biotin ligase display on yeast cells using modified biotin as substrate, a biotin acceptor was necessary. For this, the *A. aeolicus* naturally occurring biotin carboxyl carrier protein (BCCP) of acetyl-CoA carboxylase was exploited. Hereby, K117 is specifically biotinylated whereas other lysines remain unmodified. With this knowledge in mind three different presentation strategies were analyzed (Figure 32, A). The first construct involves Aga2p as a spacer in between both proteins, linking the ligase to the N- and the acceptor to the C-terminus. For the other two strategies the enzyme plus BCCP were attached next to each other on the C-terminus of Aga2p with varying linkers. Variation of linker sequences $(GGGS)_2$ or $(GGGSE)_3$ should enable more flexibility to enable biotinylation.

Of all three tested constructs, surface presentation was achieved for the $(GGGS)_2$ variant. Even tough presentation of this construct varied intensively during different experiments (Supplementary figure 6, A). The other two formats exhibited very weak to no display (Supplementary figure 6, B).

For activity evaluation of the $(GGGS)_2$ strategy, yeasts were incubated in presence of biotin or *cis- / trans*-propargyl biotin mixture, respectively, overnight. As, BCCP of different species show homology to each other (see Figure 7, C), they are also recognized by different biotin ligases. Therefore, it was important to evaluate whether the presented BCCP may already have been biotinylated upon synthesis and secretion by the yeast endogenous biotin ligase prior to presentation. However, this was not the case, since only a neglectable shift was obtained for the sample with no additionally added biotin (Figure 32, B). Upon addition of 50 μM biotin the shift to quadrant Q2 nearly doubled. However, activity was attributed to 6.25 % of the yeast population. Performance was improved to 12.6 % by addition of the co-factor Mg^{2+}, but overall turnover was weak, considering that this was a single clone and no library. For the propargyl biotin sample weaker activity was obtained. This was expected, however shifting population was comparable to the sample with omitted biotin and could be normal fluctuation of the experiment.

Thus, display of biotin ligase and BBCP did not yield promising results, due to missing presentation or overall weak performance. Besides that, presentation reproducibility of the $(GGGS)_2$ was challenging and an unreliable process. Using a single clone must lead to a robust signal, which is reliable for library

screening. In this case, discrimination between the negative control and the actual sample was challenging and not suitable for an enzyme library screening.

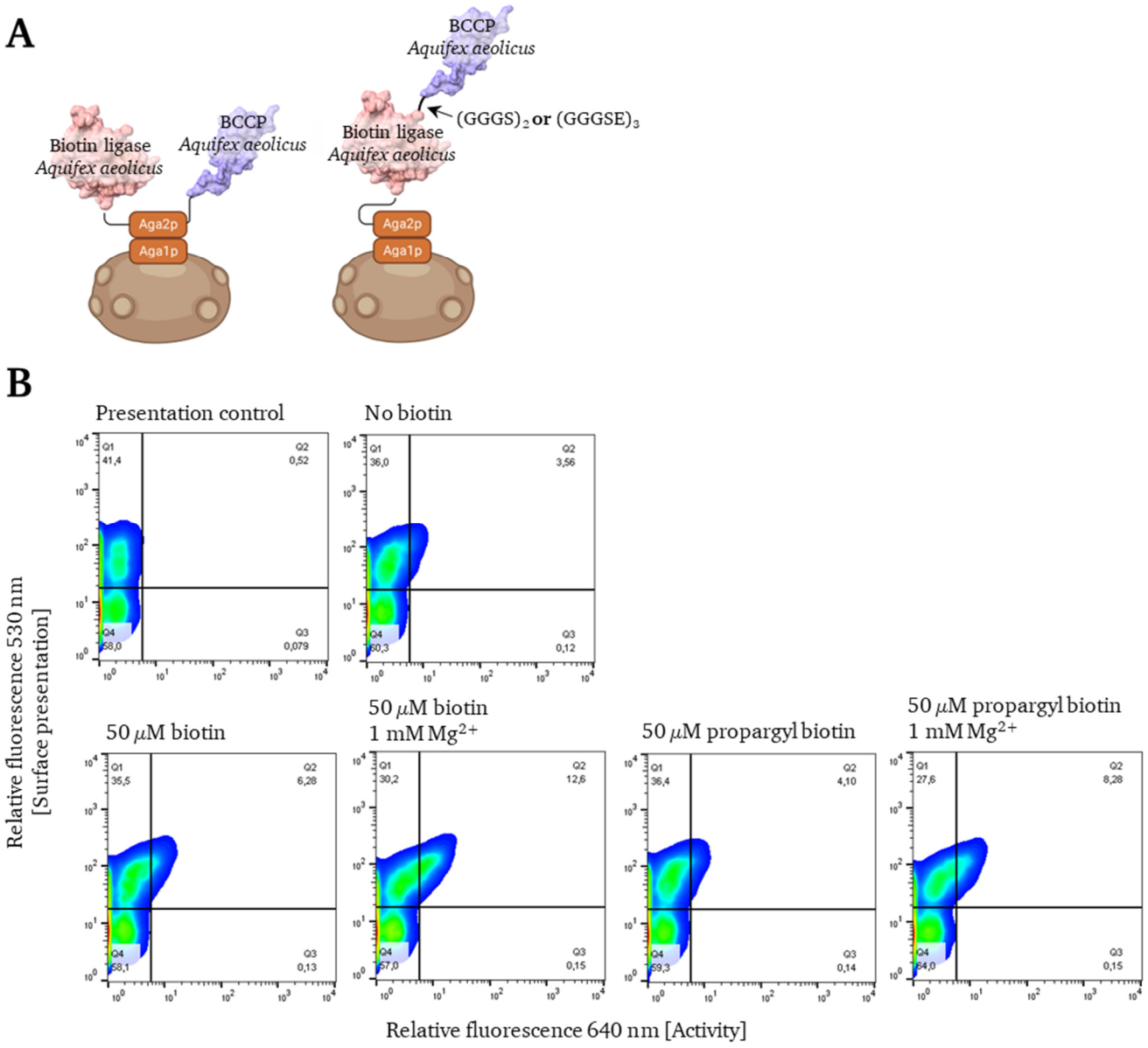

Figure 32: Schematic depiction of *A. aeolicus* biotin ligase-BCCP fusions on yeast surface display (A) and activity assay of *A. aeolicus* biotin ligase and BCCP as fusion protein ($GGGS_2$-construct). Yeast cells were incubated overnight at 30°C and 900 rpm in presence of either 50 µM biotin or a mixture of *cis*-/*trans*-propargyl biotin and 2.5 mM ATP. Impact of magnesium as a cofactor was evaluated by addition of 1 mM $Mg(OAc)_2$. Surface presentation was stained with an anti-penta His and an anti-mouse FITC antibody, activity was evaluated by a Neutravidin-DyLight 650 conjugate.

7.2.4 Summary and interim conclusion

In summary, it was not possible to identify an *A. aeolicus* derived biotin ligase, which was able to use propargyl biotin as a substrate. This might be related to the fact that it is impossible to optimize the binding pocket of the enzyme for this substrate, as the propargyl moiety is sterically demanding and

might not fit in the binding pocket. One could also consider that the right variants for propargyl biotin turnover were not present in the generated library. Diversity was calculated to be $8*10^7$ individual clones, which is relatively small when considering its error-prone PCR origin. As mutations across the whole gene sequence are possible, it is likely, that many mutations are not at the active site where they presumably must be. Furthermore, a changed presentation strategy with the enzyme's natural acceptor domain did not lead to the desired results. Even as a single clone, enzyme activity was not detectable or only very weakly. Consequently, this couldn´t be transferred to a library context. While *A. aeolicus* biotin ligase might be a robust enzyme for BioID, towards other substrates and site-specific protein conjugation it was shown not be suitable.

7.3 Generation of antibody-drug conjugates with biotin ligases

To adapt the strategy for chemoenzymatic ADC generation, a novel approach was initiated based on the identification of two biotin ligases that recognized propargyl biotin. According to published data[143], the enzyme of *Pyrococcus horikoshii* and *Saccharomyces cerevisae* can attach the small molecule to the p67 acceptor domain. Consequently, attachment of p67, which is derived by human propionyl-CoA carboxylase alpha chain, to the C-terminus of either the heavy or the light chain of trastuzumab could be a straightforward way to introduce propargyl biotin to the antibody. Subsequently, a copper click reaction with an azido-MMAE would result in the generation of an ADC. To that point this work was only focused on propargyl biotin conversion, however the desthiobiotin azide molecule would also be an interesting probe enabling SPAAC reaction and therefore being independent of copper ions.

7.3.1 Expression and activity determination of biotin ligases for conjugation

To begin, the respective enzymes for conjugation were required. Therefore, a gene for the *Pyrococcus horikoshii* biotin ligase (PhBL) was order from *Twist Biosciences*, the gene for *Escherichia coli* (EcBL) was already available in the lab, the truncated gene of *Aquifex aeolicus* promiscuous biotin ligase (ΔAaBL) was reverted to the original sequence (introducing the original R40) by site-directed mutagenesis, and lastly the *Saccharomyces cerevisiae* biotin ligase (yBL) gene was amplified from the yeast genome of the EBY100 strain. Sequencing of the yBL gene revealed several mutations in the amplified DNA when comparing it to database entries (For alignment with best BLASTP hit see Supplementary figure 7), either having been introduced during the PCR reaction or enriched by the yeast themselves. As the amino acid mutations mostly retained the same biophysical properties (e.g., hydrophobicity or hydrophilicity), work with the enzyme was continued. Genes were cloned into pET30 or pET22 expression vectors and expressed in *E. coli* cells.

As shown in Figure 33 A all biotin ligases could be identified based on their expected molecular weight after SDS-PAGE analysis meaning successful expression. ΔAaBL and PhBL showed very high purity (> 98%), whereas mayor impurities were obtained for EcBL and yBL. For yBL, it is known that the enzyme is prone to proteolytic degradation[223], explaining other protein bands. Ultimately, yields of ~ 5 – 15 mg were obtained (ΔAaBL > PhBL > EcBL > yBL).

To verify activity of the enzymes, p67 was expressed as a solitary protein and purified with Strep-Tactin® XT to remove already biotinylated protein. Solitary p67 was incubated with biotin, ATP, Mg^{2+} and a ligase for 2 h at 37°C (35°C for yBL) and the reaction mixture was coated on a microtiter plate. An ELISA with streptavidin AP was carried out to quantify biotin turnover.

All enzymes except yBL exhibited activity in biotinylation of p67 (Figure 33 B) with PhBL and EcBL showing the highest activity. Considering the impurities of EcBL sample, one could speculate that the pure enzyme might be even more active. Interestingly, there was also activity in the control without additional ATP. This was not expected since ATP is crucial for catalysis. However, it is conceivable that the enzyme already bound ATP (and biotin) during expression in *E. coli* and can therefore catalyze the reaction once. This hypothesis is supported by the "- biotin ligase" control, where weak signals, most likely due to small amounts of previously biotinylated p67, were observed.

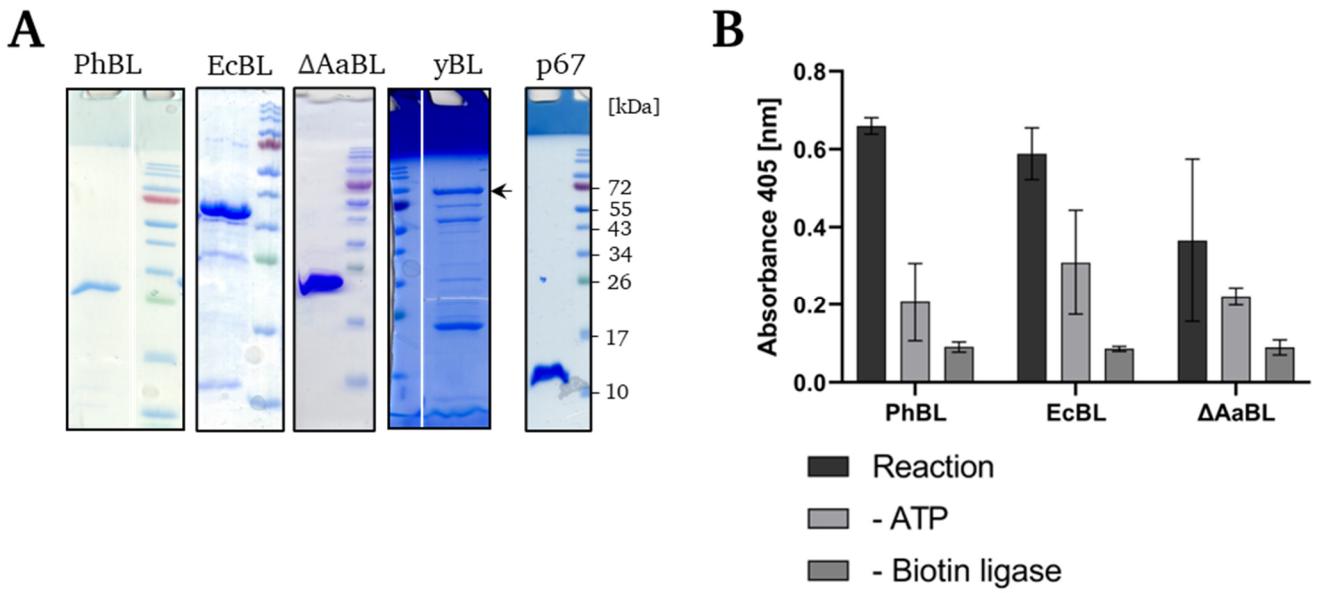

Figure 33: Expression of different biotin ligases (A) and activity assay (B). Biotin ligases from different species were expressed in *E. coli* and purified via IMAC. The dialyzed enzymes were analyzed by SDS-PAGE (← marks full-length yBL) and activity was determined in an activity assay. Hereby, 100 µg unbiotinylated p67 (50 µM) was incubated in presence of 5 mM $Mg(OAc)_2$, 1 mM biotin, 5 mM ATP and 5 µM of biotin ligase for 2 h at 37°C. The reaction mixture was coated on a microtiter plate and an ELISA-based assay using streptavidin-AP was conducted. Error bars resemble standard deviation n=3.

As already mentioned, no activity for yBL was detected (Supplementary figure 8). Literature describes an irreversible inhibition of the enzyme by imidazole[223], which was used to elute the protein from the IMAC column. To evade this, elution by acidic pH (4) was conducted, also leading to no activity. Usage of Tris puffer instead of PBS during biotinylation reaction had no impact on activity. It is possible that the attained mutations are the reason for the missing activity. Consequently, work with the enzyme was stopped at this point.

To sum it up, three of four biotin ligases were produced in sufficient yields and in an active state for further evaluation. As stated in literature it was also confirmed that p67 is recognized by PhBL and EcBL.

On top of that it was shown that the truncated *A. aeolicus* biotin ligase can be used to conjugate biotin to p67.

7.3.2 Conjugation of p67 by various biotin ligases with biotin derivatives

To verify the recognition of propargyl biotin or desthiobiotin azide by PhBL, EcBL and ΔAaBL and a possible chemoenzymatic conjugation approach, p67 was modified by the respective ligase and a biotin substrate. Therefore, the enzyme reaction was performed overnight, excess substrate was removed by purification with magnetic IMAC beads and p67 was further modified by CuAAC or SPAAC with BCN- or N_3-5-(and-6)-Carboxytetramethylrhodamine (TAMRA) (see Figure 34, A).

As shown in Figure 34 modification of p67 with EcBL or ΔAaBL did not result in successful conjugation. No fluorescence was obtained for neither the azide nor propargyl biotin variant, presumably due to the ligase reaction and/or click reaction. Failure of the enzyme mediated modification would imply no downstream turnover of the biotin derivative, while problems with the click-reaction would suggest that, for example, placement of an azide or propargyl function next to the biotin molecule may lead to sterically hindrance. In contrast, modification of p67 by PhBL appeared to work out with the azide substrate as fluorescence was obtained for both samples with desthiobiotin azide (Figure 34, PhBL, lane 3+4). Two samples for the azide substrate were prepared since chemical synthesis led to two purification fractions containing the molecule. Named desthiobiotin azide F1 (Lane 3) and F2 (Lane 4), the latter contains less impurities than the former.

A control reaction with biotin (Lane 1) also showed a weak fluorescence, however this is most likely related to unspecific interaction of the BCN-TAMRA molecule. Additionally, free BCN-TAMRA and p67 run at the same height in SDS-PAGE, making it difficult to distinguish between them. Therefore, the click products needed to be purified before analysis, which included tremendous washing of the magnetic IMAC beads. Nonetheless, TAMRA impurities in the final product were still observed, meaning unreacted BCN-TAMRA could also be an explanation for the stickiness. Interestingly, no signal was obtained for the propargyl biotin substrate. Since, it was shown that the enzyme can use propargyl biotin, the CuAAC reaction most likely failed. This must be evaluated separately in another approach.

With these first encouraging results optimization had to be performed, particularly for CuAAC. Due to the difficult handling of p67 based on its size and purification via magnetic IMAC beads, a possible alternative was the direct fusion of p67 onto a therapeutic antibody to facilitate downstream purification and optimize the conjugation strategy.

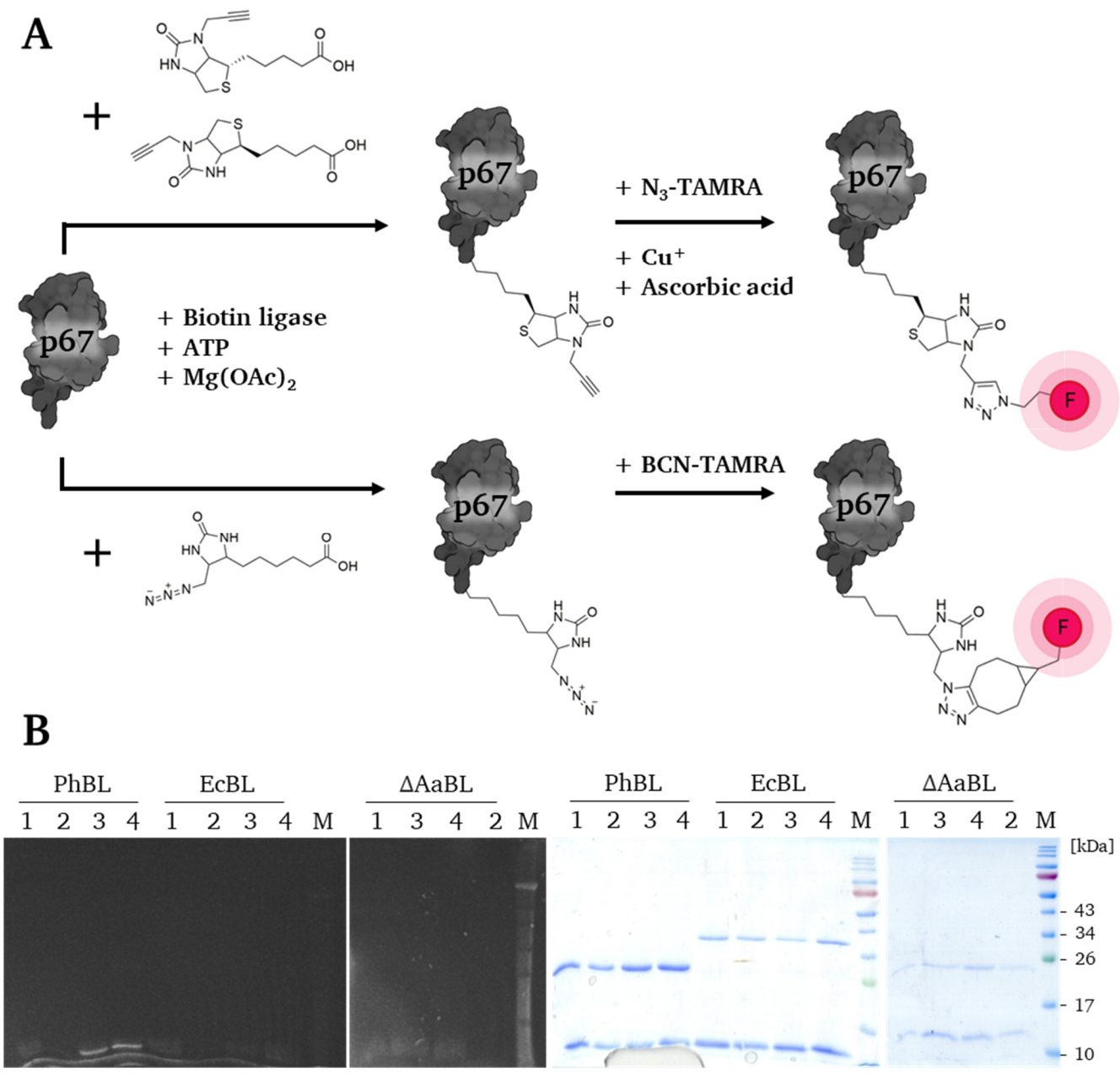

Figure 34: Conjugation of p67 by different biotin ligases with biotin derivatives. (A) Schematic depiction of reaction. Upper row is exemplary shown for trans-propargyl biotin. (B) Fluorescence excitation and coomassie stained acrylamide gel. p67 was modified with 10 eq. biotin (1), propargyl biotin (2) or desthiobiotin azide (3 + 4) by 1/10 eq. of the depicted biotin ligase in the presences of 5 mM Mg(OAc)2 and 5 mM ATP overnight at 37°C. The protein was purified by magnetic IMAC beads and conjugation was visualized by click chemistry. Biotin and desthiobiotin azide samples were incubated with 500 µM BCN-TAMRA. Propargyl biotin samples were incubated in presences of 2 eq. ascorbic acid, 1 eq. CuSO4 and 500 µM N3-TAMRA for 72 h at 22°C. The fluorophore was removed by magnetic Ni-NTA beads.

7.3.3 Expression, purification, and characterization of trastuzumab p67 fusions

For the generation of trastuzumab heavy chain p67 fusions, parts of the CH2 and the entire CH3 domain were amplified and used for a SOE-PCR with the p67-gene. The DNA fusion was ligated in an *MfeI* and *BamHI* hydrolyzed pTT5 vector carrying the trastuzumab heavy chain, with parts of CH2 and CH3 domain removed. For cloning of light chain fusions, SOE-PCR between trastuzumab LC with leader sequence and the p67-gene was performed. The product was ligated in a *EcoRI* and *BamHI* hydrolyzed pTT5 vector. After successful sequencing, variants carrying p67 at different positions (Figure 35) were expressed in Expi293F cells and the antibody fusions were purified from the supernatant by protein A chromatography.

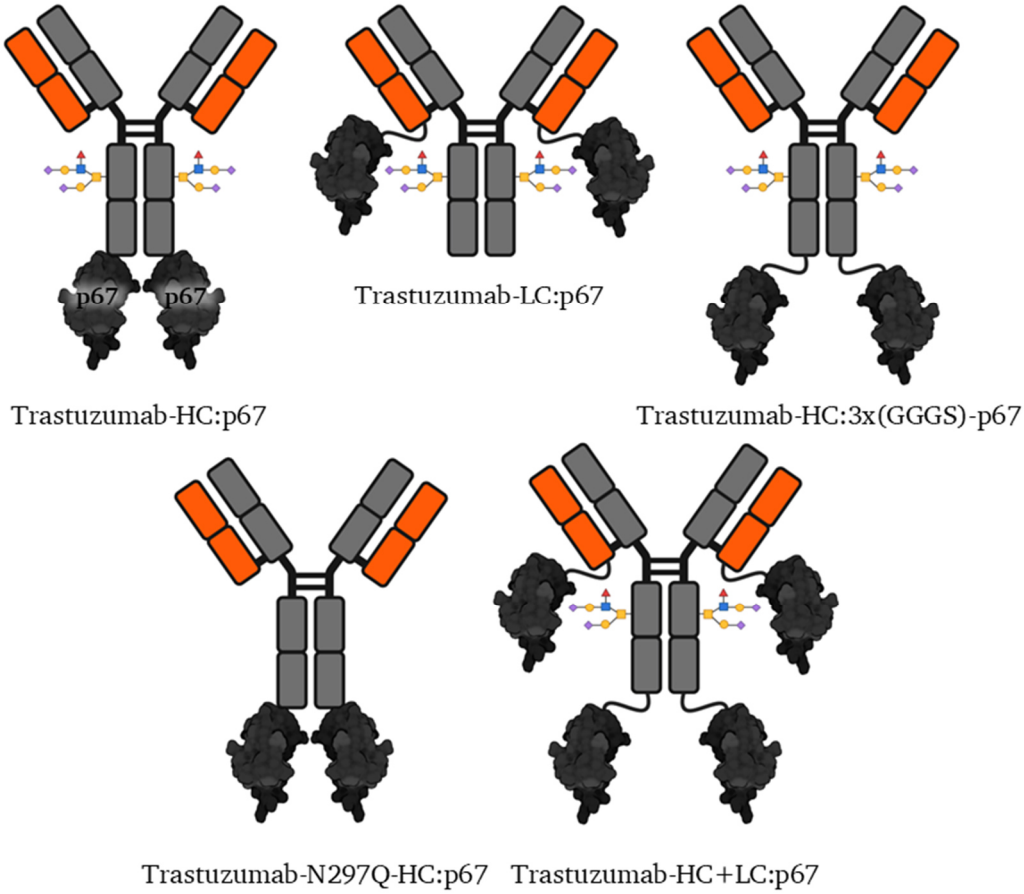

Figure 35: Schematic depiction of constructed trastuzumab-p67 fusions. Since N297 is the natural glycosylation site of IgG1 antibodies the mutations N297Q leads to an aglycosylated antibody.

After SDS-PAGE analysis, all variants with p67 on the heavy chain (fused directly, aglycosylated or with GGGS-linker) showed no aggregates or higher molecular protein bands (Figure 36, A). The heavy chain fusions exhibited the expected mass of ~ 56 kDa (HC: 49.2 kDa, p67: 6.9 kDa). However, it seemed that the glycosylated variants, were made up of two to three different heavy chain bands which were nearly

superimposed. This phenomenon was even more pronounced for the aglycosylated variant showing three distinct heavy chain bands. For the light chain fusions similar results were obtained, with the additional presence of high molecular weight bands, visible for both, trastuzumab-LC:p67 and trastuzumab-HC+LC:p67. Potentially an accessible protease cleavage site was introduced by fusing p67 to the antibody's chains promoting partial degradation and hence the appearance of three bands per chain. Whether there is an influence on enzyme recognition and conjugation must be investigated further.

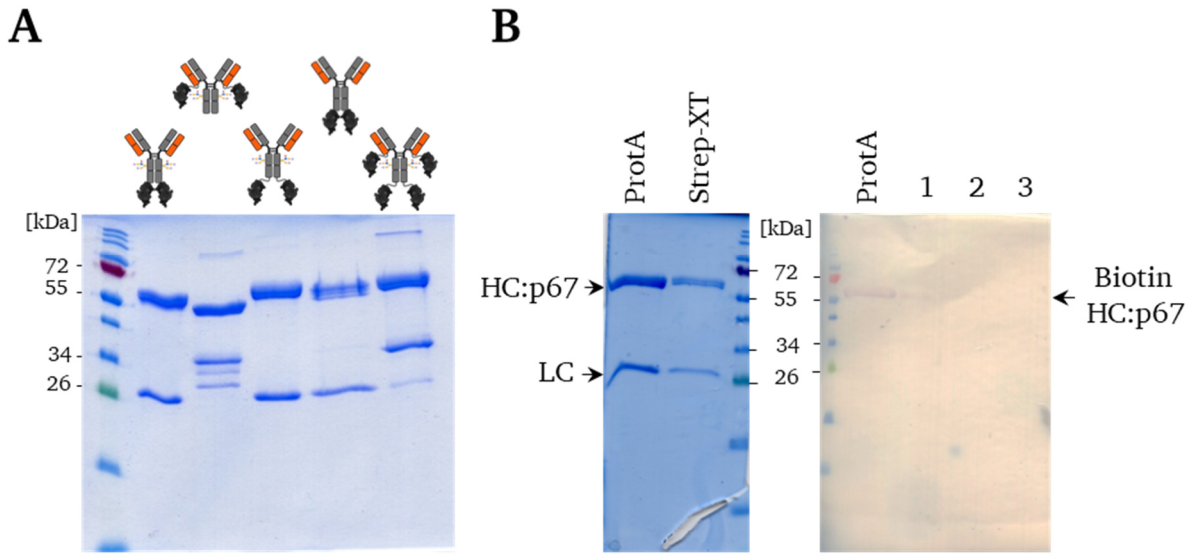

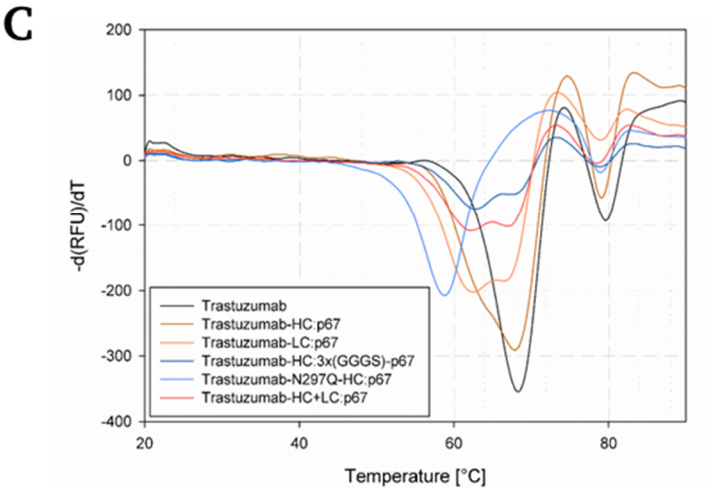

	Melting points [°C]	
Trastuzumab	68.5	79.5
Trastuzumab-HC:p67	68.0	79.0
Trastuzumab-LC:p67	66.5	79.0
Trastuzumab-HC:3x(GGGS)-p67	67.5	79.0
Trastuzumab-N297Q-HC:p67	59.0	79.0
Trastuzumab-HC+LC:p67	67.0	78.5

Figure 36: Protein A purified trastuzumab-p67 fusion constructs (A), Strep-Tacin XT purified trastuzumab-HC:p67 (B) and thermal shift assay (C). Trastuzumab-p67 fusions were expressed in Expi293F cells and purified from the cell culture supernatant with protein A. To remove already biotinylated antibody, the proteins were loaded to a Strep-Tactin XT gravity flow column for three times collecting the flow through. Purification process was exemplary analyzed for trastuzumab-HC:p67 by western blot and streptavidin-AP staining. In addition, a thermal shift assay was performed to determine the stability impact of the p67 grafting. ProtA: Protein A purified trastuzumab-HC-p67; Strep-XT: Protein A and 3x Streptactin XT purified trastuzumab-HC:p67; 1-3: Strep-Tactin XT purification count; HC:p67: heavy cain fused with p67; LC: light chain; Biotin HC:p67: biotinylated HC fused to p67.

Due to natural biotinylation and human origin of p67, it is likely that a proportion of the trastuzumab-p67 constructs were already biotinylated by the Expi293F cells during production. Therefore, purification with a Strep-Tactin® XT gravity flow column was performed, and the flow through was collected (biotinylated antibody was bound to the column). After each iteration a sample was taken and analyzed by western blot and streptavidin-AP-staining. As expected, the protein A purified sample displayed staining, confirming biotinylation (exemplarily shown for trastuzumab-HC:p67; Figure 36, B). This signal was still detectable after the first column passthrough, but vanished by the next application, resulting in a mostly unbiotinylated antibody. Typical antibody yields after complete purification ranged from 1.0 mg – 2.5 mg per 30 ml expression volume, which was a moderate result. On top of that, influence of the C-terminal p67 on overall stability of the antibodies was evaluated. Therefore, a thermal shift assay was performed using clinical grade trastuzumab as a reference (Figure 36, C). Trastzumab-p67 fusions had a neglectable stability loss in comparison to its unmodified counterpart. Solely trastuzumab-N297Q-HC:p67 had a decreased melting point of the Fc-fragment by ~ 10°C. However, this was likely attributed to the removed glycan and not to the fused p67 domain. Interestingly, all p67 constructs showed two overlapping signals at ~66°C. This could be related to the p67 fragment, which seemed to have nearly the same melting point as the Fc fragment. All in all, fusion of the p67 domain to C-termini of trastuzumab light or heavy chain did not affect thermal stability and was consequently a good basis for further conjugation experiments.

7.3.4 Propargyl biotin for generation of an antibody-drug conjugate

Initial experiments on p67 conjugation with propargyl biotin revealed no fluorescence when the protein was enzymatically conjugated by PhBL and chemically by CuAAC with a N_3-TAMRA probe (see section 7.3.2). To investigate the failed conjugation the reaction was directly performed in the antibody context enabling easier purification in between the two reactions and for instances hydrophobic interaction chromatography (HIC) as a more reliable analysis. As already mentioned in section 7.3.2 there could be two reasons for the failed conjugation. On the one hand, conjugation of the biotin derivative by the enzyme may have failed or CuAAC is inefficient. This was further investigated in the next two section.

7.3.4.1 Validation of propargyl biotin conjugation by PhBL

Despite having p67 fused directly to an IgG, no fluorescence for propargyl biotin in combination with CuAAC was observed (Data not shown), similar to the results from 7.3.2. Usually, biotin ligases bind both ATP and biotin, and keep the activated intermediate in a thermodynamically very stable enzyme-substrate complex bound until an acceptor is recognized[139]. Consequently, it is plausible, that PhBL is loaded with “common” biotin during *E. coli* expression and initially catalyzes biotinylation of the

antibody instead of propargyl biotinylation. Since, 1 μM biotin ligase was applied for conjugation of 2.3 μM antibody preloaded enzyme could be a critical problem.

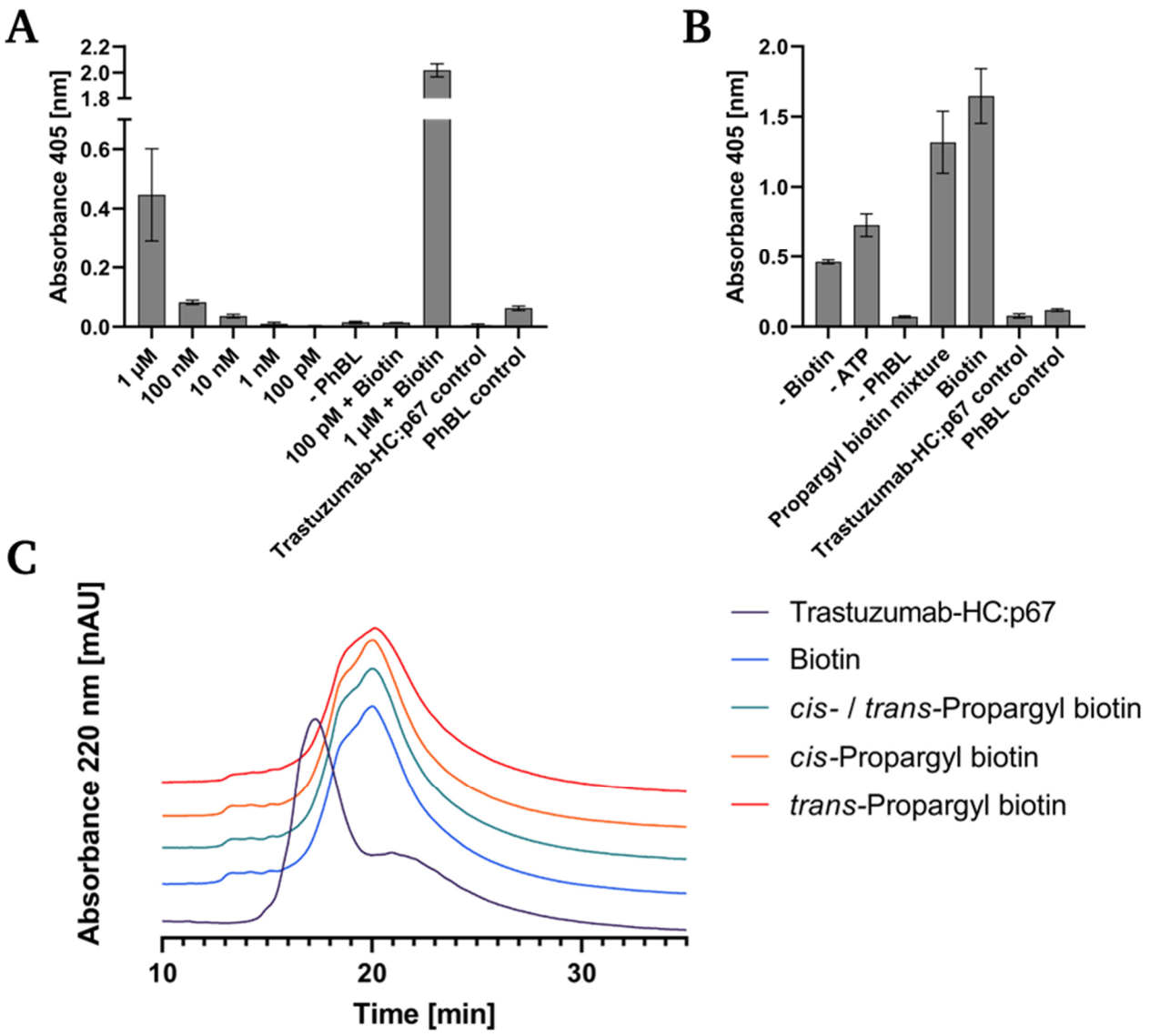

Figure 37: Investigation of trastuzumab-HC:p67 modification by PhBL. (A) Correlation between trastuzumab-HC:p67 biotinylation and PhBL concentration. 2.3 µM trastuzumab-HC:p67 were incubated in presences of 5 mM ATP, 5 mM $Mg(OAc)_2$ and different concentrations of PhBL for 2 h at 37°C in PBS with no additional biotin added. Control reactions were performed by addition of 1 mM biotin. Subsequently, reaction mixture containing 8 µg of antibody was coated on a microtiter plate and an ELISA-based assay with Streptavidin-AP staining was performed. Trastuzumab-HC:p67 and PhBL control resemble pure protein coated in same amounts as applied for the 1 µM reaction. n = 3, errors bars resemble standard deviation. (B) ELISA-based assay of trastuzumab-HC:p67 conjugated with 1 mM propargyl biotin by 1 µM PhBL. Procedure was performed analogous to (A). "- ATP", "- Biotin" and "- PhBL": Reaction mixture without the respective compound. n = 3, errors bars resemble standard deviation. (C) HIC analysis of (propargyl) biotin conjugation. Experiment was performed analogous to (A), overnight at 37°C. 35 µg of antibody was analyzed by HIC.

Figure 37 A, shows the correlation between trastuzumab-HC:p67 biotinylation and PhBL concentration without additional biotin. As hypothesized, biotinylation occurs even when no biotin was added to the

reaction. Besides, the effect was proportional to the amount of enzyme applied, with less enzyme leading to lower streptavidin-AP staining. The control reactions where 1 mM biotin was added supported the hypothesis that prebound biotin was the origin of this phenomenon. For both, absorbances were increased by a factor of ~ 4 compared to the reaction without biotin. Thus, it was crucial to keep the ratio between enzyme and antibody low to achieve propargyl biotinylation and decrease undesired biotinylation.

Next, turnover of propargyl biotin was further analyzed (Figure 37, B). Here, trastuzumab-HC:p67 was incubated with either a mixture of *cis-/trans*-propargyl biotin or "common" biotin and PhBL. Conjugation success was evaluated by an ELISA-based experiment stained by a streptavidin-AP conjugate. Comparable to A, control reactions without ATP or biotin exhibited a signal, which suggested a pre-bound substrate. Once again, the yield of biotinylated antibody was increased when 1 mM biotin was added. For the actual sample with propargyl biotin, a signal similar to the biotin reaction was achieved, which resembled successful conjugation of the derivative. Since, absorbance was increased by a factor of ~ 3 compared to the sample without added biotin, the read out had to be correlated to propargyl biotin turnover and was not a result from initially bound biotin.

As a next step, it had to be evaluated whether quantitative conversion of the antibody was occurring. It is possible that weak turnover of the antibody fused to p67 was the reason for the missing fluorescence in SDS-PAGE. So, for this undertaking the reaction yield was analyzed via HIC. Here, trastuzumab-HC:p67 was incubated with PhBL and a biotin substrate overnight and was directly applied to the column. The chromatogram for trastuzumab-HC:p67 indicated two species in the final preparation with a broad shoulder peak (Figure 37, C). For all reaction samples independent of the substrate the same peak pattern was observed with an increased retention time by ~ 2 min compared to trastuzumab-HC:p67 without substrate, which implies a more hydrophobic molecule, likely due to biotin attachment. The modest delay in retention time can be traced back to biotin being a water-soluble vitamin and thus not extremely hydrophobic in nature. As for the unmodified trastuzumab-HC:p67 the conjugates with (propargyl) biotin also exhibit a shoulder peak. This could either be explained by single and double modified trastuzumab or was a consequence of the two species obtained from the beginning. Nevertheless, no signal was observed at the retention time of unmodified trastuzumab-HC:p67, indicating that overnight incubation with PhBL resulted in complete turnover and yielded single- or double-conjugated proteins.

The investigation of propargyl biotin conjugates by an ELISA-based experiment and HIC analysis revealed that modification of trastuzumab-HC:p67 with propargyl biotin was successful. It was shown

that the ratio between biotin ligase and antibody is critical to prevent biotinylation with "common" biotin. However, unfavorable combinations of enzyme and antibody might decrease the overall yield of the desired product. Next, fluorophore conjugation of propargyl biotin by CuAAC was investigated.

7.3.4.2 Validation of CuAAC with propargyl biotin and N_3-TAMRA

From the HIC analysis and ELISA-based experiments revealing successful conjugation of propargyl biotin it was concluded that CuAAC either did not take place with a N_3-TAMRA or it occurs in very low yield only. This was investigated further.

Therefore, click reaction of propargyl biotin with N_3-TAMRA was performed in the absence of any protein to validate successful coupling. Additionally, a N_3-PEG_3-TAMRA probe was used to address the possibility of steric hindrance in the antibody-p67 construct. Analysis of the reaction was performed by RP-HPLC and mass spectrometry.

Figure 38 exemplarily shows the HPLC chromatograms of the N_3-PEG_3-TAMRA and propargyl biotin coupling. To begin with, the *cis*- as well as the *trans*-propargyl biotin molecule showed a weak signal for absorbance at 220 nm (Figure 38, top arrow 1 + 2) and no signal at 550 nm. For the TAMRA educt absorbance signals were obtained at both wavelengths and revealed impurities in the molecules sample. The CuAAC reaction sample depicted another prominent peak (arrow 3) not present in the educt samples. Furthermore, absorbance at 550 nm indicated the presence of TAMRA (arrow 4) and thus a successful product formation. These results were also validated by LC-MS (Supplementary figure 9). Observed masses reflected the calculated masses of the educts as well as the CuAAC product. The same holds true for the N_3-TAMRA molecule (Supplementary figure 10).

To summarize, propargyl biotin reacted in a copper-catalyzed azide-alkyne cycloaddition with TAMRA azide derivates. However, as for p67 alone, the antibody p67 fusion did not show successful N_3-TAMRA conjugation when analyzed and visualized by SDS-PAGE. It is known, that CuAAC is sensitive to the presences of free thiols such as cysteines[224,225]. Through the binding of copper by the sulfur moiety, it is consequently no longer available for catalysis. Notably, p67 exhibits two cysteines that might negatively interfere with copper click reaction. Copper binding ligands have been described, such as BTTAA or THPTA, known to complex Cu^+, preventing oxidation and supporting CuAAC. However, their usage did not change the outcome in any way (Data not shown). All in all, generation of an antibody-ligand conjugate by utilization of propargyl biotin proved to be ineffective and was not explored any further. The project was continued by applying the desthiobiotin azide as an alternative substrate.

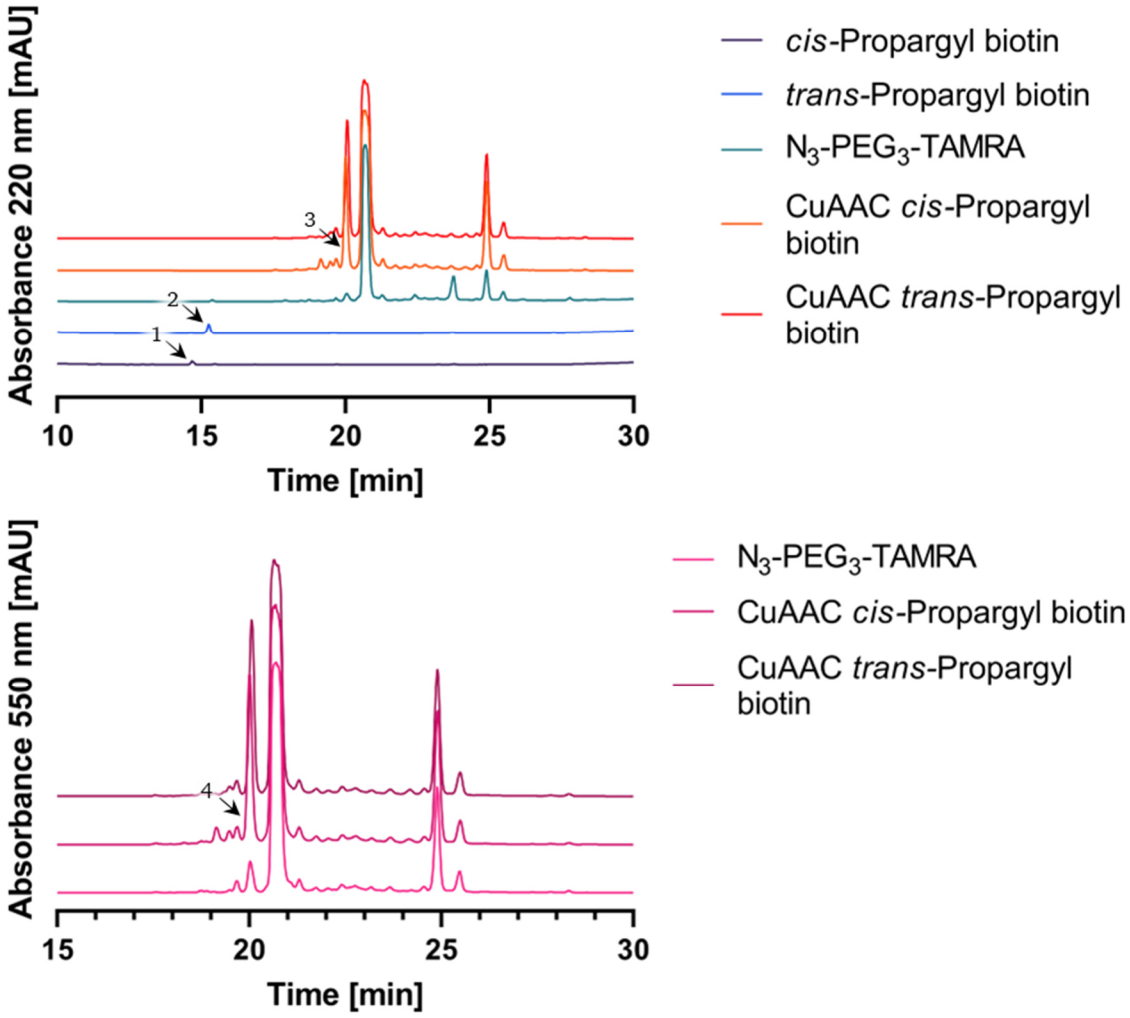

Figure 38: RP-HPLC analysis of CuAAC reaction between propargyl biotin and N_3-PEG_3-TAMRA. 2.3 mM *cis*- or *trans*-propargyl biotin, 1 mM N_3-PEG_3-TAMRA, 1 mM Cu^+ and 2 mM ascorbic acid were incubated for 5 h at 37°C. 15 µg of the educts and reacted propargyl biotin were analyzed by RP-HPLC applying a gradient 0to60%B in 32 min. 1 + 2: Propargyl biotin; 3 + 4: CuAAC product.

7.3.5 Desthiobiotin azide for generation of an antibody-drug conjugate

With the failure of propargyl biotin and the initial successful chemoenzymatic coupling of desthiobiotin azide mediated by PhBL and BCN-TAMRA by SPAAC on solitary p67, this approach was investigated further for the generation of ADCs. Consequently, experiments were carried out in an antibody-p67-fusion context (as described in 7.3.3).

7.3.5.1 Validation of desthiobiotin azide conjugation to trastuzumab-HC:p67

Conjugation of desthiobiotin azide by PhBL was analyzed for quantitative conversion by HIC. Hereby, trastuzumab-HC:p67 was incubated in the presence of a biotin derivative and PhBL overnight and analyzed by HIC.

HIC analysis of the p67 fused trastuzumab revealed a comparable elution profile (Figure 39) as measured in the propargyl biotin section (7.3.4.1). Upon closer examination the antibodies main elution peak consisted of four overlapping signals, which might be correlated to the individual heavy chains already seen in section 7.3.3. Samples containing the desthiobiotin azide modified antibody showed four individual peaks with a delay in retention time by ~ 1 – 4 min. While the origin of those peaks remained unclear, it might be the result from incomplete conjugation of the individual heavy chains. This hypothesis was supported by the biotin sample, where only three distinct elution signals were obtained. While biotin is the natural substrate for the enzyme the best conjugation results should be obtained with this substrate and elution peak pattern should be comparable. Nevertheless, the results could also be a consequence of the different heavy chain species which are quantitatively conjugated and yielded one peak per species. Independently from the origin of the different elution signals, there was no signal with the same retention time as the negative control remaining, which indicated antibody conversion and a (semi)-quantitative turnover. Consequently, chemoenzymatic conjugation of trastuzumab-HC:p67 should be conducted with a BCN-TAMRA fluorophore.

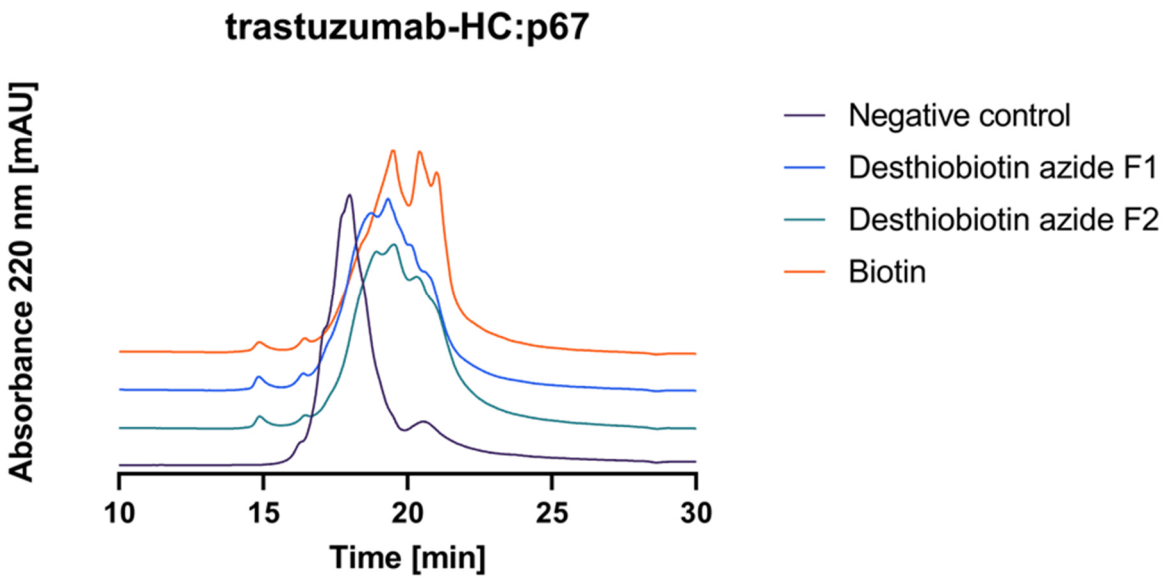

Figure 39: HIC analysis of desthiobiotin azide conjugated trastuzumab variants. Trastuzumab-HC:p67 was incubated with 50 eq. of the respective biotin substrate, 5 mM ATP, 5 mM Mg(OAc)2 and 1/10 eq. PhBL overnight at 37°C. Reaction mixture was analyzed via HIC.

7.3.5.2 Chemoenzymatic conjugation of trastuzumab-HC:p67 with TAMRA

In order to conjugate two TAMRA molecules to trastuzumab-HC:p67, the antibody was incubated with the desthiobiotin azide and PhBL overnight. After removal of excess substrate by ultrafiltration, SPAAC was performed with BCN-TAMRA molecules.

Similar to the modification of solitary p67, fluorescence was also observed for the p67-fused trastuzumab as revealed by SDS-PAGE analysis (Figure 40, A) with bands visible for both the F1- and F2- conjugated antibody. “Common” biotin behaved as expected and led to no conjugation of the fluorophore. Additionally, the fluorescence image showed that all three bands of the heavy chain (discussed in section 7.3.3) were conjugated with TAMRA when using desthiobiotin azide. Unexpectedly, the light chain was also fluorescently labeled which was surprising since p67 was fused only to the heavy chain. This could infer that the enzyme is not highly specific and recognized lysine residues in the light chain as a substrate, too. Alternatively, there may be an enzyme independent reaction occurring between the antibody and the desthiobiotin azide. Detectable side-reactions of the BCN-TAMRA with trastuzumab-HC:p67 were excluded since the biotin control revealed no fluorescence signal.

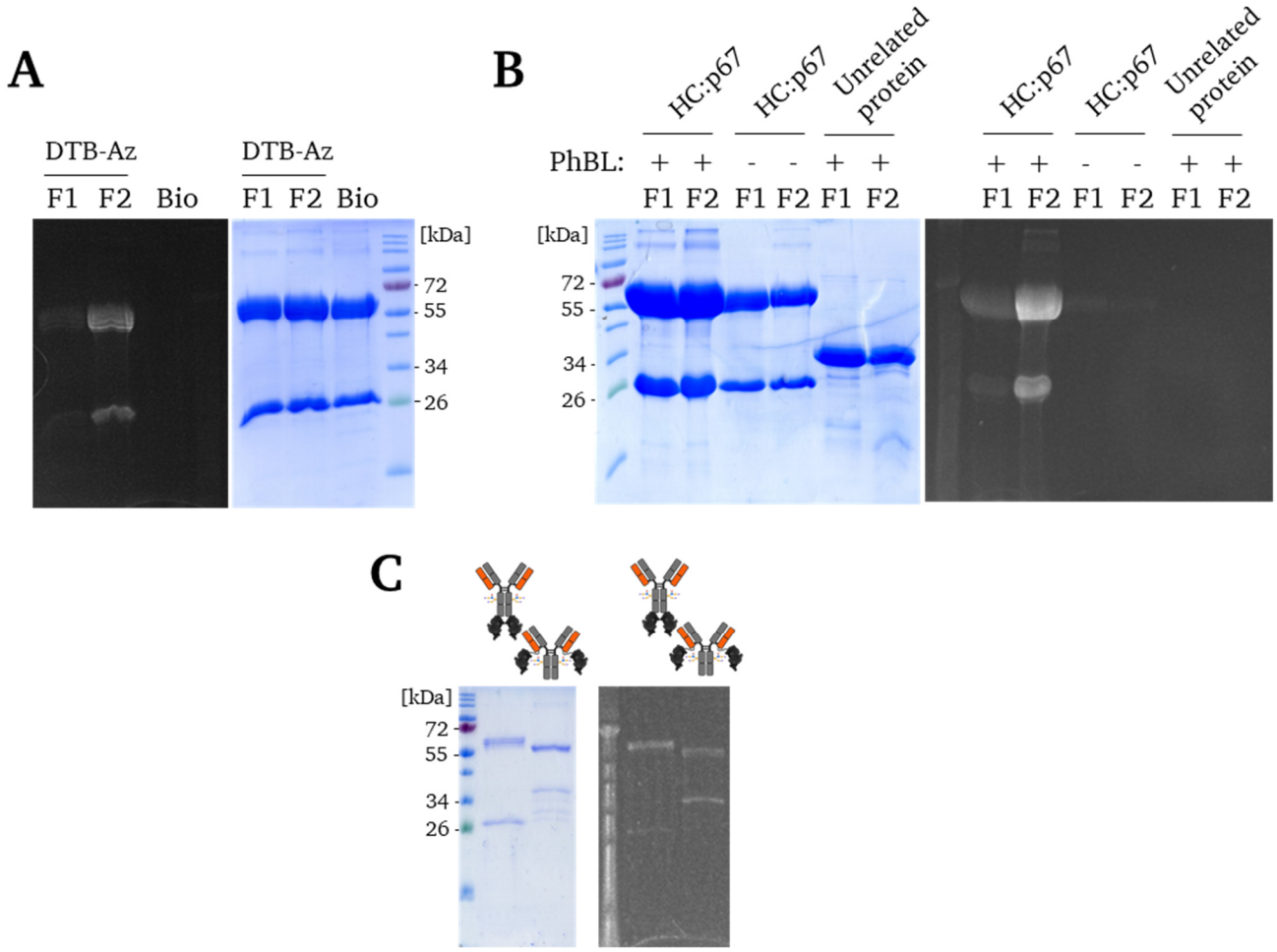

Figure 40: Chemoenzymatic modification of trastuzumab-HC:p67 with different biotin substrates (A), control reactions for validation of enzyme and SPAAC specificity (B) and comparison of trastuzumab-HC:p67 and LC:p67 modified chemoenzymatically (C). For chemoenzymatic conjugation, trastuzumab-HC:p67 was incubated with 50 eq. of biotin substrate, 5 mM ATP, 5 mM $Mg(OAc)_2$ and 1/10 eq. PhBL overnight at 37°C. The next day, excess substrate was removed by ultrafiltration. Subsequently, 20 eq. BCN-TAMRA were added, and reaction was incubated for 3 days at room temperature. Control reactions were done similar, omitting addition of the enzyme, or using an unrelated protein (tandem biparatopic EGFR-binding VHHs termed 7D9G) with no p67 acceptor domain as POI. DTB-Az: Desthiobiotin azide; F1: Desthiobiotin azide fraction 1; F2: Desthiobiotin azide fraction 2; Bio: Biotin.

For further investigation in this matter, additional chemoenzymatic approaches were conducted using no biotin ligase in the initial conjugation step, or by applying an unrelated non-p67 fused protein.

As shown before, the conjugation to trastuzumab-HC:p67 resulted in fluorophore attachment on both the heavy and the light chain for both desthiobiotin azide substrates. When PhBL was omitted or an unrelated protein was used no significant fluorescence was obtained either for the F1 or F2 substrate (Figure 40, B). Interestingly, usage of trastuzumab-LC:p67 as a conjugation partner resulted in fluorescence of both chains, too, (Figure 40, C) although p67 was fused to the light chain in this case.

This finding was further evaluated by MALDI-TOF/TOF. The aglycosylated trastuzumab-N297Q-HC:p67 (see section 7.3.3) was conjugated as mentioned before by PhBL with desthiobiotin azide F2 and was subsequently reduced by DTT. Together with the unconjugated counterpart MALDI-MS was conducted. For the aglycosylated trastuzumab-N297Q-HC:p67, masses representing the heavy and light chain were detected (Supplementary figure 11). Calculated and observed masses deviated depending on the charge of the species and the antibody chain from ~ 24 – 54 Da (light chain) and ~ 40 – 94 Da (heavy chain). Considering the size of the protein and additional unknown post-translational modifications this was a possible divergence which was still smaller than the average size of one amino acid (~ 110 Da). Interestingly, modified trastuzumab-N297Q-HC:p67 also showed these masses, however there was a small proportion obtained, which had an increased mass of ~ 505 Da. This was in the range of two attached desthiobiotin azide (Mass: 255,13 g/mol, expected mass increase of 238,13 g/mol due to eliminated hydroxy group) and would support the SDS-PAGE obtained results. MALDI signals obtained for the heavy chain, were less intense compared to the light chain. For the conjugated variant they couldn´t be distinguished from the background and therefore no predication on the conjugation degree was made.

All in all, MALDI-TOF/TOF-MS served as another analysis method to support the hypothesis, that conjugation on the light chain of the antibody occurred. In combination with the SDS-PAGE results this phenomenon must be investigated further since unspecific conjugation by the enzyme was undesired and would put the whole approach into question. A possible reason for the finding might be desthiobiotin azide because it is no optimal substrate for the enzyme. To render a biotin ligase promiscuous, as done for the BioID experiments, a single mutation is necessary. It is tempting to speculate that the same occurs when using desthiobiotin azide as a substrate due to the thiolane ring opening and introduction of the azide function. The molecule might be bound tight enough to retain specificity of the enzyme in context of unrelated proteins but when coordinated at the p67 domain unspecific release could be promoted. Something comparable is known for the interaction of desthiobiotin with streptavidin. The affinity of the

small molecule is 10^2 – 10^4-fold weaker than the of biotin[226]. In context of the enzyme introduction of the azide function might further decrease the affinity towards the substrate. To validate this assumption, it must be investigated if biotinylation of the light chain also occurs when "common" biotin is the substrate.

7.3.5.3 Analysis of unspecific biotinylation by PhBL

To confirm the hypothesis that desthiobiotin azide in combination with coordinated PhBL on the p67 acceptor domain promotes a promiscuity of the enzyme a western blot was conducted. Hereby, trastuzumab-HC:p67, trastuzumab-HC:NEJ4 (IgG negative control with mTG recognition sequence) and a non-p67 fused protein were conjugated by PhBL with biotin and desthiobiotin azide.

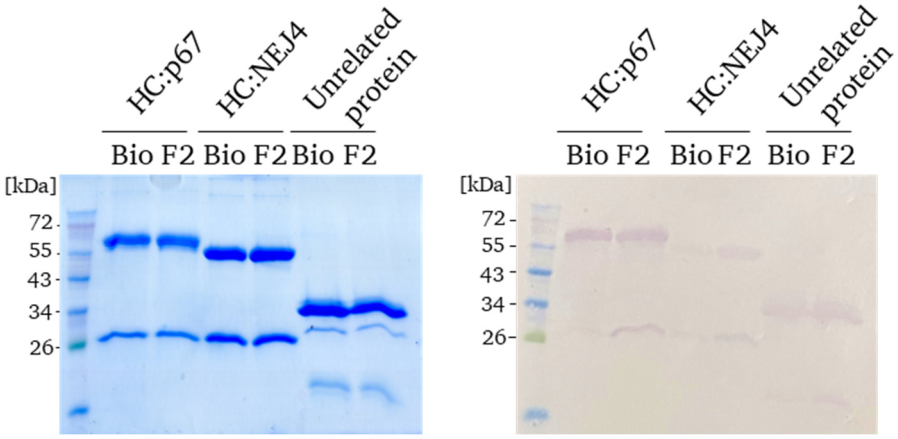

Figure 41: Western blot analysis of biotin and desthiobiotin azide modified trastuzumab-HC:p67, trastuzumab-HC:NEJ4 and an unrelated protein (7D9G). The respective protein was conjugated with biotin or desthiobiotin azide F2 at 37°C overnight applying 50 eq. of the substrate, 5 mM ATP, 5 mM Mg(OAc)2 and 1/10 eq. PhBL. Western blot was stained with a streptavidine-AP conjugate. Bio: biotin sample; F2: desthiobiotin azide F2 sample; HC p67: trastuzumab-HC:p67; HC NEJ4: trastuzumab-HC:NEJ4; Unrelated protein: tandem biparatopic EGFR-binding VHH termed 7D9G.

Western blot analysis (Figure 41) of trastuzumab-HC:p67 labeling showed as expected that modification of the heavy chain occurred for both used substrates. As hypothesized modification of the light chain occurred only for the desthiobiotin variant in a significant manner. Interestingly, there was also turnover detected for both negative controls even though intensity was lower. This finding was unexpected since it would imply that the enzyme was not highly specific. Additionally, the western blot showed a different outcome than to SDS-PAGE conducted before (Figure 40), where no modification of the unrelated protein was observed. However, this could be explained by the detection method, since visualization of fluorescence is more insensitive in comparison to an enzyme catalyzed reaction as done by alkaline phosphatase. When comparing the biotin with the desthiobiotin sample of the negative controls it was shown that band strength of the latter was stronger. For trastuzumab-HC:NEJ4 conjugation of biotin was hard to detect, whereas for the desthio counterpart proof was unproblematic. This was in accordance

with the assumption, that desthiobiotin azide is not an optimal substrate for the enzyme and might promoted release of activated intermediate.

All in all, this experiment revealed, that desthiobiotin azide as a substrate promotes unspecific modification of proteins independent of p67 presence. Additionally, PhBL is not as specific as expected. Biotinylation occurred on trastuzumab-HC:NEJ4 as well as on an unrelated VHH nanobody both exhibiting no biotin acceptor domain. It remains to be elucidated, to what extent this unwanted side reaction occurs in comparison to p67 conjugation and whether totally unspecific lysine labelling in the antibody light chain occurs or the side reaction is restricted to certain lysine residues that may be placed in steric proximity to p67-bound enzyme.

7.3.6 Summary and interim conclusion

In summary, generation of an antibody-drug conjugate by biotin ligase was not a trivial approach. ADC construction using propargyl biotin as substrate for enzymatic modification failed due to subsequent CuAAC. Addressing the alkyne moiety was only possible in an unconjugated state of the biotin derivative. After attachment to a protein conversion was not possible. Since there was no solution for that problem, propargyl biotin seemed not to be suitable for further investigations.

For the desthiobiotin azide substrate it was shown that chemoenzymatic modification of an antibody was feasible in principle. However, modification was not site-specific and therefore comparable to conventional chemical modifications done by NHS or maleimide coupling. It must be validated if reaction conditions can be tuned to decrease the unspecific modification to a degree that it could be neglected.

7.4 Generation of antibody-drug conjugates with lipoate-protein ligase A

Comparing biotin ligases with other ligases such as lipoic acid ligase shows significant similarities. They are nucleoside triphosphate dependent and catalyze activation of a substrate in order to conjugate the molecule to a desired acceptor. Whereas the previous chapter (7.3) was focused on biotin ligases, in this section the lipoate-protein ligase A (LplA) derived from *E. coli* was assessed for ADC generation. Initial experiments were done during the authors master thesis[227] showing that LplA was a highly specific enzyme leading to quantitative conjugation of the heavy chain LAP-tagged trastuzumab antibody (trastuzumab-HC:LAP, LAP = synthetic recognition sequence of LplA). This project was a cooperation with the working group Wombacher at university of Heidelberg. The state of the art of using LplA derivatives with tailor-made substrates for later biorthogonal conjugation is described in section 3.5.1 of the introduction of this thesis.

7.4.1 Characterization of trastuzumab-HC:LAP conjugates mediated by LplA

For the generation of an ADC, introduction of click chemistry-based residues into the antibody molecule was necessary. Here a BCN-substrate for LplA was used for conjugation to a heavy chain LAP-tagged trastuzumab (Figure 42 A). During the enzymatic conjugation samples were taken and reaction was terminated by addition of 0.25 M EDTA (final) since it is known to be Mg^{2+} dependent. Reaction progress was monitored by HIC. In addition to that, the BCN-activated trastuzumab was conjugated with a tetrazine-modified eGFP-LAP or rhodamine. These fluorophore-carrying antibodies were subsequently used to analyze binding behavior on SK-BR-3 cells.

As shown in Figure 42 B, a single peak at ~ 14 min indicating a pure, unmodified antibody was observed by HIC before the start of the reaction (0 min). Already after 1 min of conjugation, three individual peaks resulted, where one had the same retention time as the unmodified trastuzumab-HC:LAP. Peaks 2 and 3 had a higher elution time, implying a more hydrophobic molecule. Consequently, the middle signal most likely resembles the once modified trastuzumab with a BCN-to-antibody-ratio (BAR) of 1. Peak 3 could be assigned to a twice-modified antibody. Interestingly, no change in the chromatogram was observed after 3 min of conjugation suggesting complete conjugation within 2 - 3 min. In comparison to other enzymes used for C-terminal modification of trastuzumab, this confirms a very fast reaction to take place[133,228–230]. Hence, conjugation with LplA resulted in a very fast and straight-forward approach for enzymatic antibody modification.

To investigate any potential impact of the C-terminal conjugation on binding behavior of the antibody, on-cell K_D were determined with Her2-positve SK-BR-3 cells. As shown in Figure 42 C, trastuzumab-HC:LAP exhibited a K_D of 5.6 nM, which was in accordance with other K_D measured in literature[231,232].

This was also true for the trastuzumab-HC:LAP-BCN:MeTz-eGFP construct exhibiting equipotent binding (7.9 nM). In contrast, the trastuzumab-HC:LAP-BCN:MeTz-rhodamine construct showed a weak decrease in binding affinity to double digit nanomolar range (12.9 nM).

To sum it up, a heavy chain LAP-tagged trastuzumab was a reliable target molecule to introduce chemical handles like BCN, which may be addressed later in click-chemistry based conjugations. On top of that, constructs carrying an eGFP or rhodamine at the C-terminus behaved comparable to its unmodified counterpart. Therefore, this workflow could be adjusted for the generation of a toxin-containing ADC.

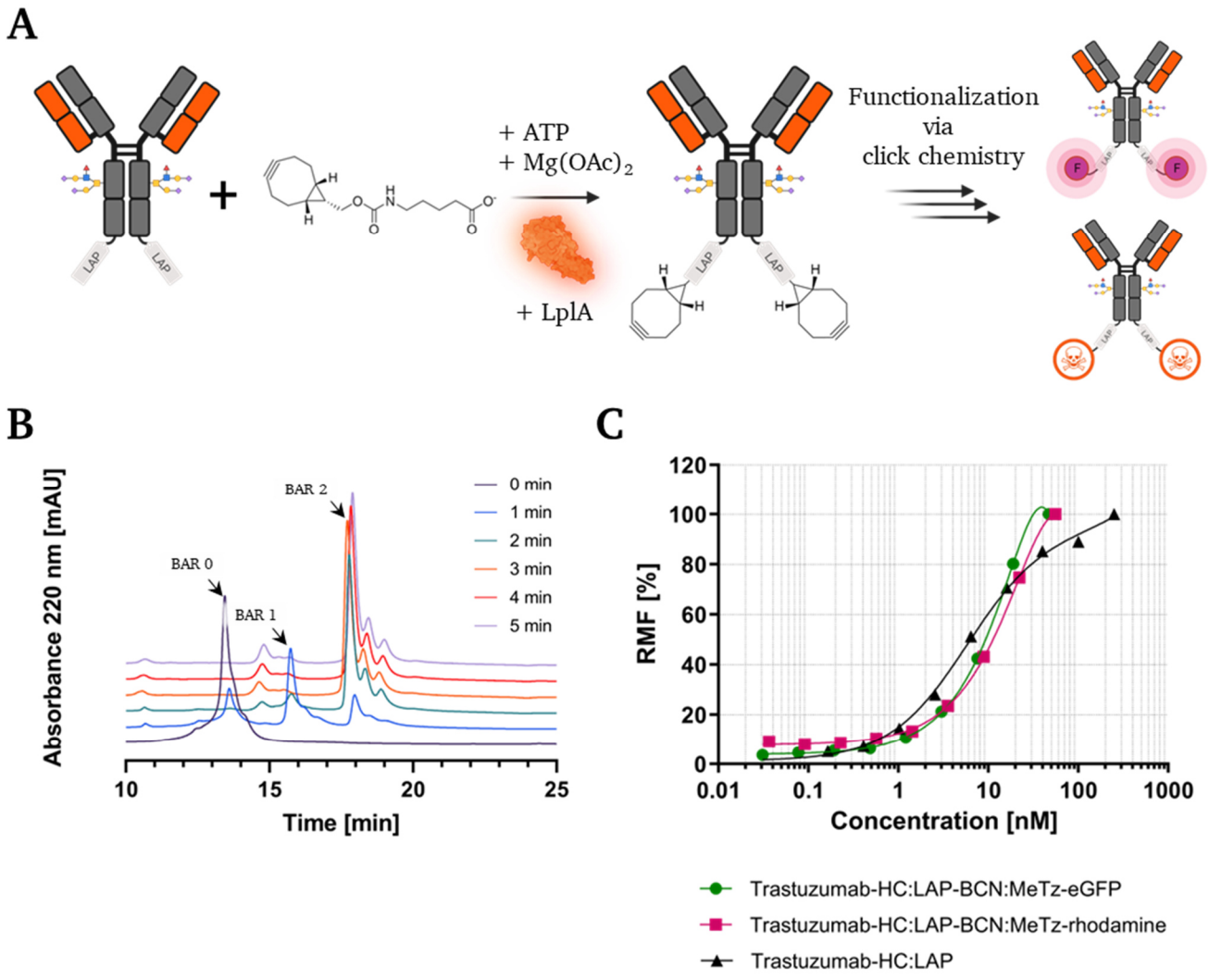

Figure 42: Characterization of trastuzumab-HC:LAP conjugates mediated by LplA. A: Schematic depiction of Trastuzumab conjugation with LplA. B: HIC analysis of LplA mediated BCN conjugation to trastuzumab-HC:LAP. A sample was taken every minute and reaction was stopped with 0.25M EDTA. Stopped reaction mixture was directly used for HIC analysis. C: K_D determination of trastuzumab-HC:LAP-BCN:MeTz-eGFP and trastuzumab-HC:LAP-BCN:MeTz-rhodamine conjugates. BCN activated trastuzumab-HC:LAP was conjugated with tetrazine-modified eGFP or rhodamine to generate a fluorophore-antibody conjugate. These molecules were serially diluted and incubated with SK-BR-3 cells. FACS analysis war carried out for determination of binding. Data adapted from [233].

7.4.2 Generation of an ADC using LplA and Azido-Val-Cit-PAB-MMAE

Chemoenzymatic conjugation of trastuzumab-HC:LAP was performed in order to generate an ADC. Therefore, the antibody was modified by LplA and its BCN-substrate. Subsequently, conjugation with azido-Val-Cit-PAB-MMAE was carried out and ultimately purified by Protein A and ultrafiltration. A cell proliferation assay was performed to analyze cellular toxicity using SK-BR-3 (Her2 positive) and CHO (Her2 negative) cells. Therefore, trastuzumab-HC:LAP and the ADC were serially diluted 8-fold and incubated on cells.

After 72 h, the ADC exhibited potent, concentration-dependent cell killing with a sub-nanomolar IC_{50} of 0.31 nM (Figure 43). In contrast, trastuzumab-HC:LAP had a neglectable impact on the SK-BR-3 cell survival. The decrease in proliferation at concentrations >10 nM could be explained by a trastuzumab-mediated growth inhibition and consequently a lower cell count in respective wells. As expected, both constructs had no impact on CHO cells, as they do not express human Her2.

To sum it up, a novel, straightforward LplA-mediated method for ADC generation was presented. The potent ADC was used to selectively kill Her2 overexpressing cells.

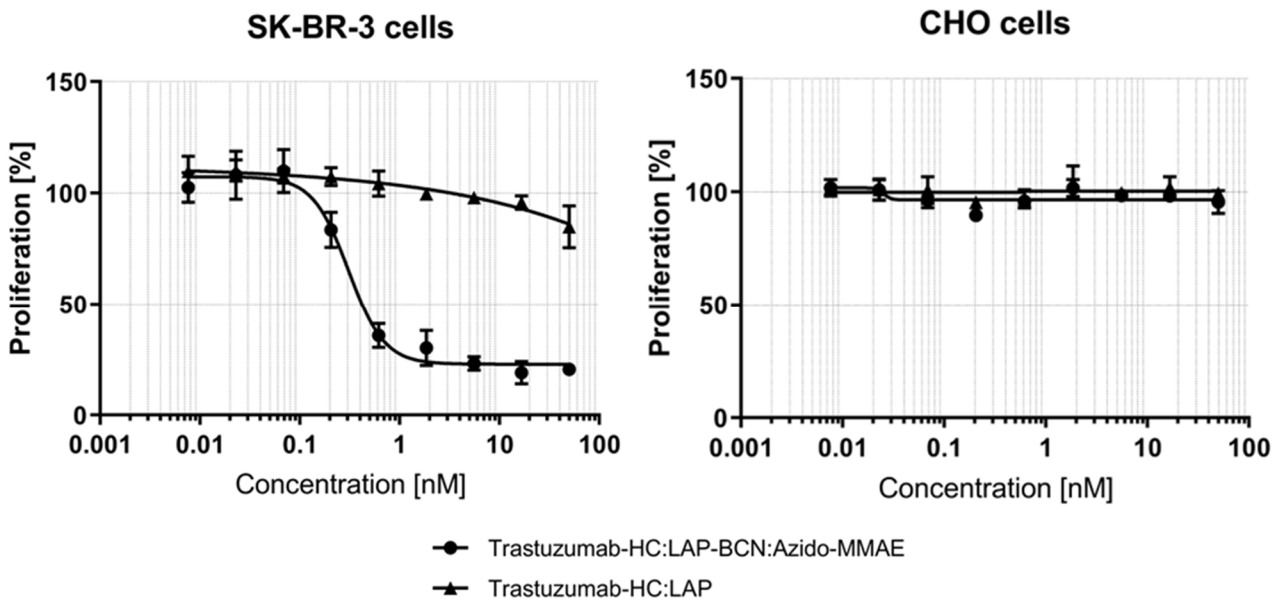

Figure 43: Cell proliferation assay using a trastuzumab-HC:LAP-BCN:Azido-MMAE conjugate. Trastuzumab-LAP was modified with BCN by LplA. Subsequently, click-reaction applying azido-Val-Cit-PAB-MMAE was carried out. For the Cytotoxicity-assay SK-BR-3 ($Her2^+$) and CHO cells ($Her2^-$) were used. Trastuzumab-HC:LAP-BCN:Azido-MMAE and trastuzumab-HC:LAP were serial diluted and incubated with cells for 80 h. Cell proliferation was measured using *CellTiter96 AQ_{ueous} One Solution Cell Proliferation Assay*. Data adapted from [233].

7.5 Identification of cell-internalizing binders out of systemic lupus erythematosus libraries

This chapter deals with the application of biotin ligases for the identification of cell-internalizing antibodies. These could become valuable tools for the study of cell functions but also on a long run for therapeutic intervention as outlined in chapter 3.8 of the introduction section. It is known that patients suffering from systemic lupus erythematosus (SLE) show evidence of antibodies, which can internalize in living cells. These antibodies and, in general internalizing proteins, are of big interest for development of drugs, since targeting of intercellular proteins might be facilitated. The starting material for this project was provided by *Merck Healthcare KGaA* in form of single chain antibody fragments obtained by PCR amplification and cloning of the B-cell repertoire of SLE patients provided in a phage display library format. Reports showed that phages presenting cell penetrating proteins or peptides are able to internalize in living cells and remained there for various hours while still being fully functional and infectious[187]. Based on this premise, the idea for a screening approach arose. To start, packaged phages presenting the whole antibody pool of a SLE patient in an scFv format should be applied to mammalian cells. ScFvs mediating cell penetration should result in transport of the phage into the cell all other bacteriophages remain outside the cell and can be removed by stringent washing steps. After lysis of the mammalian cells, *E. coli* can be infected, which ends in enrichment of internalizing phages after various rounds of screening (for workflow see Figure 44, A). This should be combined with intracellular phage biotinylation to ease enrichment of "internalizers" (see section 7.5.4).

7.5.1 Initial proof-of-concept with patient S016 BC13 λ-light chain

As an initial proof-of-concept study initial experiments were done with a single scFv library containing one patient's antibody λ-light chain pool. Hereby, phages were packaged from *E. coli* cells and analyzed by western blot. Afterwards, phages were applied to mammalian cells in four consecutive enrichment rounds, changing cell line to prevent enrichment against specific proteins on the cell surface. Each culture lysate was used to determine the output phage titer by serial dilution and infection of *E. coli*.

Analysis of bacteriophages via SDS-PAGE and western blot hinted at the effective production of phages (Figure 44, B). This was shown due to presence of the major coat protein pVIII and minor coat protein pIII detected by western blot. Unexpectedly, an scFv:pIII fusion was not detected in this approach by staining against the pIII protein. Since it is known that ratios between wild-type pIII and the pIII:scFv fusion ranging from 9:1 to 1000:1 depending on the presentation system used[234], it is likely that the fusion was undetectable by anti-pIII western blot. If the pIII:scFv fusion was successfully translated a His- and a myc-tag should be present. Thus, western blot analysis with anti-His and anti-myc staining was performed. In both blots, a band was visible at ~ 34 kDa, presumably being the free scFv. As free

scFv should not be detectable in a pure phage preparation, it was assumed that there were remaining *E. coli* cells in the final M13 phage sample. If there is no *amber* codon suppression occurring (as in most translation iterations of the mRNA), free scFv is directed to the periplasm of the cell, that could then be stained by western blot, when whole cell lysates are applied. However, despite being undesired, this was an indication that functional scFvs were translated during phage production. Exclusively for the anti-myc staining, a slight band was visible at ~ 95 kDa, likely belonging to the desired fusion protein. pIII has a molecular size of 42.5 kDa but it is known that it runs higher on SDS-PAGE (65 kDa) and therefore the pIII:scFv protein runs at ~ 95 kDa[218]. From this, it was concluded that packaging of scFv-presenting M13 phages was successful, and enrichment could be started.

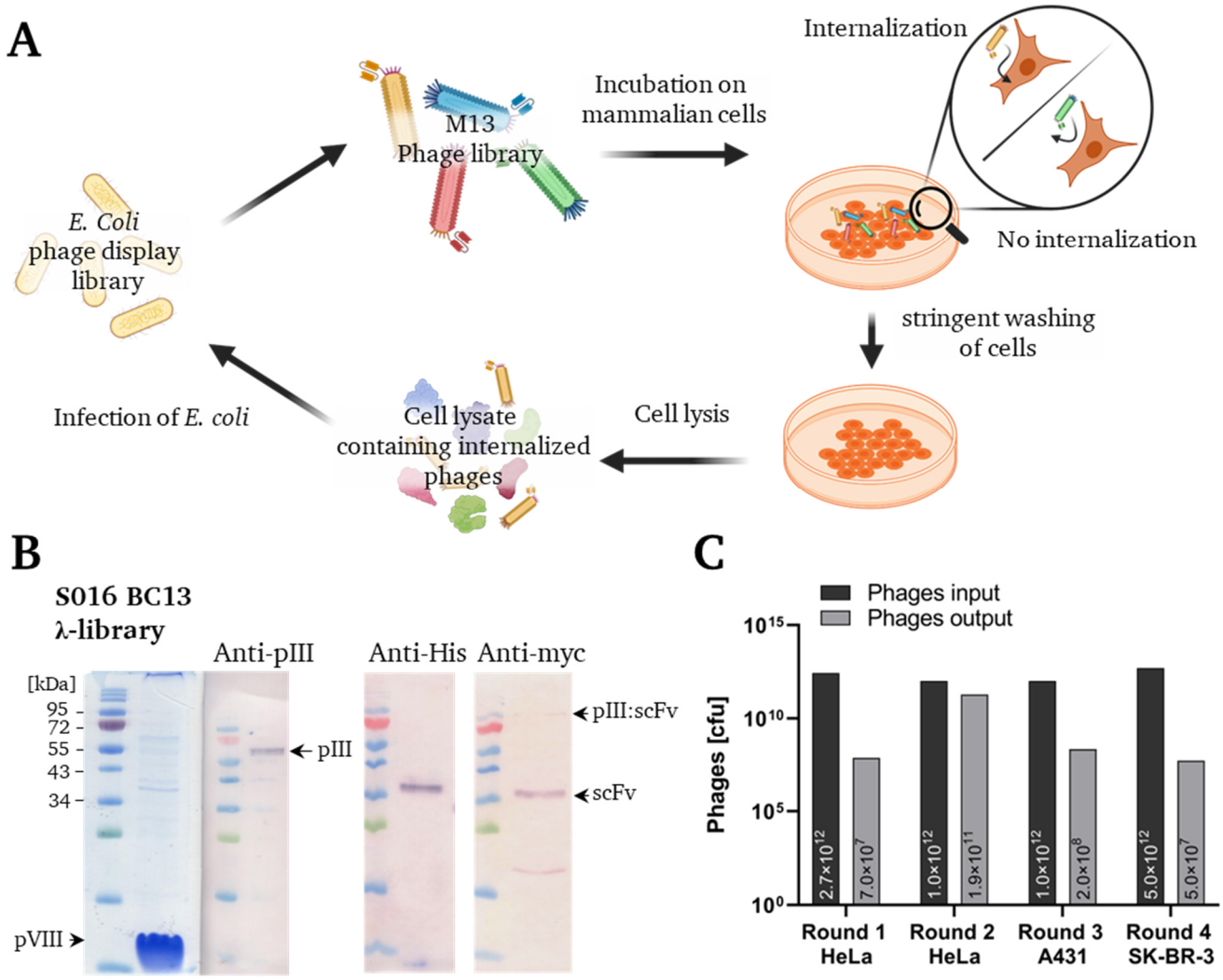

Figure 44: General enrichment workflow (A), SDS-PAGE and western blot analysis of phage preparation of S016 BC13 λ-V_L (B) and overview of enrichment rounds (C). For screening phages were applied in cell culture supernatant and incubated for ~ 17 h. After stringent washing of the cells with PBS and low pH stripping buffer, cells were lysed by freeze thaw. Cell debris was spun down by centrifugation and the supernatant was used for phage titer determination and infection of a freshly grown culture of *E. coli* XL1-blue or ER2738.

For all incubation rounds (Figure 44, C), ~ 10^{12} phages were applied to the cells depending on the preparation's phage titer. Using HeLa cells for the first enrichment, phage count was reduced by five orders of magnitude after incubation, washing and lysis of the cells. This could mean that there were either internalizing phage present in the library, or unspecific binding to the cell surface occurred and the phage particles were not removed completely. Due to the unfortunate lack of a suitable negative control, this could not be validated. Interestingly, after a second round of enrichment the output phage count increased significantly, indicating a potential enrichment. After changing the cell line to prevent receptor binding and receptor-mediated endocytosis for a third and fourth iteration the obtained bacteriophage count, was decreased. While this was desired, no significant enrichment was obtained when comparing the outcome of round 1 and 4, with ~ 10^{7} phages presumably being the background signal that was gained after each experiment.

To evaluate these results, clones derived from round 4 were tried to be amplified and sequenced by next generation sequencing. However, this did not deem successful as no PCR product for the V_H domain could be obtained. Sequencing of single clones by Sanger sequencing confirmed that no enrichment of functional phages was achieved revealing out of frame cloned genes or no sequencing result at all.

The presented experiments showed that discrimination steps for unspecific binding to the surface and internalization are crucial to execute this kind of enrichment workflow. The data suggested that by simply washing the cells it was not sufficient to reduce non-internalizing phage output to zero. Therefore, a different strategy was applied to allow better discrimination between internalizing and non-internalizing phages. To this end expression of *E. coli* biotin ligase within mammalian cells and expression of an AviTag™ on the phage might be a suitable approach. Upon internalization in cells, the M13 phage should be site-specifically biotinylated and can be purified via streptavidin or avidin-beads, which might decrease background signal by unspecific binding phages.

7.5.2 Generation of SLE phage display libraries containing an AviTag™

For generation of an SLE phage display library presenting an AviTag™, DNA of the patients was supplied by *Merck Healthcare KGaA* (PCR products of cDNA amplification). The V_H, and κ and λ V_L genes were amplified separately and were assembled to a functional scFv with a linker sequence in between *via* golden gate cloning into a the pPD1 phage display vector. Hereby, the antibody pool of patient SLE007 was used.

As depicted in Figure 45 A, amplification in general was successful. The PCR of V_H (~ 450 bp) led to byproducts, which could not be averted by optimization of the PCR reaction. Hence, gel extraction of

the correct band was conducted. This was not necessary for the κ PCRs as a single band was observed. For the λ approach, weak signals were obtained, consequently leading to low overall DNA yields. Nevertheless, the DNA was used for golden gate assembly and library generation. A final diversity of $2.5*10^{10}$ variants was estimated for the κ-library, and $1*10^{9}$ for the λ counterpart. Colony PCR after golden gate assembly resulted in more full-length genes for the κ-library (6 out of 8) than for the λ-library (1 out of 8) (Figure 45, B). This was likely attributable to the low λ DNA yields and therefore a lower DNA quality in general. Following, the κ-library was used for phage packaging and western blot served as the analysis method. In contrast to the samples derived by *Merck Healthcare KGaA* (see 7.5.1) detection of pIII:scFv fusion with anti-pIII was unproblematic, since a prominent band at ~ 95 kDa was observed (Figure 45, C). Nonetheless, the final phage preparation contained *E. coli* impurities, which ended up in the detection of free scFv with both, the anti-His and Streptavidin-AP staining. The latter suggested that there was biotinylation of the AviTag™ due to endogenous *E. coli* biotin ligase. Even though pIII:scFv fusion could not be detected by this staining method, biotinylation presumably occurred and would end up in the enrichment of false positive phages. Therefore, the desired workflow could not be performed as planned.

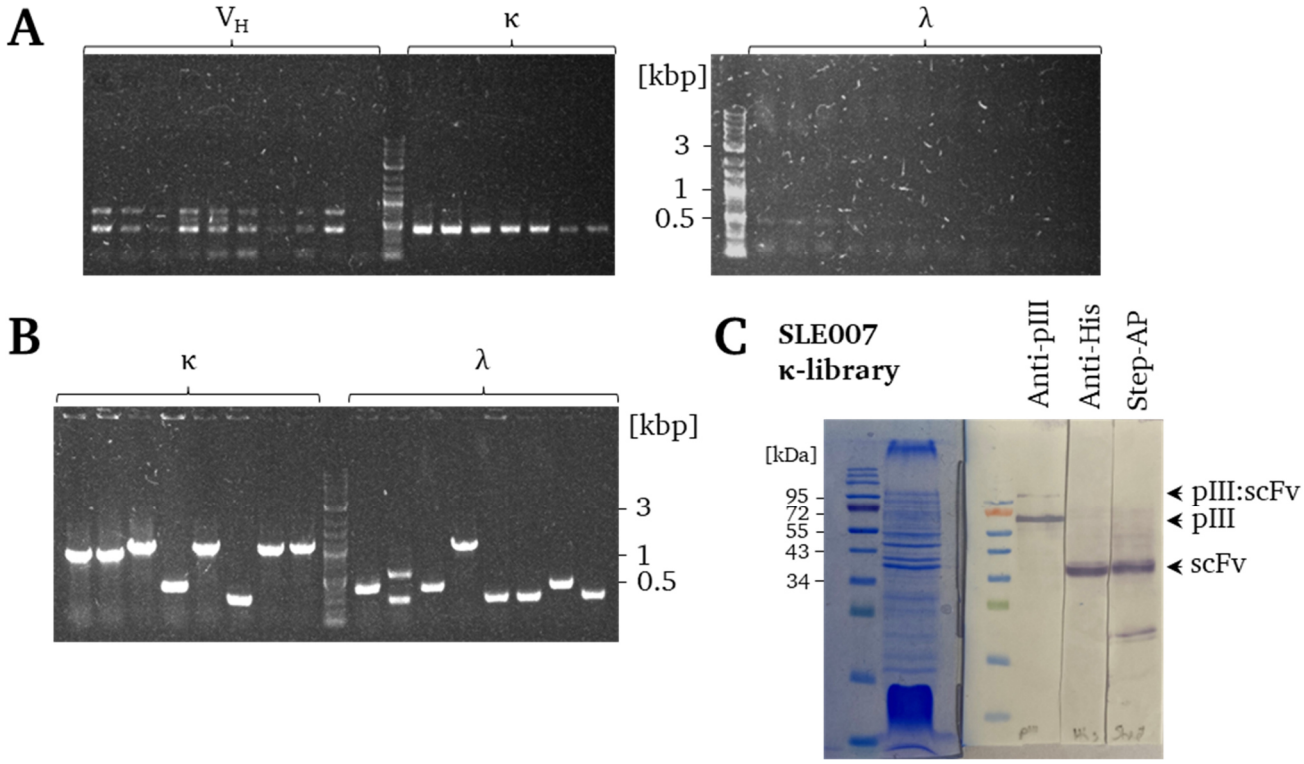

Figure 45: Amplification of SLE007s different IgG V_H and V_L germlines (A), colony PCR of clones derived from library generation by golden gate assembly (B) and SDS-PAGE and western blot analysis of packaged phages presenting scFvs made up of V_H and V_L κ-pool (C). For amplification of the patients IgG V_H and V_L various PCRs were performed. The forward primer was changed in each PCR addressing the different germlines whereas reverse primers stayed the same. In total ten reactions were conducted for the V_H, seven for the κ V_L and eleven for the λ V_L.

7.5.3 Enrichment of internalizing phages using the SLE007 κ-library

Nevertheless, since the library quality from 7.5.2 appeared to be higher than the *Merck Healthcare KGaA* derived counterpart, the approach in 7.5.1 was repeated with the SLE007 κ-library. Analysis of the constructed SLE007 κ-library revealed promising presentation of scFvs, as well as a decent assembly rate by golden gate cloning and therefore the enrichment of internalizing phages was performed. Before lysis, cells were detached from the cell culture flask by trypsin. This should further decrease unspecific binding of phages by removing surface-associated proteins. In parallel, all experiments were carried out with M13KO7 helper phage as a negative control. Besides the missing scFv on the pIII protein, M13KO7 is phenotypically identical to the library phages and should be suitable to evaluate background titer. After each enrichment round, *E. coli* cells were directly used to package phages for the next incubation round on cells. Western blot was utilized to evaluate the presence of pIII:scFv fusions and ultimately the functionality of the library.

For the two enrichment rounds of the SLE007 κ-library no significant enrichment was obtained (Figure 46). Output phage titer remained nearly unchanged and stayed in the range of the M13KO7 titer. Colony PCR after each round (Supplementary figure 12) revealed clones carrying scFv genes, however sequencing of those revealed the presence of early non-amber stop codons (Supplementary figure 12), indicating that in the first-round functional phages were already lost. However, this hypothesis was disproven by western blot analysis after library packaging. Since pIII:scFv fusions were still detectable, there had to be functional phages in the library. This finding was in accordance with section 7.5.1, where identification of functional phages after four rounds of incubation was not possible. Interestingly, most sequences obtained started with the right amino acids, expected for a human V_H framework (EVQ.., QVQ.., DIQ..). Consequently, early stop codons within the gene sequence indicate that errors occurred during amplification of the DNA or even earlier in cDNA generation.

All in all, this performed enrichment method lacked an appropriate way to recover the presenting phages. Alternative approaches to address the expressed His_6-tag between pIII and the scFv by using Ni-NTA magnetic beads were also inconclusive (Supplementary figure 12, C). Nevertheless, the overall quality of the library was questionable, being indicated by many clones containing early stop codons.

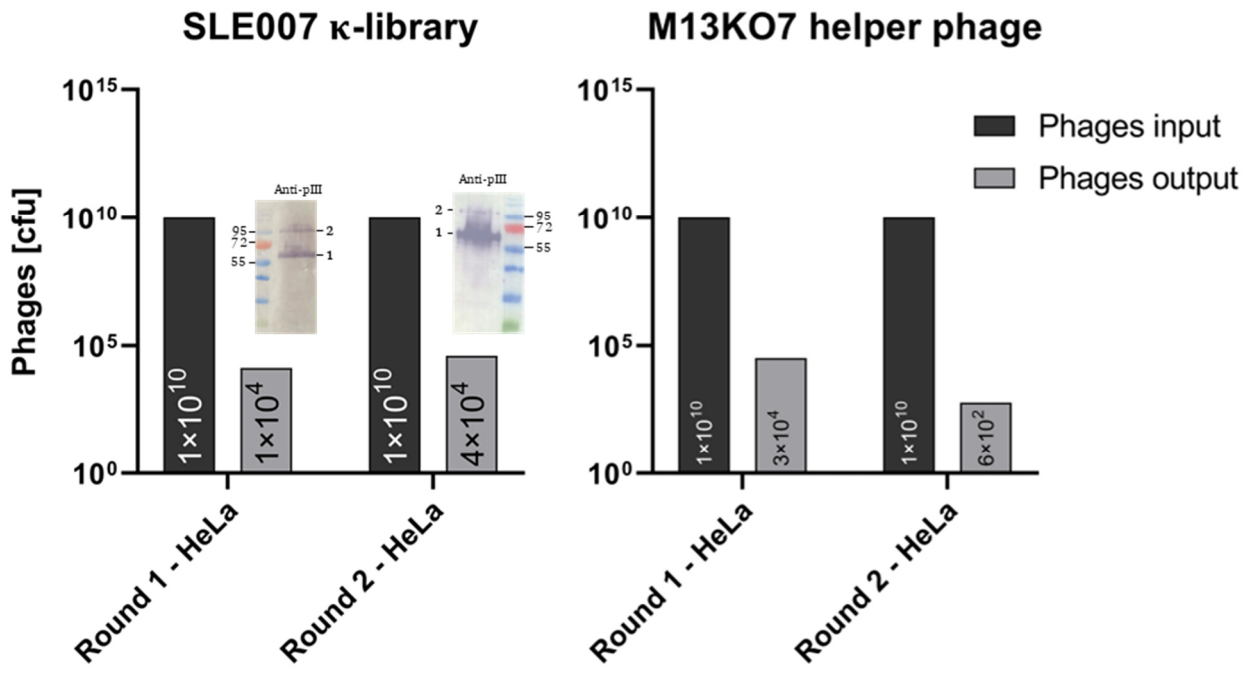

Figure 46: Enrichment of internalizing phages derived from SLE007 κ-library. SLE007 phages and M13KO7 helper phage (negative control) were incubated for ~ 17 h on HeLa cells. After stringent washing of the cells with PBS and low pH stripping buffer, cells were detached from the culture flask by trypsin and lysed by freeze thaw. Cell debris was spun down by centrifugation and the supernatant was used for phage titer determination and infection of a freshly grown culture of *E. coli* ER2738. Cells were used for packaging of new phages and western blot was performed to verify the presence of pIII:scFv fusion. **1**: pIII; **2**: pIII:scFv.

7.5.4 Generation and functional test of stable HeLa cell line expressing microID / ultraID

To draw a bow back to the beginning of this work, the presented problems were addressed by applying another approach mediated by biotin ligases. Using biotin on phages as an affinity ligand seemed to be a good strategy, since it was already used in the phage display context[188]. To prevent early biotinylation during *E. coli* packaging, the AviTag™ had to be removed and biotin had to be introduced to the phages in another way. Hereby, the promiscuous biotin ligases described earlier (7.1) came in handy. Using stably transfected mammalian cells expressing e.g., microID or ultraID in the cytoplasm could be a solution for this approach. Consequently, phages internalizing into the cytoplasm would undergo unspecific biotinylation. After cell lysis, purification by Strep-Tactin® XT beads could be carried out in order to enrich functional phages. An additional advantage of this purification strategy could be avoiding steric hinderance, which could have been the problem with Ni-NTA purification of the phages, since biotinylation likely occurs all over the surface of the phage.

For the generation of stable HeLa cell lines, expressing microID or ultraID, HeLa-EM2-11ht cells were used as previously described in literature[216,217]. Before incorporation into the genome, both biotin ligases were equipped with a nuclear export signal (NES sequence: LPPLERLTL) to ensure cytoplasmatic

localization and genes were subsequently cloned in the integration vector pSF3. Otherwise, entry in the nucleus via nuclear pores would be possible since both enzymes are very small (~ 21.1 kDa with myc-tag).

Western blot analysis of cell lysates revealed that uninduced HeLa cells showed no biotin ligase basal expression and consequently no biotinylation of proteins. In contrast, doxycycline induced mammalian cells showed the desired unspecific biotinylation of the proteosome for both, microID und ultraID (Figure 47). Interestingly, biotinylation seemed to occur only for proteins ≳ 43 kDa. Since, M13 phages are enormous compared to a single protein, it was concluded that the mammalian cells were functional for their desired application. While stable transfection with FLP-recombinase occurs highly specific at one single locus and expression levels of the enzymes should be comparable direct comparison between the microID and ultraID cells couldn´t be done since evaluation of function was done in two separate and independent western blots. However, one could assume that overall biotinylation was stronger in ultraID cells because general activity of the enzyme is known to be higher (7.1.7). However, the experiment was carried out for 17 h, which might end up in comparable turnover. This was also shown in labeling experiments done by our colleagues of the Béthune group[221].

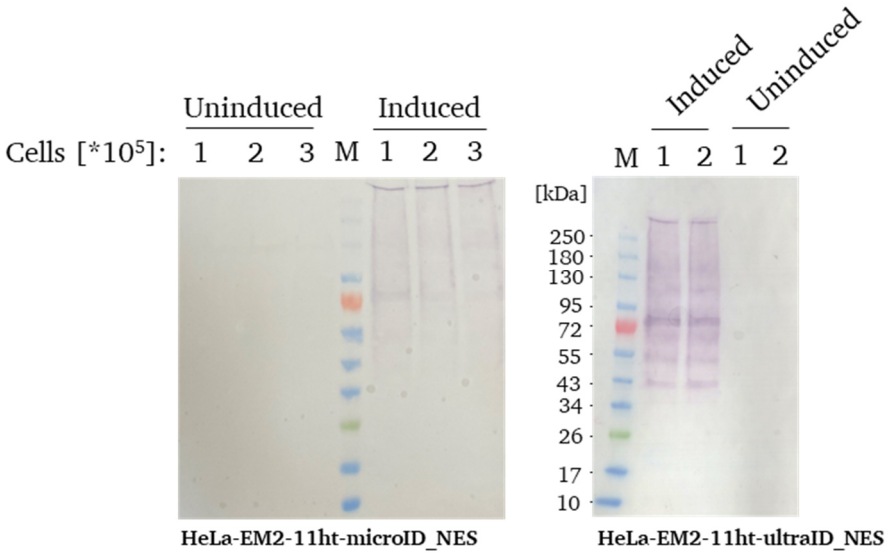

Figure 47: Western blot analysis of HeLa-EM2-11ht cell line lysates stability transfected with microID / ultraID. Different cell counts (1 – 3*10^5 cells) of stably transfected cells were seeded in a 96 well plate. The next day expression of biotin ligases was induced by addition of 1 µg/ml doxycycline. Additionally, 50 µM biotin was added. After 24 h, cells were lysed using 0.1 M EDTA, 0.5% (w/v) SDS and 10 mM Tris-HCl pH 8.0. Lysates were centrifuged at 13000 × g and supernatants were used directly for SDS-PAGE and subsequent western blot analysis with streptavidin-AP staining.

7.5.5 Enrichment of internalizing phages using different SLE libraries and anti-STAT3 VHH

Previous enrichment attempts showed that application of M13 phages on mammalian cells for identification of internalizing binders had some serious drawbacks. There was a significant quantity of phages that most likely did not internalize but rather ended up in the final cell lysate. This was also depicted by the M13KO7 negative control. Furthermore, capturing functional phages was problematic. Colony PCR in combination with sequencing of single clones revealed only mutated scFv genes, presumably resulting in non-functional proteins on the phages. However, analysis of the library by western blot suggested that there were still functional clones present.

To address both problems, phage libraries were generated lacking an AviTag™ to prevent undesired biotinylation during phage production and enable screening with the promiscuous biotin ligase cell lines (for changed workflow see Figure 48, A). Furthermore, a positive control was generated by cloning an anti-STAT3 VHH N-terminally of the pIII protein. This VHH is known to internalize in mammalian cells and could therefore verify the enrichment process[202,203].

The presentation of anti-STAT3 VHH on M13 phages was feasible, with two bands visible after western blot resembling pIII and the pIII:VHH fusion (Figure 48, B). Since a VHH is significantly smaller than an scFv (~ 14 kDa vs ~ 26 kDa), the fusion protein runs lower on SDS-PAGE or western blot compared to the protein of the SLE libraries. The SLE libraries were generated from four patients libraries and analyzed as shown exemplarily in 7.5.2 (Supplementary figure 13), ending up in comparable diversity (Figure 48, C).

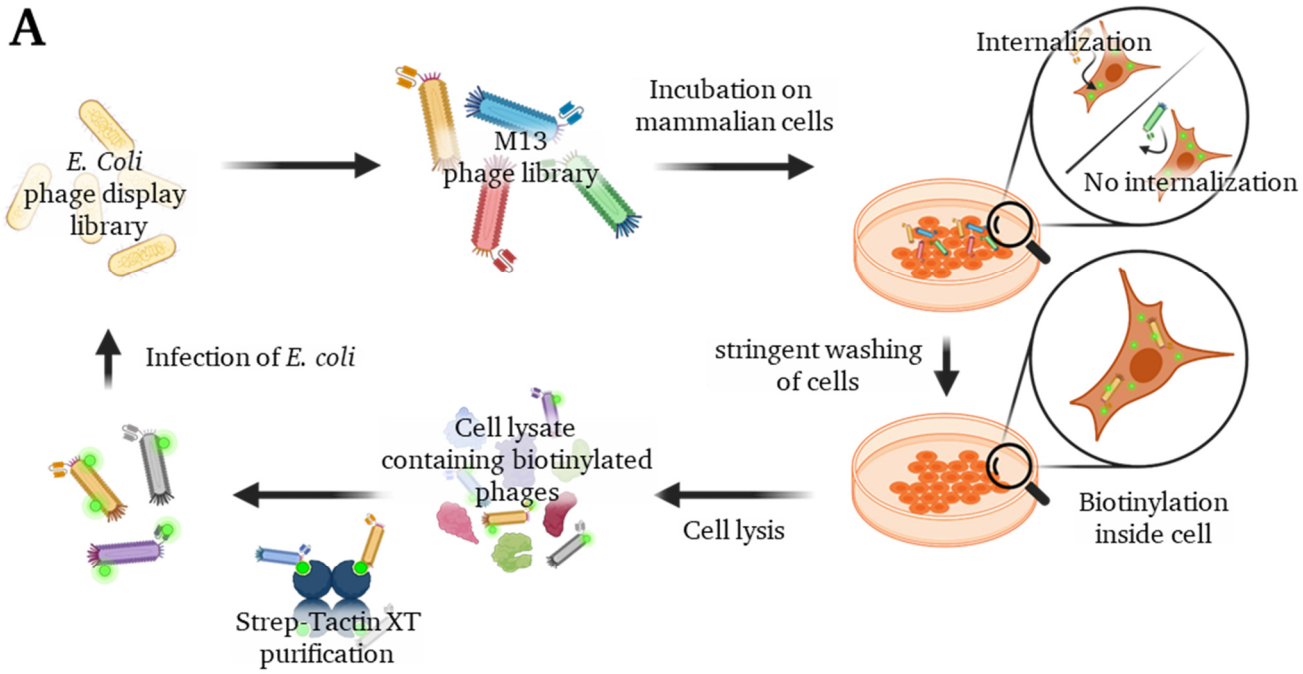

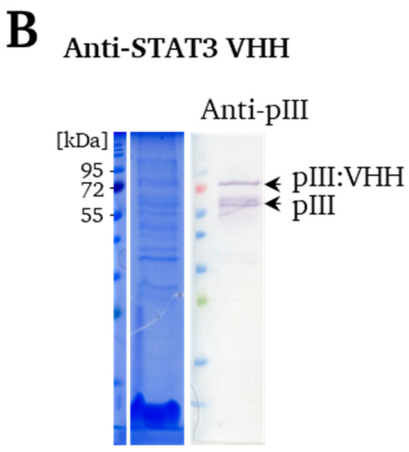

C

	Diversity	
Library	κ-library	λ-Library
SLE005	3.3E+09	3.3E+09
SLE007	3.7E+09	2.3E+10
SLE029	3.3E+09	6.6E+09
SLE043	9.9E+09	1.3E+10

Figure 48: General enrichment workflow using biotin ligase expressing HeLa cells (A), analysis of anti-STAT3 VHH phage preparation by SDS-PAGE and western blot (B) and diversity of SLE phage libraries (C). Anti-STAT3 VHH gene was cloned in pPD1 phage display vector and phages were produced in F^+ *E. coli* cells. Analysis was performed using SDS-PAGE and western blot. For library generation genes of the V_H, κ as well as the λ V_L were amplified separately and were assembled to a functional scFv via golden gate cloning into a the pPD1 phage display vector. Hereby, the antibody pool of patients SLE005, SLE007, SLE029 and SLE043 was used. Diversity was determined by serial dilution of the regenerated *E. coli* cells and growth overnight on agar plates.

For a first feasibility evaluation of the mammalian cell line and the affinity purification via Strep-Tactin® XT, anti-STAT3 VHH presenting phages (positive control) and M13KO7 (negative control) were used. The workflow was comparable to that described in the previous chapters, with the modification that the cell lysate was applied to Strep-Tactin® XT agarose beads, washed three times and phages were directly eluted in *E. coli* samples by using 3 M $MgCl_2$ or 10 mM NaOH.

The results of the experiment are summarized in Table 14. For the anti-STAT3 VHH-presenting phages, around ~ 10^2 colony-forming units (cfu) of phages were obtained. This was a reduction of 10^{10} phages since $1*10^{12}$ bacteriophages were initially applied. For the M13KO7 negative control no colonies were obtained upon *E. coli* infection and selection on kanamycin containing agar plates. While these results looked promising as no background occurred in the negative control enrichment of internalizing phages could be difficult, if $1*10^{12}$ penetrating binders lead to ~ 100 cfu. This concern was enhanced looking at the VHH / M13KO7 mixture, which fits the results obtained for M13KO7 sample. Applying both phages to the same mammalian cells in a ratio of 1:100 ($1*10^{10}$ VHH and $1*10^{12}$ M13KO7) resulted in no *E. coli* colonies. Consequently, the reduction of added internalizing phages by two orders of magnitude ended up in a zero cfu count. In addition to that, there was no significant difference between microID and ultraID cell line considering the phage output.

Table 14: Colony-forming units obtained after incubation on different mammalian cell lines and Strep-Tactin® XT purification. Anti-STAT3 VHH presenting phages or M13KO7 were incubated overnight on HeLa-EM2-11ht cells expressing a promiscuous biotin ligase. After stringent washing cells were lyzed by freeze-thaw and phages were purified via Strep-Tactin® XT agarose beads. For infection of F^+ *E. coli* cells, phages were eluted directly in the cells by using 10 mM of NaOH. Mixture: anti-STAT3 VHH + M13KO7 1:100.

	HeLa-EM2-11ht	
	microID-NES [cfu]	ultraID-NES [cfu]
anti-STAT3 VHH	> 100	> 50
M13KO7	0	0
Mixture	0	0
PBS control	0	0

All in all, experimental data hinted that the presented workflow may not be suitable for the desired application. Considering the low phage count obtained, different reasons can be considered. One could be the harsh elution conditions with 10 mM NaOH or 3 M $MgCl_2$. Consequently, most of the bacteriophages might be unfunctional, prior to *E. coli* infection. As a solution, transduction may be carried out without elution but by mixing of the Strep-Tactin® XT beads with the bacteria. Another consideration was the affinity purification. Since, all cytoplasmic proteins of the HeLa cells are biotinylated, phages are competing for binding sites of Strep-Tactin® XT. Due to the huge size of M13 bacteriophage compared to a single protein, steric hindrance likely favors binding of the latter. Lastly, anti-STAT3 VHH is known to internalize in cells, however the nanobody mediated transport of a complete phage was not shown in literature. To investigate this further, independently of these results,

the AviTag™ removed libraries were incubated on biotin ligase expressing cells. In parallel an experiment was performed where the SLE libraries were mixed 100:1 with anti-STAT3 VHH presenting phage as an internal control.

Results of both experiments are depicted in Table 15 and Table 16. As in the previous experiment cfu count was low. Analysis of the different libraries by colony PCR and sequencing (Supplementary figure 14, A and B) revealed comparable results to the enrichment attempt for the SLE007 kappa library (7.5.3). Most clones had no scFv insert (395 bp product), which was not to be expected since previous experiments showed, that phenotypic M13KO7 phages were completely removed by affinity purification. On top of that, sequencing of the "positive" clones revealed that there were once again early non-amber stop codons and consequently non-presenting phages. One clone (43.3) looked intact at first sight, however the V_H domain was truncated most likely due to a double frameshift. The experiments with mixed phage samples had a similar outcome. Colony PCR showed many (Supplementary figure 14, C) clones without insert and interestingly no anti-STAT3 VHH gene was detected in any of the SLE libraries. Thus, the enrichment of internalizing phages with promiscuous biotin ligase expressing cell lines did not demonstrate to be a successful enrichment method.

Table 15: Colony-forming units obtained after incubation of SLE libraries on HeLa-EM2-11ht-ultraID_NES and Strep-Tactin® XT purification. SLE phage libraries were incubated overnight on HeLa-EM2-11ht-ultraID_NES cells. After stringent washing cells were lyzed by freeze-thaw and phages were purified via Strep-Tactin® XT agarose beads. For infection of F⁺ *E. coli* cells, phages were eluted directly in the cells by using 10 mM of NaOH. $1*10^{12}$ phages of each library were incubated separately on HeLa-EM2-11ht-ultraID_NES cells.

	Phage output [cfu]
anti-STAT3 VHH	> 150
SLE005	~ 50
SLE007	> 100
SLE029	~ 20
SLE043	~ 50

Table 16: Colony-forming units obtained after incubation of SLE libraries mixed with anti-STAT3 VHH phages on HeLa-EM2-11ht-ultraID_NES and Strep-Tactin® XT purification. SLE phage libraries were incubated overnight on HeLa-EM2-11ht-ultraID_NES cells. After stringent washing cells were lyzed by freeze-thaw and phages were purified via Strep-Tactin® XT agarose beads. For infection of F⁺ *E. coli* cells, phages were eluted directly in the cells by using 10 mM of NaOH. $1*10^{12}$ phages of each library were mixed with anti-STAT3 VHH presenting phages in a 100:1 ratio and were incubated separately on HeLa-EM2-11ht-ultraID_NES cells.

	Phage output [cfu]
PBS control	0
anti-STAT3 VHH	29
SLE005	2
SLE007	16
SLE029	1
SLE043	0

7.5.6 Summary and interim conclusion

In conclusion, identification of cell penetrating binders via phage display was unsuccessful. Possible causes for that were diverse. Considering the workflow, it was a tightrope walk between enrichment of unspecifically bound phages on the cell surface and very stringent phage enrichment leading to nearly no phage output. Experiments where phages were applied to mammalian cells without further discrimination strategy had the drawback that background noise was high, ending up in a relatively high phage output. This went hand in hand with trouble isolating functional clones, which could be detected by western blot. Since this approach seemed to be unfeasible, a change of the strategy was necessary. Using the promiscuous biotin ligase approach looked promising at first, since the background was completely removed, being indicated by M13KO7 incubation. However, one must consider that the helper phage is phenotypically identical to a non-presenting M13 phage from the library, but genotypically there are mayor differences. The pPD1 vector, which was used for library generation uses an ampicillin resistance for selection, where in contrast kanamycin is used for M13KO7 amplification. Further pPD1 is based on an ColE1 high-copy-number origin of replication, whereas the engineered helper phage relies on a medium-copy-number p15A origin. Both could impact colony growth after infection. In theory it was possible that M13KO7 had lower colony yields in general, compared to the M13 library. For ultimate validation, empty pPD1 vector (no insert) could have been used to generate M13 phages which carry the pPD1 phagemid but phenotypically having wild type pIII, only. Besides that, the affinity-based purification by Strep-Tactin® XT agarose beads helped to distinguish functional phages from unfunctional once during the enrichment process and seemed promising. However, elution from the agarose beads was only possible under harsh conditions. In the context of the anti-STAT3 VHH positive control, a reduction of ten orders of magnitude happened. In a library context this would mean that a single clone must be present at least 10^{10} times to obtain a single *E. coli* clone afterwards, which is unrealistic for libraries with a size of $\sim 10^{9} – 10^{10}$ individual clones. Considering that, it was likely, that incubation of the libraries on ultraID expressing HeLa cells, did not achieve any successful enrichment. Nevertheless, overall library quality must be considered as well. Sequencing of single clones as well as colony PCRs showed tremendous library characteristics. Both, DNA amplification with One*Taq*® and golden gate cloning are reliable methods, where errors rarely occur, thus the initial DNA received by *Merck Healthcare KGaA* presumably contained an unacceptable high fraction of insert-less phagemids (in context of the already prepared libraries of section 7.5.1) and genes containing deletions and stop codons (for the freshly prepared libraries from section 7.5.2 and 7.5.5). This was also shown when the ready-to-use *E. coli* libraries were used for phage packaging. Detection of pIII:scFv fusions was not possible, indicating poor material quality. Indeed, as observed in this experimental setting, the

phenomenon of enrichment of phages with deletions and stop codons upon incubation with mammalian cells (in this case aimed at obtaining cell surface binders) was also reported by others[235]. In summary, identification of the internalizing binders likely failed, due to a difficult enrichment approach as well as a defective starting material.

8 Conclusion and Outlook

In this work biotin ligases have been applied and been engineered for different approaches starting with fundamental research and ending with biopharmaceutical applications. Hereby, the unique interaction between biotin and (strept)avidin was exploited (BioID and phage screening) or the small molecule served as scaffold for introduction of click chemistry handles, which were conjugated to an antibody enabling chemoenzymatic modification.

First, a novel enzyme for BioID screenings called ultraID was engineered. While based on a truncated biotin ligase derived from *Aquifex aeolicus* one single amino acid exchange (L41P) was identified which massively improves the catalytic turnover of the enzyme. During revision of the manuscript another paper has been published addressing optimization of BioID2. Using a rational approach Johnson *et al.* also discovered L41 in addition to others as important residues for optimization of the enzyme[236]. Evaluating this data, ultraID is comparable in size to microID2 and data suggest that our enzyme variant seems to be still faster in overall performance. However, this needs to be carefully analyzed in follow-up experiments. Besides that, it would be interesting to investigate whether there is potential for further optimization of the enzyme. Particularly the loop in the active site (see Figure 25 in section 7.1.4, G37 to R43) could be randomized by e.g., degenerative primers and a small sized mutant library could be generated. This approach may end up in even more active variants. Additionally, it would be interesting to screen the presented library for enzyme mutants using (solely) desthiobiotin. A comparable experiment was already done by Lu *et al*. in 2014[205] with the *E. coli* biotin ligase. Since, desthiobiotin and biotin exhibit different affinities[226] to streptavidin this could enable selective purification[237] and helps to discriminate between proteins derived from BioID and from endogenous biotinylation of the cell. It might also be applicable to perform two BioID experiments at the same time independently from each other. Thereby, the biotin and the desthiobiotin engineered enzymes are fused to different POIs at the same time. Afterwards differentiation of POI interacting proteins could be carried out by the attached biotin derivate.

Second, it was investigated to identify a propargyl biotin using biotin ligase starting off with the priorly mentioned yeast surface display library encoding biotin ligase mutants. Hereby, enrichment attempts failed. Changing the presentation strategy was also unsuccessful. There has been a directed evolution approach in the past, where a biotin ligase was engineered towards desthiobiotin[205]. So, in principle this should be feasible for other substrates, too. However, Lu and coworkers used in vitro compartmentalization for their approach. While in this work, yeast surface display was conducted there were problems with the biotin acceptor. Fusion to the same protein chain led to weak conversion which

was not suitable for further experiments. Nevertheless, following experiments showed that propargyl biotin was not suitable for the intended ADC generation and therefore screening only makes sense if ligand conjugation using copper click chemistry and propargyl biotin would have been optimized beforehand.

Third, the biotin ligase of *Pyrococcus horikoshii* was used with the biotin click chemistry derivatives propargyl biotin and desthiobiotin azide to generate an ADC. For this approach the therapeutic antibody trastuzumab was fused with the biotin acceptor domain p67 at different sites. It was shown that conjugation with propargyl biotin to the antibody was successful, however CuAAC in presence of the antibody was not possible. For the desthiobiotin azide variant chemoenzymatic conjugation of TAMRA to the antibody was successful. Nevertheless, unspecific conjugation to the light chain of the antibody as well as to non-p67 fused proteins occurred. The reason for this phenomenon was presumably the decreased affinity of the desthiobiotin azide to the enzyme which led to an undesired release of the activated intermediate. Additionally, it seemed, that the enzyme in general is not highly specific for a biotin acceptor. For further investigation it needed to be evaluated whether unwanted biotinylation could be decreased. As a straight forwards solution, this could be carried out by reaction optimization. Reactions with trastuzumab-HC:p67 and PhBL were usually carried out overnight which was necessary since the Slavoff publication[143] showed that turnover of the desthiobiotin azide was slow. Nevertheless, it should be investigated if shorter labeling decreases off-target biotinylation. Additionally, conjugation at lower temperatures might have an impact on the specificity. Since, Brownian motion is slower at lower temperatures this could also compensate unspecific release of the activated intermediate. If this approaches fail, engineering of the enzyme could be carried out with the aim to improve affinity for the substrate.

Moving away from biotin ligases, another ligase was used for generation of an ADC. Lipoate-protein ligase A was engineered in the past to conjugate bulky, click chemistry suitable molecules to LAP-tagged proteins. It was shown for the first time, that in a chemoenzymatic approach this system was applicable for ADC generation. Additionally, the enzyme had very fast turnover rates within a few minutes. However, introducing the LAP-tag at the C-terminus of the antibody may have an impact on the overall immunogenicity of the construct. A higher antigenicity is undesired and therefore needs to be further investigated. For further experiments it could also be considered to perform one-pot reactions in combination with e.g., PhBL. Since, both enzymes rely on the same co-factors this might be a feasible approach. After optimization of the PhBL conjugation, introduction of orthogonal click chemistry

moieties by both enzymes could be carried out aiming at dual-site specific modification of glycosylated antibodies within only two conjugation steps.

Last, identification of internalizing scFvs from phage display libraries derived from SLE patients was conducted. All attempts, whether they relied on solely incubation on mammalian cells or internalization discrimination by biotinylation mediated by biotin ligases, led to enrichment of nonfunctional scFv genes. Reasons for that were diverse starting from a missing purification method for enrichment of functional phage over difficulties to verify the functionality of the internalizing anti-STAT3 VHH phages and ending with an unknown quality of the obtained SLE phage library and/or DNA. In future experiments the library functionality should be assured at first. This could be carried out by yeast surface display. Hereby, assembly of the scFv could be done directly by gap repair cloning. Yeasts which present a full length scFv can be sorted out by FACS and the library containing intact genes could be transferred to the phage context. Next, a phage presenting the 3D8 transbody as described in the publication by Kim *et al.*[187] should be constructed as a positive control and mixed with the library as an internal standard. Afterwards screening with or without selection pressure by biotin ligase could be repeated. Alternatively, screening of the yeast library could be performed, too. Since, it is known that internalizing antibodies often exhibit many positively charged amino acids and binding to sulfate polysaccharides or glycosaminoglycans occurs[201] enrichment of yeasts binding to fluorescently label heparin or the like could be done. This could obviously be done with the phage library in a panning experiment against heparin, too.

9 References

1. Roser M. & Ritchie H.: Cancer. *Our World in Data* (Webpage last updated 2019) Available at: https://ourworldindata.org/cancer. (Accessed: November 4, 2022)
2. Ferlay J., Colombet M., Soerjomataram I., Parkin D. M., Piñeros M., Znaor A. & Bray F.: Cancer statistics for the year 2020: An overview. *Int. J. Cancer* **149**, pp. 778–789 (2021).
3. Sung H., Ferlay J., Siegel R. L., Laversanne M., Soerjomataram I., Jemal A. & Bray F.: Global Cancer Statistics 2020: GLOBOCAN Estimates of Incidence and Mortality Worldwide for 36 Cancers in 185 Countries. *CA. Cancer J. Clin.* **71**, pp. 209–249 (2021).
4. Bluethmann S. M., Mariotto A. B. & Rowland J. H.: Anticipating the "Silver Tsunami": Prevalence Trajectories and Co-Morbidity Burden among Older Cancer Survivors in the United States. *Cancer Epidemiol. Biomarkers Prev.* **25**, pp. 1029–1036 (2016).
5. Miller K. D., Nogueira L., Devasia T., Mariotto A. B., Yabroff K. R., Jemal A., Kramer J. & Siegel R. L.: Cancer treatment and survivorship statistics, 2022. *CA. Cancer J. Clin.* **72**, pp. 409–436 (2022).
6. Yabroff K. R., Mariotto A., Tangka F., Zhao J., Islami F., Sung H., Sherman R. L., Henley S. J., Jemal A. & Ward E. M.: Annual Report to the Nation on the Status of Cancer, Part 2: Patient Economic Burden Associated With Cancer Care. *JNCI J. Natl. Cancer Inst.* **113**, pp. 1670–1682 (2021).
7. NIH National Cancer Institute.: What Is Cancer? (Webpage last updated 2021) Available at: https://www.cancer.gov/about-cancer/understanding/what-is-cancer. (Accessed: November 11, 2022)
8. Hanahan D. & Weinberg R. A.: Hallmarks of cancer: The next generation. *Cell* **144**, pp. 646–674 (2011).
9. Hayflick L.: The limited in vitro lifetime of human diploid cell strains. *Exp. Cell Res.* **37**, pp. 614–636 (1965).
10. Nishida N, Yano H, Nishida T, Kamura T K. M.: Angiogenesis in Cancer. *Vasc Heal. Risk Manag.* **2**, pp. 213–9 (2006).
11. Boroughs L. K. & Deberardinis R. J.: Metabolic pathways promoting cancer cell survival and growth. *Nat. Cell Biol. 2015 174* **17**, pp. 351–359 (2015).
12. Dang C. V.: Links between metabolism and cancer. *Genes Dev.* **26**, pp. 877–890 (2012).
13. Dingar D., Kalkat M., Chan P.-K., Bailey S. D., Srikumar T., Tu W. B., Coyaud E., Ponzielli R., Kolyar M., Jurisica I., *et al.*: Abstract B04: In vivo BioID identifies novel Myc interacting partners. *Mol. Cancer Res.* **13**, pp. B04–B04 (2015).
14. Sharifi Tabar M., Francis H., Yeo D., Bailey C. G., J Rasko J. E., Ka Shing Cell L., Therapy Program G. & Charles Bailey C. G.: Mapping oncogenic protein interactions for precision medicine. *Int. J. Cancer* **151**, pp. 7–19 (2022).
15. Pedley R., King L. E., Mallikarjun V., Wang P., Swift J., Brennan K. & Gilmore A. P.: BioID-based proteomic analysis of the Bid interactome identifies novel proteins involved in cell-cycle-dependent apoptotic priming. *Cell Death Dis. 2020 1110* **11**, pp. 1–17 (2020).
16. Kim B. R., Coyaud E., Laurent E. M. N., St-Germain J., Van De Laar E., Tsao M. S., Raught B. & Moghal N.: Identification of the SOX2 Interactome by BioID Reveals EP300 as a Mediator of SOX2-dependent Squamous Differentiation and Lung Squamous Cell Carcinoma Growth. *Mol. Cell.*

Proteomics **16**, pp. 1864–1888 (2017).

17. Roux K. J., Kim D. I., Raida M. & Burke B.: A promiscuous biotin ligase fusion protein identifies proximal and interacting proteins in mammalian cells. *J. Cell Biol.* **196**, pp. 801–810 (2012).

18. Livnah O., Bayert E. A., Wilchekt M. & Sussman J. L.: Three-dimensional structures of avidin and the avidin-biotin complex (deglycosylated avidin/divergent evolution/x-ray crystallography/streptavidin). *Proc. Natl. Acad. Sci.* **90**, pp. 5076–5080 (1993).

19. Gitlin G., Bayer E. A. & Wilchek M.: Studies on the biotin-binding site of streptavidin Tryptophan residues involved in the active site. *Biochem. J* **256**, pp. 279–282 (1988).

20. Kim D. I., Kc B., Zhu W., Motamedchaboki K., Doye V. & Roux K. J.: Probing nuclear pore complex architecture with proximity-dependent biotinylation. *Proc Natl Acad Sci USA* **111**, pp. 2453–61 (2014).

21. Kim D. I., Jensen S. C., Noble K. A., Kc B., Roux K. H., Motamedchaboki K. & Roux K. J.: An improved smaller biotin ligase for BioID proximity labeling. *Mol. Biol. Cell* **27**, pp. 1188–1196 (2016).

22. Varnaitė R. & MacNeill S. A.: Meet the neighbors: Mapping local protein interactomes by proximity-dependent labeling with BioID. *Proteomics* **16**, pp. 2503–2518 (2016).

23. Ramanathan M., Majzoub K., Rao D. S., Neela P. H., Zarnegar B. J., Mondal S., Roth J. G., Gai H., Kovalski J. R., Siprashvili Z., *et al.*: RNA–protein interaction detection in living cells. *Nat. Methods 2018 153* **15**, pp. 207–212 (2018).

24. Branon T. C., Bosch J. A., Sanchez A. D., Udeshi N. D., Svinkina T., Carr S. A., Feldman J. L., Perrimon N. & Ting A. Y.: Efficient proximity labeling in living cells and organisms with TurboID. *Nat. Biotechnol. 2018 369* **36**, pp. 880–887 (2018).

25. Kido K., Yamanaka S., Nakano S., Motani K., Shinohara S., Nozawa A., Kosako H., Ito S. & Sawasaki T.: AirID, a novel proximity biotinylation enzyme, for analysis of protein–protein interactions. *Elife* **9**, (2020).

26. Chabner B. A. & Roberts T. G.: Chemotherapy and the war on cancer. *Nat. Rev. Cancer* **5**, pp. 65–72 (2005).

27. Nygren P.: What is cancer chemotherapy? *Acta Oncol. (Madr).* (2009). doi:10.1080/02841860151116204

28. DeVita V. T. & Chu E.: A History of Cancer Chemotherapy. *Cancer Res.* **68**, pp. 8643–8653 (2008).

29. NIH National Cancer Institute.: Chemotherapy to Treat Cancer. (Webpage last updated 2023) Available at: https://www.cancer.gov/about-cancer/treatment/types/chemotherapy. (Accessed: November 23, 2022)

30. Chen H. H. W. & Kuo M. T.: Improving radiotherapy in cancer treatment: Promises and challenges. *Oncotarget* **8**, pp. 62742–62758 (2017).

31. NIH National Cancer Institute.: Radiation Therapy to Treat Cancer. (Webpage last updated 2019) Available at: https://www.cancer.gov/about-cancer/treatment/types/radiation-therapy. (Accessed: November 23, 2022)

32. Hellerstedt B. A. & Pienta K. J.: The Current State of Hormonal Therapy for Prostate Cancer. *CA. Cancer J. Clin.* **52**, pp. 154–179 (2002).

33. Drãgãnescu M., Trestioreanu A. & Carmocan C.: Hormone Therapy in Breast Cancer. *Rev. Artic. Chir.* **112**, pp. 2017 (2017).

34. Locker G. Y.: Hormonal therapy of breast cancer. *Cancer Treat. Rev.* **24**, pp. 221–240 (1998).

35. Habash R. W. Y.: Therapeutic hyperthermia. *Handb. Clin. Neurol.* **157**, pp. 853–868 (2018).

36. Roemer R. B.: Engineering Aspects of Hyperthermia Therapy. *Annu. Rev. Biomed. Eng.* **1**, pp. 347–376 (1999).

37. Halperin E. C., Wazer D. E. & Perez C. A.: The Discipline of Radiation Oncology. Published in *Perez and Brady's Principles and Practice of Radiation Oncology* pp. 33 (2013).

38. Braathen L. R., Szeimies R. M., Basset-Seguin N., Bissonnette R., Foley P., Pariser D., Roelandts R., Wennberg A. M. & Morton C. A.: Guidelines on the use of photodynamic therapy for nonmelanoma skin cancer: An international consensus. *J. Am. Acad. Dermatol.* **56**, pp. 125–143 (2007).

39. Li X., Lovell J. F., Yoon J. & Chen X.: Clinical development and potential of photothermal and photodynamic therapies for cancer. *Nat. Rev. Clin. Oncol.* pp. 657–674 (2020). doi:10.1038/s41571-020-0410-2

40. Grand View Research.: Cancer Immunotherapy Market Size, Share & Trends Analysis Report By Product (Monoclonal Antibodies, Immunomodulators), By Application, By Distribution Channel, By End-use and Segment Forecasts, 2022 - 2030. pp. 150 (Webpage last updated 2022) Available at: https://www.grandviewresearch.com/industry-analysis/cancer-immunotherapy-market. (Accessed: November 24, 2022)

41. Tan S., Li D. & Zhu X.: Cancer immunotherapy: Pros, cons and beyond. *Biomed. Pharmacother.* **124**, (2020).

42. Waldmann T. A.: Immunotherapy: past, present and future. *Nat. Med. 2003 93* **9**, pp. 269–277 (2003).

43. Schuster M., Nechansky A., Loibner H. & Kircheis R.: Cancer immunotherapy. *Biotechnol. J.* **1**, pp. 138–147 (2006).

44. Joost Lesterhuis W., A G Haanen J. B. & A Punt C. J.: Cancer immunotherapy – revisited. *Nat. Rev. Drug Discov.* **10**, pp. 591–600 (2011).

45. Farkona S., Diamandis E. P. & Blasutig I. M.: Cancer immunotherapy: The beginning of the end of cancer? *BMC Med.* **14**, pp. 1–18 (2016).

46. Shi H., Qi X., Ma B., Cao Y., Wang L., Sun L. & Niu H.: The status, limitation and improvement of adoptive cellular immunotherapy in advanced urologic malignancies. *Chinese J. Cancer Res.* **27**, pp. 128 (2015).

47. Hinrichs C. S., Rosenberg S. A. & Carl J.: Exploiting the curative potential of adoptive T-cell therapy for cancer. *Immunol. Rev.* **257**, (2013).

48. Wang R., Pan W., Jin L., Huang W., Li Y., Wu D., Gao C., Ma D. & Liao S.: Human papillomavirus vaccine against cervical cancer: Opportunity and challenge. *Cancer Lett.* **471**, pp. 88–102 (2020).

49. Blumberg B. S.: Perspective Hepatitis B virus, the vaccine, and the control of primary cancer of the liver*. *Proc. Natl. Acad. Sci.* **94**, pp. 7121–7125 (1997).

50. Sondak V. K., Sabel M. S. & Mulé J. J.: Allogeneic and Autologous Melanoma Vaccines: Where Have We Been and Where Are We Going? *Clin. Cancer Res.* **12**, pp. 2337s-2341s (2006).

51. Castle J. C., Kreiter S., Diekmann J., Löwer M., Van De Roemer N., De Graaf J., Selmi A., Diken M., Boegel S., Paret C., *et al.*: Exploiting the mutanome for tumor vaccination. *Cancer Res.* **72**, pp. 1081–1091 (2012).

52. Kreiter S., Vormehr M., Van De Roemer N., Diken M., Löwer M., Diekmann J., Boegel S., Schrörs B., Vascotto F., Castle J. C., *et al.*: Mutant MHC class II epitopes drive therapeutic immune responses to cancer. *Nature* pp. 692–696 (2013). doi:10.1038/nature14426

53. Fehniger T. A., Cooper M. A. & Caligiuri M. A.: Interleukin-2 and interleukin-15: Immunotherapy for cancer. *Cytokine Growth Factor Rev.* **13**, pp. 169–183 (2002).

54. Cancer research UK.: Types of cancer immunotherapy - cytokines. (Webpage last updated 2021) Available at: https://www.cancerresearchuk.org/about-cancer/treatment/immunotherapy/types/cytokines.

55. Institute for clinical and economic review.: Chimeric Antigen Receptor T-Cell Therapy for BCell Cancers: Effectiveness and Value. (Webpage last updated 2018) Available at: https://icer.org/wp-content/uploads/2020/10/ICER_CAR_T_Final_Evidence_Report_032318.pdf.

56. Schroeder H. W. & Cavacini L.: Structure and Function of Immunoglobulins. *J. Allergy Clin. Immunol.* **125**, pp. S41 (2010).

57. Stoop J. W., Zegers B. J. M., Sander P. C. & Ballieux R. E.: Serum immunoglobulin levels in healthy children and adults. *Clin. Exp. Immunol.* **4**, pp. 101 (1969).

58. Murphy K. M., Travers P. & Walport M.: Die Struktur eines typischen Antikörpermoleküls. Published in *Janeway Immunologie* pp. 143–150 (2014).

59. Murphy K. M., Travers P. & Walport M.: Die Wechselwirkung des Antikörpermoleküls mit einem spezifischen Antigen. Published in *Janeway Immunologie* pp. 151–156 (2014).

60. Murphy K. M., Travers P. & Walport M.: Verteilung und Funktion der Immunglobulinisotypen. Published in *Janeway Immunologie* pp. 509–516 (2014).

61. Lu L. L., Suscovich T. J., Fortune S. M. & Alter G.: Beyond binding: antibody effector functions in infectious diseases. *Nat Rev Immunol.* **18**, pp. 46–61 (2017).

62. Forthal D. N.: Functions of Antibodies. *Microbiol. Spectr.* **2**, pp. 1 (2015).

63. Liu L. & Chen J.: Therapeutic antibodies for precise cancer immunotherapy: current and future perspectives. *Med. Rev.* **2**, pp. 555–569 (2022).

64. Shan D., Ledbetter J. A. & Press O. W.: Signaling events involved in anti-CD20-induced apoptosis of malignant human B cells. *Cancer Immunol. Immunother.* **48**, pp. 673–683 (2000).

65. Reff M. E., Carner K., Chambers K. S., Chinn P. C., Leonard J. E., Raab R., Newman R. A., Hanna N. & Anderson D. R.: Depletion of B Cells In Vivo by a Chimeric Mouse Human Monoclonal Antibody to CD20. *Blood* **83**, pp. 435–445 (1994).

66. Mössner E., Brünker P., Moser S., Püntener U., Schmidt C., Herter S., Grau R., Gerdes C., Nopora A., Van Puijenbroek E., *et al.*: Increasing the efficacy of CD20 antibody therapy through the engineering of a new type II anti-CD20 antibody with enhanced direct and immune effector cell–mediated B-cell cytotoxicity. *Blood* **115**, pp. 4393–4402 (2010).

67. Teeling J. L., French R. R., Cragg M. S., Van Den Brakel J., Pluyter M., Huang H., Chan C., Parren P. W. H. I., Hack C. E., Dechant M., *et al.*: Characterization of new human CD20 monoclonal antibodies with potent cytolytic activity against non-Hodgkin lymphomas. *Blood* **104**, pp. 1793–1800 (2004).

68. Boyerinas B., Jochems C., Fantini M., Heery C. R., Gulley J. L., Tsang K. Y. & Schlom J.: Antibody-dependent cellular cytotoxicity (ADCC) activity of a novel anti-PD-L1 antibody avelumab (MSB0010718C) on human tumor cells HHS Public Access. *Cancer Immunol Res* **3**, pp. 1148–1157

(2015).

69. Choueiri T. K., Fishman M. N., Escudier B., Mcdermott D. F., Drake C. G., Kluger H., Stadler W. M., Luis Perez-Gracia J., Mcneel D. G., Curti B., *et al.*: Cancer Therapy: Clinical Immunomodulatory Activity of Nivolumab in Metastatic Renal Cell Carcinoma. *Clin Cancer Res* **22**, pp. 5461–5471 (2016).

70. Khoja L., Butler M. O., Kang S. P., Ebbinghaus S. & Joshua A. M.: Pembrolizumab. *J. Immunother. Cancer* **3**, pp. 1–13 (2015).

71. Burger R. A., Brady M. F., Bookman M. A., Fleming G. F., Monk B. J., Huang H., Mannel R. S., Homesley H. D., Fowler J., Greer B. E., *et al.*: Incorporation of Bevacizumab in the Primary Treatment of Ovarian Cancer. *N. Engl. J. Med.* **365**, pp. 2473–2483 (2011).

72. Casak S. J., Fashoyin-Aje I., Lemery S. J., Zhang L., Jin R., Li H., Zhao L., Zhao H., Zhang H., Chen H., *et al.*: FDA Approval Summary: Ramucirumab for Gastric Cancer. *Clin Cancer Res* **21**, pp. 3372–3376 (2015).

73. Petricevic B., Laengle J., Singer J., Sachet M., Fazekas J., Steger G., Bartsch R., Jensen-Jarolim E. & Bergmann M.: Trastuzumab mediates antibody-dependent cell-mediated cytotoxicity and phagocytosis to the same extent in both adjuvant and metastatic HER2/neu breast cancer patients. *J. Transl. Med.* **11**, pp. 307 (2013).

74. Slamon D., Eiermann W., Robert N., Pienkowski T., Martin M., Press M., Mackey J., Glaspy J., Chan A., Pawlicki M., *et al.*: Adjuvant Trastuzumab in HER2-Positive Breast Cancer. *n engl j med* **14**, pp. 1273–83 (2011).

75. Maximiano S., Magalhães P., Pereira Guerreiro M. & Morgado M.: Trastuzumab in the Treatment of Breast Cancer. *BioDrugs* **30**, (2016).

76. Baselga J.: A new anti-ErbB2 strategy in the treatment of cancer: Prevention of ligand-dependent ErbB2 receptor heterodimerization. *Cancer Cell* **2**, pp. 93–95 (2002).

77. Scheuer W., Friess T., Burtscher H., Bossenmaier B., Endl J. & Hasmann M.: Strongly enhanced antitumor activity of trastuzumab and pertuzumab combination treatment on HER2-positive human xenograft tumor models. *Cancer Res.* **69**, pp. 9330–9336 (2009).

78. Boekhout A. H., Beijnen J. H. & Schellens J. H. M.: Trastuzumab. *Oncologist* **16**, pp. 800–810 (2011).

79. Harbeck N., Beckmann M. W., Rody A., Schneeweiss A., Müller V., Fehm T., Marschner N., Gluz O., Schrader I., Heinrich G., *et al.*: HER2 Dimerization Inhibitor Pertuzumab - Mode of Action and Clinical Data in Breast Cancer. *Breast Care* **8**, pp. 49–55 (2013).

80. Metzger-Filho O., Winer E. P. & Krop I.: Pertuzumab: Optimizing HER2 Blockade. *Clin Cancer Res* **19**, pp. 5552–5556 (2013).

81. Nahta R., Hung M. C. & Esteva F. J.: The HER-2-Targeting Antibodies Trastuzumab and Pertuzumab Synergistically Inhibit the Survival of Breast Cancer Cells. *Cancer Res.* **64**, pp. 2343–2346 (2004).

82. U.S. Food and Drug Administration.: HERCEPTIN® (trastuzumab) for injection, for intravenous use Initial U.S. Approval. pp. 11 DESCRIPTION (1998).

83. Carter P. J. & Presta L. G.: U.S. Patent US5821337A: Immunoglobulin variants. (1992).

84. Carter P. J. & Presta L. G.: U.S. Patent US6407213B1: Method for making humanized antibodies. (1992).

85. Buntz B.: 50 of 2021's best-selling pharmaceuticals. *Drug Discovery & Development,* (Webpage last updated 2022) Available at: https://www.drugdiscoverytrends.com/50-of-2021s-best-selling-pharmaceuticals/.

86. Simon King.: The Best Selling Drugs of All Time; Humira Joins The Elite. *Forbes* (Webpage last updated 2013) Available at: https://www.forbes.com/sites/simonking/2013/01/28/the-best-selling-drugs-of-all-time-humira-joins-the-elite/?sh=1db7d15e5110.

87. James Brumley.: The 15 All-Time Best-Selling Prescription Drugs. *Kiplinger* (Webpage last updated 2017) Available at: https://www.kiplinger.com/slideshow/investing/t027-s001-the-15-all-time-best-selling-prescription-drugs/index.html.

88. Yang Y., Wang S., Ma P., Jiang Y., Cheng K., Yu Y., Jiang N., Miao H., Tang Q., Liu F., *et al.*: Drug conjugate-based anticancer therapy - Current status and perspectives. *Cancer Lett.* **552**, (2023).

89. Zhu Y., Liu K., Wang K. & Zhu H.: Treatment-related adverse events of antibody–drug conjugates in clinical trials: A systematic review and meta-analysis. *Cancer* **129**, pp. 283–295 (2022).

90. Rudnick S. I., Lou J., Shaller C. C., Tang Y., Klein-Szanto A. J. P., Weiner L. M., Marks J. D. & Adams G. P.: Influence of Affinity and Antigen Internalization on the Uptake and Penetration of Anti-HER2 Antibodies in Solid Tumors. *Cancer Res.* **71**, pp. 2250–2259 (2011).

91. Diamantis N. & Banerji U.: Antibody-drug conjugates—an emerging class of cancer treatment. *Br. J. Cancer 2016 1144* **114**, pp. 362–367 (2016).

92. Francisco J. A., Cerveny C. G., Meyer D. L., Mixan B. J., Klussman K., Chace D. F., Rejniak S. X., Gordon K. A., DeBlanc R., Toki B. E., *et al.*: cAC10-vcMMAE, an anti-CD30–monomethyl auristatin E conjugate with potent and selective antitumor activity. *Blood* **102**, pp. 1458–1465 (2003).

93. Moldenhauer G., Salnikov A. V., Lüttgau S., Herr I., Anderl J. & Faulstich H.: Therapeutic potential of amanitin-conjugated anti-epithelial cell adhesion molecule monoclonal antibody against pancreatic carcinoma. *J. Natl. Cancer Inst.* **104**, pp. 622–634 (2012).

94. Wang Y., Liu L., Fan S., Xiao D., Xie F., Li W., Zhong W. & Zhou X.: Antibody-Drug Conjugate Using Ionized Cys-Linker-MMAE as the Potent Payload Shows Optimal Therapeutic Safety. *Cancers 2020, Vol. 12, Page 744* **12**, pp. 744 (2020).

95. Dubowchik G. M., Firestone R. A., Padilla L., Willner D., Hofstead S. J., Mosure K., Knipe J. O., Lasch S. J. & Trail P. A.: Cathepsin B-Labile Dipeptide Linkers for Lysosomal Release of Doxorubicin from Internalizing Immunoconjugates: Model Studies of Enzymatic Drug Release and Antigen-Specific In Vitro Anticancer Activity. *Bioconjug. Chem.* **13**, pp. 855–869 (2002).

96. Lee A.: Loncastuximab Tesirine: First Approval. *Drugs* **81**, pp. 1229–1233 (2021).

97. Lamb Y. N.: Inotuzumab Ozogamicin: First Global Approval. *Drugs* **77**, pp. 1603–1610 (2017).

98. Mcgavin J. K. & Spencer C. M.: Gemtuzumab ozogamicin. *Drugs* **61**, pp. 1317–1322 (2001).

99. Drago J. Z., Modi S. & Chandarlapaty S.: Unlocking the potential of antibody–drug conjugates for cancer therapy. *Nat. Rev. Clin. Oncol.* **18**, pp. 327 (2021).

100. Bouchard H., Viskov C. & Garcia-Echeverria C.: Antibody–drug conjugates—A new wave of cancer drugs. *Bioorg. Med. Chem. Lett.* **24**, pp. 5357–5363 (2014).

101. Perez H. L., Cardarelli P. M., Deshpande S., Gangwar S., Schroeder G. M., Vite G. D. & Borzilleri R. M.: Antibody-drug conjugates: current status and future directions. *Drug Discov. Today* **19**, pp. 869–881 (2014).

102. Owen S. C., Patel N., Logie J., Pan G., Persson H., Moffat J., Sidhu S. S. & Shoichet M. S.: Targeting

HER2 + breast cancer cells: Lysosomal accumulation of anti-HER2 antibodies is influenced by antibody binding site and conjugation to polymeric nanoparticles. *J. Control. Release* **172**, pp. 395–404 (2013).

103. Kung Sutherland M. S., Sanderson R. J., Gordon K. A., Andreyka J., Cerveny C. G., Yu C., Lewis T. S., Meyer D. L., Zabinski R. F., Doronina S. O., *et al.*: Lysosomal Trafficking and Cysteine Protease Metabolism Confer Target-specific Cytotoxicity by Peptide-linked Anti-CD30-Auristatin Conjugates. *J. Biol. Chem.* **281**, pp. 10540–10547 (2006).

104. Giugliano F., Corti C., Tarantino P., Michelini F. & Curigliano G.: Bystander effect of antibody-drug conjugates: fact or fiction? *Curr. Oncol. Rep.* **25**, pp. 809–817 (2022).

105. Ogitani Y., Aida T., Hagihara K., Yamaguchi J., Ishii C., Harada N., Soma M., Okamoto H., Oitate M., Arakawa S., *et al.*: DS-8201a, A Novel HER2-Targeting ADC with a Novel DNA Topoisomerase I Inhibitor, Demonstrates a Promising Antitumor Efficacy with Differentiation from T-DM1. *Clin. Cancer Res.* **22**, pp. 5097–5108 (2016).

106. Junttila T. T., Li G., Parsons K., Phillips G. L. & Sliwkowski M. X.: Trastuzumab-DM1 (T-DM1) retains all the mechanisms of action of trastuzumab and efficiently inhibits growth of lapatinib insensitive breast cancer. *Breast Cancer Res. Treat.* **128**, pp. 347–356 (2011).

107. Tai Y. T., Mayes P. A., Acharya C., Zhong M. Y., Cea M., Cagnetta A., Craigen J., Yates J., Gliddon L., Fieles W., *et al.*: Novel anti-B-cell maturation antigen antibody-drug conjugate (GSK2857916) selectively induces killing of multiple myeloma. *Blood* **123**, pp. 3128–3138 (2014).

108. Wakankar A., Chen Y., Gokarn Y. & Jacobson F. S.: mAbs Analytical methods for physicochemical characterization of antibody drug conjugates. *MAbs* **3**, pp. 161–172 (2011).

109. Tong J. T. W., Harris P. W. R., Brimble M. A. & Kavianinia I.: An Insight into FDA Approved Antibody-Drug Conjugates for Cancer Therapy. *Mol. 2021, Vol. 26, Page 5847* **26**, pp. 5847 (2021).

110. Keam S. J.: Trastuzumab Deruxtecan: First Approval. *Drugs* **80**, pp. 501–508 (2020).

111. Bruins J. J., Damen J. A. M., Wijdeven M. A., Lelieveldt L. P. W. M., Delft F. L. van. & Albada B.: Non-Genetic Generation of Antibody Conjugates Based on Chemoenzymatic Tyrosine Click Chemistry. *Bioconjug. Chem.* pp. acs.bioconjchem.1c00351 (2021). doi:10.1021/ACS.BIOCONJCHEM.1C00351

112. Van Geel R., Wijdeven M. A., Heesbeen R., Verkade J. M. M., Wasiel A. A., Van Berkel S. S. & Van Delft F. L.: Chemoenzymatic Conjugation of Toxic Payloads to the Globally Conserved N-Glycan of Native mAbs Provides Homogeneous and Highly Efficacious Antibody-Drug Conjugates. *Bioconjug. Chem.* **26**, pp. 2233–2242 (2015).

113. Xu Y., Jin S., Zhao W., Liu W., Ding D., Zhou J. & Chen S.: A Versatile Chemo-Enzymatic Conjugation Approach Yields Homogeneous and Highly Potent Antibody-Drug Conjugates. *Int. J. Mol. Sci. 2017, Vol. 18, Page 2284* **18**, pp. 2284 (2017).

114. Jeger S., Zimmermann K., Blanc A., Grünberg J., Honer M., Hunziker P., Struthers H. & Schibli R.: Site-Specific and Stoichiometric Modification of Antibodies by Bacterial Transglutaminase. *Angew. Chemie - Int. Ed.* **49**, pp. 9995–9997 (2010).

115. Pons J., Rajpal A., Strop P., Dorywalska M. G., Shelton D., Liu S.-H. & Dushin R.: US20130230543A1: Engineered polypeptide conjugates and methods for making thereof using transglutaminase. (2011).

116. Dennler P., Chiotellis A., Fischer E., Brégeon D., Belmant C., Gauthier L., Lhospice F., Romagne

F. & Schibli R.: Transglutaminase-based chemo-enzymatic conjugation approach yields homogeneous antibody-drug conjugates. *Bioconjug. Chem.* **25**, pp. 569–578 (2014).

117. Jeger S., Zimmermann K., Blanc A., Grünberg J., Honer M., Hunziker P., Struthers H. & Schibli R.: Site-Specific and Stoichiometric Modification of Antibodies by Bacterial Transglutaminase. *Angew. Chemie - Int. Ed.* **49**, pp. 9995–9997 (2010).

118. Dickgiesser S., Rieker M., Mueller-Pompalla D., Schröter C., Tonillo J., Warszawski S., Raab-Westphal S., Kühn S., Knehans T., Könning D., *et al.*: Site-Specific Conjugation of Native Antibodies Using Engineered Microbial Transglutaminases. *Bioconjug. Chem.* **31**, pp. 1070–1076 (2020).

119. Araris Biotech AG.: Building tomorrow's antibody-drug conjugates (ADCs). (Webpage last updated 2019) Available at: https://www.ararisbiotech.com/#what-we-do.

120. Boschanski M., Krüger T., Karsten L., Falck G., Alam S., Gerlach M., Müller B., Müller K. M., Sewald N. & Dierks T.: Site-Specific Conjugation Strategy for Dual Antibody-Drug Conjugates Using Aerobic Formylglycine-Generating Enzymes. *Bioconjug. Chem.* **32**, pp. 1167–1174 (2021).

121. Lee B. ill., Park M. H., Byeon J. J., Shin S. H., Choi J., Park Y., Park Y. H., Chae J. & Shin Y. G.: Quantification of an Antibody-Conjugated Drug in Fat Plasma by an Affinity Capture LC-MS/MS Method for a Novel Prenyl Transferase-Mediated Site-Specific Antibody–Drug Conjugate. *Mol. 2020, Vol. 25, Page 1515* **25**, pp. 1515 (2020).

122. Nunes J. P. M., Vassileva V., Robinson E., Morais M., Smith M. E. B., Pedley R. B., Caddick S., Baker J. R. & Chudasama V.: Use of a next generation maleimide in combination with THIOMAB™ antibody technology delivers a highly stable, potent and near homogeneous THIOMAB™ antibody-drug conjugate (TDC). *RSC Adv.* **7**, pp. 24828–24832 (2017).

123. Axup J. Y., Bajjuri K. M., Ritland M., Hutchins B. M., Kim C. H., Kazane S. A., Halder R., Forsyth J. S., Santidrian A. F., Stafin K., *et al.*: Synthesis of site-specific antibody-drug conjugates using unnatural amino acids. *Proc. Natl. Acad. Sci. U. S. A.* **109**, pp. 16101–16106 (2012).

124. Green D. E., Morris T. W., Green J., Cronan J. E. & Guest J. R.: Purification and properties of the lipoate protein ligase of Escherichia coli. *Biochem. J* **309**, pp. 853–862 (1995).

125. Morris T. W., Reed K. E. & Cronan J. E.: Identification of the gene encoding lipoate-protein ligase A of Escherichia coli. Molecular cloning and characterization of the lplA gene and gene product. *J. BIOLWICAL Chem.* **269**, pp. 16091–16100 (1994).

126. Kim D. J., Kim K. H., Lee H. H., Lee S. J., Ha J. Y., Yoon H. J. & Suh S. W.: Crystal Structure of Lipoate-Protein Ligase A Bound with the Activated Intermediate: INSIGHTS INTO INTERACTION WITH LIPOYL DOMAINS. *J. Biol. Chem.* **280**, pp. 38081–38089 (2005).

127. Fernández-Suárez M., Baruah H., Martínez-Hernández L., Xie K. T., Baskin J. M., Bertozzi C. R. & Ting A. Y.: Redirecting lipoic acid ligase for cell surface protein labeling with small-molecule probes. *Nat. Biotechnol. 2007 2512* **25**, pp. 1483–1487 (2007).

128. Puthenveetil S., Liu D. S., White K. A., Thompson S. & Ting A. Y.: Yeast display evolution of a kinetically efficient 13-amino acid substrate for lipoic acid ligase. *J. Am. Chem. Soc.* **131**, pp. 16430–16438 (2009).

129. Baruah H., Puthenveetil S., Choi Y. A., Shah S. & Ting A. Y.: An engineered aryl azide ligase for site-specific mapping of protein-protein interactions through photo-cross-linking. *Angew. Chemie - Int. Ed.* **47**, pp. 7018–7021 (2008).

130. Yao J. Z., Uttamapinant C., Poloukhtine A., Baskin J. M., Codelli J. A., Sletten E. M., Bertozzi C.

R., Popik V. V. & Ting A. Y.: Fluorophore targeting to cellular proteins via enzyme-mediated azide ligation and strain-promoted cycloaddition. *J. Am. Chem. Soc.* **134**, pp. 3720–3728 (2012).

131. Hauke S., Best M., Schmidt T. T., Baalmann M., Krause A. & Wombacher R.: Two-Step Protein Labeling Utilizing Lipoic Acid Ligase and Sonogashira Cross-Coupling. *Bioconjug. Chem.* **25**, pp. 1632–1637 (2014).

132. Best M., Degen A., Baalmann M., Schmidt T. T. & Wombacher R.: Two-Step Protein Labeling by Using Lipoic Acid Ligase with Norbornene Substrates and Subsequent Inverse-Electron Demand Diels–Alder Reaction. *ChemBioChem* **16**, pp. 1158–1162 (2015).

133. Thornlow D. N., Cox E. C., Walker J. A., Sorkin M., Plesset J. B., DeLisa M. P. & Alabi C. A.: Dual Site-Specific Antibody Conjugates for Sequential and Orthogonal Cargo Release. *Bioconjugate Chem.* **30**, pp. 1702–1710 (2019).

134. Cronan J. E.: Biotination of proteins in vivo. A post-translational modification to label, purify, and study proteins. *J. Biol. Chem.* **265**, pp. 10327–10333 (1990).

135. Satiaputra J., Shearwin K. E., Booker G. W. & Polyak S. W.: Mechanisms of biotin-regulated gene expression in microbes. *Synth. Syst. Biotechnol.* **1**, pp. 17–24 (2016).

136. Mayende L., Swift R. D., Bailey L. M., Da Costa T. P. S., Wallace J. C., Booker G. W. & Polyak S. W.: A novel molecular mechanism to explain biotin-unresponsive holocarboxylase synthetase deficiency. *J. Mol. Med.* **90**, pp. 81–88 (2012).

137. Wilson K. P., Shewchuk L. M., Brennan R. G., Otsuka A. J. & Matthews B. W.: Escherichia coli biotin holoenzyme synthetase/bio repressor crystal structure delineates the biotin- and DNA-binding domains. *Proc. Natl. Acad. Sci. U. S. A.* **89**, pp. 9257–9261 (1992).

138. Chapman-Smith A., Mulhern T. D., Whelan F., Cronan J. E. & Wallace J. C.: The C-terminal domain of biotin protein ligase from E. coli is required for catalytic activity. *Protein Sci.* **10**, pp. 2608–2617 (2001).

139. Chapman-Smith A. & Cronan J. E.: Molecular Biology of Biotin Attachment to Proteins. *J. Nutr.* **129**, pp. 477S-484S (1999).

140. Bagautdinov B., Kuroishi C., Sugahara M. & Kunishima N.: Crystal Structures of Biotin Protein Ligase from Pyrococcus horikoshii OT3 and its Complexes: Structural Basis of Biotin Activation. *J. Mol. Biol.* **353**, pp. 322–333 (2005).

141. Tron C. M., McNae I. W., Nutley M., Clarke D. J., Cooper A., Walkinshaw M. D., Baxter R. L. & Campopiano D. J.: Structural and Functional Studies of the Biotin Protein Ligase from Aquifex aeolicus Reveal a Critical Role for a Conserved Residue in Target Specificity. *J. Mol. Biol.* **387**, pp. 129–146 (2009).

142. Chen Y., Elizondo-Noriega A., Cantu D. C. & Reilly P. J.: Structural classification of biotin carboxyl carrier proteins. *Biotechnol. Lett.* **34**, pp. 1869–1875 (2012).

143. Slavoff S. A., Chen I., Choi Y. A. & Ting A. Y.: Expanding the substrate tolerance of biotin ligase through exploration of enzymes from diverse species. *J. Am. Chem. Soc.* **130**, pp. 1160–1162 (2008).

144. Kolb H. C., Finn M. G. & Sharpless K. B.: Click Chemistry: Diverse Chemical Function from a Few Good Reactions. *Angewandte Chemie - International Edition* pp. 2004–2021 (Webpage last updated 2001) Available at: https://doi.org/10.1002/1521-3773(20010601)40:11%3C2004::AID-ANIE2004%3E3.0.CO;2-5. (Accessed: February 23, 2023)

145. The Royal Swedish Academy Of Sciences.: The Nobel Prize in Chemistry 2022. Available at:

https://www.nobelprize.org/prizes/chemistry/2022/popular-information/. (Accessed: February 23, 2023)

146. Chang P. V., Prescher J. A., Hangauer M. J. & Bertozzi C. R.: Imaging cell surface glycans with bioorthogonal chemical reporters. *J. Am. Chem. Soc.* **129**, pp. 8400–8401 (2007).

147. Baskin J. M., Prescher J. A., Laughlin S. T., Agard N. J., Chang P. V., Miller I. A., Lo A., Codelli J. A. & Bertozzi C. R.: Copper-free click chemistry for dynamic in vivo imaging. *Proc. Natl. Acad. Sci. U. S. A.* **104**, pp. 16793–16797 (2007).

148. Tornøe C. W., Christensen C. & Meldal M.: Peptidotriazoles on solid phase: [1,2,3]-Triazoles by regiospecific copper(I)-catalyzed 1,3-dipolar cycloadditions of terminal alkynes to azides. *J. Org. Chem.* **67**, pp. 3057–3064 (2002).

149. Bock V. D., Hiemstra H. & Van Maarseveen J. H.: CuI-Catalyzed Alkyne–Azide "Click" Cycloadditions from a Mechanistic and Synthetic Perspective. *European J. Org. Chem.* **2006**, pp. 51–68 (2006).

150. Patel K. G. & Swartz J. R.: Surface Functionalization of Virus-Like Particles by Direct Conjugation Using Azide–Alkyne Click Chemistry. *Bioconjug. Chem.* **22**, pp. 376 (2011).

151. Pokorski J. K., Breitenkamp K., Liepold L. O., Qazi S. & Finn M. G.: Functional virus-based polymer-protein nanoparticles by atom transfer radical polymerization. *J. Am. Chem. Soc.* **133**, pp. 9242–9245 (2011).

152. Navarro L. A., French D. L. & Zauscher S.: Synthesis of Modular Brush Polymer-Protein Hybrids Using Diazotransfer and Copper Click Chemistry. *Bioconjug. Chem.* **29**, pp. 2594–2605 (2018).

153. Dommerholt J., Rutjes F. P. J. T. & van Delft F. L.: Strain-Promoted 1,3-Dipolar Cycloaddition of Cycloalkynes and Organic Azides. *Top. Curr. Chem.* **374**, pp. 1–20 (2016).

154. Subramanian N., Sreemanthula J. B., Balaji B., Kanwar J. R., Biswas J. & Krishnakumar S.: A strain-promoted alkyne-azide cycloaddition (SPAAC) reaction of a novel EpCAM aptamer-fluorescent conjugate for imaging of cancer cells. *Chem. Commun. (Camb).* **50**, pp. 11810–11813 (2014).

155. Jang S., Sachin K., Lee H. J., Kim D. W. & Lee H. S.: Development of a simple method for protein conjugation by copper-free click reaction and its application to antibody-free western blot analysis. *Bioconjug. Chem.* **23**, pp. 2256–2261 (2012).

156. Leunissen E. H. P., Meuleners M. H. L., Verkade J. M. M., Dommerholt J., Hoenderop J. G. J. & Van Delft F. L.: Copper-Free Click Reactions with Polar Bicyclononyne Derivatives for Modulation of Cellular Imaging. *ChemBioChem* **15**, pp. 1446–1451 (2014).

157. Oliveira B. L., Guo Z. & Bernardes G. J. L.: Inverse electron demand Diels–Alder reactions in chemical biology. *Chem. Soc. Rev.* **46**, pp. 4895–4950 (2017).

158. Knall A. C. & Slugovc C.: Inverse electron demand Diels–Alder (iEDDA)-initiated conjugation: a (high) potential click chemistry scheme. *Chem. Soc. Rev.* **42**, pp. 5131–5142 (2013).

159. Peng T. & Hang H. C.: Site-Specific Bioorthogonal Labeling for Fluorescence Imaging of Intracellular Proteins in Living Cells. *J. Am. Chem. Soc.* **138**, pp. 14423–14433 (2016).

160. Schoch J., Ameta S. & Jäschke A.: Inverse electron-demand Diels–Alder reactions for the selective and efficient labeling of RNA. *Chem. Commun.* **47**, pp. 12536–12537 (2011).

161. Wilson D. S. & Keefe A. D.: Random Mutagenesis by PCR. *Curr. Protoc. Mol. Biol.* **51**, pp. 8.3.1-8.3.9 (2000).

162. Fujii R., Kitaoka M. & Hayashi K.: Error-prone rolling circle amplification: the simplest random mutagenesis protocol. *Nat. Protoc.* **1**, pp. 2493–2497 (2006).

163. Zaccolo M., Williams D. M., Brown D. M. & Gherardi E.: An approach to random mutagenesis of DNA using mixtures of triphosphate derivatives of nucleoside analogues. *J. Mol. Biol.* **255**, pp. 589–603 (1996).

164. Cadwell R. C. & Joyce G. F.: Randomization of Genes by PCR Mutagenesis. *Genome Res.* **2**, pp. 28–33 (1992).

165. Tseng W. C., Lin J. W., Wei T. Y. & Fang T. Y.: A novel megaprimed and ligase-free, PCR-based, site-directed mutagenesis method. *Anal. Biochem.* **375**, pp. 376–378 (2008).

166. Fisher C. L. & Pei G. K.: Modification of a PCRBased Site-Directed Mutagenesis Method. *Biotechniques* **23**, pp. 570–574 (2018).

167. Carter P.: Site-directed mutagenesis. *Biochem. J.* **237**, pp. 1–7 (1986).

168. Stemmer W. P. C.: Rapid evolution of a protein in vitro by DNA shuffling. *Nature* **370**, pp. 389–391 (1994).

169. Stemmer W. P. C.: DNA shuffling by random fragmentation and reassembly: in vitro recombination for molecular evolution. *Proc. Natl. Acad. Sci. U. S. A.* **91**, pp. 10747–10751 (1994).

170. Stoltenburg R., Reinemann C. & Strehlitz B.: SELEX-A (r)evolutionary method to generate high-affinity nucleic acid ligands. *Biomol. Eng.* **24**, pp. 381–403 (2007).

171. Ellington A. D. & Szostak J. W.: In vitro selection of RNA molecules that bind specific ligands. *Nat. Vol.* **346**, pp. 818–822 (1990).

172. Bessette P. H., Rice J. J. & Daugherty P. S.: Rapid isolation of high-affinity protein binding peptides using bacterial display. *Protein Eng. Des. Sel.* **17**, pp. 731–739 (2004).

173. Freudl R., MacIntyre S., Degen M. & Henning U.: Cell surface exposure of the outer membrane protein OmpA of Escherichia coli K-12. *J. Mol. Biol.* **188**, pp. 491–494 (1986).

174. Hanes J. & Plückthun A.: In vitro selection and evolution of functional proteins by using ribosome display. *Proc. Natl. Acad. Sci. U. S. A.* **94**, pp. 4937–4942 (1997).

175. Ho M. & Pastan I.: Mammalian Cell Display for Antibody Engineering. *Methods Mol. Biol.* **525**, pp. 337 (2009).

176. Higuchi K., Araki T., Matsuzaki O., Sato A., Kanno K., Kitaguchi N. & Ito H.: Cell display library for gene cloning of variable regions of human antibodies to hepatitis B surface antigen. *J. Immunol. Methods* **202**, pp. 193–204 (1997).

177. Boder E. T. & Wittrup K. D.: Yeast surface display for screening combinatorial polypeptide libraries. *Nat. Biotechnol. 1997 156* **15**, pp. 553–557 (1997).

178. Kondo A. & Ueda M.: Yeast cell-surface display--applications of molecular display. *Appl. Microbiol. Biotechnol.* **64**, pp. 28–40 (2004).

179. Zhao H., Shen Z. M., Kahn P. C. & Lipke P. N.: Interaction of α-agglutinin and a-agglutinin, Saccharomyces cerevisiae sexual cell adhesion molecules. *J. Bacteriol.* **183**, pp. 2874–2880 (2001).

180. Smith G. P.: Filamentous fusion phage: Novel expression vectors that display cloned antigens on the virion surface. *Science (80-.).* **228**, pp. 1315–1317 (1985).

181. Perween R., Ahmed S., Shrivastava T., Parray H. A., Singh B., Pindari K. S., Sharma C., Shukla S.,

Sinha S., Panchal A. K., *et al.*: A rapid novel strategy for screening of antibody phage libraries for production, purification, and functional characterization of amber stop codons containing single-chain antibody fragments. *Biotechnol. Prog.* **37**, (2021).

182. Ledsgaard L., Kilstrup M., Karatt-Vellatt A., McCafferty J. & Laustsen A. H.: Basics of Antibody Phage Display Technology. *Toxins (Basel).* **10**, (2018).

183. Reljic R., George' S., Greiff V., Ferreira F., Hashem A. M., Alfaleh M. A., Alsaab H. O., Mahmoud A. B., Alkayyal A. A., Jones M. L., *et al.*: Phage Display Derived Monoclonal Antibodies: From Bench to Bedside. *Front. Immunol.* | *www.frontiersin.org* **1**, (2020).

184. Markham A.: Atezolizumab: First Global Approval. *Drugs* **76**, pp. 1227–1232 (2016).

185. Markham A.: Ixekizumab: First Global Approval. *Drugs* **76**, pp. 901–905 (2016).

186. Duggan S.: Caplacizumab: First Global Approval. *Drugs* **78**, pp. 1639–1642 (2018).

187. Kim A., Shin T. H., Shin S. M., Pham C. D., Choi D. K., Kwon M. H. & Kim Y. S.: Cellular Internalization Mechanism and Intracellular Trafficking of Filamentous M13 Phages Displaying a Cell-Penetrating Transbody and TAT Peptide. *PLoS One* **7**, pp. e51813 (2012).

188. Hoffmann K., Milech N., Juraja S. M., Cunningham P. T., Stone S. R., Francis R. W., Anastasas M., Hall C. M., Heinrich T., Bogdawa H. M., *et al.*: A platform for discovery of functional cell-penetrating peptides for efficient multi-cargo intracellular delivery. *Sci. Reports 2018 81* **8**, pp. 1–16 (2018).

189. Lupus Foundation of America.: What is systemic lupus erythematosus (SLE)? (Webpage last updated 2020) Available at: https://www.lupus.org/resources/what-is-systemic-lupus-erythematosus-sle.

190. Pons-Estel G. J., Alarcón G. S., Scofield L., Reinlib L. & Cooper G. S.: Understanding the Epidemiology and Progression of Systemic Lupus Erythematosus. *Semin. Arthritis Rheum.* **39**, pp. 257–268 (2010).

191. Pisetsky D. S. & Lipsky P. E.: New insights into the role of antinuclear antibodies in systemic lupus erythematosus HHS Public Access. *Nat Rev Rheumatol* **16**, pp. 565–579 (2020).

192. Mok C. C.: Pathogenesis of systemic lupus erythematosus. *J Clin Pathol* **56**, pp. 481–490 (2003).

193. Deng J.-S., Ballou B. & Hofmeister J. K.: Internalization of anti-nucleolin antibody into viable HEp-2 cells. *Mol. Biol. Rep.* **23**, pp. 191–195 (1996).

194. Park H., Kim M., Seo Y., Ham Y., Cho M. Y. & Kwon M. H.: Cytosolic internalization of anti-DNA antibodies by human monocytes induces production of pro-inflammatory cytokines independently of the tripartite motif-containing 21 (TRIM21)-mediated pathway. *Front. Immunol.* **9**, pp. 2019 (2018).

195. Trenevska I., Li D. & Banham A. H.: Therapeutic antibodies against intracellular tumor antigens. *Front. Immunol.* **8**, (2017).

196. Gaston J., Maestrali N., Lalle G., Gagnaire M., Masiero A., Dumas B., Dabdoubi T., Radošević K. & Berne P. F.: Intracellular delivery of therapeutic antibodies into specific cells using antibody-peptide fusions. *Sci. Reports 2019 91* **9**, pp. 1–12 (2019).

197. Kim J. S., Choi D. K., Shin J. Y., Shin S. M., Park S. W., Cho H. S. & Kim Y. S.: Endosomal acidic pH-induced conformational changes of a cytosol-penetrating antibody mediate endosomal escape. *J. Control. Release* **235**, pp. 165–175 (2016).

198. Jang J. Y., Jeong J. G., Jun H. R., Lee S. C., Kim J. S., Kim Y. S. & Kwon M. H.: A nucleic acid-

hydrolyzing antibody penetrates into cells via caveolae-mediated endocytosis, localizes in the cytosol and exhibits cytotoxicity. *Cell. Mol. Life Sci.* **66**, pp. 1985–1997 (2009).

199. Kim Y. R., Kim J. S., Lee S. H., Lee W. R., Sohn J. N., Chung Y. C., Shim H. K., Lee S. C., Kwon M. H. & Kim Y. S.: Heavy and light chain variable single domains of an anti-DNA binding antibody hydrolyze both double- and single-stranded DNAs without sequence specificity. *J. Biol. Chem.* **281**, pp. 15287–15295 (2006).

200. Inoue K., Ishizawa M. & Kubota T.: Monoclonal anti-dsDNA antibody 2C10 escorts DNA to intracellular DNA sensors in normal mononuclear cells and stimulates secretion of multiple cytokines implicated in lupus pathogenesis. *Clin. Exp. Immunol.* **199**, pp. 150–162 (2020).

201. Pravinsagar P., Im S. W. & Jang Y. J.: Pathogenic effect of a cell-penetrating anti-dsDNA autoantibody through p38 signaling pathway and pro-inflammatory cytokine stimulation in mesangial cells. *Animal Cells Syst. (Seoul).* **22**, pp. 45–53 (2018).

202. Singh S., Murillo G., Chen D., Parihar A. S. & Mehta R. G.: Suppression of Breast Cancer Cell Proliferation by Selective Single-Domain Antibody for Intracellular STAT3. *Breast Cancer (Auckl).* **12**, (2018).

203. Mbanefo E. C., Yan M., Kang M., Alhakeem S. A., Jittayasothorn Y., Yu C. R., Parihar A., Singh S. & Egwuagu C. E.: STAT3-Specific Single Domain Nanobody Inhibits Expansion of Pathogenic Th17 Responses and Suppresses Uveitis in Mice. *Front. Immunol.* **12**, pp. 724609 (2021).

204. Sunanda Singh.: U.S. Patent 9695234 B2: Single domain antibodies directed against STAT3. (2017).

205. Lu W. C., Levy M., Kincaid R. & Ellington A. D.: Directed evolution of the substrate specificity of biotin ligase. *Biotechnol. Bioeng.* **111**, pp. 1071–1081 (2014).

206. Pettersen E. F., Goddard T. D., Huang C. C., Couch G. S., Greenblatt D. M., Meng E. C. & Ferrin T. E.: UCSF Chimera—A visualization system for exploratory research and analysis. *J. Comput. Chem.* **25**, pp. 1605–1612 (2004).

207. Mullis K., Faloona F., Scharf S., Saiki R., Horn G. & Erlich H.: Specific Enzymatic Amplification of DNA In Vitro: The Polymerase Chain Reaction. *Cold Spring Harb. Symp. Quant. Biol.* **51**, pp. 263–273 (1986).

208. New England BioLabs.: NEB Tm calculator. Available at: https://tmcalculator.neb.com/#!/main.

209. Benatuil L., Perez J. M., Belk J. & Hsieh C.-M.: An improved yeast transformation method for the generation of very large human antibody libraries. *Protein Eng. Des. Sel.* **23**, pp. 155–159 (2010).

210. Engler C., Gruetzner R., Kandzia R. & Marillonnet S.: Golden Gate Shuffling: A One-Pot DNA Shuffling Method Based on Type IIs Restriction Enzymes. *PLoS One* **4**, pp. e5553 (2009).

211. Engler C., Kandzia R. & Marillonnet S.: A One Pot, One Step, Precision Cloning Method with High Throughput Capability. *PLoS One* **3**, pp. e3647 (2008).

212. Lõoke M., Kristjuhan K. & Kristjuhan A.: Extraction of genomic DNA from yeasts for PCR-based applications. *Biotechniques* **50**, pp. 325–328 (2011).

213. Sanger F. & Coulson A. R.: A rapid method for determining sequences in DNA by primed synthesis with DNA polymerase. *J. Mol. Biol.* **94**, pp. 441–448 (1975).

214. SIB Swiss Institute of Bioinformatics.: Expasy ProtParam. Available at: https://web.expasy.org/protparam/.

215. Laemmli U. K.: Cleavage of Structural Proteins during the Assembly of the Head of Bacteriophage

T4. *Nat. 1970 2275259* **227**, pp. 680–685 (1970).

216. Weidenfeld I., Gossen M., Löw R., Kentner D., Berger S., Görlich D., Bartsch D., Bujard H. & Schönig K.: Inducible expression of coding and inhibitory RNAs from retargetable genomic loci. *Nucleic Acids Res.* **37**, pp. e50 (2009).

217. Schopp I. M., Amaya Ramirez C. C., Debeljak J., Kreibich E., Skribbe M., Wild K. & Béthune J.: Split-BioID a conditional proteomics approach to monitor the composition of spatiotemporally defined protein complexes. *Nat. Commun. 2017 81* **8**, pp. 1–14 (2017).

218. Kügler J., Tomszak F., Frenzel A. & Michael Hust.: Construction of Human Immune and Naive scFv Libraries. Published in *Phage Display - Methods and Protocols* pp. 18–19 (2018).

219. Newton J. R. & Deutscher S. L.: In Vivo Bacteriophage Display for the Discovery of Novel Peptide-Based Tumor-Targeting Agents. Published in *Biosensors and Biodetection* pp. 275–290 (2009).

220. Day L. A. & Wiseman R. L.: A comparison of DNA packaging in the virions of fd, Xf, and Pf1. Published in *The single-stranded DNA phages* pp. 605–625 (1978).

221. Kubitz L., Bitsch S., Zhao X., Schmitt K., Deweid L., Roehrig A., Barazzone E. C., Valerius O., Kolmar H. & Béthune J.: Engineering of ultraID, a compact and hyperactive enzyme for proximity-dependent biotinylation in living cells. *Commun. Biol.* **5**, (2022).

222. Boder E. T. & Wittrup K. D.: [25] Yeast surface display for directed evolution of protein expression, affinity, and stability. *Methods Enzymol.* **328**, pp. 430–444 (2000).

223. Polyak S. W., Chapman-Smith A., Brautigan P. J. & Wallace J. C.: Biotin Protein Ligase from Saccharomyces cerevisiae THE N-TERMINAL DOMAIN IS REQUIRED FOR COMPLETE ACTIVITY*. *J. Biol. Chem.* **274**, pp. 32847–32854 (1999).

224. Neumann S., Biewend M., Rana S., Binder W. H., Neumann S., Biewend M., Binder W. H. & Rana S.: The CuAAC: Principles, Homogeneous and Heterogeneous Catalysts, and Novel Developments and Applications. *Macromol. Rapid Commun.* **41**, pp. 1900359 (2020).

225. Presolski S. I., Hong V. P. & Finn M. G.: Copper-Catalyzed Azide–Alkyne Click Chemistry for Bioconjugation. *Curr. Protoc. Chem. Biol.* **3**, pp. 153 (2011).

226. Levy M. & Ellington A. D.: Directed Evolution of Streptavidin Variants Using In Vitro Compartmentalization. *Chem. Biol.* **15**, pp. 979–989 (2008).

227. Bitsch S. H.: Modification of bond-forming enzymes for the generation of antibody-drug conjugates. (Technical University of Darmstadt, 2019).

228. Dennler P., Chiotellis A., Fischer E., Brégeon D. B., Belmant C., Gauthier L., Lhospice F., Ois Romagne F. & Schibli R.: Transglutaminase-Based Chemo-Enzymatic Conjugation Approach Yields Homogeneous Antibody−Drug Conjugates. *Bioconjugate Chem.* **25**, pp. 569–578 (2014).

229. Yamazaki C. M., Yamaguchi A., Anami Y., Xiong W., Otani Y., Lee J., Ueno N. T., Zhang N., An Z. & Tsuchikama K.: Antibody-drug conjugates with dual payloads for combating breast tumor heterogeneity and drug resistance. *Nat. Commun.* **12**, (2021).

230. Ebenig A., Juettner N. E., Deweid L., Avrutina O., Fuchsbauer H. L. & Kolmar H.: Efficient Site-Specific Antibody–Drug Conjugation by Engineering a Nature-Derived Recognition Tag for Microbial Transglutaminase. *ChemBioChem* **20**, pp. 2411–2419 (2019).

231. Lakayan D., Haselberg R., Gahoual R., Somsen G. W. & Kool J.: Affinity profiling of monoclonal antibody and antibody-drug-conjugate preparations by coupled liquid chromatography-surface plasmon resonance biosensing. *Anal. Bioanal. Chem.* **410**, pp. 7837 (2018).

232. Geuijen C. A. W., De Nardis C., Maussang D., Rovers E., Gallenne T., Hendriks L. J. A., Visser T., Nijhuis R., Logtenberg T., de Kruif J., *et al.*: Unbiased Combinatorial Screening Identifies a Bispecific IgG1 that Potently Inhibits HER3 Signaling via HER2-Guided Ligand Blockade. *Cancer Cell* **33**, pp. 922- 936.e10 (2018).

233. Baalmann M., Neises L., Bitsch S., Schneider H., Deweid L., Werther P., Ilkenhans N., Wolfring M., Ziegler M. J., Wilhelm J., *et al.*: A Bioorthogonal Click Chemistry Toolbox for Targeted Synthesis of Branched and Well-Defined Protein–Protein Conjugates. *Angew. Chemie - Int. Ed.* **59**, pp. 12885–12893 (2020).

234. Bazan J., Całkosiński I. & Gamian A.: Phage display—A powerful technique for immunotherapy. *Hum. Vaccin. Immunother.* **8**, pp. 1817 (2012).

235. Kramer L., Demuysere M., van Diest E., Beringer D. X. & Kuball J.: Challenges of γ9δ2TCR affinity maturation when using phage display. *bioRxiv* (2021). doi:10.1101/2021.05.20.445024

236. Johnson B. S., Chafin L., Farkas D., Adair J., Elhance A., Farkas L., Bednash J. S. & Londino J. D.: MicroID2: A Novel Biotin Ligase Enables Rapid Proximity-Dependent Proteomics. *Mol. Cell. Proteomics* **21**, pp. 100256 (2022).

237. Hirsch J. D., Eslamizar L., Filanoski B. J., Malekzadeh N., Haugland R. P., Beechem J. M. & Haugland R. P.: Easily reversible desthiobiotin binding to streptavidin, avidin, and other biotin-binding proteins: Uses for protein labeling, detection, and isolation. *Anal. Biochem.* **308**, pp. 343–357 (2002).

10 Appendix

10.1 Supplementary figures

```
microID     1    EQKLISEEDLDFKNLIWLKEVDSTQERLKEWNVSYGTALVADRQTKGRGGLGRKWLSQEG  60
Clone_1     1    ............................................................  60
Clone_2     1    ............................................................  60
Clone_3     1    ............................................................  60
Clone_4     1    ............................................................  60
Clone_5     1    ...........................................V................  60
Clone_6     1    ..................................D.........................  60
Clone_7     1    ............................................................  60
Clone_8     1    ............................................................D 60
Clone_9     1    ...........................................V................  60
Clone_10    1    ............................................................G. 60
Clone_11    1    ............................................................  60

microID     1    GLYFSFLLNPKEFENLLQLPLVLGLSVSEALEEITEIPFSLKWPNDVYFQEKKVSGVLCE  120
Clone_1     61   ............................................................  120
Clone_2     61   ............................K...............................  120
Clone_3     61   .P..........................................................  120
Clone_4     61   ............................................................  120
Clone_5     61   ............................................................  120
Clone_6     61   ...........D................................................  120
Clone_7     61   ..........................................*.................  120
Clone_8     61   ..................................................I.........  120
Clone_9     61   ..........................................................R...S....  120
Clone_10    61   ...................................L....RD.M.............  120
Clone_11    61   ...................................L.......L.............  120

microID     1    LSKDKLIVGIGINVNQREIPEEIKDRATTLYEITGKDWDRKEVLLKVLKRISENLKKFKE  180
Clone_1     121  ............................................................  180
Clone_2     121  ............................................................  180
Clone_3     121  ............................................................  180
Clone_4     121  ...........................................*................  180
Clone_5     121  ............................................................  180
Clone_6     121  ............................................................  180
Clone_7     121  ..........................................................M.....  180
Clone_8     121  ................K...........................................  180
Clone_9     121  ............................................................  180
Clone_10    121  ............................................................  180
Clone_11    121  ................N..K...G.....................................  180

microID     1    KHHHHHH*  188
Clone_1     181  .......*  188
Clone_2     181  .......*  188
Clone_3     181  .......*  188
Clone_4     181  .......*  188
Clone_5     181  .......*  188
Clone_6     181  .......*  188
Clone_7     181  .......*  188
Clone_8     181  .......*  188
Clone_9     181  .......*  188
Clone_10    181  .......*  188
Clone_11    181  .......*  188
```

Supplementary figure 1: Multiple sequence alignment of yeast single clones. In order to calculate an average mutagenesis rate for the yeast library eleven single clones were sequenced. Results were aligned to the wild-type enzyme (microID) and a mean amino acid exchange was calculated. Alignment carried out with *BLAST blastp suite 2sequences*.

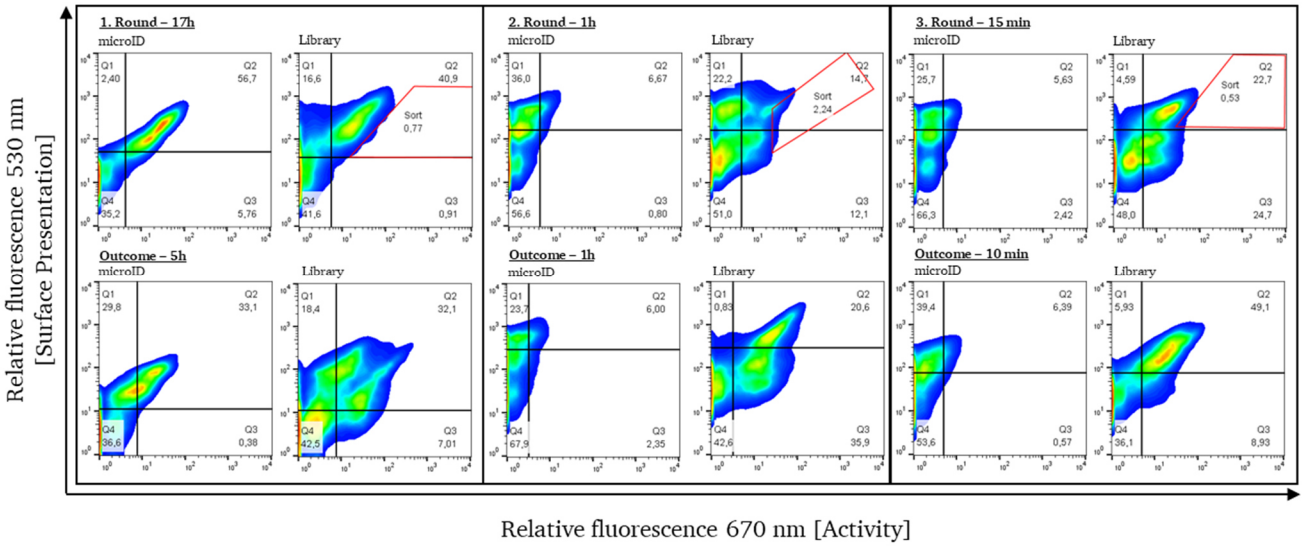

Supplementary figure 2: Directed evolution of microID by yeast surface display. For enrichment of improved microID variants the microID library and yeasts displaying the wild-type enzyme were used for a surface-biotinylation assay. Hereby, yeasts were incubated in presence of 50 µM biotin and 2.5 mM ATP and were incubated for different time periods at 30°C and 900 rpm. Cells showing surface presentation and strong activity compared to the wild-type cells were sorted out, cultivated, and used again for another enrichment. This procedure was repeated three times. Figure taken from [221].

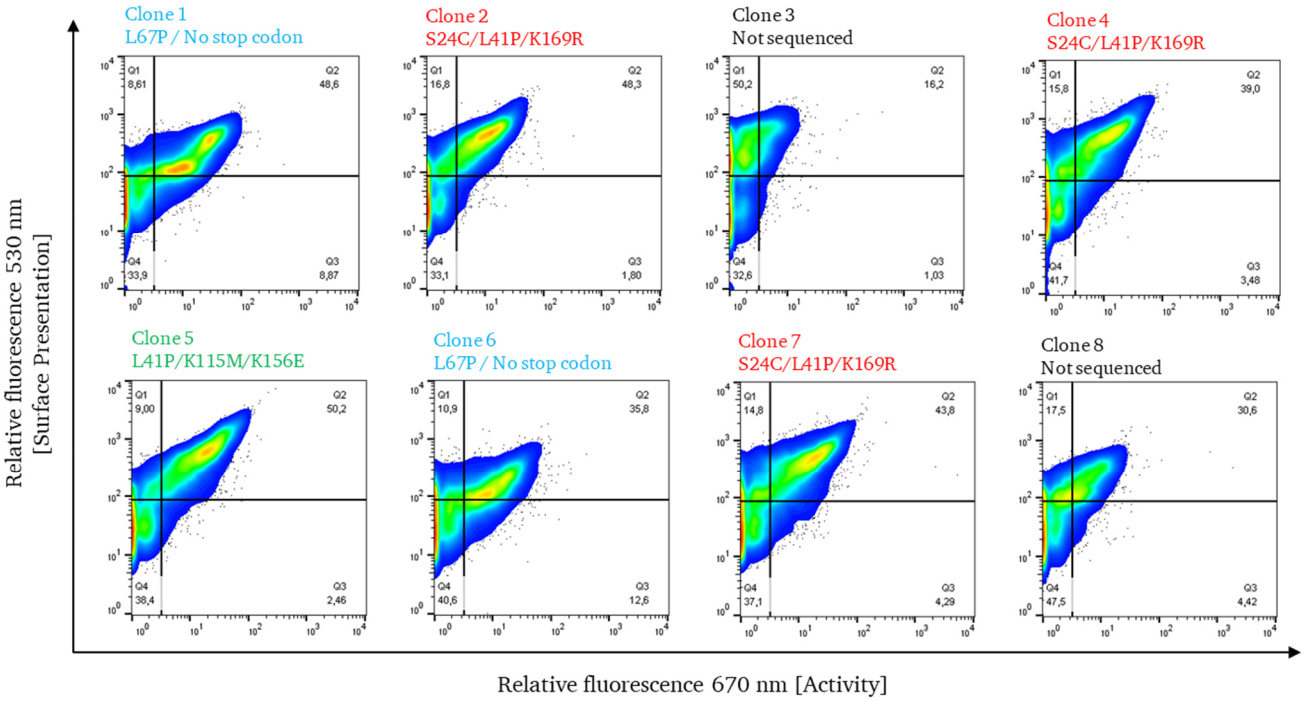

Supplementary figure 3: Single-clone analysis of round 3 yeast library. Eight single clones of the round 3 library were analyzed by YSBA. The yeasts were incubated with 50 µM biotin and 2.5 mM ATP for 10 min at 30°C and 900rpm. Subsequently surface presentation was stained with an anti-penta His and an anti-mouse FITC antibody. Activity was evaluated by a Streptavidin-APC conjugate. Figure taken from [221].

```
microID       1    EQKLISEEDLDFKNLIWLKEVDSTQERLKEWNVSYGTALVADRQTKGRGGLGRKWLSQEG  60
Clone_1       1    ............................................................  60
Clone_6       1    ............................................................  60
Clone_2       1    ................................C.................P.........  60
Clone_4       1    ................................C.................P.........  60
Clone_7       1    ................................C.................P.........  60
Clone_5       1    ............................................................  60

micro         61   GLYFSFLLNPKEFENLLQLPLVLGLSVSEALEEITEIPFSLKWPNDVYFQEKKVSGVLCE  120
Clone_1       61   ................P...........................................  120
Clone_6       61   ................P...........................................  120
Clone_2       61   ............................................................  120
Clone_4       61   ............................................................  120
Clone_7       61   ............................................................  120
Clone_5       61   ............................................................  120

microID       121  LSKDKLIVGIGINVNQREIPEEIKDRATTLYEITGKDWDRKEVLLKVLKRISENLKKFKE  180
Clone_1       121  ............................................................  180
Clone_6       121  ............................................................  180
Clone_2       121  ............................................................R.  180
Clone_4       121  ............................................................R.  180
Clone_7       121  ............................................................R.  180
Clone_5       121  ....M.....................................E..............  180

microID       181  KHHHHHH*                                 188
Clone_1       181  .......NSSRSDNNSVDVTKSTLFPLYF*           209
Clone_6       181  .......NSSRSDNNSVDVTKSTLFPLYF*           209
Clone_2       181  .......*                                 188
Clone_4       181  .......*                                 188
Clone_7       181  .......*                                 188
Clone_5       181  .......*                                 188
```

Supplementary figure 4: Multiple sequence alignment of single clones after 3rd round of enrichment. Cells sorted after 3 rounds of screening were streaked on agar plates. Eight single clones were cultivated and induced in liquid medium, followed by another YSBA and analysis by FACS. The six clones showing highest activity during single-clone analysis were sequenced.

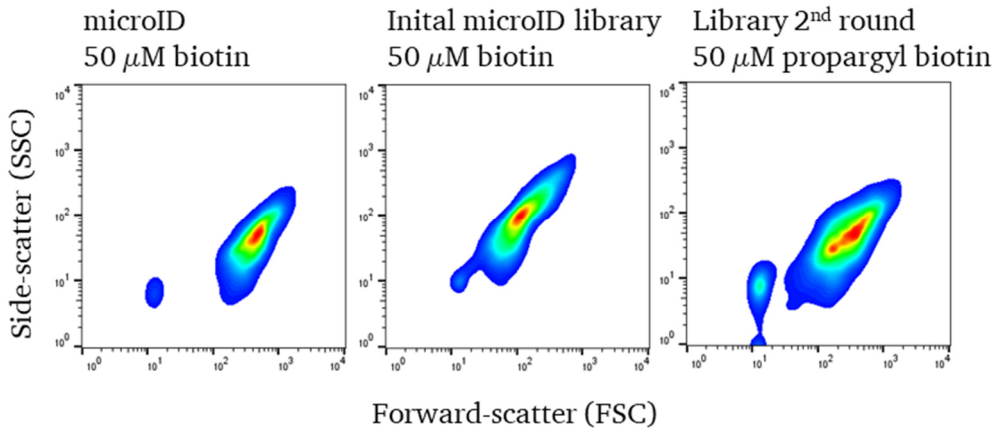

Supplementary figure 5: SSC vs FSC blots of yeasts presenting microID variants. microID 50 µM biotin: Sample which was prepared in parallel to the shown library 2nd round with 50 µM propargyl biotin. Initial microID library 50 µM biotin: Sample which was prepared during directed evolution of mircoID.

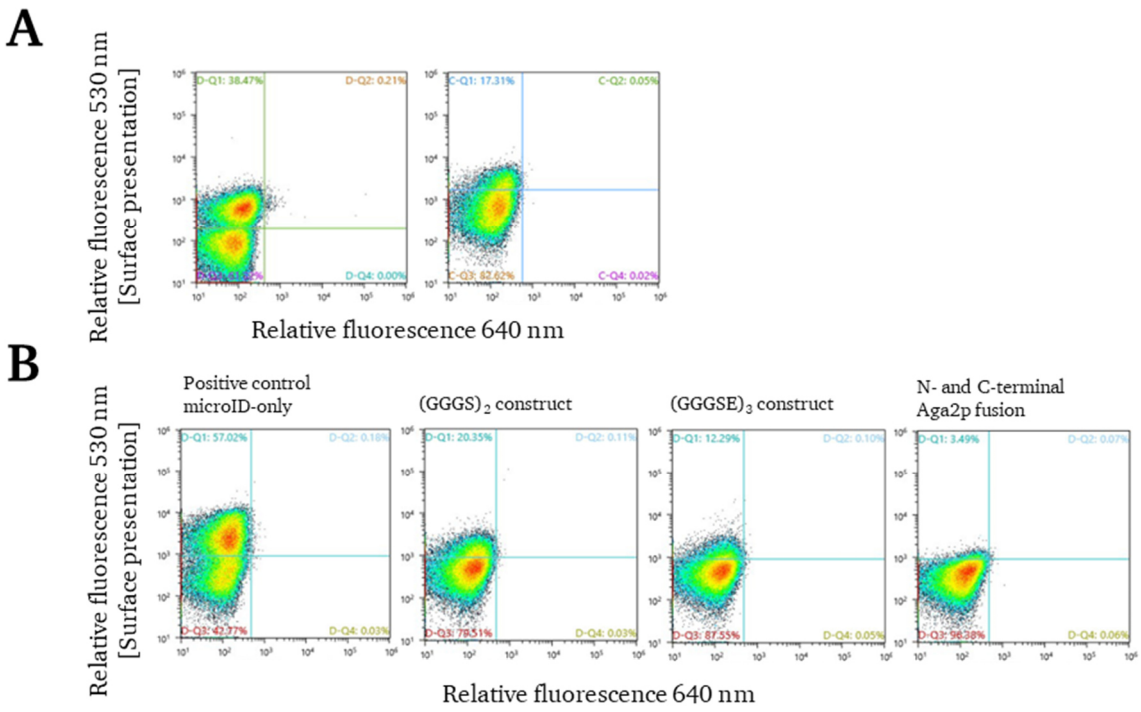

Supplementary figure 6: Presentation control of the $(GGGS)_2$ construct in independent experiments (A) and presentation control of different constructs fusing the truncated *A. aeolicus* biotin ligase with its BCCP (B). A yeast single clone was inoculated in autoinduction media and was incubated overnight. Staining for presentation was carried out with an anti-penta His and an anti-mouse FITC antibody.

```
yBL_DB   1    MNVLVYNGPGTTPGSVKHAVESLRDFLEPYYAVSTVNVKVLQTEPWMSKTSAVVFPGGAD  60
yBL_Seq  1    ............................................................  60

yBL_DB   61   LPYAQACQPIISRLKHFVSKQGGVFIGFCAGGYFGTSRVEFAQGDPTVEVSGSRDLRFFP  120
yBL_Seq  61   ...V.....................................M.....................  120

yBL_DB   121  GTSRGPAYNGFQYNSEAGARAVKLSLPDGSQFSTYFNGGAVFVDADKFDNVEILATYAEH  180
yBL_Seq  121  ........................N...................................  180

yBL_DB   181  PDVPSSDSGKGQSENPAAVVLCTVGRGKVLLTGPHPEFNVRFMRKSTDKHFLETVVENLK  240
yBL_Seq  181  ............................................................  240

yBL_DB   241  AQEIMRLKFMRTVLTKTGLNCNNDFNYVRAPNLTPLFMASAPNKRNYLQEMENNLANHGM  300
yBL_Seq  241  ..........................................................H...  300

yBL_DB   301  HANNVELCSELNAETDSFQFYRGYRASYDAASSSLLHKEPDEVPKTVIFPGVDEDIPPFQ  360
yBL_Seq  301  ............................................................  360

yBL_DB   361  YTPNFDMKEYFKYLNVQNTIGSLLLYGEVVTSTSTILNNNKSLLSSIPESTLLHVGTIRV  420
yBL_Seq  361  ..........................................................Q.  420

yBL_DB   421  SGRGRGGNTWINPKGVCASTAVVTMPLQSPVTNRNISVVFVQYLSMLAYCKAILSYAPGF  480
yBL_Seq  421  ............................................................  480

yBL_DB   481  SDIPVRIKWPNDLYALSPTYYKRKNLKLVNTGFEHTKLPLGDIEPAYLKISGLLVNTHFI  540
yBL_Seq  481  ............................................................  540

yBL_DB   541  NNKYCLLLGCGINLTSDGPTTSLQTWIDILNEERQQLHLDLLPAIKAEKLQALYMNNLEV  600
yBL_Seq  541  ............................................................  600

yBL_DB   601  ILKQFINYGAAEILPSYYELWLHSNQIVTLPDHGNTQAMITGITEDYGLLIAKELVRGSS  660
yBL_Seq  601  ..........................................................S...  660

yBL_DB   661  TQFTGNVYNLQPDGNTFDIFKSLIAKKVQS  690
yBL_Seq  661  ............................... 690
```

Supplementary figure 7: Blastp result of sequenced yBL gene (yBL_Seq) and best database hit (yBL_DB).yBL gene was amplified from *S. cerevisiae* genome and was sequenced after subsequent cloning in pET30 vector.

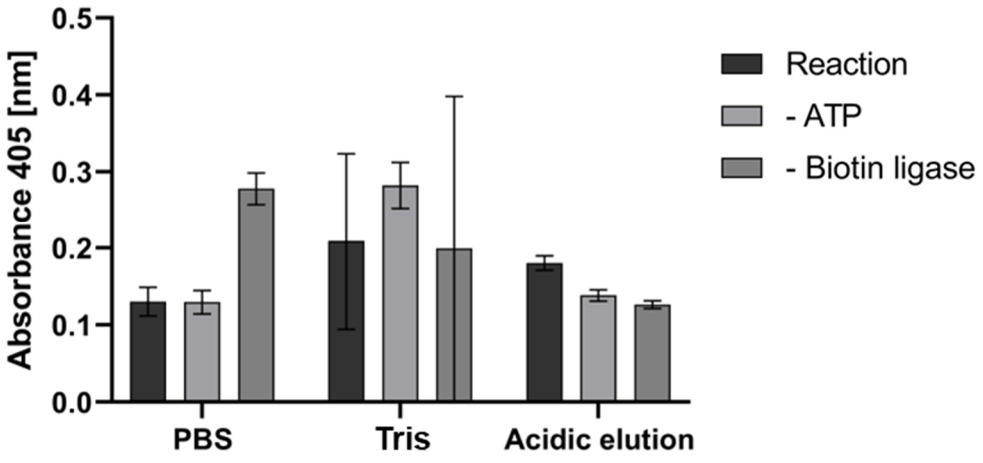

Supplementary figure 8: Activity of different yBL batches and different reaction buffers. Trastuzumab-HC:p67 was incubated in presence of 5 mM $Mg(OAc)_2$, 1 mM biotin, 5 mM ATP and 5 µM of biotin ligase for 2 h at 37°C. The reaction mixture was coated on a microtiter plate and an ELISA-based assay using streptavidin-AP was conducted. Error bars resemble standard deviation n=3. PBS: Reaction sample with PBS buffer; Tris: Reaction sample with Tris buffer; Acidic elution: Batch of yBL being eluted from IMAC column by pH 4.

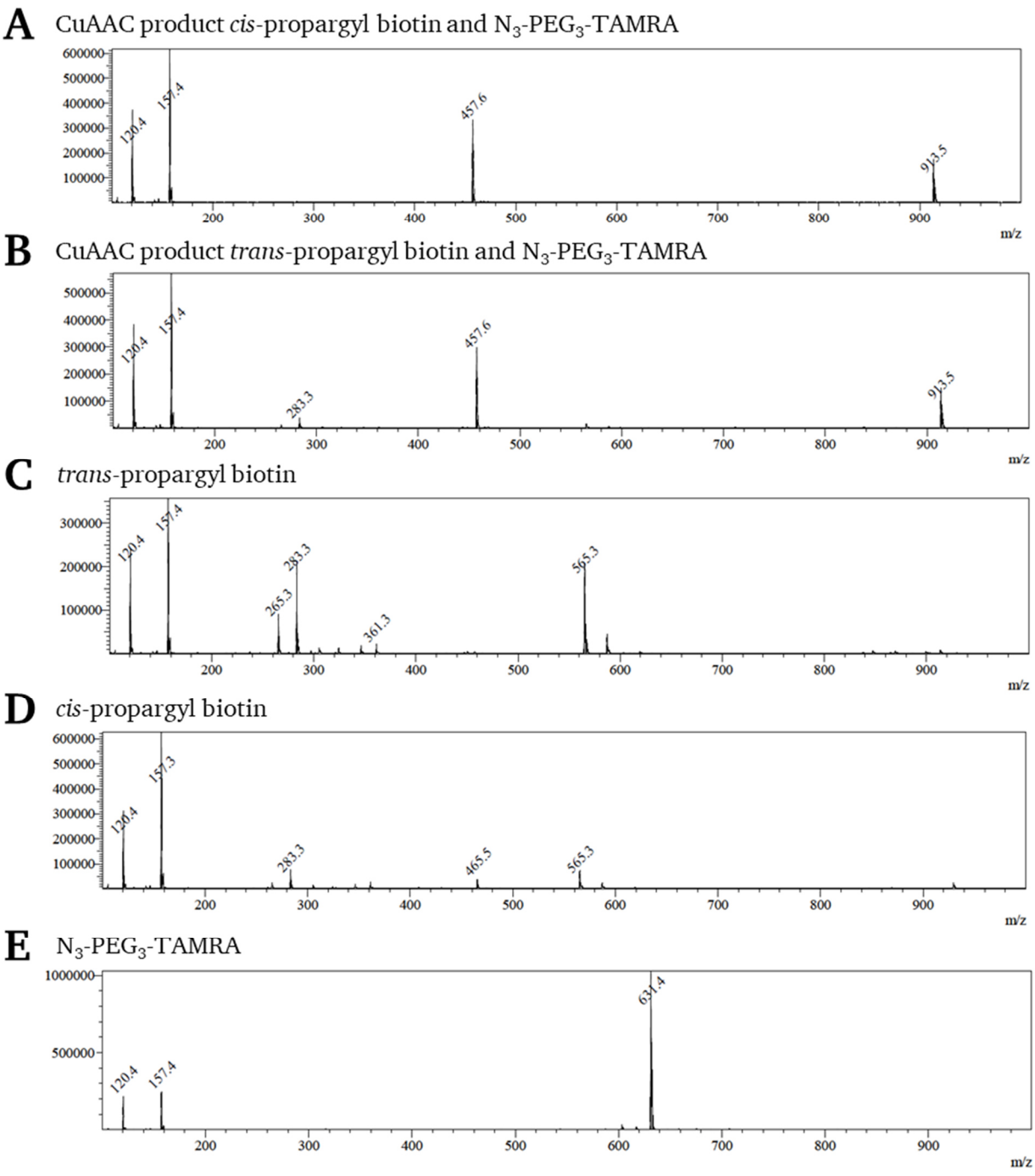

Supplementary figure 9: LC-MS analysis of CuAAC between propargyl biotin isomers and N_3-PEG_3-TAMRA. 2.3 mM *cis*- or *trans*-propargyl biotin, 1 mM N_3-PEG_3-TAMRA, 1 mM Cu^+ and 2 mM ascorbic acid were incubated for 5 h at 37°C. LC was performed 30to100%B in 20 min at 220 nm. Calc. Mass $[M+H]^+$: propargyl biotin: 282.10, N_3-PEG_3-TAMRA: 630,28, product of CuAAC: 912,38. Obs. Mass $[M+H]^+$: propargyl biotin: 283.3, N_3-PEG_3-TAMRA: 631.4, product of CuAAC: 913.5.

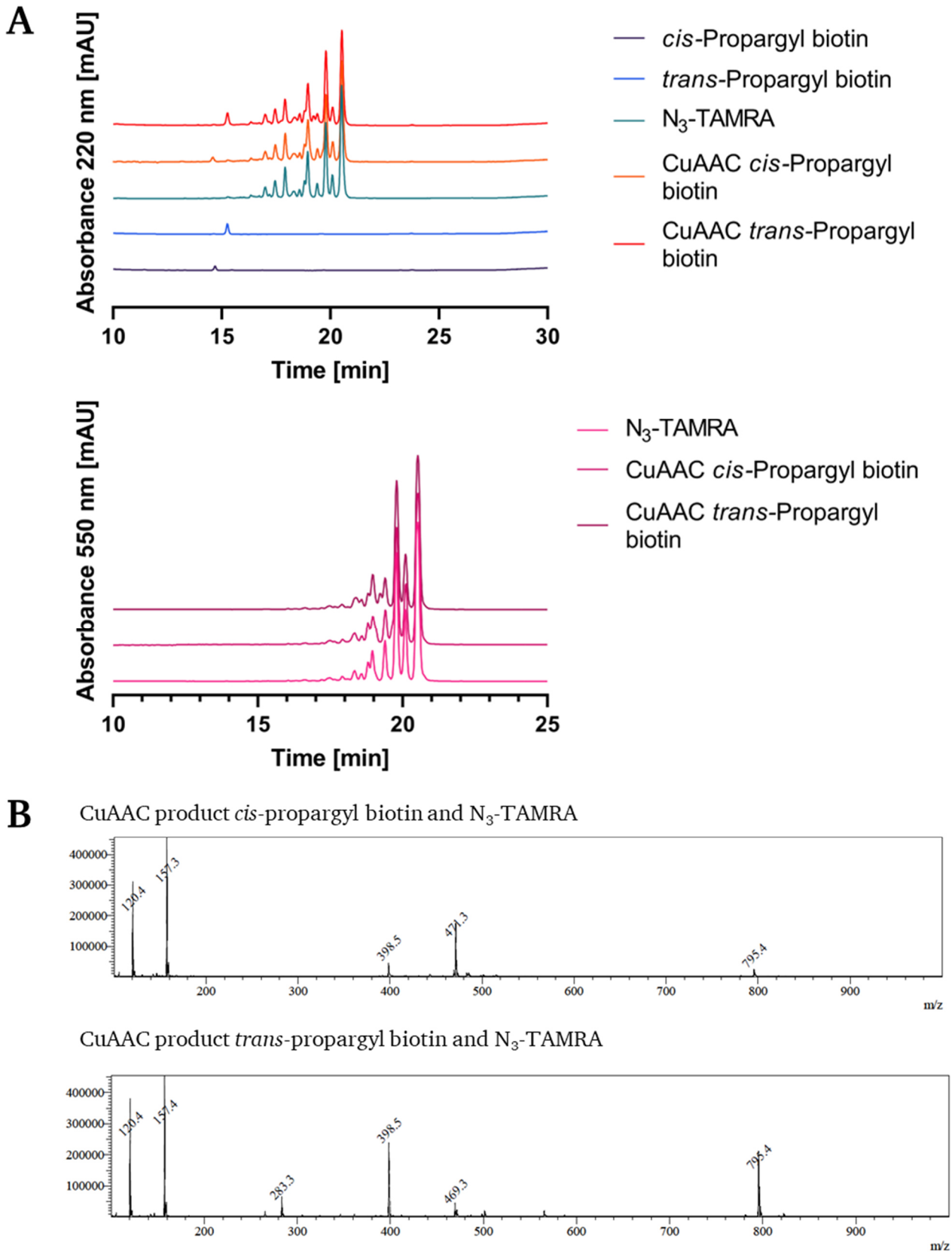

Supplementary figure 10: RP-HPLC analysis (A) and LC-MS analysis (B) of CuAAC between propargyl biotin isomers and N3-TAMRA. 2.3 mM cis- or trans-propargyl biotin, 1 mM N3-PEG3-TAMRA, 1 mM Cu+ and 2 mM ascorbic acid were incubated for 5 h at 37°C. 15 µg of the educts and reacted propargyl biotin were analyzed by RP-HPLC applying a gradient 0to60%B in 32 min. LC-MS was performed 30to100%B in 20 min at 220 nm. Calc. Mass $[M+H]^+$: Product of CuAAC: 794,32. Obs. Mass $[M+H]^+$:, Product of CuAAC: 795.4.

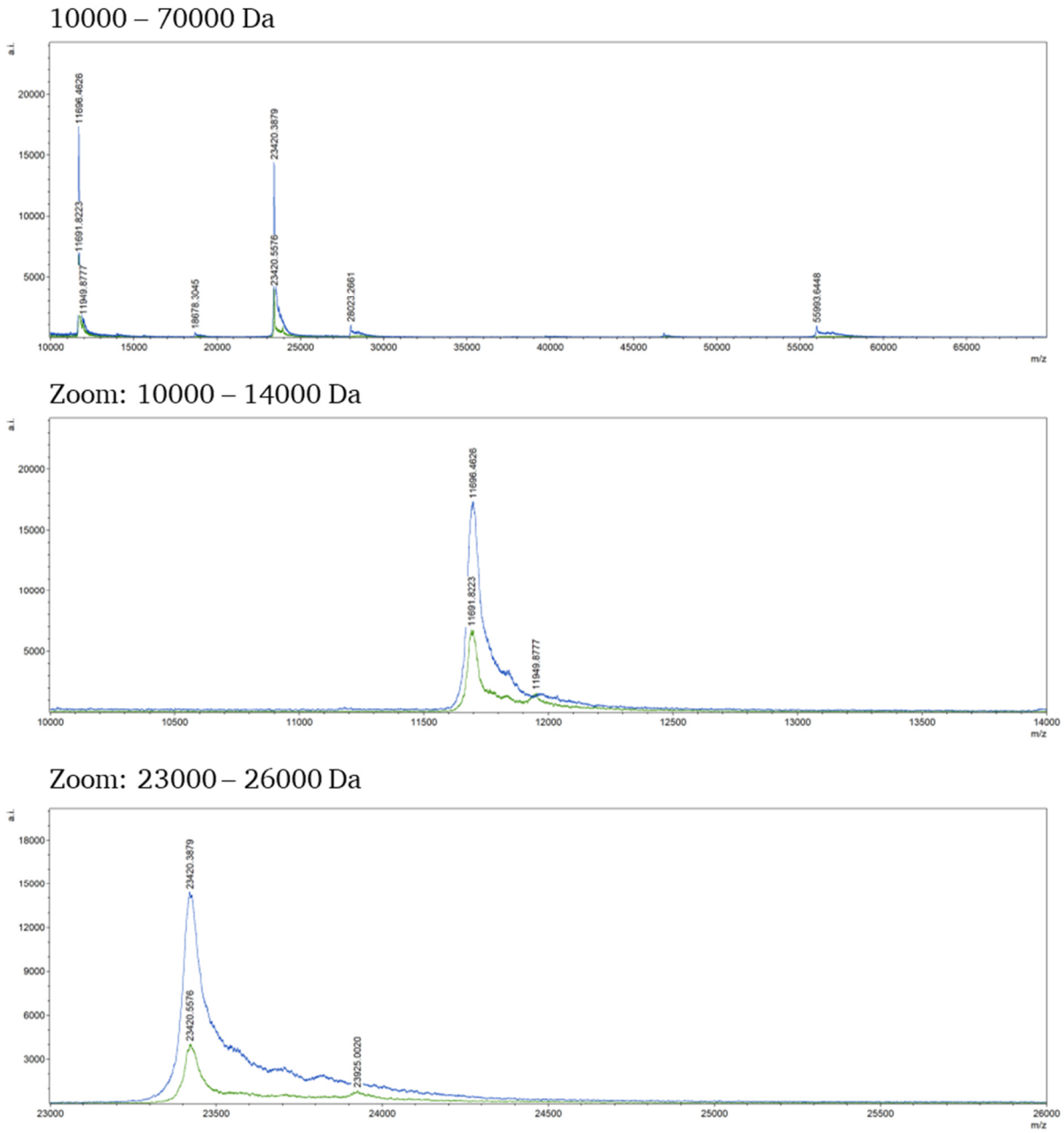

	Calc. Mass heavy chain	Obs. Mass heavy chain	Calc. Mass light chain	Obs. Mass light chain
$[M+H]^+$	56087.47	55993.64	23444.10	23420.39
$[M+2H]^{2+}$	28043.73	28023.27	11723.50	11696.46
$[M+3H]^{3+}$	18695.66	18678.30		

Supplementary figure 11: MALDI-TOF/TOF-MS analysis of unmodified trastuzumab-N297Q-HC:p67 (blue) and desthiobiotin azide carrying trastuzumab-N297Q-HC:p67 (green). Aglycosylated trastuzumab-N297Q-HC:p67 was incubated with 50 eq. of desthiobiotin azide, 5 mM ATP, 5 mM $Mg(OAc)_2$ and 1/10 eq. PhBL overnight at 37°C. After buffer exchange the purified antibodies were reduced by addition of 100 mM DTT and analyzed by MALDI-MS.

A

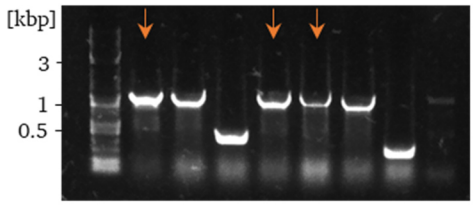

> Clone 1
MKYLLPTAAAGLLLLAAQPAMAQLQLQESGGRLSSAWGVPQTLL
FSVWVRLQYIWHALGPPSSREGAGVGLTY*... (ORF 1)

...GGGSEGGGSEGGGSEGGSDIQMTQSPSSLSASVGDTVTITC
RASQSISNYLNWYQQKPGIAPKLLIYAASALESGVPSRFSGSGS
GADFTLTISNVQPEDFATYYCQQGYGTPRTFGPGTKVDIKRTVA
APSVFGLNDIFEAQKIEWHEAAAGSEQKLISEEDLSHHHHHH*
(ORF 2)

> Clone 4
MKYLLPTAAAGLLLLAAQPAMAAGAAGGVWGTRGPAREVPKTLL
CSLWLHRHFLCHTLGPPGSRQGAGVGGTLFA*...

> Clone 5
MKYLLPTAAAGLLLLAAQPAMAQVQLVESGAEVKSPGSL*...

B

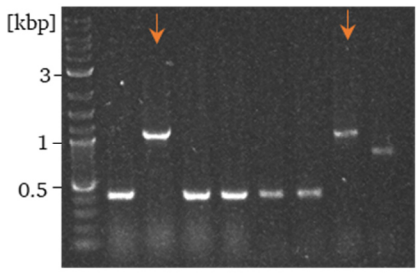

> Clone 2
MKYLLPTAAAGLLLLAAQPAMAEVQWWSLGEACYSLGGP*...

> Clone 7
MKYLLPTAAAGLLLLAAQPAMAQLSCRSRPRTGEAFGDPVPHLH
CLWWLHQKLFLELDPTARREGTGVDWSYL*...

C

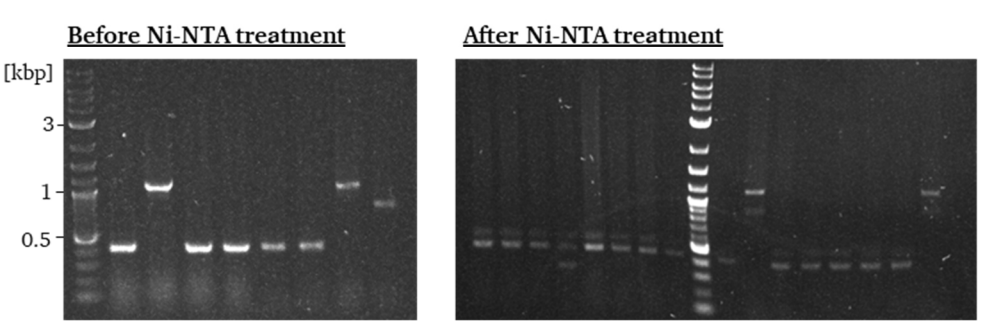

Supplementary figure 12: Colony PCR and sequencing results of enrichment round 1 (A) and 2 (B) screening SLE007 κ-library and enrichment of functional phages by magnetic Ni-NTA beads (C) Violet: pelB leader sequence; Green: scFv GGGSE linker; Dark blue: myc-Tag; Orange: His-Tag; Blue: AviTag™; *: Early stop codon.

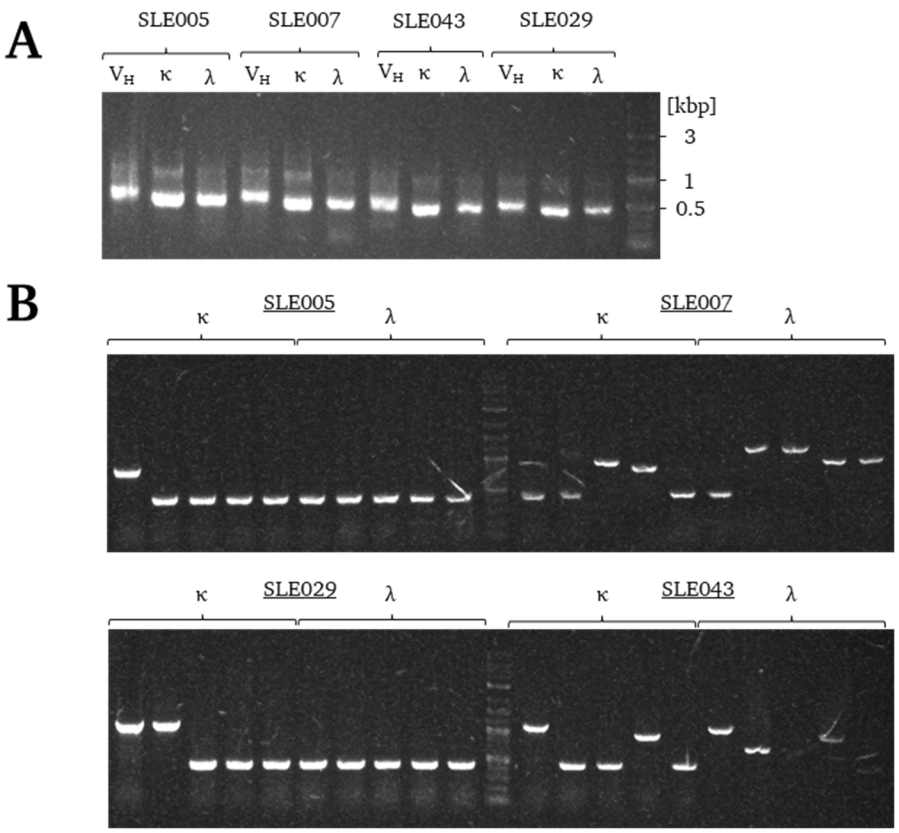

Supplementary figure 13: Pooled PCR products of V_H, κ-V_L and λ-VL of SLE patients (A) and insert rate determination of golden gate assembled clones by colony PCR (B).

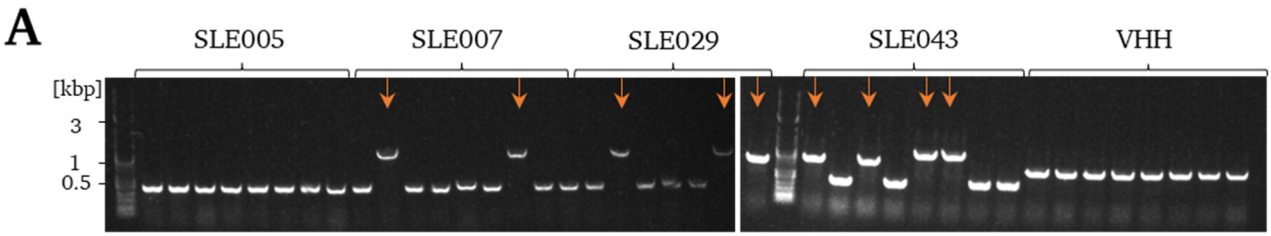

B

```
>7.2
MKYLLPTAAAGLLLLAAQPAMAQVQLQQWGLR*
>7.7
MKYLLPTAAAGLLLLAAQPAMAQIQLVQSGAEIKKPGESLKISCKGSGDSFTTN*
>29.3
MKYLLPTAAAGLLLLAAQPAMAQLQLQESGGGLIQPGGSLRLSCAASGFTVSSNYMSWVRQAPGKGLE*
>29.7
MKYLLPTAAAGLLLLAAQPAMAQVQLQQWGSLGQAWGVPNTLLCSLWIPFH*
>29.8
MKYLLPTAAAGLLLLAAQPAMAEVQLVESGGGLVKPGGSLRLSCAASGFTFSSYSMNWVRQAPGKGLEWVSSISNGSTYIYYADSVK
GRFTISRDNAKNSLYLQMNSLRAEDTAVYYCARALGQWLVRYFDYWGQGTLVTVSSASTKGPSVGGGSEGGGSEGGGSEGGSQSVLT
QPPSFWSERHLRSSENRMARSGRRF*
>43.1
MKYLLPTAAAGLLLLAAQPAMARSP*
>43.3
MKYLLPTAAAGLLLLAAQPAMAEVQLVQSGGGLVKPGGSLRLSCAASGFTFHLYGMNWVRQAPGKGLEWVSAVDITGDNTYYADSTK
GPSVGGGSEGGGSEGGGSEGGSDIQLTQSPSSVSASVGDRVTITCRASQGFSSWLAWYQQKPGKAPKLLIYAASSLQSGVPSRFSGS
GSGTDYTLTISSLQPEDFATYYCQQSKTYPWTFGRGTKVEIKRTVAAPSVFAAAGSEQKLISEEDLSHHHHHH*
>43.5
MKYLLPTAAAGLLLLAAQPAMAQVQLQQWGRRGPAWEVPETLLCSLWIHLQ*
>43.6
MKYLLPTAAAGLLLLAAQPAMAQVTLKSLGLR*
```

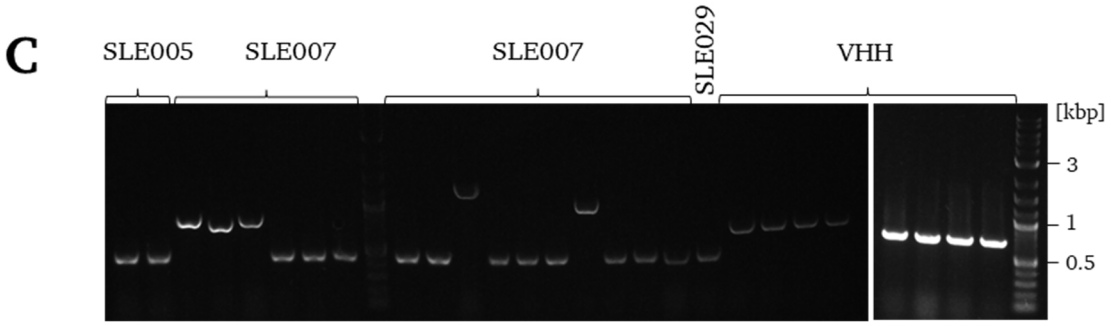

Supplementary figure 14: Colony PCR of *E. coli* infected by M13 phages yielded from mammalian cell incubation (A), sequencing results (B) and colony PCR of another independent approach were SLE libraries were mixed with 100:1 anti-STAT3 VHH (C) SLE phage libraries were incubated overnight on HeLa-EM2-11ht-ultraID_NES cells. After stringent washing cells were lyzed by freeze-thaw and phages were purified via Strep-Tactin® agarose beads. For infection of F^+ *E. coli* cells, phages were eluted directly in the cells by using 10 mM of NaOH. Obtained colonies were analyzed by colony PCR and clones with scFv genes were sequenced (Orange arrow).

10.2 List of figures

10.3 List of tables

10.4 Abbreviations

AirID	Promiscuous biotin ligase derived from ancestral organisms
AMP	Adenosine monophosphate
AP	Alkaline phosphatase
ATP	Adenosine triphosphate
BASU	Promiscuous biotin ligase derived from *Bacillus subtilis*
BCN	Bicyclononyne
BCCP	Biotin carboxyl carrier protein
BioID	Proximity-dependent biotin identification
BioID2	Promiscuous biotin ligase derived from *Aquifex aeolicus*
BirA* or BioID	Promiscuous biotin ligase derived from *Escherichia coli*
CuAAC	Copper-catalyzed azide-alkyne cycloaddition
EcBL	Biotin ligase derived from *Escherichia coli*
FACS	Fluorescence-activated cell sorting
HC	Heavy chain of an antibody
HC:LAP	LAP-tag fused to the heavy chain of an antibody
HC:p67	p67 fused to the heavy chain of an antibody
LAP	LplA acceptor peptide
LC	Light chain of an antibody
LC:67	p67 fused to the light chain of an antibody
LplA	Lipoate-protein ligase A
microID	Truncated and mutated (R40G) biotin ligase derived from *Aquifex aeolicus*
miniTurbo	Promiscuous biotin ligase derived from *Escherichia coli* engineered by YSD
MMAE	Monomethyl auristatin E
p67	Biotin acceptor domain and last 67 amino acids from human propionyl-CoA carboxylase
PhBL	Biotin ligase derived from *Pyroccocus horikoshii*
PPIs	Protein-protein interactions studies

SPAAC	Strain-promoted azide-alkyne cycloaddition
TAMRA	5-(and-6)-Carboxytetramethylrhodamine
TurboID	Promiscuous biotin ligase derived from *Escherichia coli* engineered by YSD
ultraID	Ultimate enzyme obtained from directed evolution of microID (R40G / L41P)
ultraID-4	microID variant obtained during directed evolution process
ultraID-5	microID variant obtained during directed evolution process
yBL	Yeast biotin ligase derived from *Saccharomyces cerevisiae*
YSBA	Yeast surface biotinylation assay
YSD	Yeast surface display
ΔAaBL	C-terminally truncated biotin ligase derived from *Aquifex aeolicus*

10.5 Protein sequences

microID

MGEQKLISEEDLDFKNLIWLKEVDSTQERLKEWNVSYGTALVADRQTKGRGGLGRKWLSQEGGLYFSFLLNP
KEFENLLQLPLVLGLSVSEALEEITEIPFSLKWPNDVYFQEKKVSGVLCELSKDKLIVGIGINVNQREIPEEIKDRA
TTLYEITGKDWDRKEVLLKVLKRISENLKKFKEKHHHHHH*

ultraID

MGEQKLISEEDLDFKNLIWLKEVDSTQERLKEWNVSYGTALVADRQTKGRGGPGRKWLSQEGGLYFSFLLNP
KEFENLLQLPLVLGLSVSEALEEITEIPFSLKWPNDVYFQEKKVSGVLCELSKDKLIVGIGINVNQREIPEEIKDRA
TTLYEITGKDWDRKEVLLKVLKRISENLKKFKEKHHHHHH*

***A. aeolicus* BCCP**

MMDKDFIKELINLIKNSNVKSLKIEKGDFKLQIETYKEIQPPEGVKPQKTEEYKHLEILPPSEDVKLGEQEEKKYH
VIKSPLVGTFYRSPAPGAPPFVEVGDIVSPGQVLCIIEALKVMNEIESDVRGRVEKILVENGETVEYGQPLFLIDT
NVHHHHHH*

***P. horikoshii* biotin ligase**

MLGLKTSIIGRRVIYFQEITSTNEFAKTSYLEEGTVIVADKQTMGHGRLNRKWESPEGGLWLSIVLSPKVPQKD
LPKIVFLGAVGVVETLKEFSIDGRIKWPNDVLVNYKKIAGVLVEGKGDKIVLGIGLNVNNKVPNGATSMKLELGS
EVPLLSVFRSLITNLDRLYLNFLKNPMDILNLVRDNMILGVRVKILGDGSFEGIAEDIDDFGRLIIRLDSGEVKKVI
YGDVSLRFLHHHHHH*

E. coli biotin ligase

MGEQKLISEEDLDKDNTVPLKLIALLANGEFHSGEQLGETLGMSRAAINKHIQTLRDWGVDVFTVPGKGYSLP
EPIQLLNAKQILGQLDGGSVAVLPVIDSTNQYLLDRIGELKSGDACIAEYQQAGRGRRGRKWFSPFGANLYLS
MFWRLEQGPAAAIGLSLVIGIVMAEVLRKLGADKVRVKWPNDLYLQDRKLAGILVELTGKTGDAAQIVIGAGI
NMAMRRVEESVVNQGWITLQEAGINLDRNTLAAMLIRELRAALELFEQEGLAPYLSRWEKLDNFINRPVKLII
GDKEIFGISRGIDKQGALLLEQDGIIKPWMGGEISLRSAEKHHHHHH*

p67

LRSPMPGVVVAVSVKPGDAVAEGQEICVIEAMKMQNSMTAGKTGTVKSVHCQAGDTVGEGDLLVELEHHH
HHH*

***E.coli* lipoate-protein ligase A**

MKHHHHHHHHMSTLRLLISDSYDPWFNLAVEECIFRQMPATQRVLFLVRNADTVVIGRAQNPWKECNTRRM
EEDNVRLARRSSGGGAVFHDLGNTCFTFMAGKPEYDKTISTSIVLNALNALGVSAEASGRNDLVVKTVEGDRK
VSGSAYRETKDRGFHHGTLLLNADLSRLANYLNPDKKKLAAKGITSVRSRVTNLTELLPGITHEQVCEAITEAF
FAHYGERVEAEIISPNKTPDLPNFAETFARQSSWEWNFGQAPAFSHLLDERFTWGGVELHFDVEKGHITRAQ
VFTDSLNPAPLEALAGRLQGCLYRADMLQQECEALLVDFPEQEKELRELSAWMAGAVR*

Trastuzumab-HC:p67

EVQLVESGGGLVQPGGSLRLSCAASGFNIKDTYIHWVRQAPGKGLEWVARIYPTNGYTRYADSVKGRFTISAD
TSKNTAYLQMNSLRAEDTAVYYCSRWGGDGFYAMDYWGQGTLVTVSSASTKGPSVFPLAPSSKSTSGGTAA
LGCLVKDYFPEPVTVSWNSGALTSGVHTFPAVLQSSGLYSLSSVVTVPSSSLGTQTYICNVNHKPSNTKVDKKV
EPPKSCDKTHTCPPCPAPELLGGPSVFLFPPKPKDTLMISRTPEVTCVVVDVSHEDPEVKFNWYVDGVEVHNA
KTKPREEQYNSTYRVVSVLTVLHQDWLNGKEYKCKVSNKALPAPIEKTISKAKGQPREPQVYTLPPSRDELTKN
QVSLTCLVKGFYPSDIAVEWESNGQPENNYKTTPPVLDSDGSFFLYSKLTVDKSRWQQGNVFSCSVMHEALH
NHYTQKSLSLSPGLRSPMPGVVVAVSVKPGDAVAEGQEICVIEAMKMQNSMTAGKTGTVKSVHCQAGDTVG
EGDLLVELE*

Trastuzumab-HC:LAP

EVQLVESGGGLVQPGGSLRLSCAASGFNIKDTYIHWVRQAPGKGLEWVARIYPTNGYTRYADSVKGRFTISAD
TSKNTAYLQMNSLRAEDTAVYYCSRWGGDGFYAMDYWGQGTLVTVSSASTKGPSVFPLAPSSKSTSGGTAA
LGCLVKDYFPEPVTVSWNSGALTSGVHTFPAVLQSSGLYSLSSVVTVPSSSLGTQTYICNVNHKPSNTKVDKKV
EPPKSCDKTHTCPPCPAPELLGGPSVFLFPPKPKDTLMISRTPEVTCVVVDVSHEDPEVKFNWYVDGVEVHNA
KTKPREEQYNSTYRVVSVLTVLHQDWLNGKEYKCKVSNKALPAPIEKTISKAKGQPREPQVYTLPPSRDELTKN
QVSLTCLVKGFYPSDIAVEWESNGQPENNYKTTPPVLDSDGSFFLYSKLTVDKSRWQQGNVFSCSVMHEALH
NHYTQKSLSLSPGGFEIDKVWYDLDA*

Trastuzumab heavy chain

EVQLVESGGGLVQPGGSLRLSCAASGFNIKDTYIHWVRQAPGKGLEWVARIYPTNGYTRYADSVKGRFTISAD
TSKNTAYLQMNSLRAEDTAVYYCSRWGGDGFYAMDYWGQGTLVTVSSASTKGPSVFPLAPSSKSTSGGTAA
LGCLVKDYFPEPVTVSWNSGALTSGVHTFPAVLQSSGLYSLSSVVTVPSSSLGTQTYICNVNHKPSNTKVDKKV
EPPKSCDKTHTCPPCPAPELLGGPSVFLFPPKPKDTLMISRTPEVTCVVVDVSHEDPEVKFNWYVDGVEVHNA
KTKPREEQYNSTYRVVSVLTVLHQDWLNGKEYKCKVSNKALPAPIEKTISKAKGQPREPQVYTLPPSRDELTKN
QVSLTCLVKGFYPSDIAVEWESNGQPENNYKTTPPVLDSDGSFFLYSKLTVDKSRWQQGNVFSCSVMHEALH
NHYTQKSLSLSPG*

Trastuzumab light chain

DIQMTQSPSSLSASVGDRVTITCRASQDVNTAVAWYQQKPGKAPKLLIYSASFLYSGVPSRFSGSRSGTDFTLT
ISSLQPEDFATYYCQQHYTTPPTFGQGTKVEIKRTVAAPSVFIFPPSDEQLKSGTASVVCLLNNFYPREAKVQW
KVDNALQSGNSQESVTEQDSKDSTYSLSSTLTLSKADYEKHKVYACEVTHQGLSSPVTKSFNRGEC*

Trastuzumab-LC:p67

DIQMTQSPSSLSASVGDRVTITCRASQDVNTAVAWYQQKPGKAPKLLIYSASFLYSGVPSRFSGSRSGTDFTLT
ISSLQPEDFATYYCQQHYTTPPTFGQGTKVEIKRTVAAPSVFIFPPSDEQLKSGTASVVCLLNNFYPREAKVQW
KVDNALQSGNSQESVTEQDSKDSTYSLSSTLTLSKADYEKHKVYACEVTHQGLSSPVTKSFNRGECGGGGSG
GGGSGGGGSLRSPMPGVVVAVSVKPGDAVAEGQEICVIEAMKMQNSMTAGKTGTVKSVHCQAGDTVGEGD
LLVELE*

Anti-STAT3 VHH-pIII fusion

HVQLVESGGGSVQAGGSLRLSCAASGANGGRSCMGWFRQVPGKEREGVSGISTGGLITYYADSVKGRFTISQ
DNTKNTLYLQMNSLKPEDTAMYYCATSRFDCYRGSWFNRYMYNSWGQGTQVTVSSAAAGSEQKLISEEDLS
HHHHHH*GSKDIRAETVESCLAKSHTENSFTNVWKDDKTLDRYANYEGCLWNATGVVVCTGDETQCYGTW
VPIGLAIPENEGGGSEGGGSEGGGSEGGGTKPPEYGDTPIPGYTYINPLDGTYPPGTEQNPANPNPSLEESQPL
NTFMFQNNRFRNRQGALTVYTGTVTQGTDPVKTYYQYTPVSSKAMYDAYWNGKFRDCAFHSGFNEDLFVC
EYQGQSSDLPQPPVNAGGGSGGGSGGGSEGGGSEGGGSEGGGSEGGGSGGGSGSGDFDYEKMANANKGA
MTENADENALQSDAKGKLDSVATDYGAAIDGFIGDVSGLANGNGATGDFAGSNSQMAQVGDGDNSPLMNN
FRQYLPSLPQSVECRPFVFGAGKPYEFSIDCDKINLFRGVFAFLLYVATFMYVFSTFANILRNKES*

10.6 Danksagung

An dieser Stelle möchte ich mich bei allen Personen, die mich während der Zeit meiner Promotion begleitet und unterstützt haben, herzlich bedanken!

Darüber hinaus gilt ein besonderer Dank den folgenden Personen:

Zuerst möchte ich mich bei **Prof. Dr. Harald Kolmar** für die Möglichkeit in seiner Arbeitsgruppe zu promovieren und das in mich gesetzte Vertrauen bedanken! Danke für die ständige Unterstützung, die motivierenden und thematisch anregenden Gespräche und dein zu jeder Zeit offenes Ohr. Ebenso danke, dass du stets positiv geblieben bist und es immer wieder geschafft hast, mich zu überzeugen, die Hoffnung in meine Forschung nicht zu verlieren. Ich habe die Zeit in deiner Arbeitsgruppe und auch die Kleinwalsertal Aufenthalte sehr genossen!

Bei **Prof. Dr. Viktor Stein** möchte ich mich vielmals für die sofortige Übernahme des Korreferats bedanken.

Mein Dank gilt auch **Prof. Dr. Katja Schmitz** und **Prof. Dr. Beatrix Süß** für die sofortige Übernahme der Rolle als Fachprüferinnen.

Einen besonderen Dank möchte ich meinem Namensvetter **Peter Bitsch** aussprechen. Danke für die Synthese des Propargyl-biotins. Die Enttäuschung darüber, dass daraus keine (Bitsch)^2 *et al.* Publikation entstanden ist, sitzt immer noch tief. Darüber hinaus möchte ich mich aufrichtig für deine Unterstützung außerhalb des Labors, besonders im letzten Jahr, bedanken!

Ingo Bork möchte ich für die Synthese des Desthiobiotin-azids und **Alessandro Emmanuello** für die ambitionierten Versuche andere Azid-Biotin-Derivate zu synthetisieren, bedanken!

Natürlich möchte ich mich auch bei **Carolin Dombrowsky**, **Julia Harwardt** und **Katrin Schoenfeld** für die gemeinsame Zeit im, aber auch außerhalb des Labors bedanken. Ihr Drei seid immer für einen Lacher oder einen „Grotzel“-Moment gut gewesen.

Darüber hinaus gilt mein Dank **Stefania Carrara**. Danke, dass du mir immer mit Rat und Tat zur Seite gestanden hast und ich mit dir über ELISAs und deren „dezente“ Fehleranfälligkeit lästern durfte.

Ebenso gilt mein Dank den „7. Stock Dudes“ **Ata Ali**, **Arturo Macarrón** und **Dominic Happel**. Auch wenn wir uns durch die coronabedingte Schichtarbeit fast nie gleichzeitig im Labor befunden haben, möchte ich diese Zeit nicht missen. Das gilt auch für unsere privaten Aktivitäten, sei es im Urlaub oder bei sonstigen Unternehmungen.

Ich möchte mich außerdem bei **Dana Schmidt** und **Janine Becker** für die organisatorischen Arbeiten im Labor bedanken. Ihr habt elementar dazu beigetragen, dass der Arbeitsfluss im Labor nicht zum Stocken kam.

Natürlich möchte ich mich auch bei allen nicht genannten aktuellen und auch ehemaligen Mitgliedern der AG Kolmar für die schöne Zeit und die Unterstützung bedanken. Ihr habt maßgeblich dazu beigetragen, dass ich mich hier ab dem ersten Tag wohl gefühlt habe. Als besondere Highlights werden mir immer die Aufenthalte im Kleinwalsertal und die ChemCups in Erinnerung bleiben! Ebenso wird mein Magen das sehr frühe, aber obligatorische Mittagessen um genau! 11:15 Uhr im Gedächtnis behalten.

Zu guter Letzt gilt mein besonderer Dank **meinen Eltern**. Danke, dass ihr mir in allen Lebenslagen bedingungslosen Rückhalt gebt, meine Entscheidungen unterstützt und immer da seid, falls etwas mal nicht so läuft, wie es soll! Ohne euch wäre mein ganzes Studium und auch diese Doktorarbeit nicht möglich gewesen. Von ganzem Herzen, Danke!

10.7 Affirmations

§8 Abs. 1 lit. c der Promotionsordnung der TU Darmstadt

Ich versichere hiermit, dass die elektronische Version meiner Dissertation mit der schriftlichen Version übereinstimmt und für die Durchführung des Promotionsverfahrens vorliegt.

§8 Abs. 1 lit. d der Promotionsordnung der TU Darmstadt

Ich versichere hiermit, dass zu einem vorherigen Zeitpunkt noch keine Promotion versucht wurde und zu keinem früheren Zeitpunkt an einer in- oder ausländischen Hochschule eingereicht wurde. In diesem Fall sind nähere Angaben über Zeitpunkt, Hochschule, Dissertationsthema und Ergebnis dieses Versuchs mitzuteilen.

§9 Abs. 1 der Promotionsordnung der TU Darmstadt

Ich versichere hiermit, dass die vorliegende Dissertation selbstständig und nur unter Verwendung der angegebenen Quellen verfasst wurde.

§9 Abs. 2 der Promotionsordnung der TU Darmstadt

Die Arbeit hat bisher noch nicht zu Prüfungszwecken gedient.

Darmstadt, den ……..

Sebastian Harald Bitsch